Post Excavation Changes and Preventive Conservation of Archaeological Iron

David Thickett

Thesis submitted for the degree of Doctor of Philosophy of the University of London

School of Biological and Chemical Sciences

Birkbeck College, University of London, Mar 2012

Declaration

This thesis is the result of my own independent investigation, except where otherwise stated. Other sources are acknowledged by explicit references.

David Thickett

19 March 2012

Abstract

Analysis of over 240 deteriorating (recent loss of material, new corrosion or cracking) archaeological iron objects has confirmed the pivotal role of akaganeite in their deterioration. Spectroscopic and thermoanalytical techniques have been used to characterize corrosion products, also from accelerated aged mixtures of iron powder and selected compounds. Additional species have been characterized that are known to alter the formation of akaganeite. Ferrous chloride crystals have been detected at the metal corrosion interface in freshly excavated iron and observed to transform into akaganeite via ferric chloride.

The effect of relative humidity (RH) on the main deterioration reactions has been measured, with the formation of akaganeite, and residual metal core. Associated species were found to alter corrosion rates but not the overall pattern of response. Four critical RH values (11, 16, 30 and 50-60% depending on temperature) have been defined. The effect of volatile carbonyl gases, inorganic pollutants, and their synergistic action with RH have been determined. All accelerate the reactions. When exposures are considered the risk from the carbonyl pollutants is much greater than from the inorganic ones.

Transformation of akaganeite to Goethite (α-FeOOH) has been observed on objects for the first time. The transformation is strongly affected by relative humidity. The influence of ethanoic acid was also observed on objects. Transformation to hematite, α-Fe_2O_3 was observed to occur at a much slower rate than to Goethite. Laboratory experiments require elevated temperatures, though much less than 200ºC stated in current literature. Hematite has been detected on samples of akaganeite previously removed from objects over the past four decades. Differences in synthesized akaganeites have been observed by thermoanalytical techniques and are suggested for future characterization.

Showcases to protect archaeological iron have been developed and the underlying theories of performance tested. Silica gel change schedules have been developed from modelled internal RH data in storage boxes used for iron objects and optimisation of storage procedures have been investigated.

Acknowledgements

Foremost thanks go to my superviser, Marianne Odlyha, whose support, advice, encouragement and enthusiasm has been invaluable. This work would not have been possible without the enduring and limitless support of my wife, Frances and the support and confidence of Amber Xavier-Rowe.

Within English Heritage and the British Museum, my thanks go to all the conservators, curators and scientists who have helped and supported the work, especially David Dungworth, Roger Wilkes, Nigel Meeks and Ian Freestone.

Several institutions have supported the work by allowing access to their facilities including The Victoria and Albert Museum, The National Archives and CRCC.

COST Action D42 provided invaluable financial assistance to travel to both access equipment and expertise and to carry out additional experimentation.

Terje Grontoft generously provided the results of his measurements during the MASTER project to help assess pollutant ingress into showcases.

Finally my thanks go to my parents, Ann and Richard.

Dedication

This thesis is dedicated to the memory of Graham Bulman, whose boundless enthusiasm, joie de vivre and fascination in the world around him was a true inspiration.

Table of Contents

List of Figures

List of Tables

Chapter 1 Introduction

1.1 Importance of iron in the archaeological record

Heritage benefits mankind. The interpretation of our shared past contributes to social, cultural and national identity and provides significant economic benefits (Fowler, 1992; Smith, 2006; O'Brian, 2010; English Heritage, 2010). The value in archaeological objects lies in the information that can be retrieved from them. Preserving material archives of excavations and the records that define them enables future interpretation to occur (Grossman, 2006, p5). Archaeological excavations destroy the actual site and preserving the material heritage maximises the information, both present and future, that balances this destructive process.

Iron is vastly important within the archaeological record. Iron production and manipulation has often been at the forefront of technology and its introduction still forms one of the major dating points for human history. Iron has been used for a very extensive range of objects, from the highest status Sutton Hoo helm and sword to the lowly, but essential nail. Technological study of iron artefacts is an important area of heritage science (Scott and Eggert, 2009). In temperate climates organic materials do not survive well during burial except under anaerobic conditions. When organic materials such as wood and textile are buried in close proximity to iron, the corrosion process of the iron can lead to pseudomorphic replacement of the organic materials retaining their characteristic morphological features (Jakes and Sibley, 1984). The cell patterns of wood can be used to identify the species used and microscopic features can identify textile types. Weave analysis is possible with mineral preserved textiles. Organic materials rarely survive in UK soils thus the fragile mineral preserved organic remains on archaeological iron surfaces constitute a corpus of data on organic materials.

Application of advanced analytical techniques can retrieve information from objects that were thought unimportant. X-ray radiography reveals the internal structure of many apparently shapeless lumps of iron corrosion and has been used since at least

the 1970s (Mould, 1993). X-rays were taken of archaeological objects within months of Rathgen's discovery of the technique in 1895 (Land and Middleton, 1997). Recent advances in X-ray tomography allow identification of mineral preserved organic remains within soil blocks (Ebinger-Rist et al, 2011). High resolution transmission electron microscopy has revealed the presence of carbon nanorods in Damascus steel blades (Reibold et al, 2006).

The move towards preservation in situ may increase interest in archaeological iron presently in archives. With limited opportunities for new archaeological excavations, attention may refocus towards study of material in store (Nelson and Shears, 1996).

Archaeological iron can be an inherently unstable material, at risk of deterioration and loss of the information it holds. A recent collections condition survey of English Heritage's collections (which include over 400,000 archaeological objects) identified iron as the most damaged material type (Fry et al, 2007; Xavier Rowe et al, 2008; Xavier Rowe et al 2011).

1.2 Mechanisms of iron deterioration during burial

When iron is buried, it is exposed to environments with a large excess of water and little oxygen. The exact environment depends on local conditions. The major factors influencing corrosion are shown in Figure 1.1, which emphasises the complexity and interrelations within the system. Water and oxygen availability are determined by the soil morphology and climatic conditions. The presence of soluble salt and hydrogen ions (pH) has a large effect on corrosion. The redox potential is also significant. The processes are complex with many interacting factors. For example physical weathering is determined by the water content of the soil, which in turn is determined by rainfall and soil porosity, determined by soil texture. One example of chemical weathering is determined by water, oxygen and chloride content of the soil. The chloride content is determined by soil porosity and chloride sources, salting roads, sea salt aerosol deposition and leaching of soil minerals.

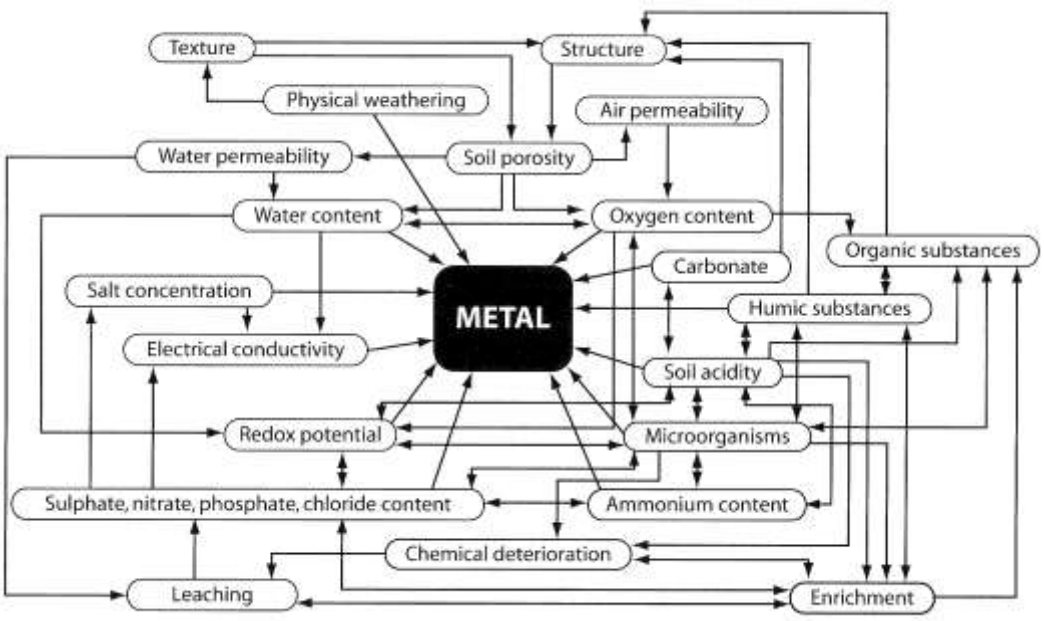

Figure 1.1 Factors in corrosion of iron during burial (after Gerwin, 1999).

Corrosion proceeds via an electrochemical process. The anodic half reaction is the dissolution of iron which occurs at the iron surface,

$$Fe_{(s)} \rightarrow Fe^{2+}_{(aq)} + 2e^- \quad (1.1)$$

The cathodic half reaction is often water reduction,

$$O_{2(g)} + 4H_2O + 4e^- \rightarrow 4OH^-_{(aq)} \quad (1.2)$$

In acidic solutions (below pH 4) hydrogen evolution can form the cathodic half reaction,

$$2H_2O + 2e^- \rightarrow H_{2(g)} + 2OH^-_{(aq)} \quad (1.3)$$

The iron ions accumulate at the metal surface. In solution the iron (II) ions exists as a hexa co-ordinated complex with water, $[Fe(H_2O)_6]^{2+}$. The co-ordinated water molecules can react with the iron(II) ions and undergo hydrolysis,

$$Fe^{2+}_{(aq)} + H_2O \rightarrow Fe(OH)^+_{(aq)} + H^+_{(aq)} \quad (1.4)$$

This causes local acidification. In the presence of dissolved oxygen, the iron (II) ions can be oxidised to iron (III) ions. The iron(III) ions can also undergo hydrolysis.

Depending on the pH, the concentration of dissolved oxygen and the concentration of other anions such as carbonate or phosphate, the iron (II) and iron (III) ions will precipitate as solids. The solids that are thermodynamically stable can be predicted using a potential pH diagram as described by Pourbaix (1977). The potential (Eh) is measured versus a standard hydrogen electrode (SHE). Figures 1.2, 1.3 and 1.4 show examples for iron. In aqueous media the two sets of dotted lines define the thermodynamic stability region for water under normal conditions at 1atmosphere pressure and 25ºC. Figure 1.2 shows the iron water system. Above line (a) water decomposes to evolve oxygen

$$2H_2O_{(l)} \leftrightarrow O_{2(g)} + 4H^+ + 4e^- \qquad (1.5)$$

Below line (b) water decomposes to evolve hydrogen

$$2H_2O_{(l)} + 2\,e^- \leftrightarrow H_{2(g)} + 2OH^- \qquad (1.6)$$

The potential, pH regions occupied by common environments are shown in Figure 1.2.

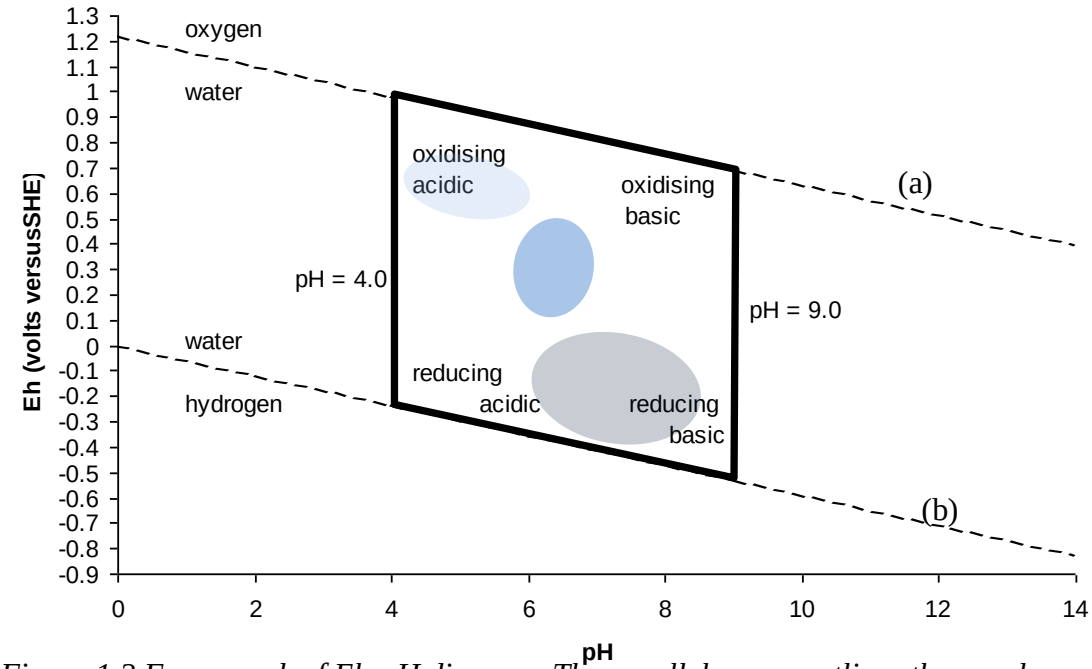

Figure 1.2 Framework of Eh-pH diagram. The parallelogram outlines the usual limits of Eh and pH found in near surface environments (after Garrels and Christ, 1965). Pale blue ellipse represents rain and streams; mid blue ellipse represents ocean; pale grey represents groundwater.

Figure 1.3 shows the Pourbaix diagram for the iron and water system at 25ºC in lower Eh region representative of soil environments.

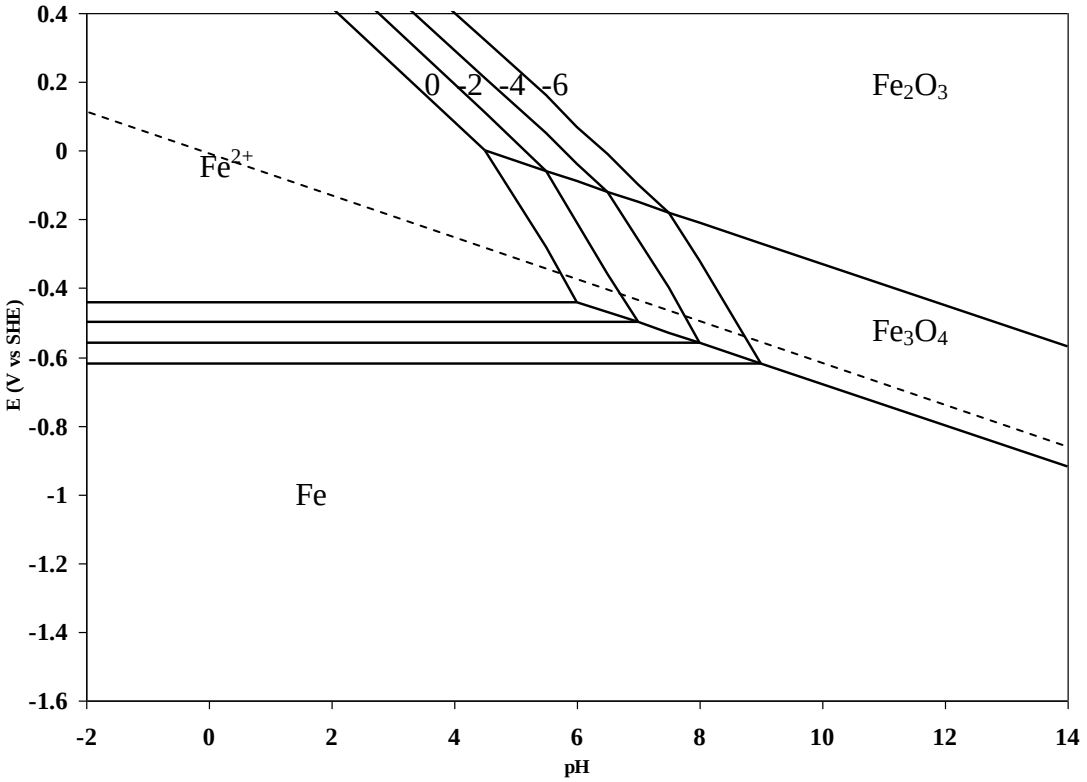

Figure 1.3 pH-Eh diagram for the system iron-water at 25ºC (after Pourbaix, 1977).

Figure 1.4 shows the different areas of thermodynamic stability.

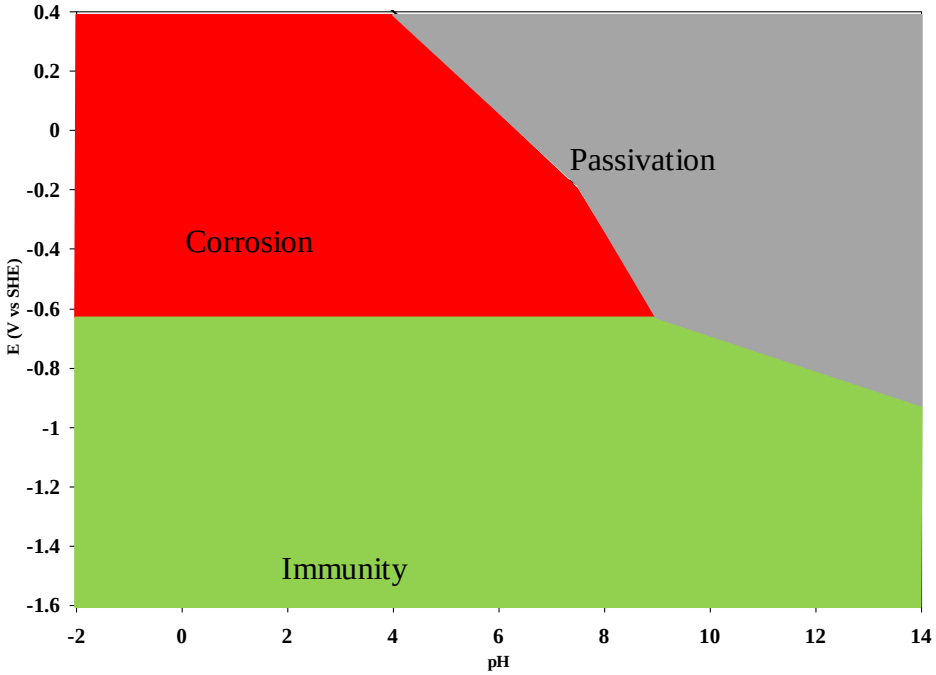

Figure 1.4 pH-Eh diagram for the system iron-water at 25ºC showing different thermodynamic areas of stability (after Pourbaix, 1977).

In normal environments (fig 1.2) iron will not be in the immunity region and will either corrode or passivate. The oxidation of iron may lead to soluble products (Fe^{2+}, Fe^{3+}, $Fe(OH)^{+}$) or insoluble products ($Fe(OH)_2$, Fe_3O_4 and Fe_2O_3). If the iron is covered by a layer of insoluble products it is rendered passive. If, however, the thermodynamically stable products are soluble, then it will corrode. The boundary between the passive and corroding regions depends on the ion concentration. At low potential the iron is thermodynamically stable, this is known as immunity. Figure 1.4 shows the passive, corrosive and immune regions.

In 1M chloride solution, Figure 1.5 the stable phases are Goethite, α-FeOOH and magnetite Fe_3O_4 and the iron will be passivated. The unstable phases are now iron (II) chloride and iron (III) chloride, and corrosion will occur.

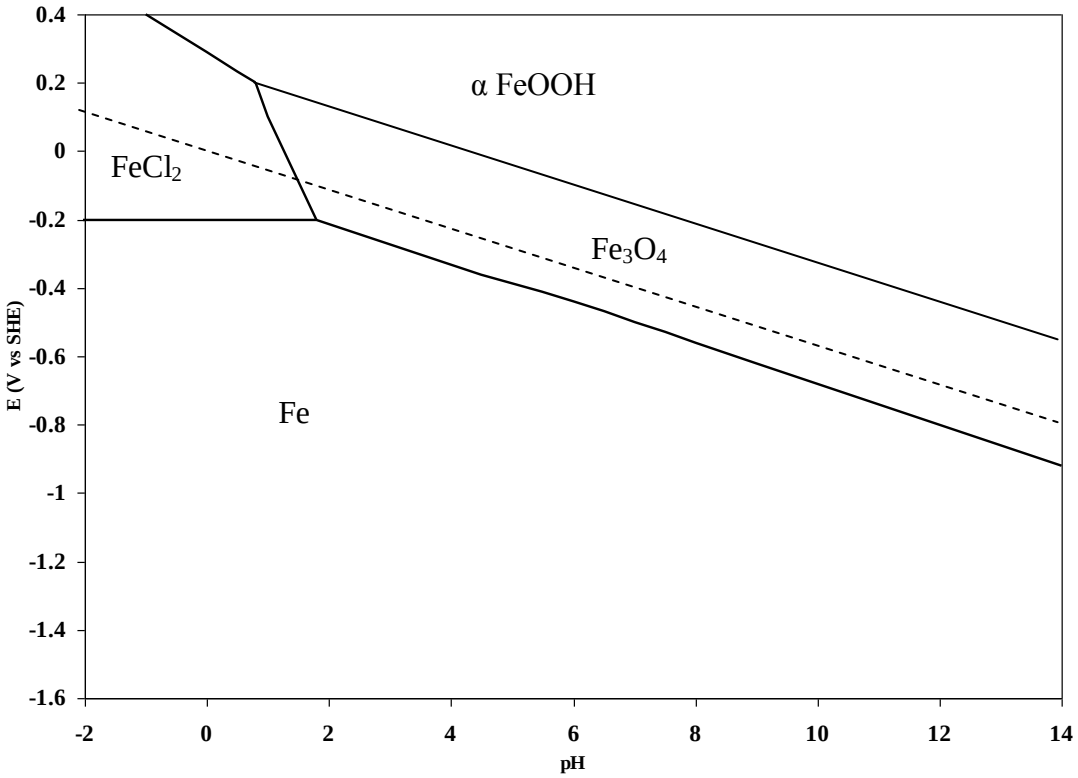

Figure 1.5 pH-Eh diagram for the system iron-water-chloride at 25ºC and 1M chloride concentration, (after Turgoose 1982a).

Above pH 6, solid iron(II) hydroxide will precipitate. In reducing conditions if carbonate or phosphate are present in sufficient concentrations siderite $FeCO_3$ or vivianite, $Fe_3(PO_4)_2.8H_2O$ will also precipitate. (Selwyn, 2004).

Once precipitated $Fe(OH)_2$ is readily oxidised to intermediate Fe(II)-(III) compounds by dissolved oxygen. The possibilities are magnetite, $FeO.Fe_2O_3$ and the green rusts. Green rusts are layered compounds with alternate positively charged iron hydroxide sheets and negatively charged chloride, carbonate or sulphate ions (Refait et al, 1997).

After a period of time buried archaeological iron is covered by layered structures of corrosion products. The outer layers are formed of iron (III) corrosion products, often Goethite, α-FeOOH. The soil components such as small stones, sand crystals, clay are often incorporated into these layers. The inner layers are of lower oxidation states, often magnetite. This layer was thought to be the 'original surface'. Many iron artefacts were cleaned to this layer. Berthalon (2000) has developed a system to determine the original surface, such that exists from observation and analysis. Near the remaining metal core, if there is any, Fe^{2+} ions will continue to be generated if corrosion proceeds. These will dissolve, accumulate and possibly hydrolyse, depending on the local pH. To maintain electrical neutrality anions are transported towards the corroding surface to balance the Fe^{2+} and H^{+} ions produced there. Chloride ions are small and have high transport numbers and tend to form the bulk of the balancing cations when available. During burial any spaces near the remaining metal surfaces; cracks, pores or voids will become filled with solution rich in Fe^{2+} and Cl^{-} ions (Turgoose, 1993).

1.3 Mechanisms of iron deterioration after excavation

When iron artefacts are excavated they enter an atmosphere with much more oxygen and much less water. Hence they will slowly dry. The complete drying of a small iron find such as a knife blade can take several years (Thickett and Odlyha, 2010) and soil retained on the surface will slow this process. Oxygen will permeate the soil and corrosion product layer enclosing the object. As these layers dry they often crack, increasing the rate of oxygen ingress. In areas where corrosion was occurring there will be high concentrations of chloride and ferrous ions near remaining metal surfaces. As water evaporates these will crystallise as iron (II) chloride, in either the dihydrate or tetrahydrate state (Turgoose, 1982a; Turgoose, 1993; Costain, 1984). If the relative humidity is equal or less than 15% then the dihydrate is the stable phase and no further changes occur (Turgoose, 1982b). If the RH is above 20% the tetrahydrate is stable and this slowly oxidises and hydrolyses to for akaganeite, β-FeOOH. Above 56% the iron(II) chloride is reported to deliquesce (Turgoose, 1982b). The presence of orange droplets on an archaeological iron surface are though to be evidence of this process. Under very high RH conditions large volumes of a liquid can form. Initially these droplets were thought to be iron (III) chloride

(Organ, 1977), Further analysis by North (1982), later verified by Knight (1982) and Turgoose (1982a) showed them to contain iron (II) chloride. If the RH decreases after drop formation, hollow brown spheres can be observed (Selwyn et al, 1999). Selwyn et al (1999) identified the shell material to be Goethite and lepidocrite, γ-FeOOH. Watkinson (2004, 2005) has refined these critical RH values. A number of species have been reported to influence the oxidation of Iron (II) chloride and formation and crystallinity of iron (III) hyroxyoxide corrosion products (Ishikawa et al, 2001; Pullin and Cabaniss, 2003; Ishikawa et al, 1998). Reguer et al (2005, 2007) have shown that beta ferrous hydroxychloride, β-$Fe_2(OH)_3Cl$, can also precipitate depending on the local conditions samples. This will rapidly oxidise to form akaganeite. Whatever the initial precipitate, there is a large volume expansion on the formation of akaganeite and this can cause massive disruption to artefacts. The iron oxyoxides have approximately three times the molar volume of iron (Selwyn, 2004). Overall the process can be described as;

$$4Fe^{2+}_{(aq)} + O_{2(g)} + 6H_2O \rightarrow 4FeOOH_{(s)} + 8H^{+}_{(aq)} \qquad (1.7)$$

The acid ions produced can disrupt the corrosion product layers and attack the remaining metal core. At higher RH values the solubilisation of large amounts of chloride absorbed on the akaganeite surfaces leads to corrosion of the remaining metal core of the object. This risks the metallurgical information retained and produces more iron and chloride rich solution to repeat the akaganeite formation process. Metallurgical information about steels present is often only contained in thin layers on the surface of the object, due to ancient steel making practices and this is particularly at risk, even though the majority of the iron core may remain unaffected. Askey et al (1993) have postulated a hydrochloric acid regeneration cycle.

$$2Fe_{(s)} + 4H^{+}_{(aq)} + 4Cl^{-}_{(aq)} + O_{2(g)} \rightarrow 2Fe^{2+}_{(aq)} + 4Cl^{-}_{(aq)} + 2H_2O \qquad (1.8)$$

$$2Fe_{(s)} + 3H_2O + 4Cl^{-}_{(aq)} + \tfrac{1}{2}\, O_{2(g)} \rightarrow 2FeOOH_{(s)} + 4H^{+}_{(aq)} + 4Cl^{-}_{(aq)} \qquad (1.9)$$

The chloride ions form a soluble salt with iron(II) ions and this solubility allows the cycle to proceed. The major difference between this and equation 1.7 is the explicit involvement of chloride ions in the corrosion process.

Beyond water vapour and oxygen, other species in the air affect the deterioration of iron in a museum environment. The industrial pollutant gases sulfur dioxide, nitrogen dioxide, ozone, hydrogen chloride and hydrogen sulfide are all known to accelerate iron corrosion (Oesch, 1996; Arroyave and Morcillo, 1995). They would be expected to attack the remaining metal core of objects in association with RH. Showcases and storage containers can have high concentrations of the carboxylic acids ethanoic and methanoic in them (Grywacz and Tennent, 1994). Both these species are known to corrode iron and will attack any remaining metal core (Donovan and Stringer, 1972; Cermkova and Vlchova, 1966). There has been little recent work in this area.

Dust particles can be a source of chloride ions and also act to concentrate pollutant gases on mineral surfaces (Corvo et al, 1995). Dust particles can act to deliquesce water due to the presence of hygroscopic components and the narrow gaps formed at the dust surface interface (Vernon, 1935; Evans, 1981; Thickett, 2008a). The condensed water could change the corrosion product mineral and is likely to cause swelling of any clay minerals present, disrupting the corrosion product layers.The porosity of the corrosion layers would very likely transport the condensed water in towards the original metal surface, enhancing further corrosion. Iron artefacts could also be damaged through heating and drying from unsuitable lighting on display and through vibration, although these are beyond the scope of this thesis.

1.4 Akaganeite

Akaganeite has been associated with ongoing deterioration of archaeological iron and been observed at the centre of corroding areas (Zucchi, 1977).

Figure 1.6 Orange akaganeite crystals levering apart Saxon iron pin with eye (Carver 1989).

Akaganeite is the beta polymorph of iron oxyhydroxide, β FeOOH. It is named after the Akagane mine near Esashi City in Iwate Prefecture, Japan. The name does not have an accent on the 'e' (Gaines et al, 1997; Burke, 2008). It has an hollandite structure with 5Å channels. The space group is I2/m with a=1.0600, b=0.30339, c=1.0513nm, β=90.24º (Post and Buckwald, 1991). The most common XRD pattern obtained is ICCD 42-1315.

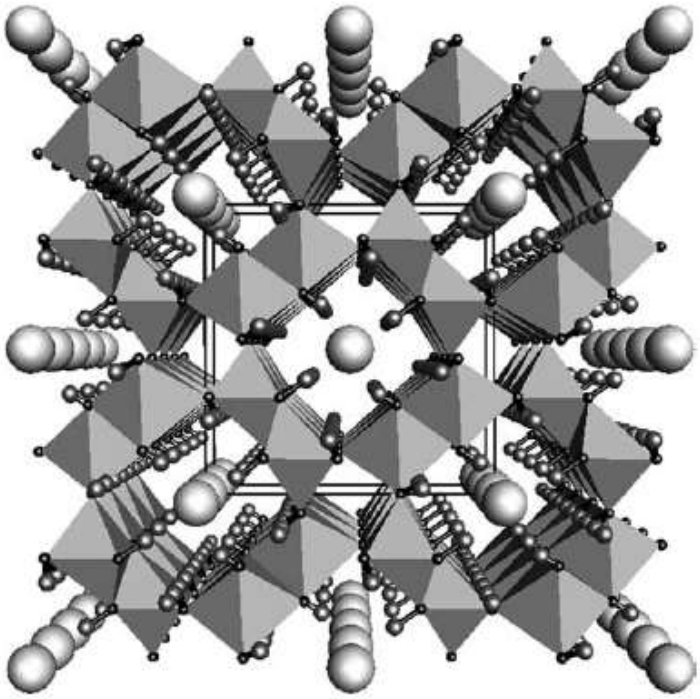

Figure 1.7 Structure of akaganeite viewed along b direction, large spheres are chloride ions, small spheres terminal hydrogen atoms (from Stahl, 2003).

The structure of akaganeite has been the subject of several investigations and our understanding has been through several refinements, mainly about the position of the chloride ions (Weisser and Milligan, 1935; Mackay, 1960; Post and Buchwald, 1991; Stahl et al, 2003). The most recent analysis gives a chemical formula of $FeO_{0.833}(OH)_{1.167}Cl_{0.167}$. Chloride is positioned at the (0.0.11,0) site with about 2/3 of those sites occupied. This chloride is balanced by hydrogen ions in structure, (Figure 1.7).

Akaganeite is thought to be only able to form in the presence of high concentrations of chloride or fluoride at relatively low pH (<5). Bland et al (1997) and DeGrigny et al (1999) have both reported akaganeite with no apparent chloride present, most authors agree on its necessity for akaganeite for form. A minimum of 0.25-0.5mmol/mol chloride seems to be essential for its stability (Ellis et al, 1976). Akaganeite is the stable polymorph formed from solutions with a chloride to hydroxide ratio greater than 8.0 (Refait and Genin, 1997), this equates to chloride concentrations in excess of 2M. Laboratory syntheses are generally from Fe(II) or Fe(III)Cl solutions at 60-100ºC. There are at least 23 published synthetic routes to form akaganeite from iron (III) compounds (Al Zahrani, 1999 p49). It can also be formed by hydrolysis of FeOCl (Keller, 1948), direct precipitation from $FeCl_3$ and K_2CO_3 (Hofer, 1946), damp oxidation of Fe(II)Cl (MacKay, 1960) and dry aerial oxidation of ferrous hydroxychloride β-$Fe_2(OH)_3Cl$ (MacKay, 1960; MacKay, 1962; Keller, 1948). The presence of too much water leads to Goethite via green rust 1 (Misawa et al, 1969; Misawa et al, 1970).

On non marine, archaeological iron (which is generally dried on excavation) akaganeite is thought to form from Fe(II)Cl crystals present from the burial corrosion process (Turgoose, 1982a). Beta ferrous hydroxychloride has been reported on archaeological iron in 31 out of 65 samples (Reguer et al, 2005; Reguer et al, 2007; Saheb et al, 2008; Chitty et al, 2005). For the terrestrial iron it was present as less than 20µm layers in the dense product layers over 1mm thick.

Chloride appears to be adsorbed onto akaganeite crystal surfaces as well as present in the channels (Al Zahrani, 1999). The presence of adsorbed chloride has been verified with extended x-ray absorption fine structure analysis and X-ray absorption

spectroscopy and X-ray diffraction. (Reguer et al, 2006; Reguer et al, 2007). A wide range of chloride concentrations have been reported for akaganeite. This is probably related to the different formation mechanisms and degrees of washing after formation.

Chloride content as reported%	Author
0.87-7.67*	Weiser and Milligan, 1935
2-4*	MacKay, 1966
4.6*	Ishikawa and Inouye, 1972
9.5*	Kaneko and Inouye, 1974
7-17*	Ishikawa and Inouye, 1975
12*	Kaneko et al, 1975
3.5-6.9*	Johnston and Logan, 1979
1.8-7.6	Childs et al, 1980
2.28-6.4	Gilberg and Seeley, 1981; Keller, 1970
3.5*	Naono et al, 1982
4.44-8.00*	Chambaere and Grave, 1984
0.1-4.9	Buchwald and Clarke, 1989
4.39-4.62*	Al Zahrani, 1999
3.0-6.24	Wang et al, 2007a
0.3-5	Watkinson and Lewis, 2005
up to 17*	Watkinson and Lewis, 2005

* synthesized akaganeite

Table 1.1 Reported chloride contents of synthetic and corrosion product akaganeite.

Adsorbed chloride has been implicated in the lowering of the critical RH for Fe(II)Cl and iron powder mixtures from 19 to 12% (Watkinson and Lewis, 2005).

Akaganeite has been reported to transform into goethite and hematite. Neither of these materials has chloride in their structure and Goethite is reported to be only able to hold 0.5% of chloride on its surface (Turgoose, 1982a). Hence when akaganeite transforms to these materials, chloride is released that can cause further corrosion of any remaining iron core. Study of these transformation reactions on archaeological iron has been highlighted as a key research area (Selwyn et al,1999).

1.5 Research aims and objectives

This research is designed to determine how much risk there is to archaeological iron objects from the environment (in terms of relative humidity, ethanoic and methanoic acid concentrations, and methanal concentrations). Methods to provide a range of suitable environments for both the display and storage of archaeological iron artefacts will be assessed and best practice for preventive conservation, devised.

Its objectives are:

- to carry out analysis on objects to determine the deterioration mechanisms and their relative importance.
- to undertake laboratory experiments to understand the influence on those mechanisms of
    - relative humidity.
    - ethanoic and methanoic acid and methanal.
    - the synergistic effects of the above and relative humidity.
    - nitrogen dioxide and sulfur dioxide.
    - the amount of chloride present in the iron.

    - the presence of copper, humic acid, akaganeite and Goethite.

- to validate the laboratory experiment results with a survey of archaeological iron displayed under different environmental conditions.
- to investigate the transformation reactions of akaganeite and determine the long term risk they pose.
- to investigate the factors that determine showcase performance and devise best practise to design showcases to display archaeological iron artefacts.
- to investigate storage methods including:
    - accuracy of measuring RH to determine when to change silica gel.
    - the feasibility of modelling RH inside storage boxes to predict when silica gel will require changing in a certain space and devising replacement schedules.
    - deterioration of the boxes presently used and any reduction in performance.
    - survey of storage box types available and identification of the most suitable box to use for new storage .

Chapter 2 General Materials and Methods

This chapter describes the materials, both standards (purchased or synthesized to test the analytical methods), objects analysed, and the general methods used throughout the thesis. Where methods have been developed, this work is reported in Chapter 3. In order to assess the performance of the analytical techniques with iron corrosion products, a series of standard minerals were purchased or synthesized. The International Centre for Diffraction Data (ICCD) X ray diffraction database contains all the known corrosion products of iron. However, no single piece of work had been reported that includes Raman and infra-red spectra for the corrosion products possible on archaeological iron. Collections of spectra for both infra-red and Raman have been published since the work began, but were not available when required. The performance of the techniques for identification and quantification of the iron corrosion products and their mixtures was assessed and results are collated and reported in Chapter 3.

2.1 Materials

The corrosion products likely to be encountered on archaeological iron were identified from a review of the literature and the results of thirty years analysis of material at the British Museum. A variety of archaeological iron objects were examined and analysed from the collections of the British Museum and English Heritage. The objects spanned the Roman, Saxon and Medieval periods.

2.1.1 Standard materials

The reported corrosion products of archaeological iron are shown in Table 2.1.

Material	Mineral name	Reference to occurrence on archaeological iron
		Pearson, 1972
Alpha-FeOOH	Goethite	North and Pearson, 1975; Zucchi et al, 1977; Knight, 1982; Scharff and Huesmann, 1995; Gettens, 1961; Selwyn et al, 1999; Maeda et al, 1992; Fell and Ward, 1998
Beta-FeOOH	Akageneite	Zucchi et al, 1977; Lehmann and Nosek, 1978; Turgoose, 1982; Knight, 1982; Scharff and Huesmann, 1995; Gettens, 1961; Selwyn et al, 1999; Maeda et al, 1992
Gamma-FeOOH	Lepidocrite	Zucchi et al, 1977; Knight, 1982; Selwyn et al, 1999
Delta-FeOOH		North and Pearson, 1975; Lehmann and Nosek, 1978
Amorphous $FeO_x(OH)_{3-2x}$		Selwyn et al, 1999
$FeO(OH).nH_2O$, n variable	Limonite	North, 1976; North and Pearson, 1975
Fe_3O_4	Magnetite	North, 1976; Zucchi et al, 1977; Pearson, 1972; Yunlan et al, 1994; Gettens, 1961; Selwyn et al, 1999; Maeda et al, 1992
Alpha-Fe_2O_3	Hematite	Yunlan et al, 1994; Selwyn et al, 1999; Maeda et al, 1992
Gamma-Fe_2O_3	Maghemite	Scharff and Huesmann, 1995
Residual Fe		Watkinson, 1983
FeO		Yunlan et al, 1994
$FeCl_2$	Lawrencite	Lehmann and Nosek, 1978; Knight, 1982
$FeCl_3$	Molysite	Lehmann and Nosek, 1978
FeOCl		North, 1976; North and Pearson, 1975; Lehmann and Nosek, 1978; Nosek, 1978

$Fe_3(PO_4)_2.8H_2O$	Vivianite	Farrer et al, 1953; Gettens, 1961; Fell and Ward, 1998
$FePO_4.2H_2O$	Strengite	Farrer et al, 1953
Fe_3S_4	Greigite	Fell and Ward, 1998
$Fe_{1.01\text{-}1.08}S$	Mackinawite	Fell and Ward, 1998
FeS_2	Pyrite	Fell and Ward, 1998
$Fe_{0.8\text{-}1}S$	Pyrrhotite	North, 1976; Pearson, 1972; Gettens, 1961
$FeCO_3$	Siderite	North, 1976; Gettens, 1961; Fell and Ward, 1998
$FeSO_4.4H_2O$	Rozenite	Scharff and Huesmann, 1995; Fell and Ward, 1998
$NaFe_3(OH)_6(SO_4)_2$	Jarosite	Scharff and Huesmann, 1995
Beta-$Fe_2(OH)_3Cl$		Bellot-Gurlet et al, 2009; Neff et al 2005; Reguer et al, 2005; Reguer et al 2006; Reguer et al, 2007; Saheb et al, 2008
Chloride Green Rust I $[Fe^{(II)}_3Fe^{(III)}(OH)_8][Cl.nH_2O]$		Unstable intermediates, as yet unreported on archaeological iron
Carbonate Green Rust I $[Fe^{(II)}_4Fe^{(III)}_2(OH)_{12}][CO_3.2H_2O]$		
Carbonate Green Rust I $[Fe^{(II)}_2Fe^{(III)}_2(OH)_{12}][CO_3.2H_2O]$		
Green rust II $4Fe(OH)_2.FeSO_4.nH_2O$		

Table 2.1 Corrosion products reported on archaeological iron.

Mineral and powder chemical samples were purchased commercially, where possible, to act as standard materials and are shown in Table 2.2. The short term

intermediates, green rust I and II, ferroxyhydrate and beta iron hydroxychloride were not considered due to the low probability of their survival in the long term experiments undertaken for this thesis. The mineral FeOCl occurs mainly in marine iron and there is some uncertainty in the identifications published with suggested misinterpretation of x-ray diffraction data (Gilberg and Seeley, 1981). The literature was examined to determine characteristic features in the analytical techniques employed, to ensure they would be recognized if present.

Each mineral was analysed with Fourier transform infra-red spectroscopy, (FTIR), X-ray diffraction, (XRD) and scanning electron microscopy with energy dispersive analysis of x-rays, (SEM-EDX). The FTIR spectra and XRD were compared to published standards to confirm the minerals identity. The purity was calculated from the iron concentration (measured by SEM-EDX). Results are shown in Table 2.2, impurities present are shown in brackets..

Material	Mineral name	Supplier	Stated Purity (%)	Impurity analysis unexpected elements in brackets		
				SEM-	XRD	FTIR
α –FeOOH	Goethite		99	99.5	Goethite	
β –FeOOH	Akageneite	RT Min	-		Goethite	
β –FeOOH	Akageneite	RT Min	-		Goethite	
β –FeOOH	Akageneite	Synthesised	-	[Cl]=5.7	Akaganeite	
β –FeOOH	Akageneite	Corrosion	-	[Cl]=9.8	Akaganeite	
γ-FeOOH	Lepidocrit	Alfa	99	99.6	Lepidocrit	
Fe_3O_4	Magnetite	Ald	99.5	99.4(Si)	Magnetite	silicate
Fe_3O_4	Magnetite	Alfa	99.999			
α -Fe_2O_3	Hematite	Ald	99.998			
γ-Fe_2O_3	Maghemite	Alfa	99.9	99.9	Maghemite	
$FeCl_2.2H_2O$	Lawrencite	Alfa	99.99	100	Lawrencite	
$FeCl_3$	Molysite	Alfa	99.8	99.8	Molysite	
$FePO_4.2H_2O$	Strengite	Ald	97.17	98.9	Strengite	
FeS_2	Pyrite	RT Min	-	99.5	Pyrite	
$Fe_{0.8-1}S$	Pyrrhotite	Alfa	99.9	99.9	Pyrrhotite	
$FeCO_3$	Siderite	RT Min	-	99.8	Siderite	
$FeCO_3$	Siderite	RT Min	-	96.3(Si),	Siderite	silicate
$FeCO_3$	Siderite	RT Min	-	98.4 (Ca)	Siderite	calcite
$FeSO_4.4H_2O$	Rozenite	Ald	99	99.3	Rozenite	

Alfa Alfa Aesar

RT Min Richard Taylor Minerals Ltd

Ald Aldrich

- no purity stated, mineral samples

Table 2.2 Standard minerals and their analyses.

2.1.1.1 Synthesis of akaganeite

None of the commercial mineralogical samples of akaganeite actually had any akaganeite present. These mineral samples were from meteorites on which akaganeite had been analysed. Akaganeite was synthesized from 500ml of 0.3M $FeCl_3$, heated at 70ºC in a sealed glass flask for 48 hours. The solution was heated in a oven with magnetic stirring. The precipitate was collected on a 0.45µm PTFE filter and then washed six times in a centrifuge, with fresh 18.2MΩ water each time and then air dried (Cornell and Schwertmann, 1996). Four batches of akaganeite were produced for the experiments in this work which took place over a 10 year period.

2.1.2 Archaeological objects analysed

Roman, Saxon and Medieval archaeological objects were examined for a number of purposes;

to determine the cause of deterioration of objects from museum environments.

to determine the environment and presence of foreign species around the deterioration centres in those objects.

a series of objects from two excavations were monitored over a period of five years after post excavation conservation, when they were deposited as an archaeological archive.

a large number of objects subjected to different environments, were surveyed and any deterioration analysed.

two objects were analysed immediately after excavation to determine the species present.

2.1.2.1 Deteriorating objects

Deteriorating objects from both display and storage contexts were examined. Objects from the sites listed in Table 2.3 were investigated. These were objects that had shown obvious visual deterioration in a few years. The number of objects and their contexts are also shown in Table 3. Many of the objects were displayed for the first

time. In these instances they were recently removed from dry silica gel storage, had good quality condition photography and had undergone conservation assessments that would have highlighted any existing active deterioration. Hence the deterioration observed could safely be assigned to the period on display, which is also included in Table 2.3.

Site	Context	Date analysed	Dates of excavations#	Number of objects analysed	Years on display
Sutton Hoo	display and storage	2002 2001 2003	1939 1970s 2000	5 9 2	50 35 3
Wetwang	display and storage	2003	2000	5	9
Stonea	storage	2002	1980-1984	14	-
Uley	storage	2001	1977-1979	18	-
Buckland	storage	2001	1951-1953	12	-
Kirkburn	display	2001	1987	7	-
Ashby Winkworth	storage	2002	1974	6	-
River Thames	storage	2001	1973	3	-
Portchester Castle	display	2003-4	1961-1979	14	6
Pevensey	display	2007	1906-1908	5	5
Lullingstone Roman Villa	Storage	2007	1949-1961	34	-

St Augustines Abbey	display	2006	1983-1993	5	9
Hailles Abbey	display	2009	1906-1909	8	30
Scarborough Castle	display	2006	1888, 1970s	4	4
Whitby Abbey	display	2007	1923-1925, 1958 1993-2001	21	7
Chesters Roman Fort	display	2005-7	1843, 1880s, 1967	42	85
Corbridge Roman Fort	display	2004-5	1906, 1947, 1952-1953, 1980	18	20
Helmsley Castle	display	2004	1957, 1985, 1994	15	6
Castle Acre Priory	display	2005	1972-1976	8	4
Peverill Castle	display	2007	1936	4	5
Carisbroke Castle	display	2010	1976-1981	7	10

dates of excavations from which artefacts were examined, many sites had several other excavations.

Table 2.3 Objects examined, excavation details and length of time on display.

2.1.2.2 Recently excavated objects

Recently excavated objects from two sites were studied in more detail to determine any early signs of deterioration and define the corrosion environment. Soil samples were collected from the excavations.

The Sutton Hoo ship burial is thought to date from the 7th century AD. Recent work developing a visitor centre on the Tramner House area, to the north of the burial mounds, was preceded by a rescue excavation. This revealed several graves, thought to date somewhat earlier than the famous ship burial (the earliest between approximately 525 and 550 AD). After excavation in the summer of 2000, the iron finds from these graves were stored in polypropylene boxes (Stewart type) with dried silica gel incorporated to keep the RH low. The material was accessioned into the British Museum in July 2000. Of the 125 iron objects, twelve representative of the type, size and degree of corrosion of the set were chosen for in depth examination. Soil was retrieved from the Sutton Hoo Tranmer House site to a depth of 2m using a spade. A solid section of soil was retrieved and stored in a polyethene bag sealed with an airtight plastic clip (Mitsubishi Chemical Ageless RP system).

Wetwang forms part of a series of East Yorkshire burials from the 3rd century BC to the 1st century AD. It is one of the very small number of chariot burials found in the UK. Initially dated to the 1st century BC, because of the lack of similarity with other chariot burials (the date range of which spans the 1st century BC to the 1st AD), the discovery after radiography of an inverted brooch in an iron corrosion block pushed the date back to late 1st century AD. This illustrates the vital importance of iron in the archaeological record. The major iron artefacts were the chariot wheels and associated fittings, a total number of 18 artefacts containing iron. A much larger proportion, 8 of these objects were studied. It was not possible to retrieve soil samples from the Wetwang excavation site. However, several of the objects were excavated with significant soil deposits present. These were mechanically removed. Small samples of soil were also removed from the objects during the examination. Two stratigraphic soil samples were removed from one of the wheels excavated. One sample was taken from directly next to the dense product layer, whilst a second was taken at the outer edge of the soil concretion lifted with the wheel, a distance of 10cm above that layer.

Any changes in the objects from these two excavations were observed over a period of five years. Whilst many of the objects remained in dry storage, the wheel fragments were too large for this method and were stored in open wooden drawers in a room at ambient conditions. Several objects were displayed in showcases over this period.

2.1.2.3 General survey of iron on display at English Heritage sites

The different room conditions, showcase air exchange rates and silica gel loadings generate different RH conditions inside showcases at different sites. The different construction materials of showcases generate different concentrations of ethanoic and methanoic acid and methanal inside the cases. In order to verify the environmental thresholds (RH and carboxylic acids and aldehydes) derived from experiments in chapter 5, a large survey was carried out of archaeological iron objects on display under different conditions. The sites surveyed are shown below.

Site	Number of objects	Silica gel	Wood products present in showcases	Years on display when examined
Battle Abbey	22	Y	Y	7
Byland Abbey	3	Y	N	3
Carisbroke Castle	35	Y	Y	5
Castle Acre Priory	7	Y	Y	3
Chesters Roman Fort	309	N	Y	10
Corbridge Roman Fort	64	N	Y	10
Hailles Abbey	8	N	Y	25
Helmsley Castle	24	Y	Y	5
Jewel Tower	1	N	Y	10
Launceston Castle	15	N	Y	7
Lullingstone	54	Y	N	2

Roman Villa				
Pevensey	22	Y	N	4
Peverill Castle	8	N	Y	3
Portchester Castle	44	Y	N	3
Revieux Abbey	8	N	Y	7
Scarborough Castle	21	N	Y	4
St Augustines Abbey	45	Y	Y	8
St Peters Church	3	Y	N	3

Table 2.4 Objects surveyed.

Each object was examined visually with a good quality LED torch. The degree of surface corrosion, flaking and cracking was assessed using a criteria anchored methodology (Suensen-Taylor et al, 1999). Details are given below;

Degree	Surface corrosion	Cracking	Flaking
None			
Some	1 or 2 spots, <1% coverage	1 or 2 cracks, <1mm total length	1 or 2 flakes, <1% coverage
Medium	3 to 10 spots, <5% coverage	1 or 2 cracks , <5mm total length	3 to 10 flakes, <5% coverage
Heavy	>10 spots, >5% coverage	Multiple cracks, >5mm total length	>10 flakes, >5% coverage

Table 2.5 Criteria for object assessment.

Each object was assessed for surface corrosion, cracking and flaking and given a degree score for each damage type. The worst degree of damage in those categories was used for the overall object score.

2.2 Methods

A wider variety of analyses than those described in 2.1.2 were required to achieve the aims of the work:

- analyses of the causes of deterioration of archaeological iron to determine the species involved and how frequently each causes deterioration. Is akaganeite predominantly associated with deterioration? Is it solely associated with deterioration?
- analyses of the species present at and in close proximity to the deterioration centres to determine the composition of experiments and assess the effects of each.
- analyses of the amount of akaganeite formed in exposure experiments to a variety of environments. These analyses need to be undertaken in the presence of other species.
- characterisation of the mineralogy of complete archaeological objects to monitor any changes over a number of years. In situ, non invasive analyses are required as these are accessioned museum objects and will require multiple analyses, ideally at the same point to determine any changes.
- analyses of the pollutant gases; methanoic acid, ethanoic acid, sulfur dioxide, nitrogen dioxide, ozone, and hydrogen chloride.
- analyses of the dust deposition and the dust's chloride concentration.
- analyses of the deterioration of polyethylene and polypropylene boxes used to store archaeological iron.

A variety of analytical methods and sampling techniques have been used to accomplish this. Most analyses required multiple techniques. Archaeological iron is

a complex material with many corrosion products, soil components and conservation materials potentially present. Many of the corrosion phenomena occur on a microscopic scale and several materials are often in close proximity. The techniques used, and their suitability for these applications are described below. The exact application and any sample preparation are described in the relevant chapters.

2.2.1 Fourier Transform Infra Red (FTIR)

Fourier transform infra red spectroscopy detects transitions between molecular vibrational modes. A particular chemical bond gives rise to an absorption at a particular frequency (Kellner et al, 1998). The selection rule is that transitions are active if they result in a change in dipole moment. FTIR is therefore most sensitive to polar bonding and suitable for identifying the ionic compounds of interest in this thesis.

Fourier transform infra red spectroscopy uses an interferometer to generate a interferogram. Many instruments, including the three used, utilize Michelson interferometers. A schematic is shown in Figure 2.1.

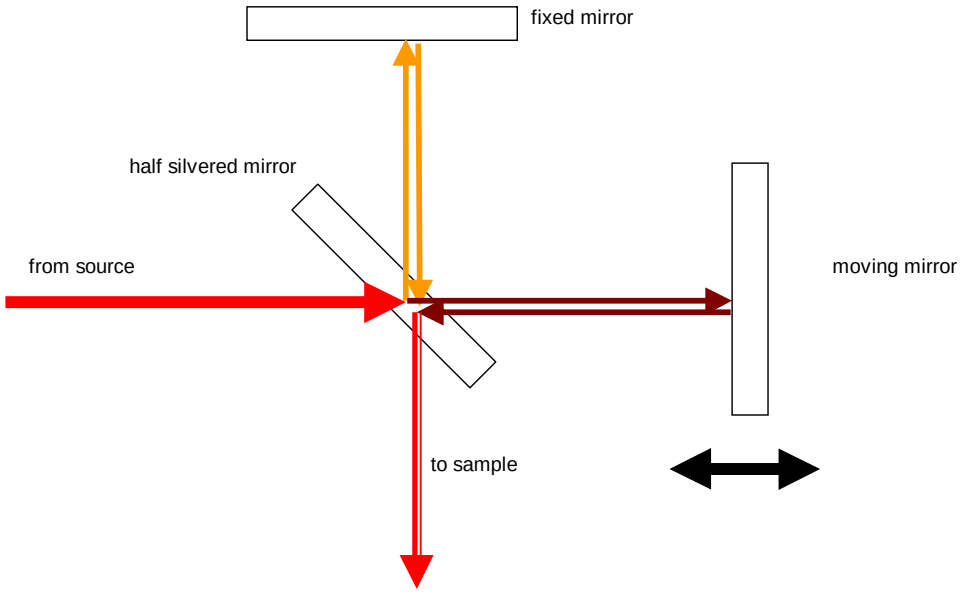

Figure 2.1 Michelson interferometer.

A Michelson interferometer consists of a half silvered mirror that splits the infra-red beam from the instrument source into two perpendicular beams. One beam reflects from a fixed mirror, the other from a moving mirror. The two beams are combined at the half silvered mirror and then pass through the sample to the detector. As the moving mirror sweeps out full or half wavelengths of particular infra red wavelengths, constructive and destructive interference occurs.

2.2.1.1 Potassium bromide disc (KBr)

For transmission spectroscopy the sample has to be suspended in the infrared beam. Potassium bromide disks are the most common method for this. They require about 3mg of sample, depending on how strongly the material absorbs. The sample is intimately mixed with potassium bromide, limiting its use for further analysis. Potassium bromide can also ion exchange with ionic solids. However, this method is generally unaffected by spectral artefacts and produces high quality spectra and has been used for quantification.

2.2.1.2 Diamond cell and beam condenser (DC)

It is essential to minimise sample size in all cultural heritage applications. Additionally, many of the corrosion products encountered only occur in small amounts, less than is required for a potassium bromide disc. A diamond cell with beam condenser can reduce the sample size required by a factor of twenty. The technique is non destructive, although the sample is flattened. The sample can be readily removed from the diamond cell after analysis for further analyses.

The “Diasqueeze” diamond cell used consists of two matched, type IIA diamond plates. Each plate is mounted into a circular metal frame. The sample is placed between the two plates, which fit into a holder, with three small guide pins to keep the diamond plates parallel. A rubber “O” ring fits between the plates to regulate the pressure. The top piece of the holder is screwed down using finger pressure to compress the sample between the diamond plates to form a thin film. The diamond cell is placed in the beam condenser and the x-y-z stage aligned to achieve maximum energy throughput.

The diamond plates absorb strongly in the IR region. Fortunately the major absorption bands occur between 1750 and 2500 cm^{-1}, where there are likely to be very few absorptions of interest when dealing with a sample, although this does slightly overlap into the region for carbonyl stretching absorption bands. The background spectrum of the diamond plates and of atmospheric carbon dioxide and water is first recorded and is then automatically subtracted from any subsequent spectra. This process is not perfect, as the path of the IR beam through the diamond plates changes slightly as the plates are moved apart by the sample, especially hard mineral samples. The choice of beam-condenser for use with a diamond cell is a compromise. A high factor condenser produces finer focus and higher energy density through the sample and therefore allows a smaller sample size. However, it also increases the path-length through the diamond plates, losing more of the energy in the process. A three times beam-condenser is reported to be the ideal for this application. Since this piece of equipment is not commercially available, a four times beam-condenser was used.

2.2.1.3 Attenuated total reflectance (ATR)

When a beam of radiation impinges on medium interface of lower refractive index, if the incident angle is greater than the critical angle, then the beam is fully reflected. The critical angle depends on the refractive indices of the medium the beam is travelling in and the medium beyond the interface. The field intensity in the lower refractive index medium is non zero. There is an instantaneous normal component of energy flow into this medium, the time average of which is zero. Thus, there is no loss of energy and the radiation is totally internally reflected. An evanescent wave penetrates the lower refractive index material perpendicular to the interface. The term evanescent is derived from the latin root evanescere ‘to tend to vanish or pass away like vapour’. The intensity of the field decreases with increasing distance into the rarer medium (Drude, 1902; Harrick and du Pre 1966).

$$E = E_o \exp(-2\pi/\lambda(\sin^2\Theta - n_{21}^2)^{1/2} z) \qquad (2.1)$$

Where

E is the field strength at depth z

Eo is the field strength at the surface of the crystal, z=0

λ is the wavelength of the radiation in the ATR crystal = λ/n_1

θ is the incident angle of the beam

n_{21} is the ratio of the refractive indices of the sample material and the ATR crystal = n_2/n_1

z is the depth from the crystal surface

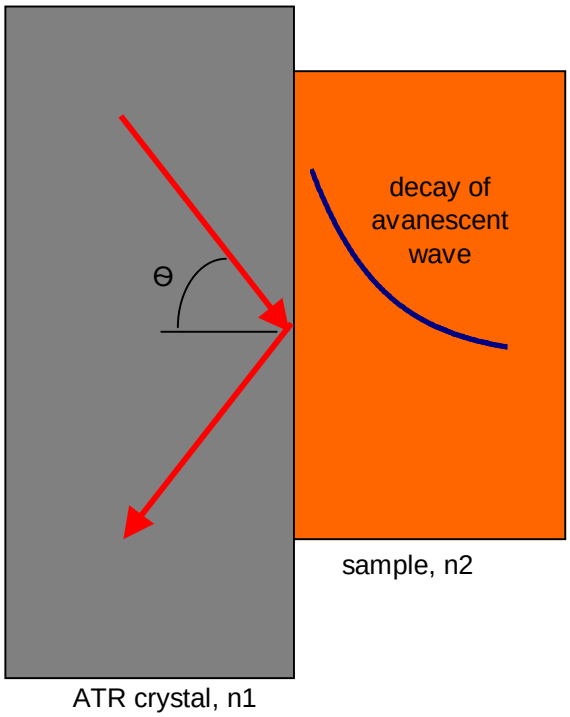

Figure 2.2 Schematic of a single bounce ATR accessory showing the radiation path and evanescent field strength.

Harrick and du Pre (1966) proposed a parameter known as penetration depth, d_p, defined as the depth at which the field strength drops to $E_o\exp(1)$, i.e. the depth into the lower refractive index medium where the amplitude is 37% of its original value. At 3 times d_p the field strength is 5% of it's original value and this figure can be used as an approximation of the information depth, as spectral information from closer to the surface will dominate. This has been validated by Lu et al for cadmium fluoride crystals (1998).

$$d_p = \lambda/(2\pi(\sin^2\theta - n_{21}^2)^{1/2}) \quad (2.2)$$

Where

d_p is the approximate information depth (90% of the information comes from this depth)

λ is the wavelength of the radiation in the ATR crystal = λ/n_1

n_1 is the refractive index of the ATR crystal

θ is the incident angle of the beam

n_{21} is the ratio of the refractive indices of the sample material and the ATR crystal = n_2/n_1

The SensIR Durascope uses a diamond ATR plate on a zinc selenide waveguide. This gives a 1.8mm diameter sampling area. The sample can be viewed through the crystal to confirm placement and optical contact. A metal arm with pressure sensor allows precise repeatable pressure to be applied to the sample. The Thermo Nicolet Smart Orbit ATR has a diamond plate with KRS5 (thallium bromide, thallium iodide) wave-guide. The sample cannot be viewed with this system.

Advantages of the ATR technique are the lack of sample preparation, high degree of control of pressure, and controlled sample path. The technique is non destructive and the sample can be retrieved for further analysis. The working range depends on the crystal selected. Zinc selenide and Germanium absorb lower energy infra-red radiation and limit the practical working range to 650 – 4000cm^{-1}. A KrS 5 wave-guide has a working range of 200-4000cm^{-1}, limited to 400-4000cm^{-1} by the KBr beamsplitter used in the spectrometer. The diamond has strong absorptions, but these are generally removed by background subtraction and away from the regions of interest. Hard samples require high pressures to ensure optical contact. These can deform the crystals and alter the wave-path slightly, meaning the background compensation is not perfect.

The standard minerals gave good quality spectra by ATR. The wavelength dependence on the information depth is clear, with the lower wavenumber bands having higher intensities.

Qualitative ATR spectroscopy was undertaken on Perkin-Elmer 2000 with Globar source and TGS detector and a SensIR technologies Durascope. Spectra were collected with 32 scans, between 650 and 4000 cm^{-1} resolution of 4cm^{-1} and strong Norton-Beer apodisation. The Durascope has a diamond ATR and the optics focus the beam on a 1mm diameter circle. A Nicolet Avatar 380 with Smart Orbit ATR was used identification and quantification of degradation and crystallinity of the plastic storage boxes in Chapter 8. The source and detector were of the same type and spectra were collected for 32 scans between 400 and 4000cm^{-1} resolution of 4cm^{-1} and Happ-Genzel apodisation.

There are a number of issues with using ATR for quantification.

the wavelength dependence of penetration depth gives greater absorption on the longer wavelength side of an absorption band, contributing to band distortion.

non absorbing, optically transparent materials show a continuous decrease in refractive index with increasing wavelength. Materials that can absorb energy show an increase in refractive index at longer wavelengths in the region of the absorption, anomalous dispersion. This effect is well known in transmission spectroscopy, but typically small and often ignored. In ATR this effect can change the critical angle and penetration depth. The resultant spectrum is neither a true measure of the absorption index or the refractive index, but a complex function of both.

ATR-FTIR has been used for quantification of the degree of crystallinity of polypropylene in this thesis. The quantification was based on the peak ratios of three absorptions at 973, 942 and 900cm^{-1} (Yakimets et al, 2004). Independent measurements with differential scanning calorimetry were used to confirm the results.

2.2.1.4 Infrared microscopy

Infrared spectroscopy is a powerful analytical technique, capable of distinguishing the vast majority of the corrosion products of iron under ideal conditions. However, the requirement for sample removal for most methods to collect spectra, and the complexity of spectra from mixtures, limit its utility. An inspection type infrared microscope manufactured by Nicolet has been found to be able to acquire identifiable spectra from many types of solid surfaces, without taking a sample. Details are provided in Chapter 3.

2.2.1.5 Diffuse reflectance (DRIFTs)

When radiation impinges on a surface it can be reflected in two basic ways. If the angle of incidence equals the angle of reflection this is specular reflection. All other angles are diffuse reflection. For powders and rough surfaces diffuse reflection tends to dominate. In Diffuse Reflection in Infrared Fourier Transform Spectroscopy, DRIFTS, the diffusely reflected infrared radiation from a surface is collected using parabolic or elliptical mirrors onto the infrared detector (Coblentz, 1905; Derrick et al, 1995). The interaction of diffuse and specular components can lead to derivative peak shapes. In DRIFTS these are avoided by blocking the specular reflection or designing the mirrors so no specular component is transmitted to the detector.

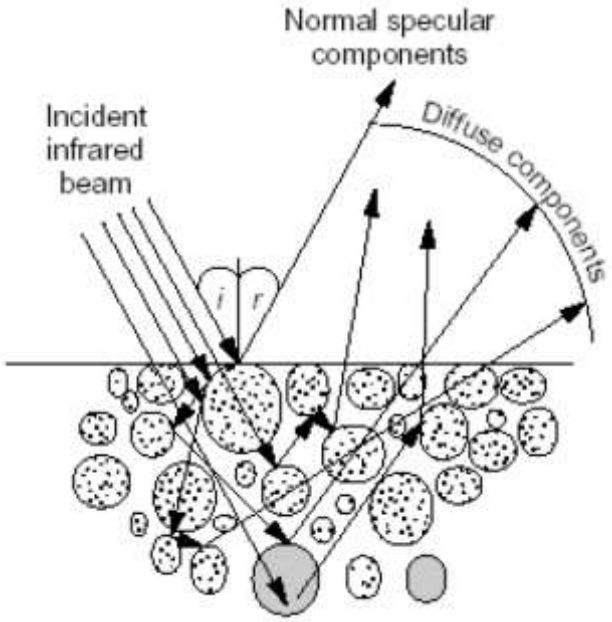

Figure 2.3 Beam paths of infrared radiation during diffuse and specular reflection (from Amaroli et al, 2004).

In the early stages of the project the requirement to detect small amounts of lead carbonate coatings on basic lead carbonate powder arose. DRIFTS is reported to be very sensitive to surface layers (Bak and Kindl, 1997; Bak, 2002). The technique is also easy to perform with powders. Attenuated total reflectance FTIR was not yet available. Although the ATR would have very good surface sensitivity, the high pressure applied can deform powders. In this process the underlying powder can push through the surface into contact with the ATR plate and reduce the surface sensitivity.

2.2.2 Raman

Raman spectra are obtained by inelastic scattering of light at molecules. The effect was first observed in 1923 (Raman and Krishnan, 1928; Smekal, 1923). The selection rule is for there to be a change in polarisability ellipsoid for a vibration to be Raman active. For any molecule with a centre of symmetry, the symmetric vibrations are Raman active and IR inactive and the antisymmetric vibrations are Raman inactive and IR active. The two techniques give complementary information. When laser light impinges on a sample, about 10^{-8} parts of the incident light are scattered elastically (Rayleigh lines), and only about 10^{-10} parts lead to excitations of

rotation and vibration levels of the ground electronic state. This causes an energy loss of the incident radiation and a shift to longer wavelengths. The effect is very weak and instrumentation relies on lasers and very good notch filters.

A typical Raman instrument has one or more lasers which can be focused onto the sample. The laser power is often filterable to reduce heating effects. The reflected light is passed through a notch filter to remove the Rayleigh lines at the same wavelength as the laser. The lower wavenumber limit of the instrument is limited by the notch filter, 70 cm^{-1} is achievable. The inelastically scattered radiation is focused onto a CCD. Focusing is achieved with a microscope, and if a confocal arrangement is used (a very fine hole at the focal point of the microscope), then mainly radiation emitted from a defined volume is collected. High magnification lenses can achieve small analytical volumes. Iron corrosion products absorb strongly and scatter weakly and hence are difficult samples for Raman spectroscopy. The utility of Raman micro-spectroscopy was investigated because it is able to identify very small sample volumes in mixed corrosion situations Low wavenumber information is also available, which is particularly useful for oxides and halides. This is reported in Chapter 3.

2.2.3 Powder X-Ray Diffraction (XRD)

When monochromatic X-rays interact with a crystalline solid, geometric considerations lead to Bragg's Law. Constructive interference will only occur when the following condition is met.

$$n\lambda = 2d\sin\theta \qquad (2.3)$$

where n is the order of diffraction (an integer),

λ is the wavelength of the X-ray,

d is the interplane spacing and

θ is the angle of incidence of the X-ray.

Instruments consist of a X-ray tube, metal foil target, slits to collimate the X-ray beam and a detector. The beam and detector geometry is varied to sweep through a range of θ. Iron minerals fluoresce strongly which produces a strong background signal and tends to reduce the sensitivity of XRD. This can be improved by using specific wavelength radiation, (Co K_α X-ray tube reduces the effect) or by altering the settings on a linear detector, so called pulse height discrimination. If the lower discrimination level is lowered (the linear detecter can detect 11º of 2θ angle and normally a window from approximately 6-10º of 2θ angle is collected to reduce the effect of charge sharing and produce a cleaner diffractogram. If the lower angle collected is reduced and the overall window size increased (4-10º of 2θ angle), then the peak intensity reduces, but the background fluorescence intensity reduces more. Hence the peak to background ratio is improved. XRD can only detect crystalline materials with crystallites above a certain size and a number of materials of interest are amorphous or microcrystalline. The sample size required is relatively large, in the order of a few mg. Detection limits in mixtures can be relatively poor, between 5 and 10%, depending on the materials and peaks used.

Two instruments were used. A Phillips 1830/1840 diffractometer with Co tube operating at 40V and 40mA. A Bruker D8 advance with Cu tube operating at 40V and 40mA and a Lynxeye linear detector time with pulse height discrimination set to suppress fluorescence (discriminator lower level 0.19, discriminator window width 0.08). All diffractograms were collected with 2θ angles from 5 to 70°. Samples were ground with industrial methylated spirit and dispersed on amorphous silica plates for analysis. Phase identification used the International Centre for Diffraction Data, (ICDD) 2 database. No evidence of preferential orientation was observed as the diffractograms matched the intensity ratio of the ICDD standard patterns. All crystalline iron corrosion products can by distinguished by XRD if three diffraction lines are present, with the possible exception of magnetite and maghemite. These minerals have almost identical crystal parameters, both cubic lattices with dimensions of 0.8396 nm for magnetite and 0.835nm for maghemite. The XRD of magnetite shows all the diffractions of maghemite and can only be distinguished if the additional weak lines are present.

The detections limits of Goethite in the presence of akaganeite were determined. Mixtures were made by thoroughly grinding together mineral powders of akaganeite

and Goethite. On both instruments strong diffractograms were obtained for the pure materials. The 10% akaganeite mixture in Goethite could not be detected, whilst the 20% mixture yielded diffraction lines for akaganeite.

2.2.4 Scanning Electron Microscopy – Energy Dispersive Analysis of X-Rays (SEM-EDX)

SEM-EDX combines imaging of a sample with elemental analysis and is useful to complement the characterization of materials. As many sample sizes are very small, the high magnification was extremely useful. SEM-EDX uses a focused electron beam to generate secondary and back scattered electrons and X-rays from the point of interest. The X-rays were detected with a Germanium detector with super thin window. The detector is cooled with liquid nitrogen so all the electrons remain in the valence band and no current flows when a voltage is applied across the crystal. When an X-ray enters the crystal, its energy is absorbed. This results in the formation of an electron-hole pair and the crystal becomes conducting and the electrons are swept to the rear contact because of the applied voltage. Each X-ray generates a voltage pulse. An electronic circuit measured the height of the pulses which are proportional to the X-ray energies.

All samples were prepared as polished sections. The samples were then analysed in a Joel 840 SEM (10mm height, 25keV accelerating voltage and 1nA beam current) with Oxford Instruments germanium detector with ISIS software. The instrument was calibrated with certified reference x-ray microprobe standards supplied by Micro-Analysis Consultants Ltd (Registered standard number 1158 minerals). As the standards did not have any iron or copper and chloride containing minerals the calibration was checked with high purity samples of Goethite, lepidocrite, ferrous chloride and ferric chloride, copper oxide and copper chloride.

Quantification of chloride (detected as chlorine) was of particular interest. Rimmer (2010 p112) quotes a ‘detection limit for chlorine of c. 0.2%, and the relative precision is 10% in the concentration range 5-20%, deteriorating as the detection limit is approached’ for the same model SEM-EDX. A comparable performance would be expected from the system used (Freestone, 2010; Dungworth, 2005). Koshy et al (1992) compared SEM-EDX with spectrophotometric methods and

found the results agreed well in the range 0.11 to 0.78% (wt/wt). Precautions were taken to avoid chloride contamination of samples. All preparation equipment was washed five times in 18.2MΩ water before use and checked by swabbing and ion chromatography analysis. A low chloride epoxy was used for embedding (Struers EpoThin). A low chloride oil based lubricant (Buehler ISOCUT) was used for any cutting or polishing to avoid chloride migration from water.

2.2.5 Thermo-gravimetric Analysis (TGA)

Thermo-gravimetry is a technique in which the mass of the sample is monitored against temperature while the temperature of the sample, in a specified atmosphere, is programmed (ICTAC, 1991). The balance is an opto-electronic one. Current is applied to an electromagnet to drive the balance bar controlled by a photocell which is occluded when the bar is horizontal. The system keeps the balance bar horizontal and the current flowing is a measure of the mass. This system gives a sensitivity of 1μg. The experimental factors that determine the results and accuracy are the sample packing and particle size, gas type and flow rate, crucible material and geometry (open, open or sealed, hole size in the lid sealing).

The standard minerals were all measured to confirm the literature assignments. The results of TGA depend on the exact experimental conditions used. Hence it was necessary to measure the standard minerals to determine the results from the TGA7 under these experimental conditions. Thermo-gravimetry was undertaken on a Perkin Elmer TGA7 with an open platinum crucible. The sample size was approximately 3mg and all samples were ground in a pestle and mortar. The furnace was flushed with 60ml/min of zero grade nitrogen. The furnace was calibrated for temperature using the induced magnetization weight losses at the Curie points of Alumel (163ºC), Nicoseal (354ºC) and iron (780ºC). The balance system was calibrated with a 100mg reference mass. The heating rate was 10°C/min. The transitions reported in the literature are included in Table 2.6.

Temperature range of Transition (ºC)	Weight Loss (%)	Reactant	Product	Reference	Technique
Goethite α-FeOOH					
190-380*	10.10*	Goethite	Hematite	MacKenzie, 1970	DTA*
258-320	10.34-11.29	Goethite		Schwertmann et al, 1985	DTA,TGA
Akaganeite β-FeOOH					
270-320		Akaganeite	Maghemite	Gonzalez-Calbet and Alario Franco, 1982	TGA, XRD, ED, HREM
340-367	-	Maghemite	Hematite		
250-300		Akaganeite	Maghemite	Paterson et al, 1982	DTA
400-450	-	Maghemite	Hematite		
125-300		Akaganeite	Maghemite	MacKenzie,1970	DTA
	-	Maghemite			
Lepidocrite γ-FeOOH					
220-270		Lepidocrite	Maghemite	Dinesen et al, 2001	
435-510	-	Maghemite	Hematite		
270		Lepidocrite	Maghemite	Schwertmann and Wolska, 1990	
500	-	Maghemite	Hematite	Wolska et al, 1992	
300-350	10.10*	Lepidocrite	Maghemite	MacKenzie, 1970	DTA*
400-500	-	Maghemite	Hematite		
Feroxyhyte, δ-FeOOH					
150-230		Feroxyhyte	NS	Cornell and Schwertmann, 1986 p490	DTA

100-320		Feroxyhyte	Hematite	MacKenzie, 1970	DTA
Ferrihydrate $Fe_5HO_8.4H_2O$					
150-230		Ferrihydrate	NS	Carlson and Schwertmann, 1981	DTA
280-320		NS	Hematite		
Magnetite, Fe_3O_4					
350-400		Magnetite	Maghemite	MacKenzie, 1970	DTA
650-800		Maghemite	Hematite		
Maghemite γ-Fe_2O_3					
397-597*		Maghemite	Hematite	Karmazsin et al, 1983	XRD, dilatometry, TM
275-800		Maghemite	Hematite	Bozorth, 1951	
Siderite					
400-550		Siderite	Magnetite*	Gallagher and Warne, 1981	TGA, TM, EGA, XRD
Pyrites					
440-667		Pyrites	Pyrrhotite	Hu et al, 2003	TGA, XRD

NS not specified

XRD X-ray diffraction

ED electron diffraction

HREM high resolution electron microscopy

EGA evolved gas analysis

* in DTA at this date the weight loss would have been calculated by weighing the sample before and then after analysis

Hematite has no reported thermal transitions below 1000ºC

Table 2.6 Thermal transitions reported in literature.

Compound	Measured onset temperature (°C)	Measured endset temperature (°C)	Weight loss (%)	Process
Goethite α-FeOOH	267	309	9.1	Dehydroxylation
Akaganeite β-FeOOH synthetic first preparation	253	451	9.8	Dehydroxylation
Akaganeite β-FeOOH synthetic second preparation	223	432	10.0	Dehydroxylation
Akaganeite β-FeOOH synthetic third preparation	261	473	9.9	Dehydroxylation
Akaganeite β-FeOOH synthetic fourth preparation			not determined	Dehydroxylation
Akaganeite β-FeOOH corrosion	236	443	10.4	Dehydroxylation
Lepidocrite γ-FeOOH	210	265	11.1	Dehydroxylation
Maghemite γ-Fe_2O_3	steady increase from 328°C		~ 4%	Oxidation
Strengite $FePO_4.2H_2O$	133	177	13.0	Dehydration
Pyrites FeS	461	515	3.1	
	957	974	1.8	
Rozenite $FeSO_4.4H_2O$	106	138	27.0	Dehydration
	461	515	3.1	
	957	974	1.8	
Siderite $FeCO_3$	458	507	29.6	

Table 2.7 TGA table corrosion products.

Thermogravimetry is a quantitative technique and was used to confirm FTIR or XRD quantifications of akaganeite samples. A slower heating rate of 2°C/min was used for quantification of akaganeite. The amount of akaganeite present in samples was

calculated from the mass loss of transitions occurring between 190 and 450°C and the reaction;

$2FeOOH_{(s)} \dashrightarrow Fe_2O_{3(s)} + H_2O_{(g)}$ mass loss 18% (2.4)

Figure 2.4 shows a typical TGA.

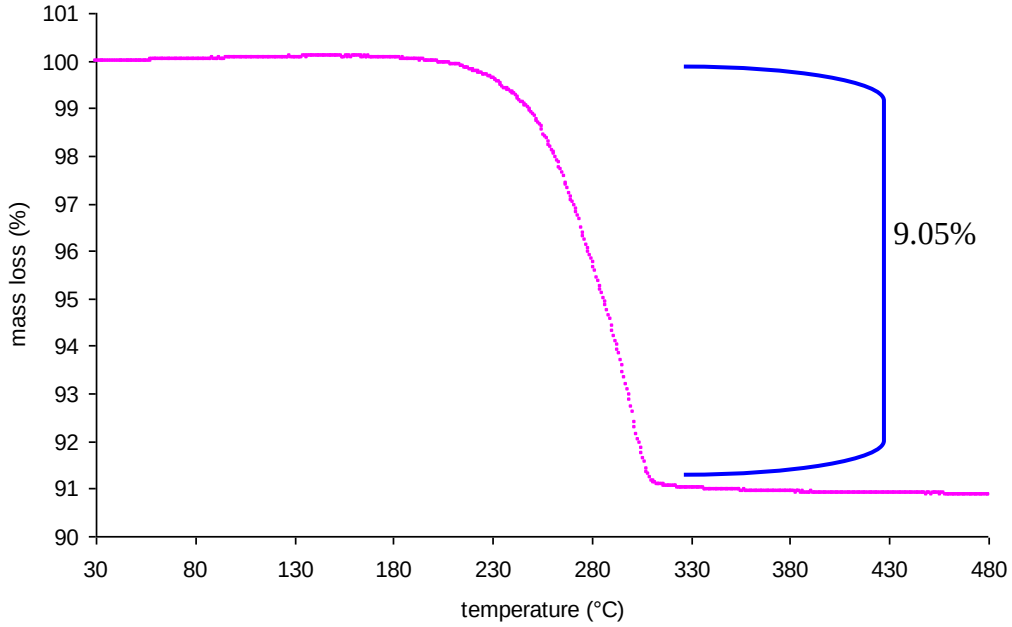

Figure 2.4 TGA of akaganeite formed in experiments (Chapter 5).

In Figure 2.4 the measured mass loss is 9.05%. If the sample were pure akaganeite this would be expected to be 18%, equation 2.4. Hence there is 9.05/18 = 50.28% akaganeite present.

TGA was also used to quantify the water in the samples in Chapter 5. Closed aluminium crucibles were used with a hole in the lid. This geometry is best for moisture content determination.

2.2.6 Differential Scanning Calorimetry (DSC)

Differential scanning calorimetry is a technique in which heat flow between the sample and an empty crucible are monitored against temperature while the temperature of the sample, in a specified atmosphere, is programmed (ICTAC, 1991). DSCs are categorized into two basic types. A power compensation DSC has

platinum resistor sensors and the power is provided separately to the sample and reference cells, Figure 2.5. The Japanese Industrial Standards define power compensation DSC as a technique in which difference of thermal energy that is applied to the sample and the reference material per unit of time is measured as a function of the temperature to equalize their temperature, while temperature of the sample unit, formed by the sample and reference material, is varied in a specified program (JIS, 1994).

A heat flux DSC has thermocouple sensors and uses a single heat source to both the sample and reference chambers, Figure 2.4. The Japanese Industrial Standards define heat flux DSC as a technique in which the temperature of the sample unit, formed by a sample and reference material, is varied in a specified program, and the temperature difference between the sample and the reference material is measured as a function of temperature.

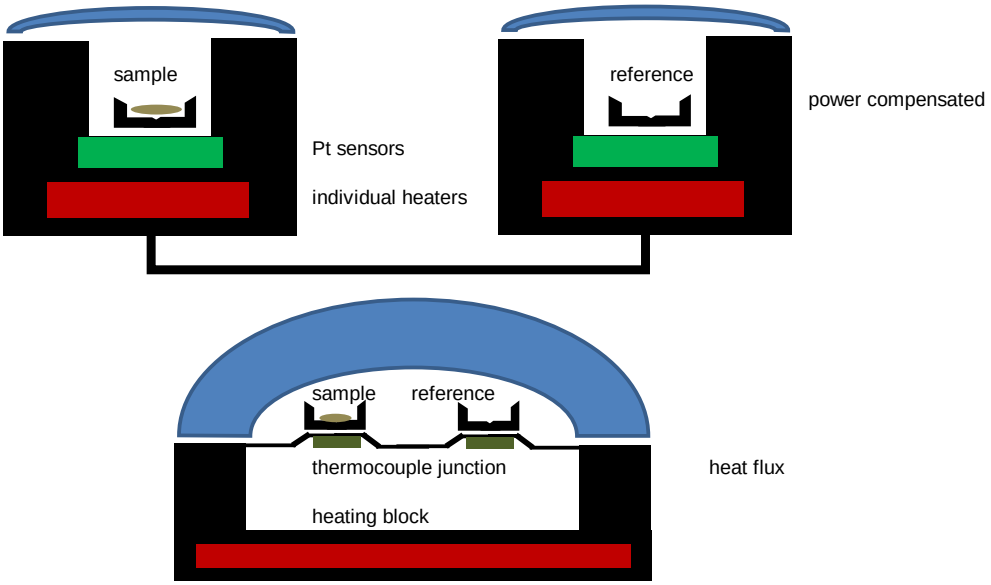

Figure 2.5 Types of differential scanning calorimetry.

In this work DSC has been used for two purposes;

To determine the degree of crystallinity of polyethylene and polypropylene boxes used to store archaeological iron.

DSC has also been undertaken of the standard iron minerals to clarify the transitions reported in the literature and determine their start and end temperatures and enthalpies.

A Shimadzu DSC 50 (heat flux) with open aluminium crucibles (L5116) under 60ml/min of nitrogen was used for the degree of crystallinity (20 to 500°C at 10°C /min) and standard mineral analyses. The furnace temperature and heat flow was calibrated with indium, zinc and tin.

After, the DSC samples were analysed with FTIR to confirm the products of any reaction. Where intermediates were reported in the literature, or suspected from the DSC traces, additional runs were undertaken and stopped just after the transition temperatures. The intermediates were analysed with FTIR to identify them. The results of the DSC analyses are shown in Table 2.8.

compound	DSC parameters				Product		
	Peak	Onset	Endset	Enthalpy (J/g)	FTIR peaks (cm^{-1})	Raman peaks (cm^{-1})	identification
Goethite	298	283	311	196.6*	645,525,440	226,292,411, 612	hematite
Akaganeite synthetic first preparation	207	175	254	137.0*	461,580,642, 704,3675	381,486,670	akaganeite
	592	571	606	72.0	646,525,440	226,292,411,497, 612	hematite
Akaganeite synthetic third preparation	207	175	254	137.0*	461,580,642, 704,3675	381,486,670	akaganeite
	592	571	606	72.0	646,525,440	226,292,411,497, 612	hematite

Akaganeite corrosion	303	278	340	228.7*	459,580,646, 700,3677	381,670	maghemite
	568	538	637	102.9	643,526,441	226,292,411,612	hematite
Lepidocrite	57	32	82	34.5*	750,1018	252,379,638	lepidicrite
	250	219	270	143.0*	459,580,650, 701,3675	381,486,670,718	maghemite
	446	432	462	55.8	645,525	226,292,245 411,612	hematite
Magnetite	396	311	448	62.6	647,525,440	226,292,411,497, 612	hematite
Hematite	No transitions observed						
Maghemite	584	556	614	26.8*	645,526,441	226,292,612	hematite
Strengite	74	33	91	24.2*	589,1039, 1634,3372	not done	iron phosphate hydrate
	145	129	162	78.0*	589,1039	not done	iron phosphate
	580	527	592	21.9	645,525,440	226,292,411, 612	hematite
Pyrites	149	145	156	7.2*	none	none	
	554	457	480	12.3*	645,525,440	226,292,411,497, 612	hematite
Siderite	411	406	433	293.2*	460,580,650, 700,3675	381,486,670,718	maghemite
	536	521	561	11.5*	645,525	226,292,245 411,612	hematite
rozenite		583	707	29.6	645,525,440	226,292,411,612	hematite

* endothermic effect

Table 2.8 Transitions observed for iron corrosion products by means of DSC.

2.2.7 Ion Chromatography

Ion chromatography is a derivative of high performance liquid chromatography. The column is an ion exchange resin. For example the Dionex Ionpack AS14 column consists of 9µm diameter surface-functionalized alkyl quaternary ammonium ion beads. When a flow of anions, in a suitable eluent, is forced through the column the different ions interact with the column to different degrees and gradually separate in the eluent stream. The technique has been applied for analysis of gases (Gibson et al, 1997b), dust (Gysel et al, 2004) and soils (Pfaff, 1993).

In this work ion chromatography has been used to detect anions and cations in solutions from soil, diffusion tubes and dust or fabrics. The solution was filtered (0,45 µm PTFE) and analysed with a Dionex 600 ion chromatograph. The injection loop volume was 10µL and detection was by temperature controlled conductivity. Anions were separated with a Dionex AS14A column with 0.02M sodium bicarbonate and 0.018M sodium hydrogen carbonate eluent at a flow rate of 0.5ml/minute. This method gives sensitivities of 0.01ppm for chloride, nitrate and sulfate ions. Calibration was with Dionex standards containing fluoride, chloride, nitrate, phosphate and sulfate at 5 concentration levels. Cation analysis was carried out with a Dionex CS12 column with 0.018M methane sulfonic acid eluent at a flow rate of 1ml/minute. This gave sensitivities of 0.05ppm for lithium, sodium, ammonium, potassium, magnesium and calcium ions. Calibration was with Dionex standards containing lithium, sodium, ammonium, potassium, magnesium and calcium at 5 concentration levels.

Ion chromatography was also used to detect ethanoate and methanoate ions from diffusion tubes. The same column and conditions were used as for anions. The ethanoate and methanoate eluted between fluoride and chloride. Sensitivity was a little worse at 0.5ppm. Calibration was with solutions prepared from Analar sodium ethanoate and methanoate at 5 concentrations levels.

2.2.8 Gas analysis

2.2.8.1 Diffusion tubes

Diffusion tubes were used to determine the airborne concentration of sulfur dioxide, nitrogen dioxide, ozone, hydrogen chloride, methanoic and ethanoic acids. A typical tube of the Palmes type is shown in Figure 2.6 (Palmes et al, 1976).

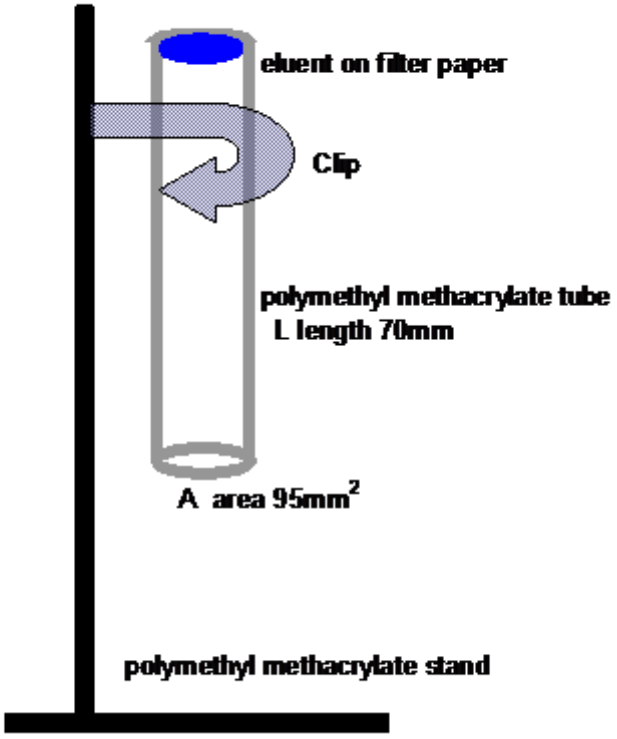

Figure 2.6 Schematic of Palmes diffusion tube.

The exposure begins when the cap is removed and stops when it is replaced. After exposure the amount of the species of interest is determined in the adsorbent from the tube. The adsorbent was 20µL of 1M KOH on Whatman number 1 filter paper. The airborne concentration is related to the mass uptake of the sampler by;

$$C = \frac{ML}{DAt} \qquad (2.5)$$

Where

C is the concentrations of the species in the air (µg/m^3)

M is the mass uptake of the species collected in the potassium hydroxide (μg)

L is the diffusion pathway (length of tube 70mm)

A is the area of the opening, 95mm^2

t is the exposure time, hours

D is the diffusion constant

Diffusion constants were taken from the literature (Gibson et al, 1997a; Makkonen and Juntto, 1997; Glasius et al, 1999; Ivanov et al 2007).

Diffusion tubes are ideal for use in showcases as they are small and do not require power. The major alternative is forced sampling with a pump (Schieweck, 2009). This draws large volumes of air through the sampler and has lower detection limits. However, the units generally require power and are large and difficult to fit into some showcases. Additionally the air flow over wood-based material surfaces increases the emission rate of carbonyl pollutants and can also affect the air exchange rate of the showcase.

2.2.8.2 Ethanoic and methanoic acids

The airborne concentration of carboxylic acids was analysed using diffusion tubes following the methodology developed by Gibson et al (Gibson et al, 1997b). Each measurement involved exposing four diffusion tubes for approximately twenty eight days. The large number of measurements was used due to reports of widely differing values between duplicate tubes (Bommel et al, 1997). Outliers could be evaluated statistically when four replicate tubes were used. The replicates also allowed a statistical evaluation of the errors in the technique. The extracts from the tubes were analysed with ion chromatography as described previously.

The standard deviation of each tube was calculated from;

$$S_X^2 = d^2(S_R^2/n+S_C^2) \qquad (2.6)$$

Where S_X is the standard deviation of an individual tube

d is the dilution factor used in the extraction

S_R is an estimate of the replication error from multiple injections

S_C is an estimate of the calibration error from the linear fit used to calibrate the ethanoate response of the ion chromatograph.

The individual tube errors were then combined to provide a standard deviation for each measurement.

Where space allowed diffusion tubes were deployed, clipped upside down to a polymethyl methacrylate sheet vertically so there was a 30mm gap between the lower, open end of the tube and the stand base. Polymethyl methacrylate is known to be a very weak adsorber for the gases being analysed and is used for the diffusion tube material (Gibson, 2005). In order to provide a stable vertical stand a large base is required.

Some of the showcases were not tall enough or did not have enough free area to deploy the diffusion tubes this way. In these instances the tubes were exposed horizontally, ontop of the polyethylene sheet, so that the open ends were more than 30mm away from any surface. Differences due to the deployment method were assessed. Three duplicate sets of readings were taken in larger showcases with tubes deployed both vertically and horizontally. Results are shown in Table 2.9.

	Tube 1	Tube 2	Tube 3	Tube 4	mean
Case 1 horizontal	685 ± 41	633 ± 48	613 ± 47	695 ± 52	656.4 ± 94.3
Case 1 vertical	585 ± 51	621 ± 55	633 ± 56	620 ± 52	614.7 ±107.1
Case 2 horizontal	592 ± 58	804 ± 61	660 ± 65	819 ± 54	718.6 ± 119.3
Case 2 vertical	572 ± 55	774 ± 65	760 ± 61	832 ± 81	734.5 ± 122.7
Case 3 horizontal	1530 ± 70	1666 ± 74	1594 ± 68	1728 ± 81	1629.4 ± 146.8
Case 3 vertical	1620 ± 68	1638 ± 70	1652 ± 75	1685 ± 65	1648.8 ± 139.2

Table 2.9 Results of triplicate measurements of ethanoic acid concentration in a showcase with diffusion tubes placed vertically and horizontally.

The differences between the measurements with tubes horizontal and vertical are not significant.

2.2.8.3 Sulfur dioxide, Nitrogen dioxide, Hydrogen chloride

The airborne concentrations were analysed using a modification of the diffusion tube method developed by Gibson et al (1997). The anions in the extracts from the tubes were analysed with ion chromatography. The sulfate formed from sulphur dioxide, nitrate formed from nitrogen dioxide and chloride from the hydrogen chloride, all elute after the organic acids. The airborne concentrations were then calculated from the concentrations on the adsorbent. The method was tested against commercial diffusion tubes for sulfur dioxide and nitrogen dioxide supplied and analysed by Gradko International Ltd for ten analyses.

As many of the analyses were of maritime locations the ingress of any fine sea salt aerosol through the 10μm filter on the end of the diffusion tube was assessed and corrected for. The eluents were analysed for sodium ions with a Dionex CS12 column with 0.018M methane sulfonic acid eluent at a flow rate of 1ml/minute. The molar equivalent of the sodium concentration in chloride was subtracted from the chloride result for the analysis. This was less than 4% in all analyses undertaken.

2.2.8.4 Ozone

All ozone measurements were carried out with diffusion tubes supplied and analysed by Gradko International Ltd. The analytical method was in house method GLM2.

2.2.9 Dust analysis

Analytical chemistry has been mainly concerned with the analysis of airborne dust for effects on health. Conservation is mainly interested with the amount of dust depositing on an object.

Previous work has used impactors or pumps to collect airborne dust and glass slides, fabric and self adhesive labels or sticky carbon pads to collect deposited dust (Adams and Ford, 1999; Howell et al, 2002; Ligocki et al, 1990). As this thesis was investigating dust deposition inside showcases impactors and pumps were impractical as they require power and large air volumes. Glass slides were used to

collect deposited dust due to their low cost, suitability for microscopy and low soluble ion content. The soluble ion content of the dust was also investigated.

Dust was collected on glass slides exposed for twenty eight days. The surface coverage of deposited dust was analysed using microscopy and image analysis (Howell et al, 2002). The analysis measures 50 approximately 1mm by 1mm areas on the slide surface. The light intensity of the microscope was set using the image processing routine on a graticule standard from the National Physical Laboratory. Particle size distributions were calculated from the areas of each particle detected, by assuming the particles were circular.

Some slides were extracted with 5ml of 18.2MΩ water and analysed with ion chromatography.

2.2.10 Provision of controlled environments

A variety of experiments have been used to determine the effect of the environment on the reactions occurring in archaeological iron. These required a series of environments to be generated.

2.2.10.1 Relative humidity

For fine control of RH, glycerol solutions were used (Miner and Dalton, 1953). The solutions were prepared by weight from Analar glycerol and 18.2MΩ water for accuracy. This allows very accurate (± 0.1%) RH environments to be generated. The RH has no temperature dependence up to 100°C and most of the experiments took place in a laboratory with no particular temperature control. The RH generated above glycerol solutions at different temperatures is shown in Figure 2.7. The values were taken fromMiner and Dalton (1953).

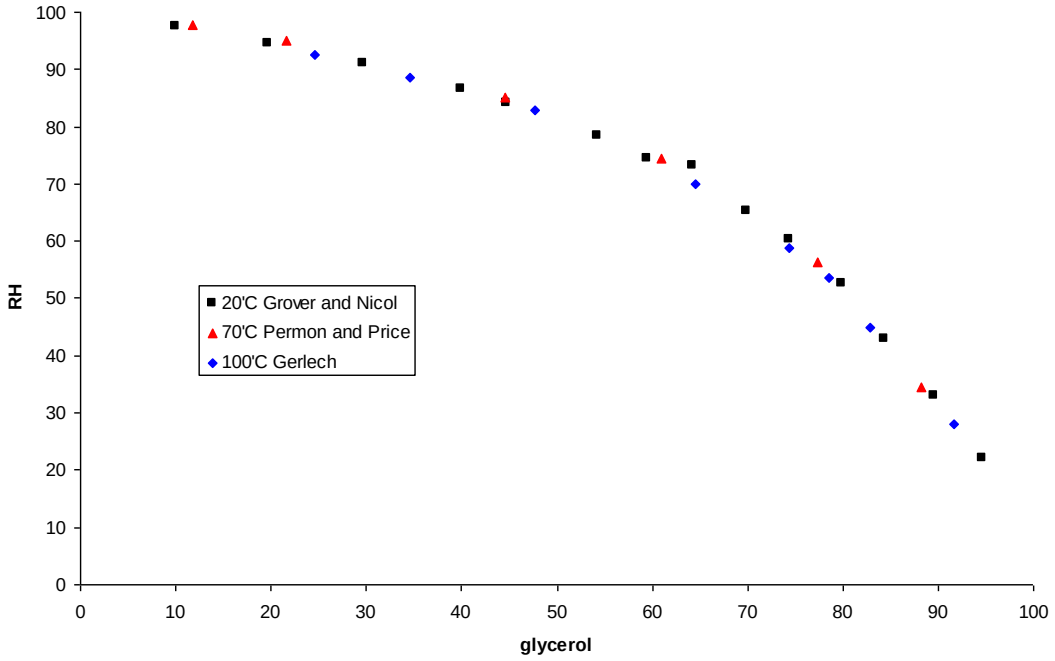

Figure 2.7 Relative humidity above glycerol solutions at different temperatures. Data taken from Miner and Dalton (1953).

Conditioned Prosorb silica gel was used to control RH in the oxygen depletion experiments. The use of solutions in near proximity to objects is an unnecessary risk and was avoided. The pore size distribution of Prosorb is designed to make it work efficiently around 50% RH. The gel was mainly used as supplied from the manufacturer. When gel needed reconditioning, this was done by drying at 80°C and then wetting with 18.2MΩ water until the mass specified on the suppliers information sheet was reached. The gel was then placed in sealed polyethylene nags for two days to equilibrate. The RH in the bag was checked with a Rotronic hygrolog data-logger.

2.2.10.2 Ethanoic acid, methanoic acid and formaldehyde and relative humidity

The carboxylic acid and aldehyde environments were generated above solutions with saturated salts to control the RH to approximately 33, 54 and 75%. This method was used as it has been used and examined by several workers (Thickett, 1996; Tetreault et al, 1998; Brokerhof and van Bommel, 1996). The RH generated above the salt

solutions is temperature dependant and the RHs at different temperatures are shown in Figure 2.8.

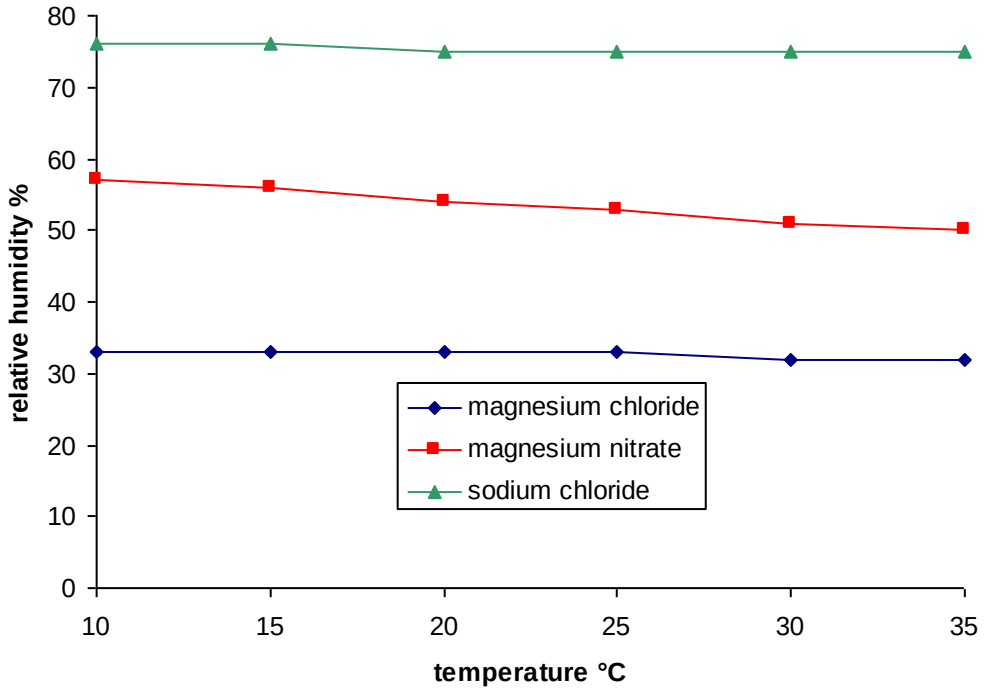

Figure 2.8 Relative humidity above saturated salt solutions at different temperatures.

The magnesium nitrate hexahydrate is particularly affected as seen in Figure 2.8.

To overcome this controls were run of the experiments above pure salt solutions (no acid or aldehyde) and the amount of akaganeite formation measured ratioed to these controls.

It has been recently reported that sodium nitrate and ethanoic acid can generate nitrogen oxide species (detected with a Draeger tube that cannot distinguish between the different nitrogen oxide species) and this can be in the order of ppm at the highest ethanoic acid concentration used (Tetreault, 2010). The impact of this additional pollutant is assessed in terms of the nitrogen dioxide exposure.

Chapter 3 Method Development

Methods were developed to optimize the characterization of corrosion. The potential and weaknesses of FTIR with several sampling accessories for archaeological iron corrosion products was investigated. The use of a fixed focus infrared microscope was developed to allow very rapid, non-invasive identification. Quantification of samples prepared as potassium bromide discs was investigated for the main iron corrosion products. No full investigation into the use of Raman for archaeological iron corrosion products was available at the start of this work and the full range of corrosion products and their characterization were investigated.

Thermo-magnetometry (TM) was applied to standard corrosion products and developed to quantify the amounts of elemental iron, magnetite and hematite. This technique also produces thermogravimetric information which was used to quantify akaganeite in samples. A tracer gas based decay method for determining air exchange rate was developed with carbon dioxide and its use for showcases and storage boxes investigated. The discrepancy between published ethanoic acid concentrations above salt solutions was investigated

3.1 Fourier Transform Infra-red Spectroscopy

Fourier transform infra-red spectroscopy has been used by several authors to identify iron corrosion products (Turgoose, 1982; Raman, 1991). No complete listing of spectra of the species occurring on archaeological iron has been published. No work has been published analysing the overlaps and potential and weaknesses of this technique. Different sampling techniques, potassium bromide discs, attenuated total reflectance, DRIFTs and a fixed focus infrared microscope were investigated.

3.1.1 Potassium Bromide Discs

3.1.1.1 Identification of Archaeological Iron Corrosion Products

Approximately 1mg of each standard material (Table 2.2) was ground with 300mg of dry potassium bromide in an agate mortar. The ground powder was double pressed in a hand press and 13mm die to 10tonnes pressure. Spectra of the potassium bromide

disc were collected on a Nicolet Avatar 360 FTIR spectrometer with Globar (heated silicon carbide rod) source and triglycine sulfate, TGS detector. Happ Genzel apodisation was used and 32 scans co-added for each spectrum. The wavenumber range was 400 to 4000 with 4cm^{-1} resolution. Spectra are shown in Figures A1.1 to A1.8 in Appendix 1. Table 3.1 shows the peaks recorded from the spectrum of each material.

Position (cm^{-1})	Goethite	Akaganeite	Lepidocrite	Hematite	Maghemite	Magnetite	Siderite	Phosphate	Sulfide	Sulfate	Peak assignment
	α-FeOOH	β-FeOOH	γ-FeOOH	α -Fe_2O_3	γ-Fe_2O_3	Fe_3O_4	$FeCO_3$	$FePO_4.2H_2O$	FeS	$FeSO_4.7H_2O$	
406	M										Antisym Fe-O
421					W	W[2]					[2] Fe-O stretch tetrahedral
434									W	M[2]	[1] S-S [2]SO_4 tetrahedra internal
445				M[1]	M[2]						[1] O displacement [2] FeO_6
463		M[1]							W		[1]Fe-O
473			S[1]		W				W		[1]oxide lattice
547				S[1]				M[2]	W		[1] O displacement [2] Fe-OH_2
560					S						Fe-O stretch
567						S					Fe_o stretch octahedral
575					W			W[3]			[3]Fe-OH2
596							W		W		
616	M[1]									M[2]	[1]sym Fe-O [2] SO_4 tetrahedra
638					S						n
659									W		
670	W										
694		W[1]			M[2]						[1]Fe-O [2]n
731							M				in plane bending CO_3
746			M								OH out of plane bend
775											
801	S[1]		W								[1]OH def v
812									W		
852		S									O-H⋯Cl hydrogen bond
863							M				out of plane bending CO_3
886			W						W		
902	S										OH bend delta
1028			M[1]					S[2]	W		[1] OH in plane bend [2]Fe-O
1087									W		
1099										S	SO_4 tetrahedra internal
1129									W		

1141	W										
1157			W								Del OH
1358								W			
1365								W			
1382				S^1	M^2						^{1}n ^{2}n
1417							S				asymm CO_3 internal
1628			M		W		W	M^2		W	^{2}HOH deformation
1665	W										
1711								W			
1803	W						W				
2076										W	
2288										W	
2497							W				
2850					W		W				
2924		W			W		W				
3103									W		
3126	M^1		S								^{1} OH stretch
3382										S	OH stretch
3413								M			n
3426			S^1		M		M				^{1}OH stretch
3453										S	OH stretch
3572				W							
3618		W									OH stretch

s, strong > 70% of maximum Abs exhibited by spectrum

m, medium 10% < m < 70% of maximum Abs exhibited by spectrum

w, weak < 10% of maximum Abs exhibited by spectrum

n reported but not assignment could be found in the litterature

Table 3.1 Observed absorption bands in Fourier transform infra red spectroscopy of standard materials.

With the exception of magnetite and maghemite, each mineral has a unique spectrum and can be identified in most mixtures with FTIR. There is some overlap ($801cm^{-1}$ band of Goethite overlaps with a medium intensity band from lepidocrite) and several bands are within $30cm^{-1}$ of each other, but examination of the rest of the whole spectrum would produce enough information to identify each mineral in mixtures. The literature was surveyed for reported FTIR absorptions. These were found to agree with peaks identified in this work, Table 3.2.

Material	Mineral name	Reference
$Fe(OH)_2$		Misawa et al 1969
Alpha-FeOOH	Goethite	Cambier 1986, Schwertmann et al 1985, Raman et al 1991, Ishilawa et al 1998, Lewis and Farmer 1986, Weckler and Lutz 1998
Beta-FeOOH	Akageneite	Ishilawa 1998, Raman et al 1991, Nyquist and Kagel 1971, Weckler and Lutz 1998
Gamma-FeOOH	Lepidocrite	Lewis and Farmer 1986, Raman et al 1991, Nyquist and Kagel 1971, Weckler and Lutz 1998
Delta-FeOOH		Misawa et al 1974, Okamato 1968, Weckler and Lutz 1998
Amorphous $FeO_x(OH)_{3-2x}$		Misawa et al 1974
$FeO(OH).nH_2O$	Limonite	
Fe_3O_4	Magnetite	Ishilawa 1998, Nyquist and Kagel 1971, Raman et al 1991
Alpha-Fe_2O_3	Hematite	Serna et al 1982, Wilson 1994, Nyquist and Kagel 1971, Raman et al 1991
Gamma-Fe_2O_3	Maghemite	Nyquist and Kagel 1971
Fe		
FeO		
$FeCl_2$	Lawrencite	Nyquist and Kagel 1971
$FeCl_3$	Molysite	

FeOCl		
$Fe_3(PO_4)_2.8H_2O$	Vivianite	Nyquist and Kagel 1971
$FePO_4.2H_2O$	Strengite	Nyquist and Kagel 1971
Fe_3S_4	Greigite	
$Fe_{1.01-1.08}S$	Mackinawite	
FeS_2	Pyrite	Nyquist and Kagel 1971
$Fe_{0.8-1}S$	Pyrrhotite	
$FeCO_3$	Siderite	Raman et al 1991, Nyquist and Kagel 1971
$FeSO_4.4H_2O$	Rozenite	Raman et al 1991, Nyquist and Kagel 1971
$NaFe_3(OH)_6(SO_4)_2$	Jarosite	
Beta-$Fe_2(OH)_3Cl$		Remazeilles and Refait 2008
Chloride Green Rust 1 $[Fe^{(II)}_3Fe^{(III)}(OH)_8][Cl.nH_2O]$		Misawa et al 1969
Carbonate Green Rust 1 $[Fe^{(II)}_4Fe^{(III)}_2(OH)_{12}][CO_3.2H_2O]$		Legrand et al 2001, Taylor 1980
Sulfate Green Rust 2 $[NaFe^{(II)}_6Fe^{(III)}_3(OH)_{18}\text{-}(SO_4)_2.12H_2O$		Ahmed et al 2010

Table 3.2 Published FTIR spectra of iron corrosion products from literature.

3.1.1.2 Quantification of Archaeological Iron Corrosion Products

For each mineral, a characteristic peak for quantification was selected. Only medium or strong intensity peaks were used. As far as possible, peaks were selected that did not overlap with other mineral peaks. The characteristic peaks are marked in orange in Table 3.1.

The response of that peak was then calibrated against the amount of mineral. Potassium bromide discs were produced from approximately 3mg accurately weighed sample, made up to 300mg with ground potassium bromide. The infra-red spectrum was recorded in triplicate on a Perkin Elmer 2000 FTIR spectrometer using 32 scans. The disc was split into two portions using a scalpel, one portion was weighed and re-ground. The weight was made up to 300mg with freshly ground potassium bromide, the powders mixed and another disc pressed and weighed. The FTIR spectra were collected and the process repeated seven times to give a series of spectra collected with sample weights ranging from 3 to 0.001mg. This method reduced the need to weigh out very small amounts of sample accurately for the calibration, and reduced the dependency on accurate weighing. The slope of the calibration line is mainly dependant on the mixing accuracy of the dilutions. Even a large error in the initial weight of sample used would have little effect on the slope. Solid state mixing of fine powders is difficult to achieve and the efficiency of this process was verified by determining the iron content in the discarded parts of the potassium bromide discs with atomic absorption spectroscopy. The calibration discs, from finest and coarsest sample powder, lepidocrite and siderite, were analysed. The discarded parts of the discs (150mg) were dissolved in dilute hydrochloric acid and the concentration of iron determined with a Perkin Elmer atomic absorption spectrometer. The iron concentrations are shown in Table 3.3.

	Amount of iron present (mg)					
	Lepidocrite		Akaganeite		siderite	
	expected	by AA	expected	by AA	expected	by AA
First KBR disc	3.053	3.051	2.998	2.996	3.024	3.023
Second KBr disc	1.524	1.522	1.493	1.491	1.500	1.497
Third KBr disc	0.741	0.732	0.746	0.742	0.742	0.733
Fourth KBr disc	0.343	0.341	0.349	0.339	0.360	0.353
Fifth KBr disc	0.153	0.151	0.161	0.161	0.174	0.173
Sixth KBr disc	0.053	0.053	0.076	0.067	0.073	0.065

Table 3.3 Expected and measured amount of iron present in lepidocrite, akaganeite and siderite calibration KBr discs.

The amounts of iron were found to match the expected values calculated from the mixing weights, within the experimental error of the atomic absorption technique 0.5%.

The calibration lines were plotted using both the peak height and area for the characteristic peaks selected previously; Figure 3.1 shows the calibration plot for akaganeite. Errors in the calibration for akaganeite were assessed by triplicate analyses of the calibration. The weighted errors are included in Figure 3.1. All of the plots showed negative deviations from straight line at higher absorbance values. The limit of linearity is important as it sets a maximum concentration, above which, the linear calibration is not valid. Limits of linearity were calculated for each calibration by comparing an independent estimate of the variance derived from the duplicate measurements (pure error mean square) with one derived from assuming a linear model (lack of fit mean square). Detection limits for the materials were determined as the lowest concentration at which a 95% confidence interval did not contain zero (IUPAC, 1997).

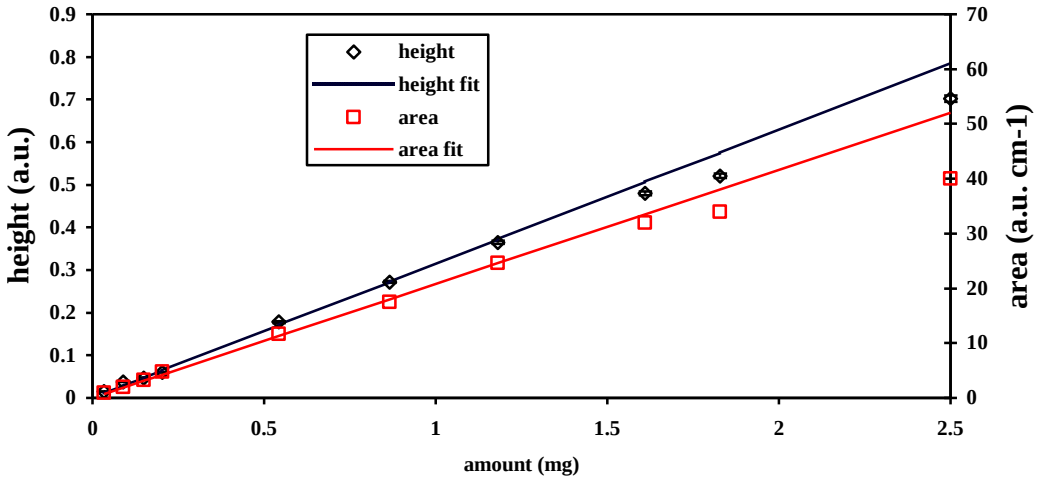

Figure 3.1 Akaganeite Calibrations against peak height and peak area for the 852cm^{-1} absorption band.

Calibrating against the peak area was found to give an extended linear range compared to calibrations against the peak heights. However, peak height is less affected by slight peak overlap, which is very likely, considering the broad nature of several of the peaks and the mixtures likely to be encountered. Hence peak height was used. The calibration information is included in Table 3.4.

Material	Peak		Calibration		
	Position (cm^{-1})	Whh (cm^{-1}) type	Slope (Abs/mg)	Limit of linearity (mg)	Detection Limit (mg)
α – FeOOH	798	44 M	0.7713	0.884	0.050
β – FeOOH	852	53 M	0.3146	1.181	0.040
γ – FeOOH	746	32 L	0.1687	1.135	0.005
Fe_3O_4	567	41 L	0.0105	1.378	0.400
α – Fe_2O_3	548	78 L	0.2318	0.798	0.035
γ – Fe_2O_3	638	35 L	0.1653	1.263	0.050
$FeSO_4.4H_2O$	1100	131 L	0.263	0.975	0.010
FeS_2	1130	253 M	0.0056	1.257	0.355
$FeCO_3$	1418	178 M	0.4226	0.975	0.055
$FePO_4.2H_2O$	1028	231 M	0.9788	0.674	0.015

Whh width at half height
Type peak type
L Lorentzian
M mixed (Lorentzian+Gaussian)

Table 3.4 Peaks used for quantification of iron corrosion products and their calibration parameters.

As can be seen, magnetite and iron sulfides give a very weak response for infra-red spectroscopy. Both of these materials also frequently occur as hard, well adherent layers (and in the case of iron sulfides, extremely thin layers) which are difficult to sample.

Potassium bromide discs have been used to quantify the amount of akaganeite formed in Chapters 5 and 6. With iron (II) chloride and iron mixtures this technique was found to work extremely well as neither the iron, iron (II) chloride or iron (III)

chloride intermediate have absorptions in the mid infra red. The detection limit was 0.04mg of akaganeite in the 3mg samples used to prepare the KBr discs, 1.33% by mass. Where no akaganeite was detected a larger sample (30mg) was made into a KBr disc, giving a 0.13% detection limit. The additional mixtures with humic acid, copper chloride, lepidocrite, magnetite, iron sulfate, iron carbonate and hematite did not interfere with akaganeite detection.

3.1.1.3 Quantification of Akaganeite in the Presence of Goethite

Goethite has absorption bands on either side of the akaganeite 852cm^{-1} absorption band. A series of experiments were undertaken to determine the sensitivity of FTIR to akaganeite in the presence of Goethite. Mixtures were made by thoroughly grinding together mineral powders of akaganeite and Goethite. Spectra of pure akaganeite and Goethite are shown in Figure 3.2.

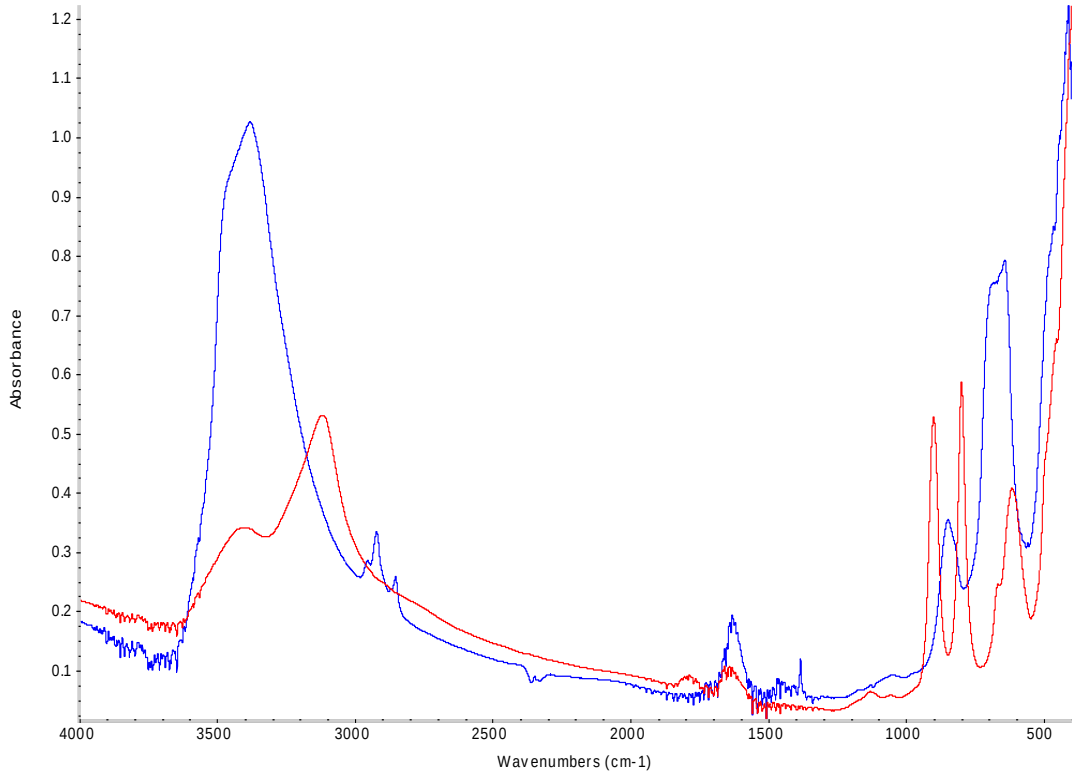

Figure 3.2 FTIR spectra of KBr discs of akaganeite (blue) and Goethite (red).

Although the spectra are quite distinctive, there is significant overlap with almost all the bands. Quantification using the peak heights at 850cm^{-1} for akaganeite and 798 cm^{-1} for Goethite was tested. The base lines was set to 990 and 551cm^{-1} to allow for the 903cm^{-1} and 602cm^{-1} peaks of Goethite. Mixtures were prepared with 1, 5 , 10, 20, 40, 50, 60, and 80% akaganeite. Small samples, 2mg were prepared as KBr discs.

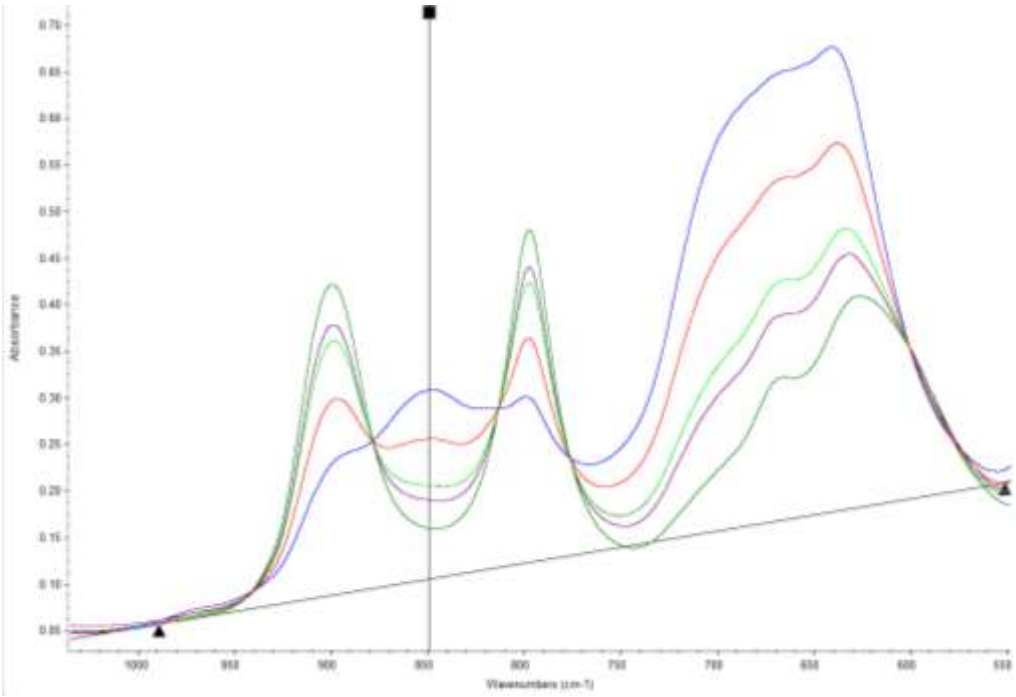

Figure 3.3 Peak Ratio method for quantification of akaganeite and Goethite mixtures. Black lines show height determination and baseline for akaganeite. The spectra are; 5% akaganeite (dark green), 10% akaganeite (purple), 20% akaganeite (green), 40% akaganeite (red), 60% akaganeite (blue).

3.1.1.4 Quantification of water

Quantification of water in samples was undertaken utilizing the method developed by Libowitzky and Rossman (1997) with KBr discs. The KBr was dried for several days at 250ºC to remove any water.

3.1.2. Infra-red Microscopy

A fixed focus Nicolet Inspect IR microscope, running from a Nicolet Avatar 360 FTIR bench was used at 4cm^{-1} resolution, collecting 128 scans between 650 and

4000cm^{-1} with Happ Genzel apodisation. The microscope uses the Avatar Globar source and beamsplitter and its own MCT-A detector. The microscope collects reflected radiation from a circle approximately 0.1mm in diameter. The analysis area is visualised with a digital camera and the camera and microscope focus are matched, so that the infrared focus can be estimated from the digital video image. The small analysis area and fixed geometry of the microscope often allow spectra to be reproduceably collected from complex surfaces. Problems can be encountered due to anomalous dispersion giving abnormal peak shapes. Several attempts from adjacent areas were often required to generate a good quality, identifiable spectrum. Where possible, spectra were collected from areas approximately flat and horizontal. To verify the technique, spectra were collected from the standard corrosion product and mineral samples. These were compared to spectra of those materials collected via transmission techniques such as potassium bromide discs and diamond cell.

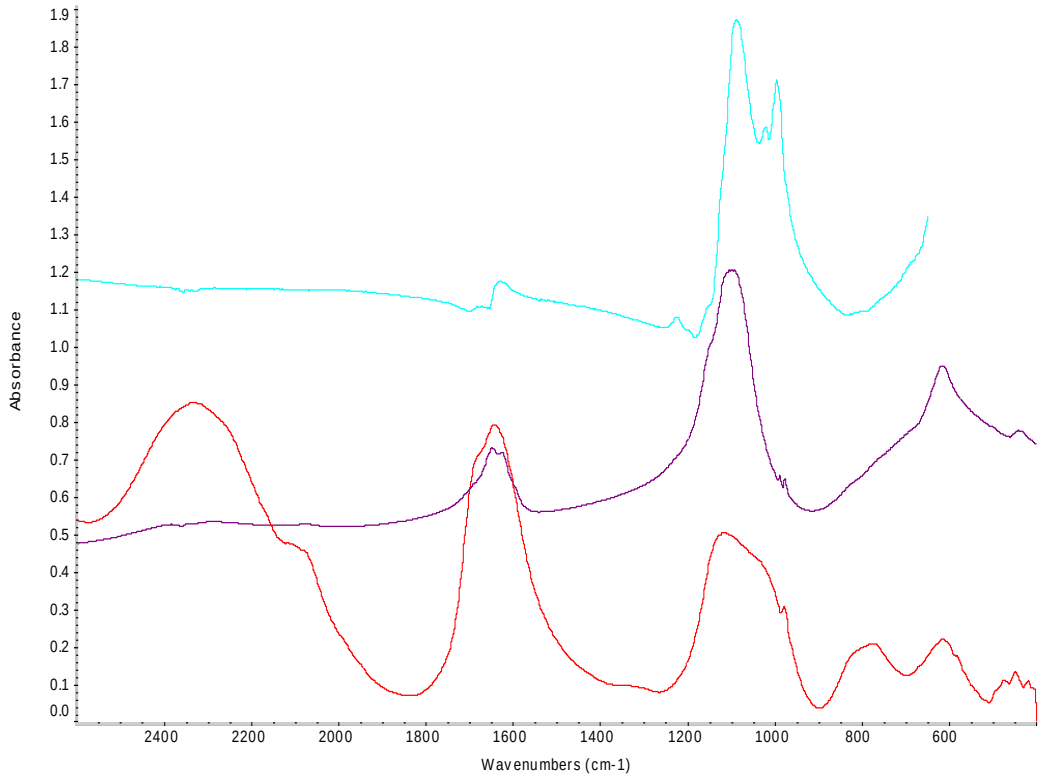

Figure 3.4 KBr, DC and microscope spectra of iron sulfate, lower spectrum DC, middle spectrum KBr, upper spectrum microscope.

The object sample spectra were compared to standards run using the same method and stored in a search library to allow swift identification.

3.1.3 Diamond cell, DRIFTS and ATR

Spectra of each of the standard materials were collected on a Nicolet Avatar 360 FTIR spectrometer with diasqueeze diamond cell on a four times beam condensor. Happ Genzel apodisation was used and 64 scans co-added for each spectrum. The wavenumber range was 400 to 4000cm-1. Spectra are shown in Figures A1.1 to A1.8 in Appendix 1. The spectra compared to the KBr disc spectra. They were of poorer quality and more noisy, but certainly of sufficient quality for identification purposes.

DRIFTs produced good quality spectra in many instances similar to the KBr discs. Several samples had to be diluted with KBr to produce well resolved spectra.

ATR produced excellent spectra of all the standard corrosion products.

3.2 Raman

Raman confocal micro-spectroscopy was carried out with two systems.

- a Horiba Jobin Yvon Infinity Raman microscope with 532nm and 780nm lasers. The Horiba system gave analytical volumes with a depth of 10.8µm and a diameter of 9.1µm with a 100µm confocal hole and the x50 objective lense and 3.8µm and diameter 4.5µm with the x100 objective lense.

- a Renishaw System 1000 Ramascope with He-Ne ion laser (632.8nm)

The standard materials were run with both Raman systems. Unique spectra were obtained for each mineral including strong responses for magnetite and iron sulfides. Spectra were also produced for ferrous chloride and ferric chloride. The 532nm laser was found to give a better response than the 780nmm laser on the Horiba system.

Position (cm^{-1})	Goethite	Akaganeite	Lepidocrite	Hematite	Maghemite	Magnetite	Siderite	Phosphate	Sulfide	Sulfate
	α-FeOOH	β-FeOOH	γ-FeOOH	α -Fe_2O_3	γ-Fe_2O_3	Fe_3O_4	$FeCO_3$	$FePO_4.2H_2O$	FeS	$FeSO_4.7H_2O$
130								m		
145				w						
195					w					
199							m	m		
206	w									
215			w							w
226				s						
249	w		s							
266								m		
291				s						
302	m		w			m				
309									s	
313		s								
336									m	
373			m							
376									m	
380						s				
383							m			
390	s									
394		s						m		
408				m						
443										w
459										m
480	w							m		
495				w						
499		m								
516							m			
525			w							
541		m								
544			w							
553										
556	m					w				
571					m					
599										w
610		m		w				w		
639			w							
650										
654				w						
664								w		
669					s					
676						s				
680	m									
684							w			
722		s				m				
728							w			

768								w		
919		w								
991										s
1002	w									
1017										w
1042								m		
1072							s			
1102								s		
1114	w									
1157		w								
1161								m		
1191								m		
1306	m									
1511							m			

s, strong > 70% of maximum intensity exhibited by spectrum

m, medium 10% < m < 70% of maximum intensity exhibited by spectrum

w, weak < 10% of maximum intensity exhibited by spectrum

Table 3.5 Observed absorption bands in Raman spectroscopy of standard materials.

Material	Mineral name	Reference
$Fe(OH)_2$		Melendes et al 1992, Odziemkowski et al 1998, Oblonsky and Devine 1995, Thibeau et al 1978
Alpha-FeOOH	Goethite	Nauer et al 1985, Oshtsuka et al 1991, Thierry et al 1991, Boucherit et al 1991, De Faria et al 1997, Bellot-Gurlet et al 2007
Beta-FeOOH	Akageneite	Oshtsuka et al 1991, Dunnwald and Otto 1989, De Faria et al 1997, Bellot-Gurlet et al 2007
Gamma-FeOOH	Lepidocrite	Nauer et al 1985, Thierry et al 1991, Boucherit et al 1991, Beattie and Gilson 1970, De Faria et al 1997, Bellot-Gurlet et al 2007

Delta-FeOOH		Oshtsuka et al 1991, Dunnwald and Otto 1989, Bellot-Gurlet et al 2007
Amorphous $FeO_x(OH)_{3-2x}$		
$FeO(OH).nH_2O$	Limonite	
Fe_3O_4	Magnetite	Nauer et al 1985, Thierry et al 1991, Beattie and Gilson 1970, De Faria et al 1997
Alpha-Fe_2O_3	Hematite	Nauer et al 1985, Thierry et al 1991, De Faria et al 1997, Bellot-Gurlet et al 2007
Gamma-Fe_2O_3	Maghemite	Thierry et al 1991, Boucherit et al 1991, Dunnwald and Otto 1989, De Faria et al 1997, Bellot-Gurlet et al 2007
Fe		
FeO		Dunnwald and Otto 1989
$FeCl_2$	Lawrencite	Blunt et al 1989
$FeCl_3$	Molysite	Sharma 1974
FeOCl		
$Fe_3(PO_4)_2.8H_2O$	Vivianite	Ross 1972
$FePO_4.2H_2O$	Strengite	Ross 1972
Fe_3S_4	Greigite	Ross 1972
$Fe_{1.01-1.08}S$	Mackinawite	Ross 1972
FeS_2	Pyrite	Ushioda 1972, Vogh et al 1982
$Fe_{0.8-1}S$	Pyrrhotite	Ross 1972

$FeCO_3$	Siderite	Melendes et al 1992, , Bellot-Gurlet et al 2007
$FeSO_4.4H_2O$	Rozenite	Ross 1972
$NaFe_3(OH)_6(SO_4)_2$	Jarosite	Ross 1972
Beta-$Fe_2(OH)_3Cl$		Reguer et al 2006, Bellot-Gurlet et al 2007
Chloride Green Rust 1 $[Fe^{(II)}_3Fe^{(III)}(OH)_8][Cl.nH_2O]$		Boucherit et al 1991
Carbonate Green Rust 1 $[Fe^{(II)}_4Fe^{(III)}_2(OH)_{12}][CO_3.2H_2O]$		Legrand et al 2001, Taylor 1980
Sulfate Green Rust 2 $[NaFe^{(II)}_6Fe^{(III)}_3(OH)_{18}\text{-}(SO_4)_2.12H_2O$		Boucherit et al 1991

Table 3.6 Reported Raman spectra of iron corrosion products from literature.

Some of the iron corrosion products undergo low temperature thermal transitions. The oxihydroxides emit water vapour at between 200 and 300˚C. Iron chlorides, hydrated sulfates and phosphates also show low temperature reactions. The high absorption of these materials renders them liable to heating under the laser illumination, especially when focused under a microscope. Such thermal transitions can easily lead to mis-identification if sufficient care is not taken. Keeping the laser filter below 10% was found to reduce heating to such a level that thermal transitions did not occur.

Fluorescence is a major limitation with archaeological material. Extended illumination can reduce this effect, but care needs to be taken because of the heating and reactions described previously. Analyses from several points can sometimes yield a non-fluorescent spectrum.

Raman has been found to be able to characterize all the iron corrosion products. It is particularly useful for magnetite (which is difficult with IR and can easily be confused for maghemite by XRD). The very small analytical volume is useful when dealing with complex, mixed corrosion products. There are some limitations to its application for archaeological iron as described above.

3.3 Thermo-Magnetometry (TM)

Thermo-magnetometry is the study of the effects of heat on the magnetic properties of materials. The technique has been used to study metal alloying with ferromagnetic metals such as iron, cobalt and nickel and their alloys. The oxidation behaviour of iron and many of its compounds including, hematite, carbonate and various sulfides have been studied (Warne et al, 1988).

The degree of corrosion of a metal is normally measured by the amount of elemental metal remaining after corrosion. The number of potential corrosion products on metals means that the weight gain can give a misleading measure of the amount of metal converted. Stripping treatments are commonly used to determine the amount of elemental metal retained (ASTM G1, 1999). An ideal stripping reagent will remove just the corrosion products whilst leaving the metal unaffected, such a reagent is rarely encountered and procedures have to be used to overcome the inaccuracies caused by the stripping reagent dissolving the metal. Iron is also very prone to post stripping corrosion and careful rinsing and drying procedures need to be adopted to ensure the mass measured is not affected. Hence stripping procedures are time consuming and also lose all the information about the corrosion products, which are removed.

Thermo-magnetometry (TM) was thought to have the potential to determine not only the amount of elemental iron left in a sample, but also to determine the amounts

of other corrosion products in a material. The reported magnetic transitions of iron minerals are shown in Table 3.7.

Material	Magnetic Structure	Magnetic Susceptibility ($l0^{-8}$ m^3kg^{-1})	Neel T_N or Curie T_C Temperature (°C)
Iron	Ferromagnetic	50,000	780 T_C
Goethite α-FeOOH	Antiferromagnetic	26-280	127 T_N
Akaganeite β-FeOOH	Antiferromagnetic	-	17 T_N
Lepidocrite γ-FeOOH	Antiferromagnetic	40-70	-196 T_N
Limonite $FeOOH.nH_2O$	Antiferromagnetic	66-74	
Hematite α -Fe_2O_3	Ferromagnetic	10-760	683 T_C
Maghemite γ-Fe_2O_3	Ferrimagnetic	40,000-50,000	547-713 T_N
Magnetite Fe_3O_4	Ferrimagnetic	20,000-110,000	577 T_N

Table 3.7 Common corrosion products of iron and their magnetic properties.

The Curie temperature is defined as the temperature at which a ferromagnetic material becomes paramagnetic. If iron is analysed with TM, with the magnet placed below the sample, a sudden drop in weight is observed when it is heated above its

Curie temperature (780˚C). The loss of magnetism is a very sharp transition due to its collaborative nature, in-fact such effects are used to calibrate the temperature for TGAs, due to their fixed and sharp nature. Examination of the mass losses occurring indicated that any TM effect due to goethite, would be masked by water loss. Akaganeite was below the calibration range of the TGA used and lepidocrite's Neel transition occurred at far too low a temperature to be observed. Iron, magnetite, hematite and maghemite could be analysed. This would provide a valuable adjunct to the other analytical techniques.

The thermal transitions of iron minerals were characterized with thermogravimetry. None of these transitions form ferromagnetic products that would show significant magnetic effects below the temperature range of interest.

Thermo-magnetometry was carried out with a Perkin Elmer TGA7, with 40cm^3min^{-1} of nitrogen flowing over the sample and a magnet precisely positioned to apply a magnetic field. Some development of the temperature program was undertaken and the final program used was:

Room temperature to150ºC at 50º$Cmin^{-1}$

hold for 2 min, the magnet is positioned during this period

150 to700ºC at 200º$Cmin^{-1}$

700 to 840ºC at 20º$Cmin^{-1}$

cool to room temperature

The slow heating to 150ºC and 2 minutes isotherm at that temperature allowed adsorbed water to diffuse out of the sample. Placing the magnet at this point allowed the initial magnetization to be determined. The amount of water was calculated from the weight drop between 30 and 150ºC. Although this temperature is somewhat higher than normally used, the long dwell time at 150ºC allowed the water loss to be viewed easily if the graph was plotted against time. It also reduced the time taken for the overall analysis, an important factor with the relatively large number of samples to be processed. The fast heating rate to 700ºC reduced the analysis time. The very slow heating rate over the iron Curie temperature allowed an accurate determination of the elemental iron content. A typical TM for iron is shown in Figure 3.5.

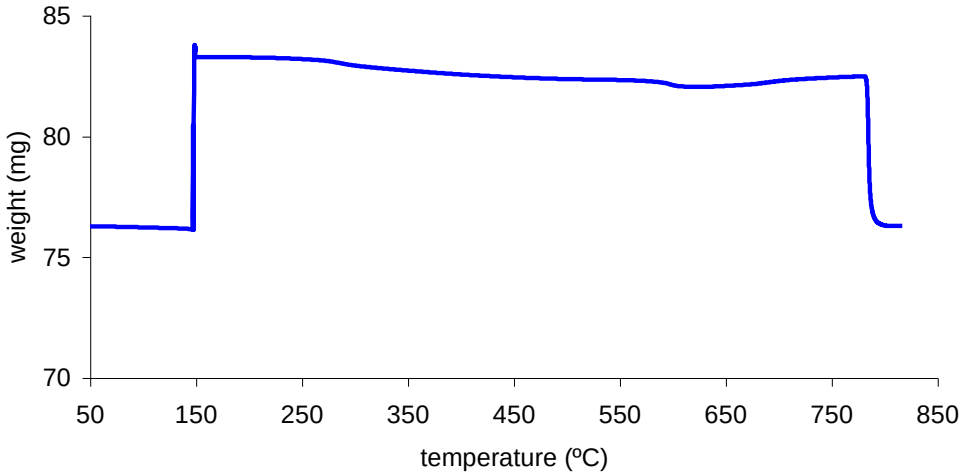

Figure 3.5 Thermo-magnetometry of sample from archaeological nail from Stonea.

A sharp rise in apparent weight can be seen when the magnet was applied at 150˚C. There is a weight loss between 250 and 450ºC due to akaganeite. A further apparent drop in the weight is observed at 580˚C, this is due to the Neel temperature (ferrimagnetic to paramagnetic transition) of the of magnetite present. At 780˚C the loss of ferromagnetism of the iron appears as a rapid weight loss.

The reported thermal transitions of iron corrosion products are summarized in Tables 2.6 and 2.7.The thermo-magnetic transitions (grey) shown by the standard materials are shown in Table 3.8. Thermo-gravimetric (white) effects for the same samples are included for comparison.

	Measured Onset Temperature (ºC)	Measured Endset Temperature (ºC)	Weight loss (%)	
Goethite α-FeOOH	267	309	9.11	Dehydroxylation

Akaganeite β-FeOOH synthetic	253	451	9.82	Dehydroxylation
Akaganeite β-FeOOH corrosion	236	443	10.38	Dehydroxylation
Lepidocrite γ-FeOOH	210	265	11.12	Dehydroxylation
	374	425	-1.18	
	425	480	2.50	Neel temperature
Magnetite Fe_3O_4	558	667	22.32	Neel temperature
Hematite α -Fe_2O_3	683	713	0.16	Neel temperature
Maghemite γ-Fe_2O_3	steady increase from 328ºC		~ 4%	Oxidation
	333	685	29.48	Neel temperature
Strengite $FePO_4.2H_2O$	133	177	13.04	Dehydration
	506	583	2.53	
Pyrites FeS	461	515	3.06	
	957	974	1.80	
	554	559	2.49	Neel temperature
	595	722	12.69	Neel temperature
Rozenite $FeSO_4.4H_2O$	106	138	27.04	Dehydration
	461	515	3.06	
	957	974	1.80	
Siderite $FeCO_3$	458	507	29.60	

Thermomagnetometric (observed only when the magnet was in place) effects are in grey

Table 3.8 Thermo-magnetometric and thermo- gravimetric results for the standard iron corrosion product samples.

None of the materials would interfere with the analysis of magnetite or iron. Siderite, $FeCO_3$ shows a weight loss, with the carbonate decomposing between 450 and 530ºC, generating maghemite which is observed in thermo-magnetometry. Siderite, akaganeite and lepidocrite all generate maghemite during thermal decomposition. Whether this occurs below the Neel temperature and would be detected by thermo-magnetometry depends on the crystallite size and degree of crystallinity of the precursors. These reactions could possibly interfere with the analysis of other maghemite present. However this mineral has only very rarely been reported on archaeological iron. Both akaganeite and lepidocrite should be distinguishable from their lower temperature dehydroxylation reactions.

The TGA7 was initially calibrated against discs of pure iron with masses ranging between 17mg (the smallest disc that could be pressed) and 130mg (the balance limit), Figure 3.6. Two calibrations were undertaken to check the reproducibility.

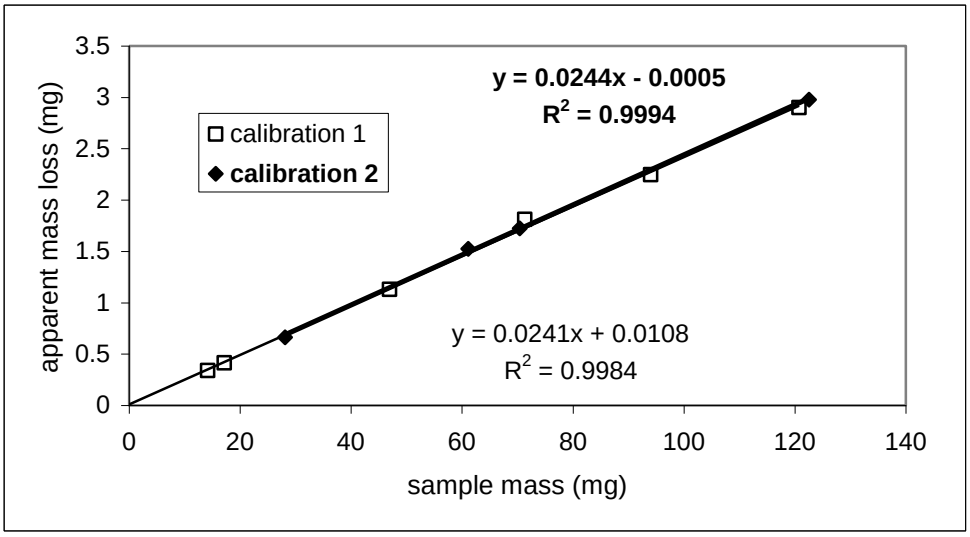

Figure 3.6 Two calibrations for thermo-magnetometry for discs of pressed iron powder.

The calibrations gave extremely good linear fits and were very close to each other. The calibrations for weight produced very similar slopes (0.0244 and 0.0241) and intercepts not significantly different from 0, ($P<0.05$).

As an estimate of the precision of the technique, iron discs were prepared using approximately the same mass and then abraded with 100 grade silicon carbide paper to produce discs of 74.15 $\pm$ 0.05mg. These discs were then analysed. The

repeatibility for discs of 74mg weight was very good, with a standard deviation in the apparent weight change of less than 0.23%. Converting these figures to weight of iron, using the calibration in Figure 3.6, gives values between 74.07 and 74.21mg, with a standard deviation of 0.091mg. The detection limit was estimated to be 0.01mg of iron (IUPAC, 2010)

The TGA 7 was then calibrated with samples of known composition to accurately determine the amount of both iron and magnetite in a disc, from the size of the magnetic effects at the Curie and Neel temperatures of these materials. Magnetite is ferrimagnetic and exhibits paramagnetism at temperatures above the Neel temperature.

The calibration graphs for magnetite from the mixed discs for iron and magnetite are shown in Figure 3.7.,

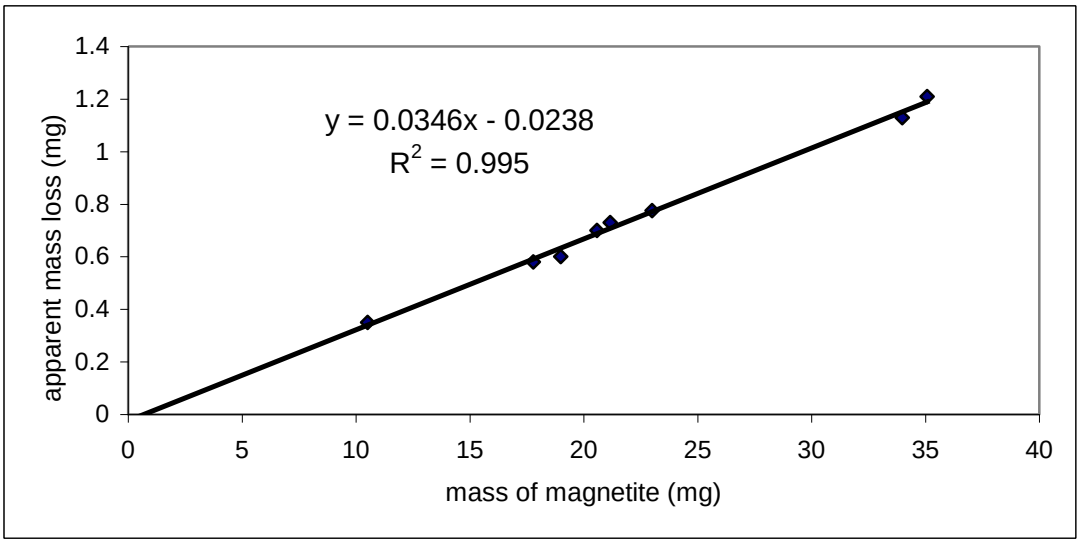

Figure 3.7 Calibrations for thermo-magnetometry for magnetite from discs of pressed iron and magnetite powders.

The technique is slightly more sensitive to the magnetite used with a coefficient of 0.0346 compared to 0.0240 for iron. This is consistent with the reported magnetic volume susceptibilities of 3.9×10^{-12} for iron and up to 5.7×10^{-12} for magnetite (Hunt et al, 1995). The intercept was significantly different from zero ($P>0.05$). Magnetic transitions are co-operative, i.e. the magnetic domains need to align. At a

certain low concentration the domains are too widely separated to align, this appears to be approximately 0.023mg (in 300mg) for the magnetite examined.

Discs were pressed of iron and magnetite, and mixtures of Goethite and lepidocrite powders were added to mimic the expected morphology of the corroded iron discs, i.e. a metal core, with a thin magnetite layer overlain with powdery corrosion products.

3.4 Air Exchange Rate Measurement

There are two basic types of tests that have been developed to measure air exchange rates; pressurisation tests and tracer gas tests. Pressurisation tests require a hole in the showcase for a fan to run through. These tests are more repeatable than tracer gas based tests and faster, but the hole requirement is a major drawback for showcases.

Both types of test can be performed as constant parameter tests, where the pressure or concentration of carbon dioxide is kept constant. The fan is run or more tracer gas injected to keep a constant value and the amount of air or tracer gas injected used to calculate the AER. An alternative method is decay tests, where a set amount is injected and the decay monitored and analysed to determine AER. Tracer gas decay tests have been used due to the simplicity of the test. Carbon dioxide because of the availability of good quality loggers (Vaisala GMD222 probe and GMD70 logger), imminent banning of SF_6 and reported adsorption of nitrous oxide on silica gel. The reported tracer gases are summarised in Table 3.9.

Gas	Relative molecular mass	Background concentration	UK WEL *	Reactivity	Notes	Reference to use in conservation
Water vapour	18	Variable	None	High	Any organic material will	(Padfield, 1966; Thomsen, 1977)
Carbon dioxide	44	350-1500ppm	5000 ppm	Med		(Brimblecombe and Rarner,
Sulfur hexafluoride			1000 ppm	Very Low	Now banned in UK by Kyoto	(Cass et al., 1989)
Nitrous oxide	44	0.03ppm	100 ppm	Low	Reported to be adsorbed by silica gel (Schwieck, 2009)	(Stanley et al., 2003; Zucchi et al., 1977)
Oxygen	32	20.9%	none	Low*		(Brimblecombe and Rarner, 1983; Daniel and Maekawa,

* 8 hour time weighted average reference period

Table 3.9 Tracer gases used to test showcase air exchange rates.

Two relevant standards already exist for measuring air exchange rates of buildings. However, the significant differences between buildings and showcases mean that these standards cannot be simply applied in this instance (ASTM, 2001; ISO, 2000). The major difference is that showcases often show significant temperature differences with the room they are in, due to thermal gain from lighting or equipment in the showcases. This can result in a strong diurnal effect on the air exchange rate. The error calculations in both ASTM E714-00 and ISO12596 use the variance from a straight line for a plot of ln concentration against time as an estimate of error. For showcases with strong diurnal variations in temperature, and therefore air exchange rate, this will give very large and inappropriate errors. Both standards use reciprocal hours as the unit, as many buildings have air exchange rates around 1 $hour^{-1}$, however few showcases are as leaky as buildings and air exchange rates are generally less than 3 day^{-1} (Thicket et al, 2007). Reciprocal days is a better unit for showcase air exchange rates as it avoids the use of very small fractions as would be

the case with reciprocal hours. For example, an air exchange rate of $0.1day^{-1}$ is $0.00416hour^{-1}$.

A series of experiments were undertaken to optimize the test method.

3.4.1 Injecting the Tracer Gas

The higher the initial concentration of tracer gas the longer a showcase with a particular air exchange rate will be measureable. Very leaky cases will lose gas quickly and require higher initial concentrations. However, injecting a high concentration of tracer gas will increase the internal pressure and hence air exchange rate of a showcase.

The amount of tracer gas required for carbon dioxide was investigated by injecting approximately 10000ppm into a Perspex case and determining the air exchange rate in 24 hour intervals. The injection was repeated six times and the case air exchange rate was such that this allowed five determinations over 24 hour periods per injection. The 24 hour air exchange rates are plotted against the initial carbon dioxide concentration in figure 3.8.

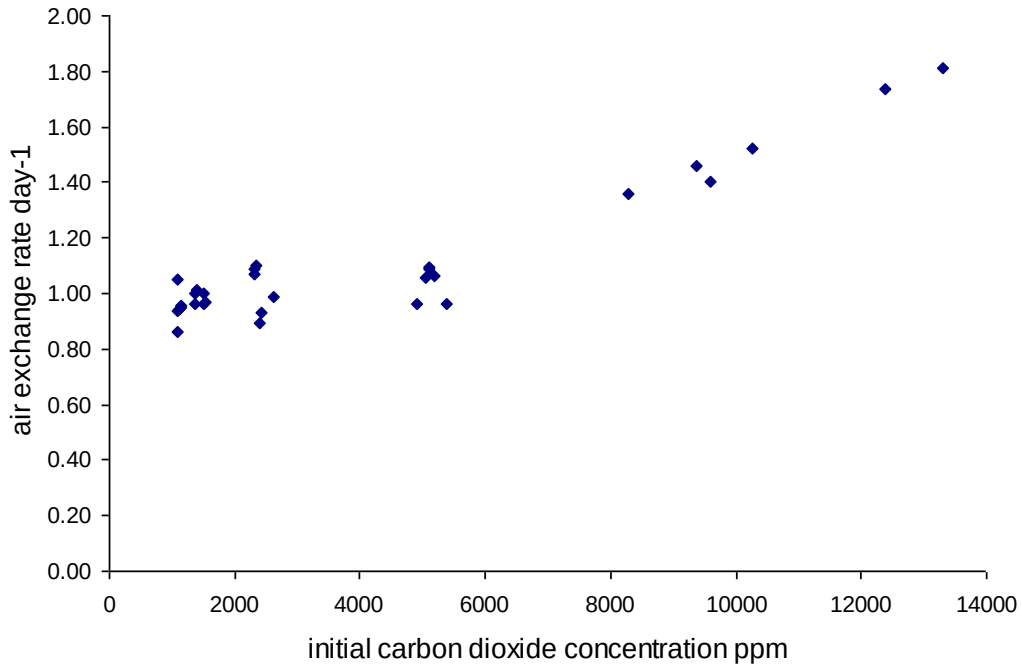

Figure 3.8 Air exchange rate versus initial carbon dioxide concentration.

The air exchange rates cluster around approximately $1day^{-1}$ when the carbon dioxide concentration is below 6000ppm, but get higher when this concentration is exceeded. The first measurement after injection is consistently and statistically significantly higher (1-tailed t-test at 95 per cent confidence levels) than the rest of the measurements. A maximum concentration of 6000ppm seems a reasonable limit to use for most showcases. For a showcase with air exchange rate of $1day^{-1}$, this will give at least 72 hours of useable data, for one with $3day^{-1}$, at least 24 hours. Higher air exchange rates will require more gas to be injected.

It is important that the tracer gas is thoroughly mixed before the measurements begin. It is possible to add a small fan to the case running off a battery and timer to mix the air for example 30minutes. This however introduces another piece of equipment into the case (which can be difficult to position with a dressed case) and in some instances longer mixing times are required. Alternatively the tracer gas can be allowed to mix naturally. This process takes anything up to 14 hours and extends the test and requires a logger with superior battery life. Figure 3.9 shows the mixing phase of three tests and the start point for the calculation in each instance is marked with an arrow.

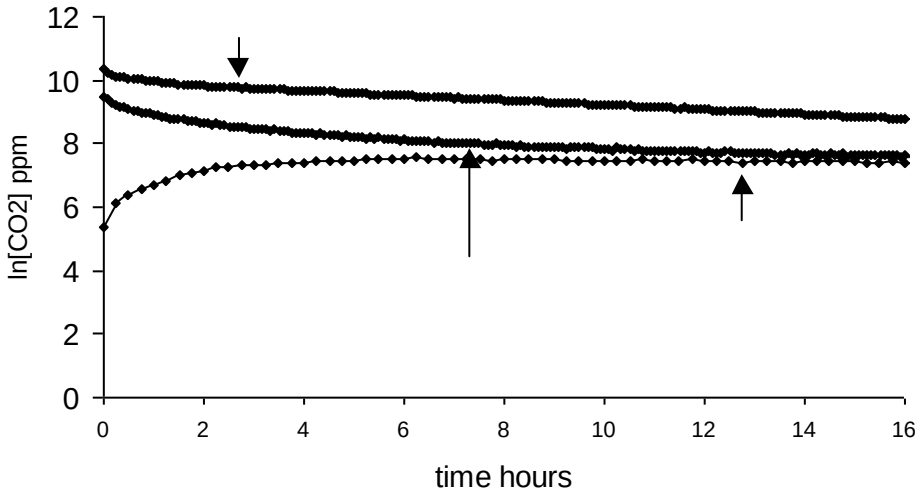

Figure 3.9 Mixing of carbon dioxide after injection.

3.4.2 Time Frame for Tests

A showcase with a heat source inside it, or acting on it, is likely to show a diurnal variation in air exchange rate. This means that calculating the air exchange rate of anything less than a 24 hour period will not be representative and can lead to major differences in measurements. Figure 3.10 shows data from a case that runs 2°C warmer than the room during the day.

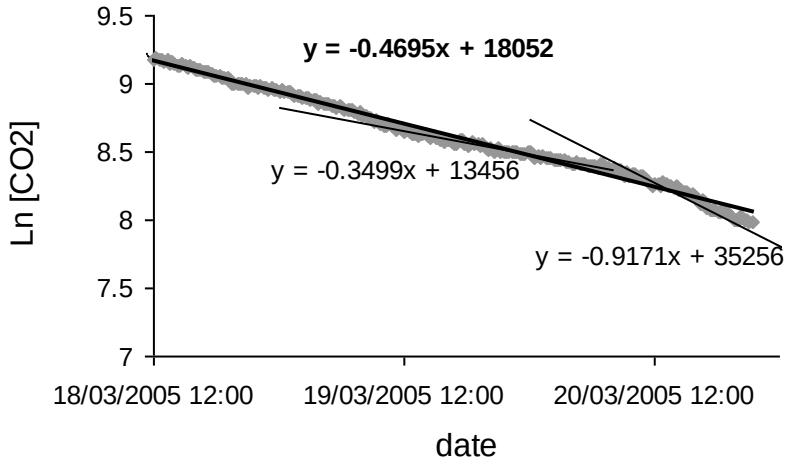

Figure 3.10 Differences in air exchange rate resulting from using short time periods.

The average air exchange rate over the 48 hour measurement period shown is 0.47day^{-1}. Two 8 hour periods are also shown on the graph, which give AERs of 0.35 and 0.92day^{-1}. Many of the preventive conservation factors of interest are long term averages. Certainly for external pollutant and dust ingress, damage accumulates over a period of months. Although corrosion from internal pollutant concentration can occur over a few days, a daily average is sufficient. Relative humidity damage can be rapid, but most showcases contain a certain amount of hygroscopic material, MDF boards, dressing fabric etc, meaning they do not respond rapidly and hence a 24 hour average is sufficient in the vast majority of instances.

Extremely high air exchange rate showcases will not hold tracer gases beyond a certain time and measurements will be limited by this. Short measurement intervals will be required in such instances.

3.4.3 Accuracy of Tests

The accuracy of tests is determined by a number of factors;

- the accuracy of the logger used.
- the correct determination of starting and end points for the calculation
- the barometric conditions in the room when measurements are carried out.
- the reproducibility of door sealing for the showcase being measured.

In order to estimate some of the errors a series of tests were carried out using a 50 by 50 by 50cm Perspex chamber with a hinged door with compression seal. The tests were undertaken in an unconditioned room in an historic house. Carbon dioxide was investigated by injecting approximately 10000ppm into a Perspex case and measuring the carbon dioxide concentration. The air exchange rate was determined in 24 hour intervals. The injection was repeated six times and the case air exchange rate was such that this allowed five determinations over 24 hour periods per injection. The 24 hour air exchange rates are plotted in Figure 3.11.

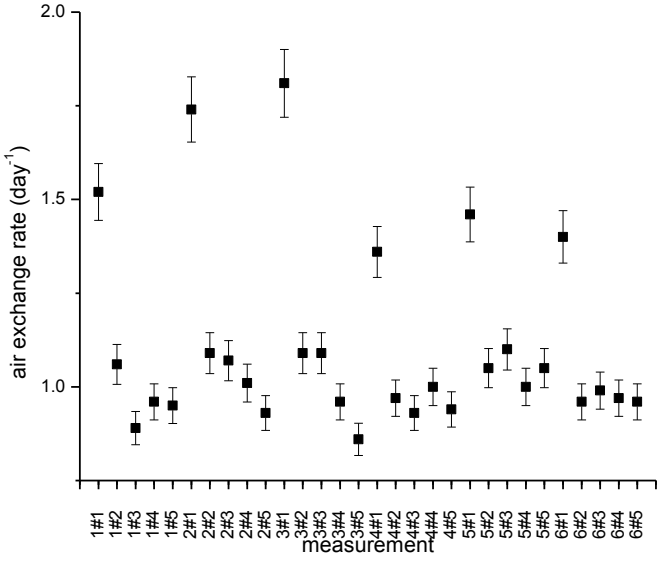

Figure 3.11 Repeated air exchange rate measurements in a single showcase.

If the initial injections are ignored (see section Injecting the Tracer Gas) the reproducibility is 11% between readings. A second series of experiments were undertaken to understand the influence of the door opening and closing and the seals reseating. A bicycle tyre valve was inserted into the Perspex wall of the case and sealed with silicone. The power lead for the Vaisala logger was also fed through the Perspex wall and sealed in place and the door closed. The logger continuously measured the carbon dioxide concentrations and approximately 6000ppm of carbon dioxide was introduced via the valve into the case when the concentration approached 700ppm. Again, air exchange rates were calculated for consecutive 24 hour periods. Results are shown in Figure 3.12.

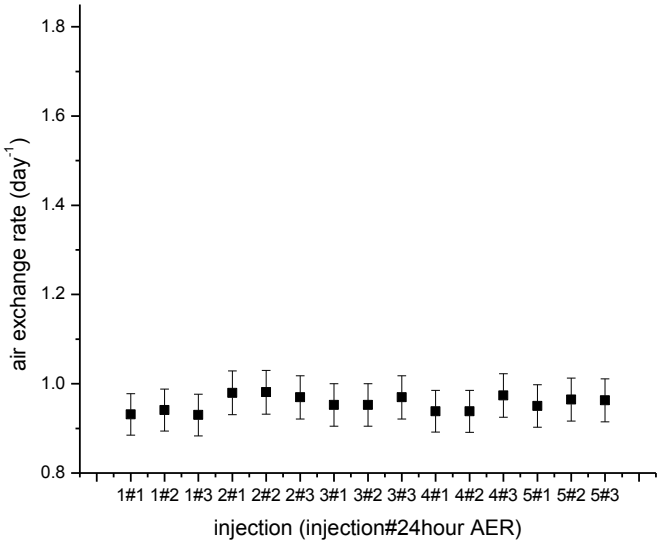

Figure 3.12 Repeat air exchange measurements without opening door.

The reproducibility dropped dramatically to approximately 7%, confirming that the door sealed slightly differently each time it was closed

3.4.5 Adsorption onto silica gel

Silica gel was present in most of the showcases tested. It was desirable not to remove the gel for testing as this posed a risk to the iron artefacts and there were storage issues, with some sites having over 200kg of gel present in cases. The effect of adsorption of carbon dioxide onto silica gel was assessed by making six sets of

measurements in the Perspex chamber. The AER was measured three times with an empty chamber and three times with 6kg of dried silica gel added. No difference in AER was observed.

3.4.6 Negative effects of carbon dioxide

The tests were carried out in showcases containing objects, and any potential negative effects of the carbon dioxide concentration used, were assessed first.

3.4.6.1 Production of carbonic acid

Carbon dioxide is in equilibrium with carbonic acid on a surface. The level of CO_2 is elevated for the test period, the pH of the equilibrium concentration of carbonic acid at 5000ppm was compared to the pH of ethanoic acid at concentrations commonly encountered. Ethanoic acid concentrations measured in showcases are reported in Chapter 7. A concentration of 1000µgm^{-3} was assumed to be the value present in most showcases in non air conditioned buildings. This is in equilibrium with 0.003112M ethanoic acid, which will have pH of 3.65. The maximum carbon dioxide concentrations used in the tests is 5000ppm . This is in equilibrium with 0.004M carbonic acid, which will have a pH of 4.37. The carbon dioxide concentrations will decay rapidly in the test and a test takes no longer than four days.

3.4.6.2 Effect of carbon dioxide on hydrocerrusite

Carbonaceous materials are in equilibrium with the carbon dioxide vapour. The ratio of cerussite to hydrocerussite in a lead pigment gives important archaeometric information on its production method (Rosi et al 2009, Milani et al 2009). Hydrocerussite has been reported to convert to lead carbonate at carbon dioxide concentrations above 1500 ppm (Taylor and Lopata, 1984). The concentrations used for measurements are above this level, so an experiment was designed to determine if this would occur. Hydrocerussite powder was exposed to 20,000 ppm of CO_2 for 7 days in stainless steel DRIFTs cups. The powder was analysed by using FTIR on a

diffuse reflectance accessory (DRIFTS) which is extremely sensitive to impurities on the surfaces of powders.

Spectra were collected on a Nicolet Avatar 360 with Spectratech DRIFTS accessory. Spectra of lead carbonate (BDH Analar 99.95%) and basic lead carbonate (BDH Analar 99.95%) powders and mixtures were collected at 4cm^{-1} resolution for 50 scans. The powders were procured in a fine particle size as DRIFTS works best with particles below 10µm. Six spectra were run for each sample due to the reported low repeatability of DRIFTS. The powder thickness was at least 2mm as this has also been reported to affect results. (Armaroli et al, 2004). Spectra were corrected using the Kubelka-Munk algorithm as there is no linear relationship in DRIFTS between the band intensity and concentration (Kubelka, 1948). The composition of the standard powders was confirmed with x-ray diffraction. The spectra for cerussite (lead carbonate and hydrocerussite (basic lead carbonate) are shown in Figure 3.13.

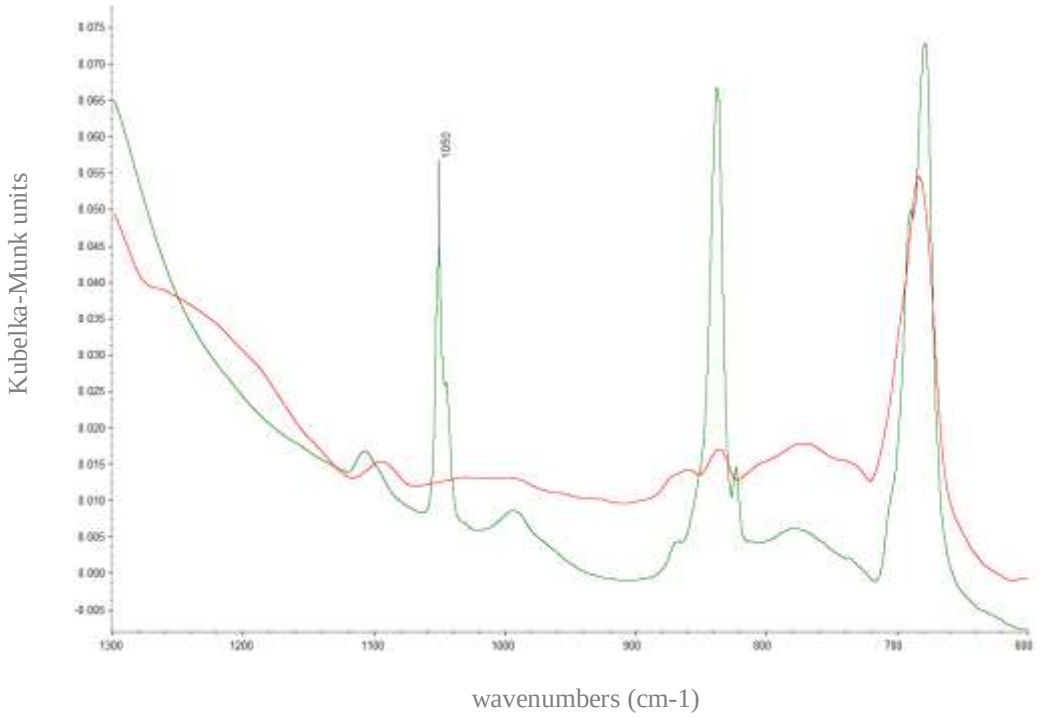

Figure 3.13 DRIFTS spectra of cerussite (green) and hydrocerussite (red).

The spectra are very similar due to the similar structure, however, cerussite has an absorption band at 1050cm^{-1}, which is absent in hydrocerussite.

Experiments with mixtures of lead carbonate and basic lead carbonate had indicated that less than 1 per cent of cerussite could be detected by examination of the absorption band at 1050 cm^{-1} with this method in hydrocerussite. No cerussite was detected in the exposed sample.

3.5 The use of ethanoic acid and soluble salt solutions

Air phase salt migration has been reported for some soluble salts. To check this effect samples of Whatmans number 1 filter paper were placed above the salt solutions used for 30 and 90 days. The filter paper was extracted with 18.2MΩ water and analysed with ion chromatography for the presence of any magnesium, sodium, chloride or nitrate ions. Very low deposition rates were analysed (<0.022 $\mu g/cm^2/day$) in the filter paper after exposure. This indicates the effect is not significant for the salts used.

Significant non linearity in ethanoic acid concentrations generated above acetic acid and salt mixtures was reported by Brockerhof and Van Bommel (1996) in contradiction of Tetrault's (1997) findings. The ethanoic acid and salt were prepared in 250ml jars and the airborne acid concentration determined for four consecutive fourteen day periods with duplicate diffusion tubes (Gibson et al, 1997b). This confirmed that the concentrations were within the 7% instrumental error of the diffusion tube analyses for the two month period. No systematic decrease in ethanoic acid concentration was detected (t-test at 99% confidence interval) over the test period. The use of an impermeable aluminum laminate (Moistop 622) barrier on the bakelite reaction vessel top negated the need to change the solutions monthly. Tests were undertaken on the screw top, glass reaction vessels proposed for the tests. A hole was drilled in one tap and a carbon dioxide probe inserted with a silicone ‘o’ ring. The air tightness was confirmed with a chlorofluorocarbon sniffer. Carbon dioxide tracer gas tested were undertaken with the modified top on several reaction vessels. The average air exchange rate was $0.02day^{-1}$. If the top was loosened by an eigth of a rotation, the air exchange rate increased to $5.8day^{-1}$. The differences between this and Tetreault's, and Brockerhof's results are most likely due to different reaction vessels used, particularly in the permeabilities of the lid materials and sealing of the lids. The ethanoic acid solution concentration was checked by

analysing the solution when the tests were complete with ion chromatography, confirming very little loss of ethanoic acid during the tests.

3.6 Conclusions

Fourier transform infra red spectroscopy and Raman micro spectroscopy are good complementary techniques for iron corrosion products. For non-invasive object examination the fixed focus infrared microscope is a very fast survey technique and Raman can be used to confirm the identification and detect magnetite and, hematite which the infrared microscope is insensitive to. Raman can also be used to identify individual corrosion crystals, which is extremely useful with the small scale, intimately mixed corrosion products often encountered on archaeological iron. The infrared sampling accessories generated essentially identical spectra. For experimental work where a representative analysis is required potassium bromide discs are an appropriate method. Raman microscopy can be used to analyse any slightly darker crystals to detect very low concentrations of akaganeite.

Thermo-magnetometry has been developed as a technique to quantify the amount of iron, magnetite and hematite in a sample. Neither infrared or Raman can detect elemental iron. Magnetite is weakly detected in infrared and quantification of large heterogeneous samples with Raman is extremely time consuming.

Appropriate experimental parameters for carbon dioxide tracer gas air exchange rate measurements for showcase have been developed. The errors and potential adverse affects have been investigated.

The mixed ethanoic acid and soluble salt method to generate ethanoic acid concentrations at different RH values has been validated. Reproduceability of tightening and the permeability of the tops used on screw top glass reaction vessels is important for consistent results.

Chapter 4 Analyses of Archaeological Iron Objects

4.1 Introduction

A number of analyses have been carried out on archaeological iron artefacts to identify the materials present. This was important to identify species that may affect the deterioration reactions and hence needed to be included in the experiments in Chapter 5 'Formation of Akaganeite and reaction of iron'. Three groups of analyses are reported in this chapter;

analyses of species in pits on freshly excavated objects, in order to investigate the initial reactions occurring on exposure to air.

determination of any changes to objects that have recently been excavated (within previous year). Observations were made over a three year period.

analyses of archaeological iron objects observed to be deteriorating or changing

More detailed analyses were undertaken on yellow surface layers observed on orange akaganeite samples identified in 4.3.1.3. These are reported in Chapter 6 'The transformation of akaganeite'.

The association between akaganeite and actively deteriorating archaeological iron was first reported in 1977 (Zucchi et al., 1977). There are different theories in the literature describing the post excavation deterioration of archaeological iron. Other corrosion products have been associated with archaeological iron deterioration, including iron sulfates (Wang, 2007a). The exact nature of the dense product layer has been elucidated by the work of Dillman, (Reguer et al, 2005; Reguer et al, 2007; Saheb et al, 2008; Neff et al, 2005). The iron corrosion products reported in archaeological iron are shown in Table 2.1 (Chapter 2).

This work investigates whether akaganeite is the major corrosion product associated with deteriorating archaeological iron, through examination of objects observed to be changing. Species associated with the akaganeite that are reported to affect its formation have also been investigated. The stability of the akaganeites found on archaeological iron has also been examined. Conversion of akaganeite to other minerals will almost certainly release chloride. Akaganeite contains a considerable amount of chloride within its structure and bound to its surface, other iron minerals can hold much less chloride, for example a maximum of 0.5% has been reported for Goethite (Turgoose, 1989). The released chloride can initiate further corrosion reactions in objects with remaining metal cores. The potential for instability in mineral preserved organic remains on the iron surfaces was also assessed. These phenomena have been elucidated by studying deteriorating and recently excavated material.

4.2 Materials and Methods

4.2.1 Materials

4.2.1.1 Freshly Excavated Objects

Freshly excavated artefacts were analysed immediately after excavation.

Nine iron artefacts were examined with portable radiography. Six showed evidence of sub surface pits. Of these the archaeologist allowed two to undergo analysis. The objects were transported in anoxic enclosures. Several potential pits were located from the radiographs. A small hole was carefully excavated into each pit using a 2mm drill bit. The ambient RH in the laboratory during the analyses was 56-64%. Pale yellow crystals were observed with microscopy at the bases of the pits on the magnetite layer and analysed with confocal Raman spectroscopy (Renishaw RamanSystem1000 using a 514.5nm Spectra-Physics argon ion laser).

4.2.1.2 Recently Excavated Objects

Recently excavated objects were studied in more detail to determine any early signs of deterioration and define the corrosion environment. The objects were selected less than a year after excavation when they entered the collections of the British Museum. Soil samples were collected from the excavations where possible.

The Sutton Hoo ship burial is thought to date from the 7th century AD. Recent work developing a visitor centre on the Tramner House area, to the north of the burial mounds, was preceded by a rescue excavation. This revealed several graves, thought to date somewhat earlier than the famous ship burial (the earliest between approximately 525 and 550 AD). After excavation in summer 2000, the iron finds from these graves were stored in polypropylene boxes (Stewart type) with dried silica gel incorporated to keep the RH low. The material was accessioned into the British Museum in July 2000. Of the 125 iron objects, twelve representative of the type, size and degree of corrosion of the set were chosen for in depth examination. Soil was retrieved from the Sutton Hoo Tranmer House site to a depth (2m) using a spade. A solid section of soil was retrieved and stored in a polyethene sealed with an airtight plastic clip (Mitsubishi Chemical Ageless RP system).

Wetwang forms part of a series of East Yorkshire burials from the 3rd century BC to the 1st century AD. It is one of the very small number of chariot burials found in the UK. Initially dated to the 1st century BC, because of the lack of similarity with other chariot burials (the date range of which spans the 1st century BC to the 1st AD), the discovery after radiography of an inverted brooch in an iron corrosion block pushed the date to late 1st century AD. This illustrates the vital importance of iron in the archaeological record. The major iron artefacts were the chariot wheels and associated fittings, a total number of 18 iron containing artefacts. A much larger proportion, 8 of these objects were studied. It was not possible to retrieve soil samples from the Wetwang excavation site, however, several of the objects were excavated with significant soil deposits present. These were mechanically removed. Small samples of soil were also removed from the objects during the examination

Any changes in the objects from these two excavations were observed over a period of five years, whilst many of the objects remained in dry storage, the wheel fragments were too large for this method and were stored in open wooden drawers in a room at ambient conditions. Several objects were displayed in showcases over this period.

4.2.1.3 Deteriorating Objects

Over 260 apparently deteriorating objects from both display and storage contexts were identified and examined and analysed. The objects either had fresh powdery corrosion beneath them or had undergone visual change (often new corrosion sites, as identified from condition photographs. Details of the sites and objects were given in Table 2.3 in Chapter 2. These were objects that had shown obvious visual deterioration in a few years, either fresh powder underneath the object or fresh corrosion products or cracks identified from condition photography. Many of the objects were displayed for the first time. In these instances they were recently removed from dry silica gel storage, had condition photography and had undergone conservation assessments that would have highlighted any existing active deterioration. Hence the deterioration observed could safely be assigned to the period on display. Those objects examined from storage were identified by metals conservators and then checked against condition photography.

4.2.2 Methods

4.2.2.1 Sample Assessment

Recently formed corrosion products were analysed from objects observed to be deteriorating (fresh powder or documented changes by photography). The mixtures of compounds present were analysed to elucidate the proportions of other species present in close proximity to the deterioration. A number of species are reported to interfere with the formation and crystallinity of akaganeite, chapter 1.3. Over two hundred examples of deteriorating archaeological iron were examined from display and storage. The morphology and type of deterioration was also recorded. Three major types were observed;

- a surface powdering.
- a plug of material being raised by the formation of elongated orange crystals, this was almost always associated with pits in the iron surface. Although these were often not revealed until the deterioration had taken place.
- levering apart of corrosion layers, by elongated orange crystals.

Samples of the major corrosion products were taken with a scalpel. They were analysed with Fourier Transform Infra-Red Spectroscopy, Raman spectroscopy and scanning electron microscopy with energy dispersive analysis. Thirty larger samples were also analysed with XRD.

4.2.2.2 Sample Analysis

4.2.2.2.1 Fourier Transform Infra-Red Spectroscopy (FTIR)

All FTIR was undertaken with a Perkin Elmer 2000 or Nicolet Avatar 360 as described in Chapter 2. Small samples were analysed with diamond cell, Durascope and diamond single bounce ATR or Nicolet Inspect IR microscope using direct reflection or with ATR heads. The corrosion products were identified by a combination of characteristic bands in their distinctive mid IR spectra (Thickett, 2005a). Amorphous iron corrosion products were observed in some of the FTIR spectra, indicating large relatively amounts of these materials present. To detect smaller amounts, all samples were extracted with 1% sodium hydroxide solution and the extract dried on a gold coated glass slide and analysed using multiple reflection with FTIR (Perkin Elmer 2000 with AmplifIR on Durascope). The crystalline polymorphs goethite, akaganeite and lepidocrite have very low sodium hydroxide solubility and would be excluded by the extraction procedure (Cornell, 2003).

In over thirty instances larger samples were removed and analysed quantitavely as potassium bromide discs, Chapter 3.1.1.

The presence of relatively large amounts of organic material in the corrosion products was indicated by absorption peaks at 2950 and 2870 cm^{-1}, CH stretching. In some instances distinctive FTIR spectra of humic and fulvic acids could be

detected in the sodium hydroxide extracts. However in many cases absorptions from the amorphous iron hydroxides covered the distinctive lower wavenumber regions. Organic conservation materials would also give 2950 and 2870 cm^{-1} absorptions which could be misinterpreted as humic or fulvic acids. The extracts were treated with acetone, the acetone extract dried and similarly analysed. This method would extract and allow identification of acrylics and polyvinyl acetates, the two most commonly used organic conservation materials.

These methods give two figures for the amorphous iron hydroxide, detection in the original spectrum indicating that a high proportion of the sample was an amorphous hydroxide, and detection during the sodium hydroxide extract only, indicating a much smaller amount present in the sample.

.

4.2.2.2.2 Raman

All of the samples were also analysed with confocal Raman micro spectroscopy. Two instruments were used, Dilor Infinity with 532 and 780nm lasers and Labram with 630nm laser. The laser power was filtered and the spectra checked as acquired to ensure the samples were not transforming under the focussed laser illumination (Robinet and Thickett, 2003). The Raman was especially useful to confirm magnetite which absorbs very weakly in the mid infra-red.

4.2.2.2.3 Radiography

Most archaeological iron is radiographed soon after excavation. The original film radiographs of objects that were found to be suffering from deep pitting corrosion (from Stone and Uley excavations) were digitised using a Radview digitiser and re-examined to determine any signs of the pits on excavation. A portable digital radiography system was used on freshly excavated archaeological iron to identify objects that were pitted under the corrosion layers. This analysis was also fundamental to assess the objects and allow the archaeologist to release objects for scientific analysis before the normal archaeological assessment process.

4.2.2.2.4 Thermo-magnetometry and thermo-gravimetry

In a few instances large enough samples were available for thermo-magnetometry and thermo-gravimetry. A number of nails from the Stonea excavation had been earmarked for disposal and thermo-magnetometry was carried out on these, as sample size was not an issue. Each nail was cut into several small pieces and the pieces analysed. One object, a coffin clamp from the 1978 Sutton Hoo excavation had a large amount of akaganeite on its surface. The initial analyses indicated this was relatively pure and it was further analysed as a KBr disc by FTIR and thermo-gravimetry. The wheels from Wetwang deteriorated to such an extent that samples were available. Samples were ground and analysed as described in 2.2.6 and 3.3.

4.2.2.5 Description of Recently Excavated Objects Corrosion layers

The corrosion layers and morphology on the recently examined objects were described using the system developed by Berthalon (2000). The system assigns each layer to a material type, the principal code. For each code the layers are numbered running in from the outside, i.e. CP1 is the outer corrosion product layer, CP2 the corrosion product layer inside CP1.

Type	Code	Cohesion	Adhesion	Colour	Morphology	Other Descriptors
Corrosion Products	CP	Y	Y	Y		
Soil	S	Y	Y	Y		granulometry
Deposit	D	Y	Y	Y	Y	Crystallinity
Metal	M			Y	Y	Magnetism
Corroded Metal	CM	Y	Y	Y	Y	
Void	V				Y	remnant structures, fossil structures
Non-metallic Material	NMM	Y	Y	Y		
Pseudomorphic Organic Material	POM	Y	Y	Y		

Table 4.1 Descriptive method for corrosion layers on archaeological metal artefacts after Berthalon (2000).

The colour of each corrosion layer was described with the Munsell notation with examination in strong sunlight (Munsell, 2009). The Munsell system seperates colour into hue, value (lightness) and chroma (colour purity) as perceptually uniform and independent dimensions

The corrosion products present in each layer were analysed with FTIR microscopy and Raman, Chapter 3.1.2 and 3.2. These techniques are non invasive and non destructive. They were found to yield a full identification of the materials present and could detect any changes in mineralogy.

4.2.2.3 Soil Analysis

Soil samples were extracted from a series of distances from the soil surface, accurately weighed and heated in an oven at 110ºC. The samples were reweighed and the water content calculated. The water soluble anion and cation concentrations of the soil samples were determined with ion chromatography. The extract concentrations were then converted to a weight percent based on the weight of the original dried soil sample. Three soil samples were kindly analysed by Tony Osborn of UCL Department of Earth Sciences as part of Nora Bartolomé Gutiérrez's MSc work. The samples were dissolved in concentrated nitric acid and the concentration of aluminium, calcium, copper, iron, potassium, manganese, phosphorous, lead and zinc analysed for with a Horoba JY Ultima 2C inductively coupled plasma – atomic emission spectrometer.

4.2.2.4 Air Analysis

The airborne concentration of carboxylic acids was analysed using diffusion tubes following the methodology developed by Gibson et al (Gibson et al., 1997a). The extracts from the tubes were analysed with ion chromatography.

4.2.2.6 Oxygen Depletion Measurements of Deterioration Rate.

Corrosion rates are often determined in industrial applications by measuring oxygen depletion (Shashoua and Matthiesen, 2010). The oxygen concentration is measured in a sealed container, if it drops, oxygen reduction is occurring as a cathodic reaction and the rate can be determined if the reaction is known. The method has been adopted for use with archaeological metals (Thickett, 2008c). The object was

acclimatised to 50% RH in an anoxic environment and then placed in sealed corrosion vessel with silica gel conditioned to 50% RH. The oxygen concentration was measured periodically over twenty two days with a Gas Sensor Solutions GSS450 oxygen sensor. The amount of akaganeite generated was calculated from Turgoose's equation (Turgoose, 1982a)

$$4Fe^{2+} + O_2 + 6H_2O \rightarrow 4FeOOH + 8H^+ \qquad (4.1)$$

4.3 Results and Discussion

4.3.1 Freshly Excavated Objects

Of the nine iron artefacts examined with portable radiography, six showed evidence of sub surface pits and two were analysed. Holes were drilled into several potential pits located from the radiographs. The ambient RH in the laboratory during the analyses was 56-64%. Pale yellow crystals were observed with microscopy at the bases of the pits on the magnetite layer. Analysis with confocal Raman spectroscopy identified these as ferrous chloride. After a few days the edges of the crystals turned brown, analysed as ferric chloride and eventually this expanded to cover the crystals and converted to akaganeite. Figure 4.1 shows the Raman spectra of the two species.

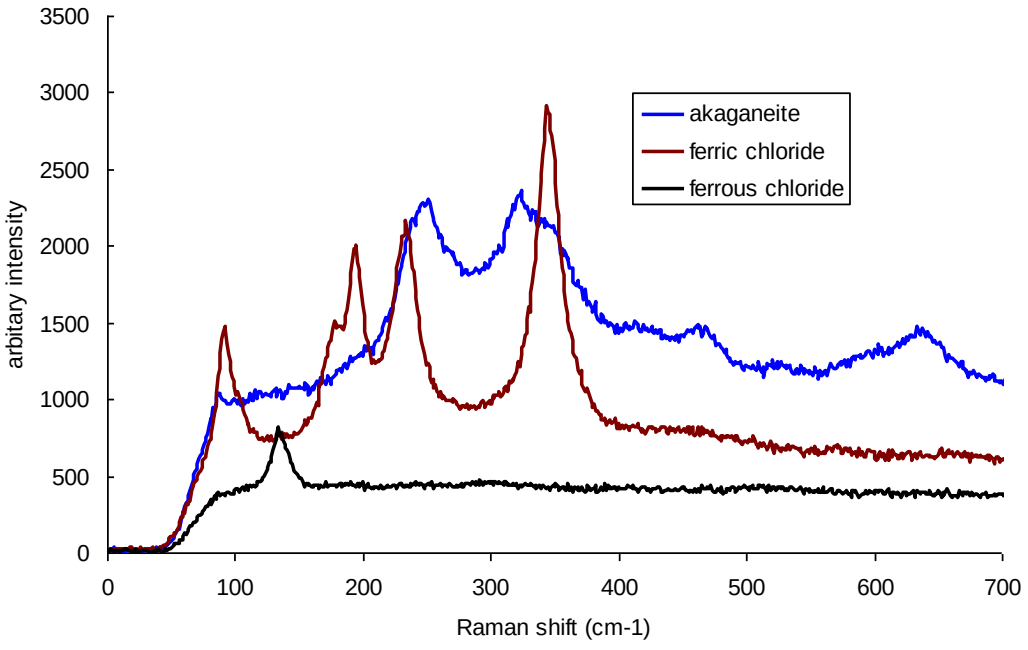

Figure 4.1 Raman spectra of species initially present in pits and formed over a few days on exposure to air.

4.3.2 Recently Excavated Objects

The corrosion layers and morphogy on the objects were described using the system developed by Berthalon (2000). A representative object from the Sutton Hoo site is shown in Figure 4.2 and the description and analyses of the corrosion layers shown in Table 4.2.

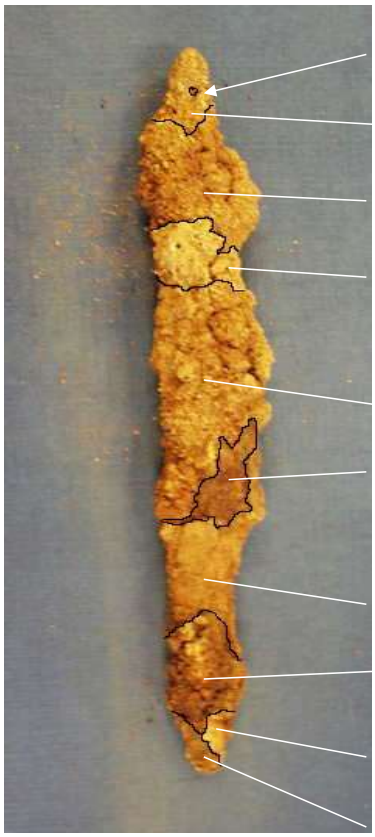

Figure 4.2: Description of corrosion morphology of typical Sutton Hoo object.

Layer	Location	Colour Description, Munsell value	Description	Identification with FTIR microscope and Raman
Soil 1 S1	Mainly above CP3, sometimes above CP2, no CP3 over	Very pale brown, 10YR 8/4	Loosely adherent fine aggregate	Quartz, kaolinite, + some lepidocrite
Deposit 1, D1	On CP3	Very dark grey, 7.5YR N3/	Adherent granular aggregate	Magnetite
Corrosion Product 3 CP3	Over CP1	Reddish yellow, 7.5YR 6/6	Loosely adherent, very fine dusty aggregate over vitreous quartz crystals	Quartz + lepidocrite
Corrosion Product 2 CP2	Over CP1	Reddish yellow, 7.5YR 6/8	As CP2, more iron present	goethite + quartz
Corrosion Product 1 CP1	Over M1	Strong brown, 7.5YR 5/6	Loosely adhrerent powderish	Goethite
Metallic 1 M1	Above metal core	Very dark grey, 7.5YR N3/	Adherent Submetallic, sparse globular blisters	Magnetite goethite

Table 4.2 Corrosion description for Sutton Hoo objects.

Very small iron corrosion crystals were intimately adhered to the large quartz crystals concreted over some of the object surfaces in the corrosion product layers, CP2 and CP3. The granules were identified as quartz by direct FTIR microscopy. No absorptions beyond those reported for quartz could be observed by direct microscopy or with the attenuated toal reflectance microscope heads (silicon and germanium). The extremely small size of these crystals (less than 3µm) and the large amount of quartz present made both FTIR and XRD analysis impossible, as these techniques are insensitive to low concentrations of phases. Physical removal could not be achieved and any chemical removal could have converted or destroyed the iron corrosion products. SEM-EDX indicated an iron and oxygen based corrosion product with the iron to oxide ratio comparative to Goethite or lepidocrite (akaganeite was not feasible as no chlorine was detected). Raman micro-spectroscopy identified the material although care had to be taken with the laser power as this was prone to convert to mpaghemite due to heating (Robinet and Thickett, 2005). The presence of the quartz in intimate contact with the iron corrosion product probably exacerbated this effect with the low thermal conductivity of the quartz increasing the heating effect.

Small hollow blisters (less than 0.5mm in diameter) were observed on several of the objects. A typical example is shown in Figure 4.3.

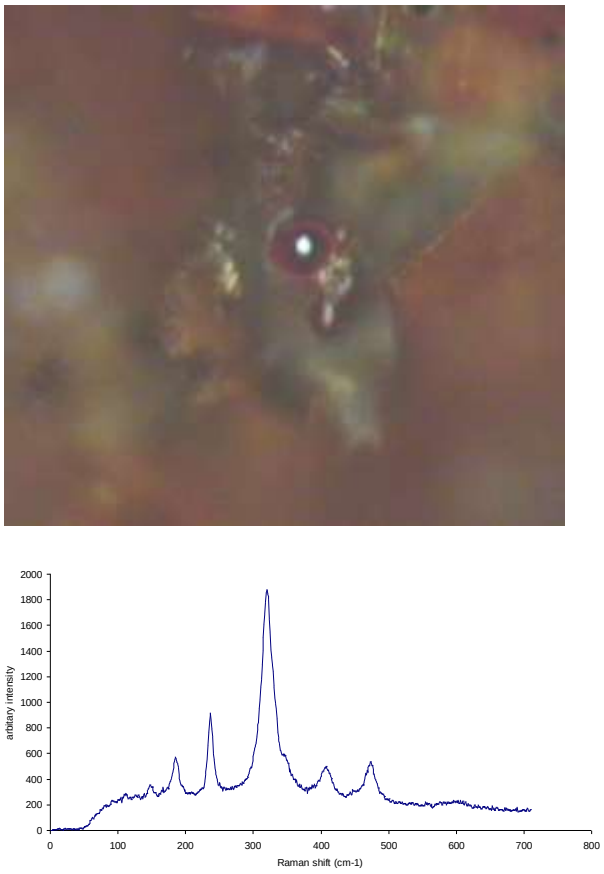

Figure 4.3: Blister found on Sutton Hoo material, field of view is 1mm. Raman spectrum from blister identified Goethite.

The blisters have most likely formed from a solution. Such a mechanism was described by Selwyn et al (Selwyn et al, 1999). The small scale of the blisters and their very thin walls made removing sufficient sample for FTIR analysis, impossible, even when using the more sensitive silicon attenuated total reflectance, ATR head on the microscope. Raman microscopy identified the wall material on some blisters as goethite (bands at 243, 299, 385, 479, 550, 685 and 993cm^{-1}), and on others as akaganeite (311, 393, 494, 535, 721, 920cm^{-1}). The grey, black layer on which the blisters all formed as magnetite (bands at 301, 533 and 662 cm^{-1}). Examination by SEM-EDX confirmed these analyses with iron and oxygen being detected in the blister wall material and a lower ratio of oxygen being present with the iron in the grey/black layer consistent with Fe_3O_4. Selwyn reported similar blisters to be formed of lepidocrite, although the objects had been exposed to very

high relative humidity values to encourage blister formation (Selwyn et al, 1999). Several white or colourless crystals were found to be associated with the blisters and a cluster of crystals was often observed inside the blister. Raman identified many of the crystals as quartz (bands at 128, 208 and 465cm^{-1}), but a significant number produced no spectrum. Silicon and oxygen were detected in some, but not all of the crystals. Several of the crystals were found to contain sodium and chlorine and are most likely sodium chloride. This material is Raman inactive.

The soluble ion contents of the Sutton Hoo soil samples are shown in Table 4.3.

Depth below surface (cm)	Ion Concentration (% wt/wt)								
	Sodium	Ammonium	Potassium	Magnesium	Calcium	chloride	Nitrate	Phosphate	Sulfate
0-33	0.0041	0.008	Bd	Bd	Bd	0.0085	Bd	0.0075	0.0151
33-66	0.0035	0.0101	0.0006	0.0003	0.0033	Bd	Bd	Bd	0.0001
66-100	0.0046	0.0101	0.0012	0.0009	0.0072	0.0065	Bd	0.0088	0.014
100-133	0.0046	0.008	0.0008	0.0007	0.0072	0.0058	Bd	0.0119	0.014
133-166	0.0053	0.007	0.0007	0.0007	0.0066	0.0057	Bd	0.009	0.0095
166-200	0.0056	0.0112	0.0013	0.0012	0.0099	0.0048	Bd	0.006	0.0077

Bd below detection limit

Table 4.3 Soluble ion concentrations from large soil samples from Sutton Hoo excavation.

The soil samples contained chloride, phosphate and sulfate as the major anions, with sodium and calcium as the major cations. The chloride concentrations are not particularly high. The high concentration of chloride detected in the akaganeite blisters shows the concentration that occurs during the corrosion process (Turgoose, 1984). Phosphate is likely to have originated from the burial context.

The ICP-AES results are shown in Table 4.4.

	amount (g/g)					
	Sutton Hoo 0-1m		Sutton Hoo 1-2m		Wetwang	
Element	amount	SD	amount	SD	amount	SD
Al	0.001034	0.000199	0.001227	0.000128	0.009688	0.000097
Ca	0.00092	0.000104	0.000791	0.000131	0.007705	0.000933
Cu	bd	0.000017	bd	0.000031	bd	0.000008
Fe	0.009428	0.002705	0.012357	0.004134	0.027891	0.005084
K	0.000019	0.000076	0.000152	0.000041	0.000694	0.000011
Mn	0.000066	0.000044	0.000066	0.000037	0.001129	0.000027
P	0.000293	6.34E-05	0.000363	0.000104	0.000685	3.16E-05
Pb	bd	2.31E-05	bd	1.01E-05	bd	5.51E-06
Zn	1.03E-05	6.8E-06	8.29E-06	8.37E-06	4.53E-05	8.65E-06

Table 4.4 Elemental analysis of three soil samples by ICP-AES.

The low concentrations of the elements detected is consistent with the mainly quartz composition of the Sutton Hoo soil. The iron concentration is elevated due to the Goethite crystals on the quartz crystal surfaces.

The Wetwang material had a different corrosion structure to that from Sutton Hoo. The soil was much finer and contained a considerable amount of a kaolinite clay, identified from its characteristic hydroxyl absorption bands at 3697 and 3620 cm^{-1} in the infrared and much less quartz. Aluminium and calcium were elevated due to the clay and there was some iron due to the close proximity of the sample to a corroding

object. Many of the objects were much more corroded with less iron remaining as observed in break sections in the objects and radiographs. The corrosion layer description is shown in Table 4.5.

Layer	Location	Colour Description, Munsell value	Description	Identification
CP3/S	Fine layer over CP1	Reddish yellow, 10YR 7/6	As CP2, more iron present	goethite + kaolinite
CP2	Over M1	Dark reddish brown 5YR 3/3	Loosely adhrerent powderish	Goethite
M1		Very dark grey, 7.5YR N3/	Adherent Submetallic	magnetite
V			Void	
CP1		Very dark grey, 7.5YR N3/	Thin, lamella strips, possibly contains metal core	magnetite and goethite

Table 4.5 Corrosion description for Wetwang objects.

Sample	Ion Concentration (% wt/wt)			
	Chloride	Nitrate	Phosphate	Sulfate
wheel soil 10ml	0.053	0.016	0.020	0.079
wheel soil above metal	0.060	0.009	0.033	0.034
Wsoil	0.104	0.048	0.024	0.530
Wsoil2	0.757	0.107	<0.050	0.408
TS4	0.080	0.014	0.074	0.043
TS1	0.043	<0.050	<0.050	0.055
TS2	0.222	0.058	0.339	0.180
332AS	0.056	<0.050	<0.050	0.072
332AN	0.054	0.028	0.043	0.042

Precision is 1% of value quoted.

Table 4.6 Soluble ion contents from small soil samples removed from Wetwang objects.

The very small sample sizes may not be representative of the material as the samples were from soil adhering to the objects. Again chloride and sulfate were the major anions present in the Wetwang soil samples. The sulfate concentration was again higher than the chloride. Significant phosphate was also detected in the Wetwang soil. This almost certainly originated from the body or offering of pork present in the grave (Hill, 2001; Hill, 2002). The amount of phosphate was found to correlate reasonably well with an objects' position in the grave, the body was found at the southern end and phosphate concentrations reduced towards the north. Low concentrations of nitrate were also detected.

The Wetwang wheel fragments continued to crumble for 3 years after excavation. The deterioration rate was determined by oxygen depletion (Thickett, 2008c), through measuring the oxygen concentration in a sealed container. One piece of the wheel was acclimatised to 50% RH in an anoxic environment and then placed in sealed corrosion vessel with silica gel conditioned to 50% RH. The pieces were placed in a 1000ml glass corrosion jar with Escal film clamped over the top opening. Self adhesive VICAL seals were placed over the centre of the Escal to allow sampling of the 5ml of the air within the jar with a Mapcheck oxygen meter. Representative results of six readings taken over three weeks are shown in Figure 4.4.

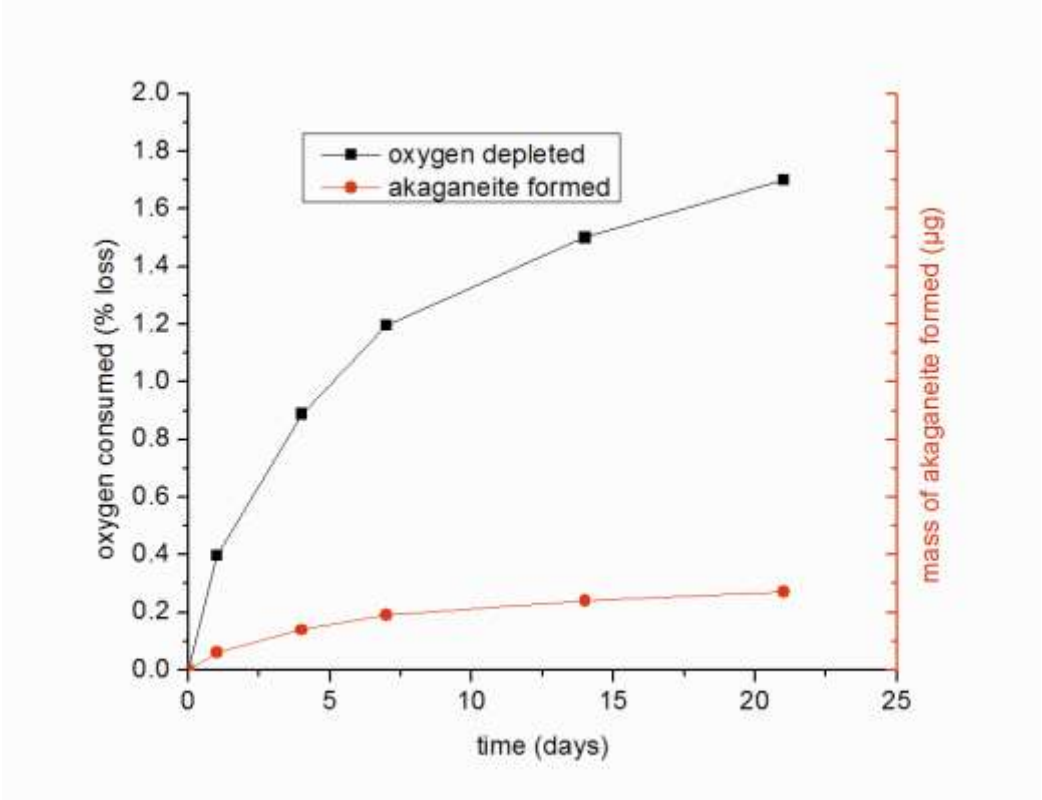

Figure 4.4 Oxygen Consumption of Wetwang wheel fragment.

As can be seen in Figure 4.4 the oxygen concentration reduces dramatically over this period. The mass of akaganeite produced from this oxygen was calculated assuming equation 4.1 holds true and oxygen reduction is the only cathodic reaction occurring. After fourteen days acclimatisation to 50% RH the mass of the wheel fragment was 80.72g, after the oxygen depletion test this had risen to 80.98g, an increase of 0.26g. This compared favourably with the calculated amount of akaganeite formed from equation 4.1, 0.26g.

The ethanoic acid concentrations measured in the storage boxes ranged from 1127 to 1865µgm^{-3}. The methanoic acid was much lower ranging between 47 and 270 µgm^{-3}. The methanoic acid emission rate from wood is below 15% of that for ethanoic acid for most wood species (Arnie and Cochrane, 1966; Gibson, 2010).

Representative Thermo-magnetometry and thermo-gravimetry analyses from the wheels are shown in Figure 4.5.

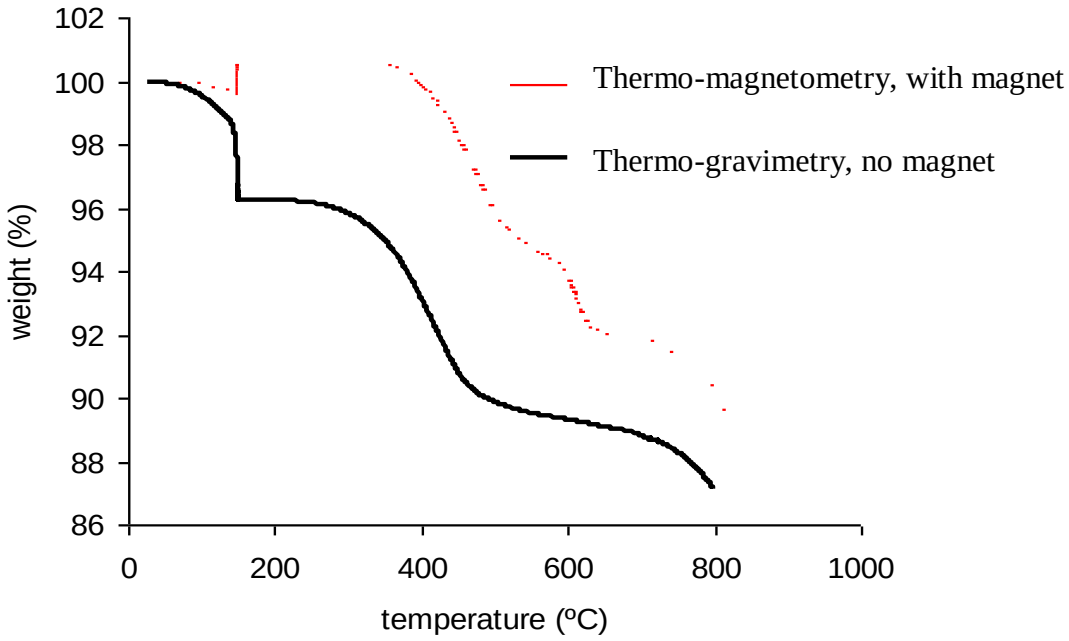

Figure 4.5 thermo-gravimetry and thermo-magnetometry of samples from the Wetwang wheels.

A large amount of magnetite was indicated by the large apparent weight loss at 580ºC. This effect was not observed with TGA because it is caused by a magnetic transition. Aside from water, two other weight losses were observed, one occurring between 400 and 500ºC, and the other 650 and 800ºC on both TM and TGA. These were tentatively assigned to iron carbonate (siderite) and calcium carbonate (calcite), respectively. Large amounts of carbon dioxide were evolved by two thermal events. The identifications were verified with FTIR spectroscopy. Absorption bands characteristic of both the calcium carbonate (1796, 1422, 874 and 744cm^{-1}) and iron carbonate (1810, 1414, 866 and 712 cm^{-1}) were observed, confirming the presence of these materials, see below.

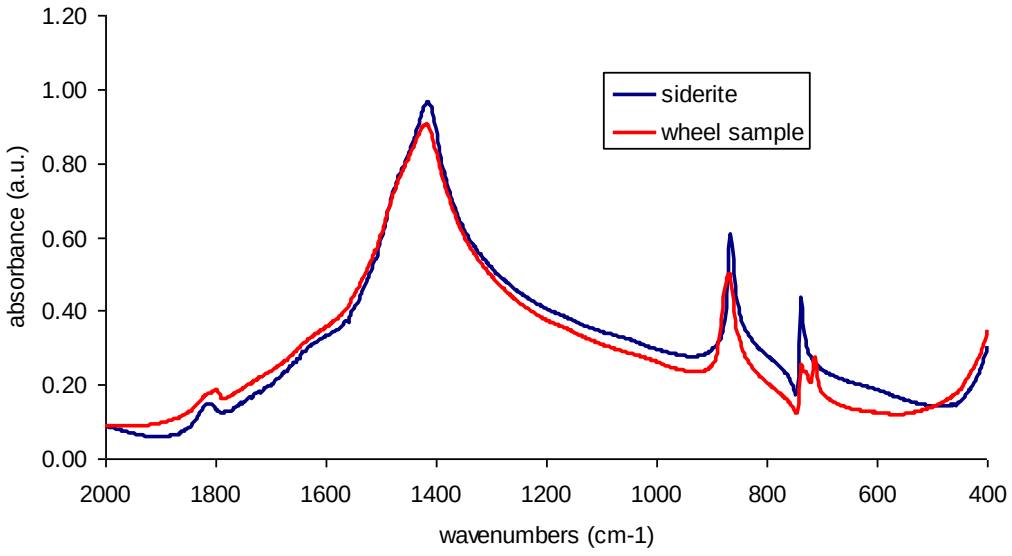

Figure 4.6 Infrared spectrum of sample from Wetwang wheel (red) and standard spectrum for siderite (blue), additional absorption bands at 744 and 1796 (shoulder) cm^{-1} are due to the presence of calcite.

Magnetite was confirmed by the presence of peaks at 308, 542 and 667 cm^{-1} with Raman spectroscopy. Elemental iron was detected with thermo-magnetometry, in

only one of the six samples and occurred as a very thin sheet in the centre of the void. Radiography showed this was localised to one very small (less than 1cm) portion of the tyres.

It would appear that the tyres were at the very end of the mineralisation process when excavated. Despite this they underwent rapid physical deterioration, with akaganeite forming in the central void and splitting them apart. The burial was discovered with a metal detector and it appears that the magnetic component detected was the magnetite.

One of the terrets was displayed in a showcase with RH values ranging between 35 and 52%. Within six weeks deterioration was observed with akaganeite crystals. The ethanoic acid concentration in the showcase was 560 μgm^{-3} and the methanoic acid concentration 87 μgm^{-3}. The other terret was stored in dry silica gel, nominally at 5% and exhibited no visible deterioration.

4.3.1.3 Deteriorating Objects

Analytical results from the over two hundred examples of deteriorating archaeological iron are shown in Figure 4.7 and Table 4.6.

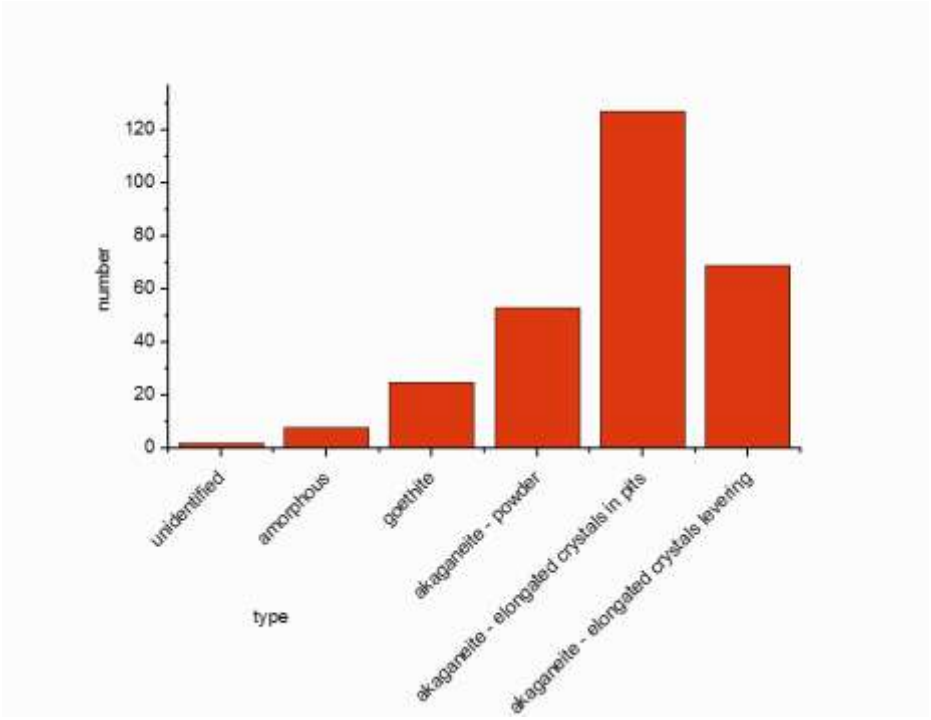

Figure 4.7 Numbers of samples from deterioration centres of archaeological iron artefacts analysed by FTIR.

Akaganeite appears to be instrumental in 85% (242/284) of the instances of deterioration observed. A typical spectrum is shown below.

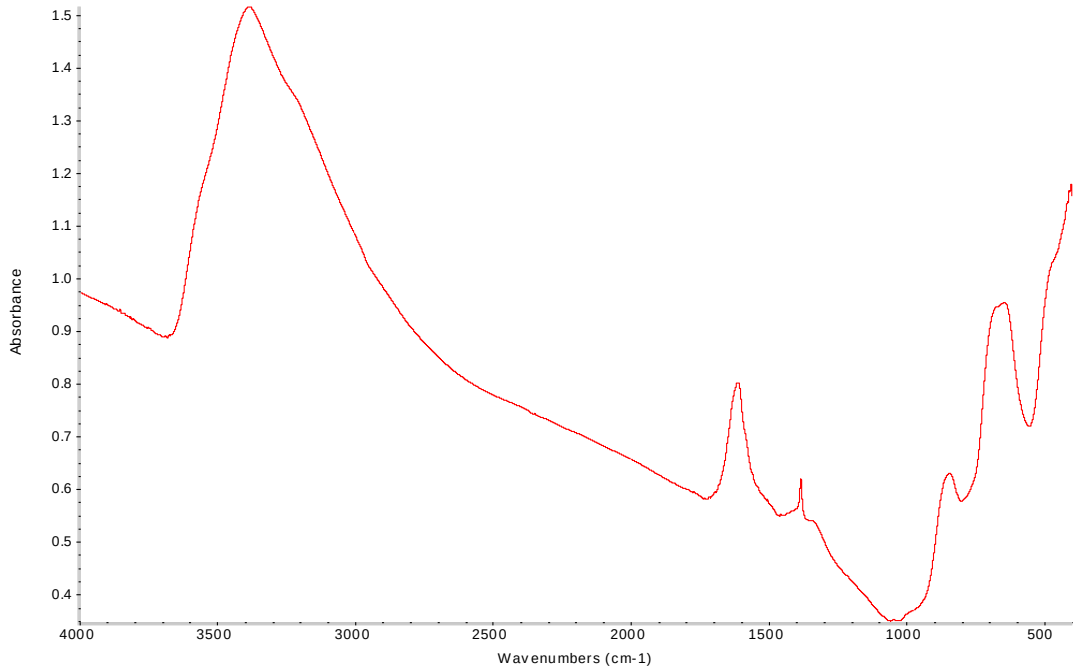

Figure 4.8 Infrared spectrum of akaganeite from deteriorating Uley object.

Goethite was detected when powdering was observed.

Major Corrosion Product	Detected on proportion of objects analysed	Associated Species (proportion present in instances identified / % of instances)						
		Amorphous visible in FTIR	Amorphous by extraction	Goethite	Lepidocrite	Magnetite	Copper	Organic
Unidentified	0.5%	81	100	100		100		100
Amorphous	2.5%	100	100	40	20	100	20	60
Goethite (all powder)	8.5%	41	100	59	41	94	29	94
Akaganeite (powder)	18.5%	52	97	56	21	97	35	75
Akaganeite (elongated crystals – pits)	46%	31	92	57	19	97	41	81
Akaganeite (elongated crystals – levering)	24%	47	96	60	36	96	28	84

Two figures are given for the amorphous material. When large amounts are present and it is visible in FTIR (identified from spectra given by Raman et al (1991)) and when smaller amounts are present and it is only detected after extraction with sodium hydroxide.

Table 4.7 Compounds detected in close association with the main corrosion products on deteriorating archaeological iron artefacts analysed with FTIR, Raman and SEM-EDX.

A wide range of other iron corrosion products , copper ions and organic material was detected in near association with the akaganeite. Many of these materials are reported to affect the oxidation of Fe(II) ions or the crystallisation of akaganeite (Ishikawa et al, 2001; Pullin and Cabaniss, 2003; Ishikawa et al, 1998). Magnetite and amorphous iron corrosion products (detected by extraction) and organic material were present in almost all cases. The common occurrence of amorphous corrosion products has not been commented on by previous authors, this is likely due to the widespread use of X-ray diffraction which cannot detect these materials and Raman spectroscopy which has limited sensitivity towards amorphous materials (Raman et el, 1991). Goethite and lepidocrite were commonly found around akaganeite crystals. The formation mechanisms often give different polymorphs depending on the exact local conditions (especially pH, eH and chloride concentration (Pourbaix, 1977). Akaganeite appears to occur at corrosion centres whereas Goethite or lepidocrite occur when conditions are not as acidic or the chloride concentration is reduced. No ferrous oxy chloride was detected in any sample. This compound is readily identified with XRD and Raman (which was undertaken on over 180 of the samples). No infra-red spectrum has been published to date. Its very high chloride content (17.9%) would be expected to allow it to be discriminated from akaganeite by back scattered electron imaging with SEM-EDX. The back scattered electron imaging parameters were adjusted for all the grain mounts of iron corrosion products using two samples of akaganeite as standards, one with 7.2% chloride, one with 13.8% chloride. The parameters were adjusted to discriminate these two samples. It is likely that any areas of samples with chloride contents over 20%, such as ferrous oxychloride would be observed. Any samples with apparently higher chloride concentration areas were mapped for chlorine and Raman analysis undertaken on the high chloride areas.

The chloride concentrations of the akaganeite samples determined by SEM-EDX are shown in Figure 4.9.

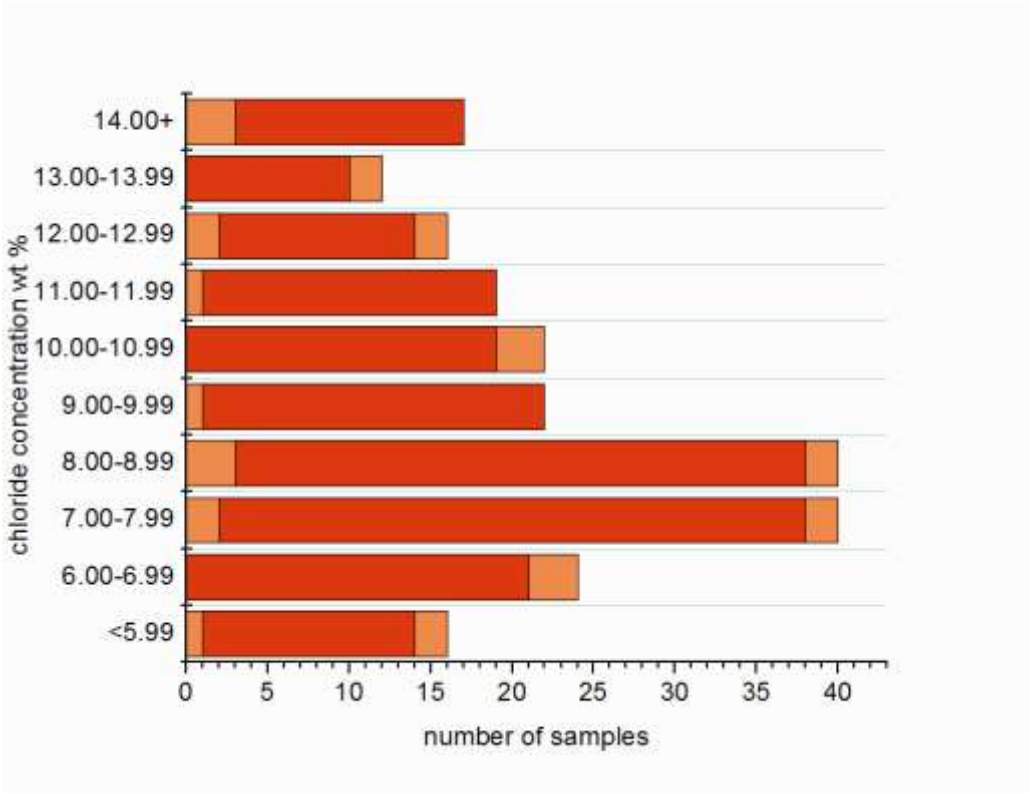

Orange coloured bars indicate number of samples within analytical error of the chloride concentration band above (right hand side) or below (left hand side)

Figure 4.9 Chloride content in akaganeite crystals analysed on deteriorating archaeological iron objects.

Most of the samples analysed had higher chloride concentrations than that determined by Stahl et al in the latest refinement of the akaganeite formula, $FeO_{0.833}(OH)_{1.167}Cl_{0.167}$ which is equivalent to 6.23% mass percent (Stahl et al., 2003). This is probably due to chloride adsorbed on the surface of the akaganeite in the manner postulated by Al-Zahrani (1999) and characterised by Regeura et al (2005, 2006). Twelve samples had lower concentrations of chloride, which is probably due to the sample contained iron minerals other than akaganeite. None of the chloride contents approached the 17.9% value found for beta iron hydroxyl chloride (Reguer et al, 2006).

4.3.1.3.1 Pitting

The presence of deep pitting corrosion was characteristic of many of the deteriorating objects examined. Radiographs taken very soon after excavation in

1974 for the Stonea and Uley material were re-examined to determine any evidence of these pits. Features could be discerned in the radiographs after digitisation and manipulation, Figure 4.10 (Lang and Middleton, 1997; Clogg and Caple, 1996). These features corresponded with the position and shape of the pits observed after the corrosion layer was fractured off. The features could not be determined by visual examination of the original film radiographs. Radiographs have high optical densities and often low contrast, the Radview digitiser ued is a 14 bit system producing 16384 grey scales, whilst the human eye can distinguish on average between 60 and 90. In the digitized radiograph the darker areas indicate more dense material (residual iron and the dense product layer) or thicker material. The paler areas are voids or in this case pits below the corroded surface.

Examination with optical microscopy and Raman spectroscopy indicated that the magnetite layer was not homogeneous and contained a large proportion of other iron corrosion products. Two small, unimportant surface flakes were mounted as horizontal sections in epoxy resin, to allow closer examination of this effect with SEM-EDX and Raman. The brown orange areas were found to be akaganeite and SEM-EDX analysis indicated the presence of significant concentrations of chlorine, above 7%, almost certainly chloride within these areas. The akaganeite was intimately mixed with the magnetite and under low magnification the mixture has a pale grey/black colour which is easily mistaken for pure magnetite.

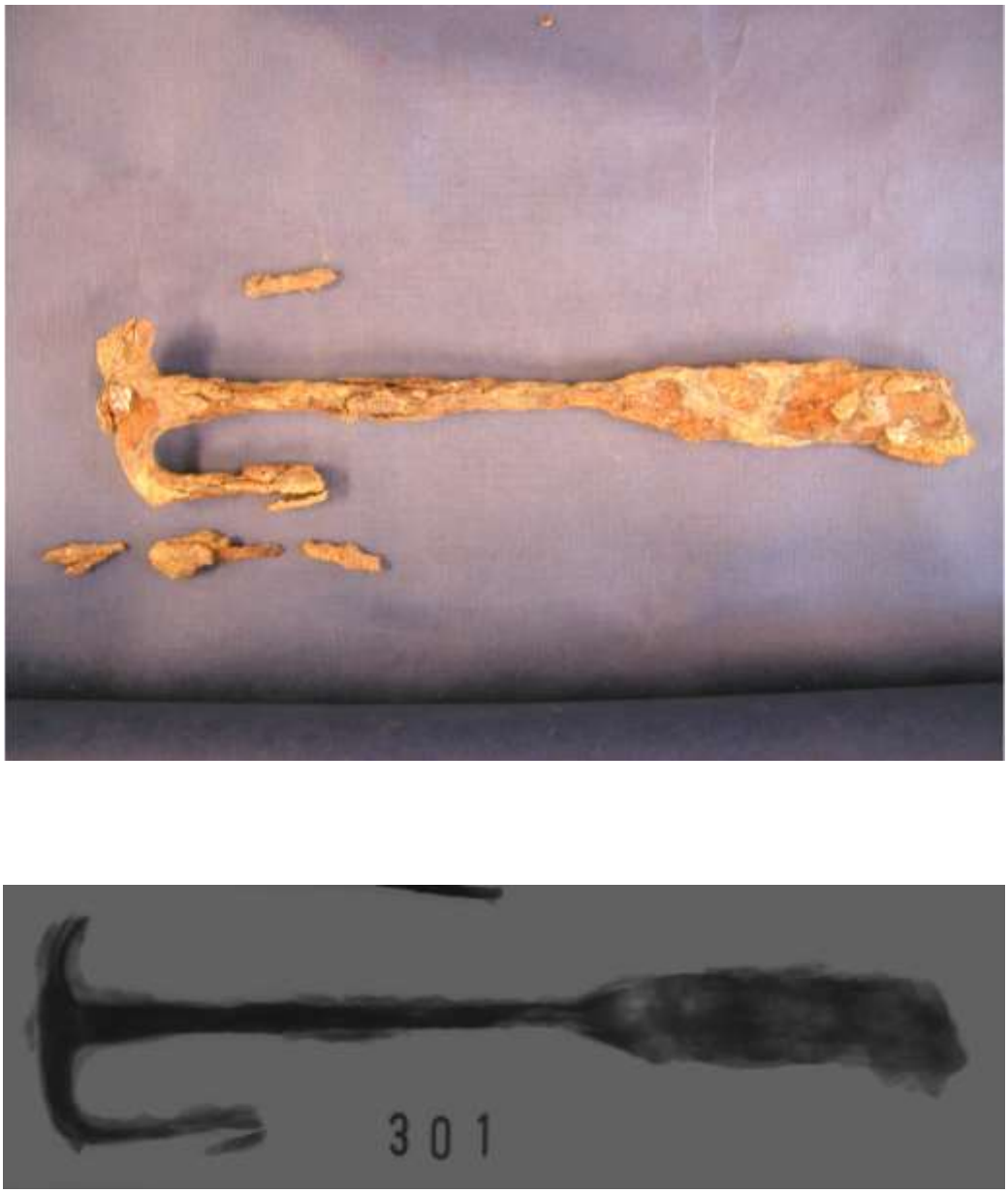

Figure 4.10 Radiograph and object from Stonea, Pits in object became obvious upon deterioration with covering material levered off. The pits are visible on the radiograph taken soon after excavation in 1974, after digital processing.

4.3.1.3.2 Thermo-magnetometry of Stonea nails

Results of a representative Stonea nail Thermo-magnetometry analysis are shown in Figure 4.11.

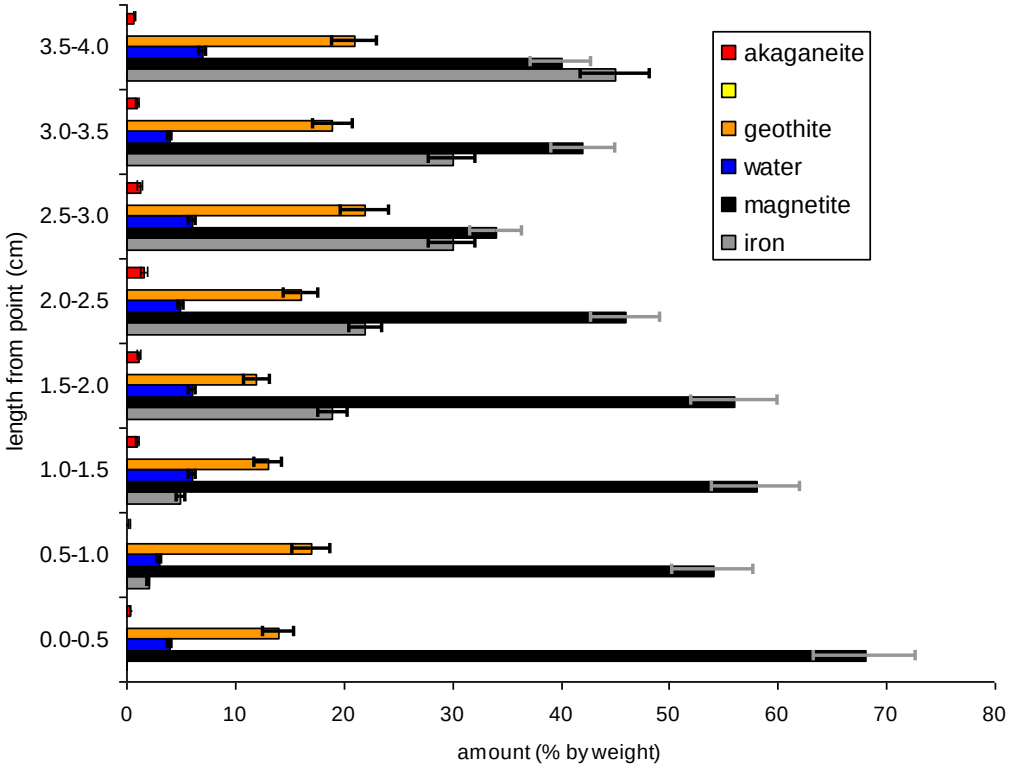

Figure 4.11 Analysis of species present in nail from Stonea by thermo-magenometry.

The composition is very variable through the length of the nail, with the tip totally mineralised. Akaganeite is only present in a small proportion (less than 1.6% by weight).

4.3.1.3.3 Surface Layers on akaganeite

Many of the orange/brown akaganeite crystals examined from the old Portchester Castle displays, the Stonea and Ulea and Lullingstone materials from storage were observed to have fine, pale yellow crystals forming at their edges, Figure 4.12.

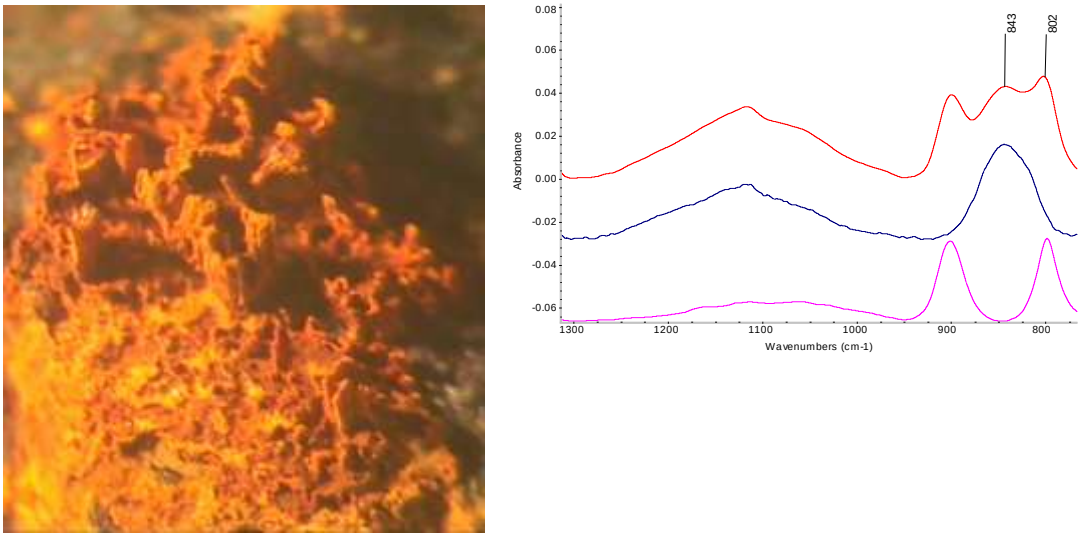

Figure 4.12 Pale yellow layer on top of akaganeite crystals, field of view is 0.3mm. FTIR spectrum by germanium ATR is on red spectrum upper (from the pale yellow layer, blue spectrum (middle) is standard of akaganeite, purple spectrum (lower) is standard of Goethite.

Raman micro-spectroscopy could not distinguish these crystals from the akaganeite that they overlay, probably due to their extremely small size. The information depth of the confocal system depends on the lens used and the diameter of the confocal hole, but the minimum is 2.8µm with the maximum magnification lense (x100) and the hole set to 100µm. Identifiable spectra could not be obtained with smaller confocal hole settings, even with very long collection times. The FTIR spectra of the orange areas were consistent with akaganeite with bands and 742, 894 and 3522cm^{-1}, and no differences could be detected in the yellow edge areas using direct reflectance. However when the ATR heads were used on surface mounted crystals, absorptions due to goethite (670, 798, 902, 1141, 1665, 1803, 3126cm^{-1}) were also observed in addition to those expected from akaganeite. These absorptions appeared more strongly when using the zinc selenide ATR crystal compared to a silicon ATR crystal. Iron, oxygen and chlorine were detected in the orange brown areas, whereas a much lower chlorine concentration was detected in the yellow areas. The Portchester display was unusual in that calibrated temperature and relative humidity monitoring records exist for its full fifteen years. The silica gel in the cases was changed every six months and this results in the characteristic pattern of RH dropping to 10% when the gel is changed and slowly rising over the next six months.

There was no environmental data available for the Stonea, Uley or Lullingstone storage areas.

The average maximum RH values from the fifteen years (thirty values from every 6 months) are shown for the three cases with iron in Table 4.8. Results of the ethanoic and methanoic acid diffusion tube analyses are also included. The analyses were undertaken over the summer period when high temperatures promote off-gassing from the chipboard showcase construction. The measurements were taken over a two week period just before the silica gel was changed when the chipboard was exposed to the highest RH, as higher RHs also promote off-gassing (Thickett, 1998b).

Case	Object	RH maxima	Case dimensions (m) width x depth x height	Carboxylic Acid Concentration μgm^{-3}	
				Ethanoic	Methanoic
Roman	Arrowhead 1	29-35	1.0 x 0.4 x 1.3	1189 $\pm$ 64	124 $\pm$ 26
	Arrowhead 2				
	Arrowhead 3				
Saxon	Purse mount	46-51	0.5 x 0.3 x 0.5	1835 $\pm$ 87	206 $\pm$ 31
Medieval	Bolt	25-31	1.0 x 0.4 x 1.3	1243 $\pm$ 64	128 $\pm$ 26
	Pliers				

Table 4.8 Environmental parameters for showcases displaying Portchester objects where Akaganeite conversion was detected .

The Saxon case experienced higher maximum RH values due to its higher air exchange rate. More of the akaganeite appeared to have converted in the fifteen years on display. The ethanoic acid concentration was also higher in this case than the others, probably due to a higher surface area to volume ratio of chipboard being

present. These higher acid concentrations may also be the cause of the thicker conversion layers. The Roman and Medieval cases appeared to behave similarly, the conversion layers in the Roman case appear to be slightly thicker. That may be related to higher RH values, as the acid concentration was slightly lower.

Similar Goethite conversion layers were observed on objects from storage from the Stonea, Uley and Lullingstone sites. All of these materials were stored in cardboard boxes, which would be expected to generate ethanoic acid atmospheres at least as concentrated as those inside the Portchester showcases. No environmental monitoring had been undertaken in the storage areas. The objects were stored in cardboard boxes, as was common practice at the time of their excavation in the early 1970s. Spot RH measurements with data-loggers placed quickly inside the boxes, yielded an RH that was probably the average of that experienced over the past thirty days or so due to the buffering of the cardboard. However, unconditioned buildings often suffer a wide annual cycle of both temperature and RH, hence the last month's average may not be representative. Monitoring data for an adjacent room was also kindly supplied by the Victoria and Albert Museum, who share the storage facility. Unfortunately room conditions can vary widely due to differences in building fabric, building services, ventilation and aspect. Temperatures tend to be less variable than RHs and in these rooms the maximum temperatures reach 24-31°C in late summer. This is generally accompanied by the maximum RHs experienced.

4.3.1.3.4 Further analyses of akaganeite from Sutton Hoo coffin clamp

Results of the infrared of the sample are shown in Figure 4.13.

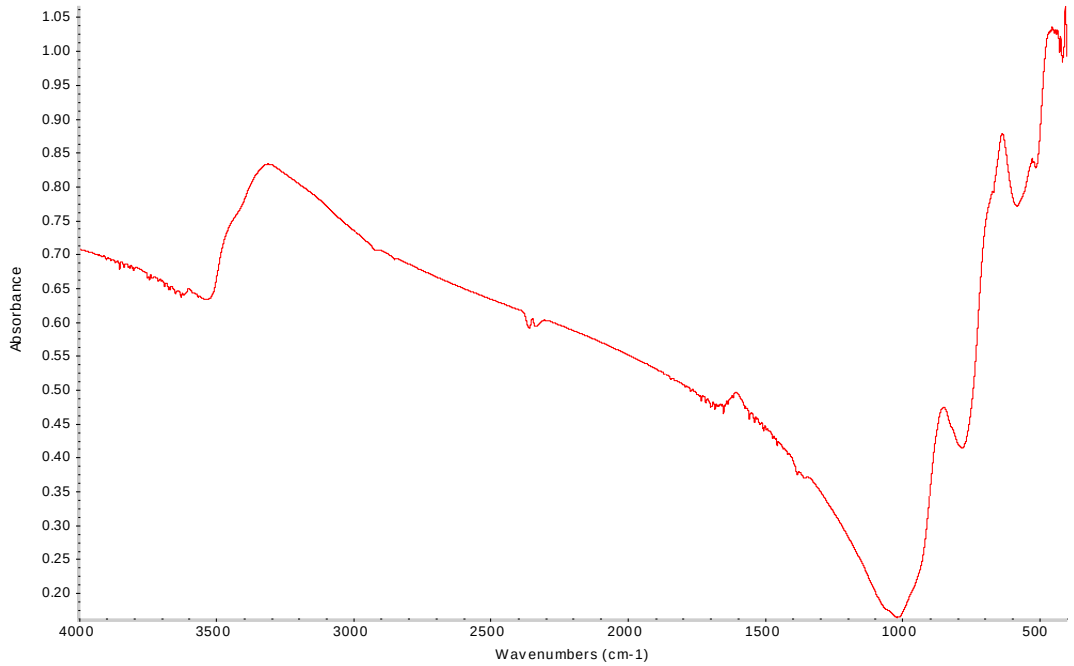

Figure 4.13 Infrared spectrum (KBr disc) of akaganeite from Sutton Hoo coffin clamp.

The absorptions match published analyses for akaganeite (Murad and Bishop, 2000; Raman et al, 1991). The therrmogravimetry analysis is shown in Figure 4.14.

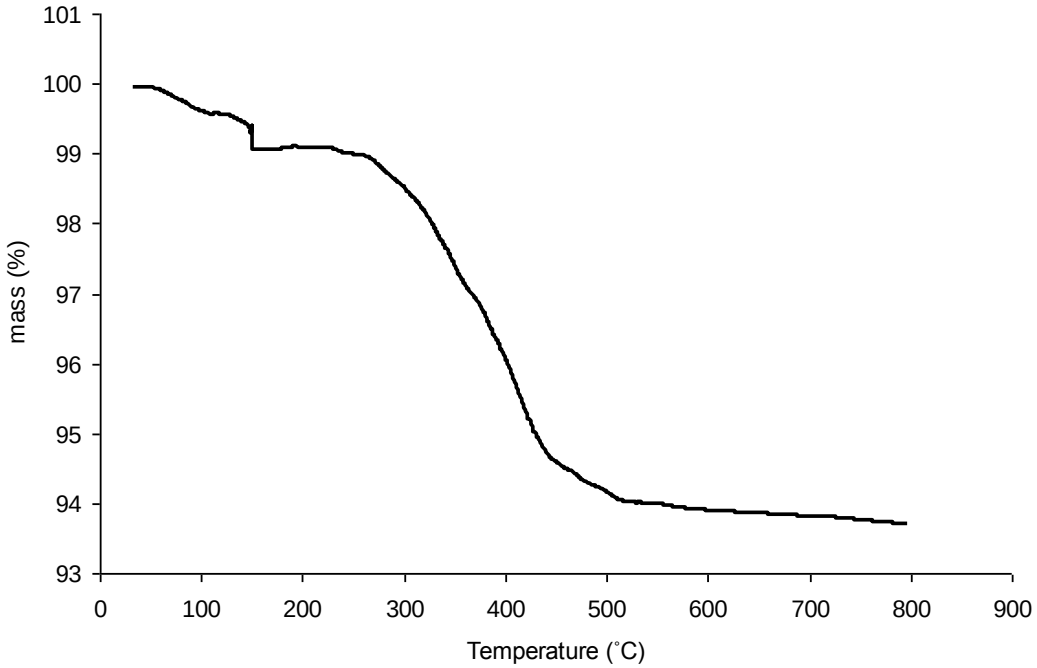

Figure 4.14 Thermo-magnetometry of akaganeite sample from Sutton Hoo coffin clamp. Drop in mass at 150ºC is water desorbing during 2 minute isotherm.

The sample had a large amount of adsorbed water, which was lost on heating to and holding at 150ºC. The total mass loss due to water was 1.9%. There was a major mass loss between 230 and 430ºC with an apparent inflection in the mass loss curve around 380 ºC. The thermo-magnetometry trace was almost identical to the TGA. There was no mass increase when the magnet was applied, indicating that no elemental iron, magnetite or hematite was present in the sample.

4.4 Discussion and Conclusions

Akaganeite has been confirmed as the major corrosion product associated with deterioration of the iron. Different morphologies were observed, with the elongated crystals caused more damage than the powder. Many of the akaganeite crystals analysed appeared to have excess chloride adsorbed on their surfaces. Goethite also appears to be an important corrosion product linked with deterioration.

Archaeological iron contains significant levels of impurities, some of which are reported to affect the oxidation and hydrolysis reactions of ferrous chloride. Three species that are reported to affect ferrous oxidation and akaganeite crystallisation were detected in close proximity to the akaganeite. Their affect on the akaganeite formation reactions will be investigated under the conditions found in archaeological iron in Chapter 5.

There is some evidence of conversion of akaganeite to goethite on archaeological iron. This phenomena has not been observed previously on archaeological iron. This appears to be a slow process, with only minimal transformation after fifteen years. The extremely thin layers detected explain the reported stability of akaganeite as they would by invisible to bulk analytical methods such as XRD previously used in this area. The conversion to goethite was often associated with high ethanoic acid levels. Investigations into these processes will be reported in Chapter 6. The study of possible conversions of akaganeite was highlighted by Selwyn as an important area for further research (Selwyn, 2004).

A magnetite layer mixed with akaganeite was identified on the Stonea and Uley objects. This has not been reported previously. Dillman has reported magnetite mixed with Goethite, maghemite and β $Fe_2(OH)_3Cl$, but not akaganeite (Neff et al, 2005; Reguer et al, 2005, 2007). Blister walls were also identified as akaganeite.

There was no visible deterioration of the recently excavated material when it was kept in dry storage. The objects under ambient relative humidities deteriorated and akaganeite was associated with this process. The continuing deterioration of the Wetwang wheel is of particular interest as there appears to be no elemental iron present in the object. This behaviour appears to contradict the theory that only objects with remaining metal core should deteriorate (Watkinson, 1992). It is possible that the wheel fragments were at the very end of their mineralisation and some iron remained in solution inside the voids at the centre of the object or in the porosity of the corrosion products. Taking the average corrosion rate figure of

4μm/year derived by Saheb et al (2008), this would equate to 7.6mm of corrosion since the late 1st century AD, which is in reasonable agreement with the objects thickness. Such an analysis would seem reasonable for this site as it did not show pitting corrosion, which would invalidate such an approach.

The analysis of freshly excavated iron identified ferrous chloride in the bottom of pits. On exposure to air this oxidised to ferric chloride and then converted to akaganeite. This confirms that the theory postulated by Turgoose (1982a) that ferrous chloride is formed on drying near the metal interface. It shows that the iron and ferrous chloride mixtures first used by Turgoose and then Watkinson, are a valid analogue for the processes undergone in at least some archaeological iron artefacts after excavation. The intermediate formation of ferric chloride has not been reported previously on archaeological iron.

5. Formation of Akaganeite and reaction of iron in laboratory simulated aging.

5.1 Introduction

The aim of this chapter is to elucidate the risk to archaeological iron from the environment using simulated tests.

The concept of value, and the impact of damage on it, is evolving within conservation (Michalski, 2008). The value of archaeological iron artefacts is the archaeological information contained within them. As new forms of analyses are applied an objects value can increase as new information becomes accessible. Within this work two general types of damage will be considered. The physical deterioration of an object caused predominantly by the physical expansion when akaganeite forms. This damage will disturb the shape of the object and interfere with morphological analyses (Doren and Hodson, 1975). A range of metallurgical surface finishes, tinning, silvering and gilding were used with iron. Sometimes only microscopic residues remain as evidence and any physical deterioration can result in their loss. Within the UK soil environment organic artefacts, on the whole, do not survive well. The corrosion process of iron can preserve the morphology of associated organic materials (Jakes and Sibley, 1984). In many instances the information preserved in this way is our only source of information. These mineral preserved organic remains are quite fragile and can easily be lost.

Iron is an important resource for archaeo-metallurgy. Loss of the metal core can destroy this information. At higher relative humidities electrochemical corrosion rates become appreciable and present the higher risk to archaeological iron with remaining metal core. The major control of electrochemical atmospheric corrosion is the availability of electrolyte. Deliquescence of ferrous chloride is the main potential source of electrolyte in archaeological iron. Observations of this have been reported as ‘weeping’ (Selwyn et al, 1999; Wang, 2007b; Knight, 1990). The exact relative humidity at which deliquescence of iron (II) chloride occurs has been subject to some uncertainty.

Several studies have been reported investigating the effect of RH on the formation of akaganeite. There is still some uncertainty in the RH threshold. Turgoose reported 15% in one publication and 18% in another (Turgoose, 1982b, 1985). The exposures he used relied on lithium chloride to produce the lowest RH. Different values have been reported for the RH generated above saturated lithium chloride solutions (Watkinson and Lewis, 2005). A series of experiments have been reported to underpin the conservation of the SS Great Britain (Watkinson and Lewis, 2004). The experiments were carried out in flowing air. There are reported differences in RH response of lead exposed to ethanoic acid, in still and moving air (Tetreault et al, 1998; Niklasson, 2007). The experiments lasted fourteen days. There is anecdotal evidence of archaeological iron taking up to three years to show signs of deterioration on display.

Whilst the effects of internally generated pollutant gases, such as methanoic and ethanoic acid are widely recognised on the corrosion of iron and steel, only one study on their effects on archaeological iron has been published (Lee, 1995). This showed that very high concentrations of ethanoic acid accelerated the deterioration reactions. However, the effect was not quantified, and the concentrations used for the experiments, were much higher than those likely to be encountered in most museum display and storage situations.

The effect of relative humidity, ethanoic and methanoic acid and methanal will be investigated. Whilst previous work has found thresholds for RH, it is not always possible to achive these very low RH values in practise. The risk when they are exceeded is extremely important and allows an informed assessment. English Heritage has a large number of showcases with archaeological iron and replacing them is not an immediate option. A way of prioritising a replacement or re-fitting program based on present risk is required. A small amount of work has been undertaken to determine the relative effect of the industrial pollutants, sulphur dioxide and nitrogen dioxide. Experiments have been undertaken to characterise the

deliquescent point of ferrous chloride over a range of temperatures normally experienced by archaeological stores in the UK. The dissolution rate of iron has been characterised in the akaganeite formation experiments to give an indication of the rate of loss of iron at higher relative humidities.

Archaeological iron is often a very complex material with several species present from the burial environment. A number of the species detected in Chapter 4 are reported to affect the oxidation of ferrous chloride or the crystallisation of akaganeite.

- Copper is often used in conjunction with iron, and in chloride burial environments, cuprous chloride can form. Ishikawa et al (2001) have shown that cuprous ions do not affect the crystallisation of akaganeite from iron (III) solutions. However, cuprous chloride deliquesces at a low RH and its affect on the critical RH was investigated.
- The presence of organic soil components, such as humic and fulvic acids, has a significant effect on several of the important reactions relating to iron corrosion. It stabilises iron (II) ions, affects the rate of oxidation of those ions to iron (III) and affects the crystallisation of iron (III) compounds (Pullin and Cabaniss, 2003). Many important archaeological iron objects originate from inhumations.
- Iron oxides and oxyhydroxides affect the mix of corrosion products formed (Ishikawa et al, 1998) and the effect of the most common; Goethite, lepidocrite and magnetite, was investigated.
- The presence of akaganeite has been reported to lower the RH at which more akaganeite forms from 19 to between 12 and 15% (Watkinson and Lewis, 2005). A series of experiments has been carried out to elucidate the effect.
- The chloride content of archaeological iron is highly variable and can also vary greatly within an object. The analyses reported in Chapter 3 found chloride concentrations of akaganeites to range between 6 and 12%. All previous work has used a 1:1 ratio of iron to iron chloride. The effect of different chloride ratios was investigated.

5.2 Experimental

Iron and iron (II) chloride powder mixtures have been used to simulate the most reactive species present in archaeological iron on excavation. The analysis of freshly excavated objects reported in Chapter 4 confirmed these species are indeed present.

5.2.1 Effect of RH

One to one mixtures of iron (Fluka 99.98%) and ferrous chloride (Alfa 99.5%) powders, by weight, were placed in inert polyethylene containers and exposed to different relative humidity atmospheres generated above glycerol solutions (Miner and Dalton, 1953). Solutions were prepared to give 5% RH intervals between 15 and 80%. Additional solutions were prepared to give intermediate RH values of 16, 17 and 18%. The high density of solutions at the low RHs were designed to investigate the threshold at which akaganeite begins to form. The prepared glycerol/water solutions generated RH values of 15.0, 16.1, 16.7, 18.1, 20.1, 24.9, 30.1, 35.0, 40.2, 44.9, 50.1, 55.0, 59.9, 64.8, 70.2, 75.0 and 79.9%. The viscous nature of glycerol makes exact weighing difficult. Glass jars with screw fit Bakelite tops were used as reaction vessels. A circle of Moistop 622 was cut out to fit the underside of the tops and neoprene rubber rings used to improve the sealing of the jars. For long term tests, low air exchange rates are vital to retain the desired RH atmosphere. Measurements with carbon dioxide tracer gas decay indicated an air exchange rate of 0.02 per day for the modified jar; 2.3 per day for the normal jar with the top tightly screwed on; and 6.9 per day with the top loosely screwed in place (Vaisala GMP2000 probe) (Calver et al, 2005). Glycerol/water solutions were selected as the method to control relative humidity, as fine relative humidity intervals can be generated and the relative humidity is not temperature dependent, unlike that generated above soluble salt solutions. The experiments were carried out in a laboratory in which the temperature varied within a 15ºC range over the forty eight month duration. Air phase migration of some salts has also been reported (Baranski et al., 2004). Environmental chambers often produce a variation in relative humidity of around 2-3% and were not used in these experiments. One drawback with glycerol solutions is that they are not self controlling, as saturated salts are to some degree, Any loss of water vapour (either from the container or through reaction) will increase the glycerol solution strength, hence decreasing the equilibrium relative

humidity. A control jar with each relative humidity solution, was weighed at monthly intervals to monitor any loss of water vapour. The relative humidity in the chambers was also checked periodically.

5.2.1.1 Mass gain, amount of akaganeite formed and water content.

The powders were weighed with a five figure decimal balance (Oertling 164) after one, three, six, twelve, twenty four, thirty six and forty eight months. Small samples of the mixtures were taken at these intervals. The samples were taken through the depth of the powder mixture with a spatula to ensure they were representative. The samples were prepared as potassium bromide discs and analysed with Fourier Transform infra-red spectroscopy as described in Chapter 3.1.1 to quantify the amount of akaganeite formed. Raman spectroscopy was undertaken on any darker regions in the sample, to confirm the absence of akaganeite. The samples after twenty four months were analysed with TGA to complement the FTIR analyses and to quantify the amount of free water present in the mixtures.

5.2.1.2 Volume expansion

The volume expansion undergone by the powders was estimated by measuring the height of the powder in the polyethylene holder with a micrometer. The measurement was taken by bracing the end of the micrometer over the top of the polyethylene holder and lowering the metal guide bar down to the level of the powder mixture. Whilst this is a relatively inaccurate measurement ($\pm$ 0.5mm), the changes were quite large. To further investigate the expansion of the mixture when akaganeite is formed, a series of more accurate experiments were undertaken. 500 mg of the mixture was placed in a Tyvek bag, the bag was placed in a pellet press for producing potassium bromide discs for infra-red spectroscopy. The die was added to the press so it flattened the powder in the bag. A linear differential voltage transducer was mounted so that, as the die raised (as akaganeite was formed and the powder mixture expanded), the transducer head was forced back, Figure 5.2. The whole assembly was placed in a Perspex chamber conditioned to a set relative humidity. The transducer was conditioned with a RDP Transducer controller, and the expansion of the mixture against the weight of the die, was recorded with an SR007 data-logger. This combination gives an accuracy of 1.77µm. These experiments were performed at 30, 35, 50 and 70% relative humidity.

5.2.1.3 Iron loss

Thermo-magnetometry (Chapter 3.3) was carried out on the powder samples after twenty eight months, including a control kept at 15%.

5.2.1.4 Ferrous chloride deliquescence

The deliquescent point of ferrous chloride would be expected to coincide roughly to a rapid acceleration in consumption of elemental iron (as liquid water is now available to act as an electrolyte) and shift in the predominant deterioration mechanism from physical forces caused by expansion on akaganeite formation to electrochemical corrosion. Experiments have been undertaken to characterise the deliquescent point of ferrous chloride from 5 to 35 ºC. Saturated pure iron (II) chloride (Aldrich 99.98%) solution was placed in a Rotronic calibration enclosure, along with a freshly calibrated Rotronic A1 probe. The calibration enclosure and probe were sealed into Escal film with 200g of Ageless RPA to ensure an oxygen free environment. This prevented the iron (II) chloride oxidising to iron (III) chloride, which is expected to have a higher deliquescent point. The oxygen concentration within the Escal enclosure was determined with a Gas Sensor Solutions GMP450 meter. The enclosure was cooled in a refridgerator at 3ºC and allowed to heat to room temperature with the relative humidity and temperature recorded every few minutes.

5.2.2 Effect of carbonyl pollutants

Several volatile organic compounds are reported to accelerate the corrosion of iron or carbon steel. In a museum storage or display environment the carbonyl compounds; ethanoic and methanoic acid and methanal are those most commonly encountered. Since ethanoic acid is the most damaging and most common, its effects on the akaganeite formation reaction were investigated (Rance, 1958; Gryzwacz, 1993). A range of ethanoic acid concentrations were used to mimic situations frequently encountered and measured (results in Chapter 7), see Table 5.1. The values are expressed in terms of average concentration, as the off-gassing from wood products is very strongly influenced by temperature and relative humidity (Thickett,

1997), and in naturally ventilated museums the airborne concentration experiences a very strong seasonal variation.

Average Concentration ($\mu g/m^3$)	Typical concentration of carbonyl pollutant in particular location (from measurements in Chapter 7)		
	ethanoic acid	methanoic acid	methanal
Zero *	good storage, Stewart boxes (not in wooden cupboards), metal and glass showcase – no wood products, all materials tested and rated suitable for permanent use		
750	good quality showcase, wood products used for base-board and back-board only and Moistop wrapped or Selabond coated to reduce emissions		showcases with some wood products with Dacrylate 103-Y coatings
1500	showcases with some wood products with no barriers or with Dacrylate 103-Y coatings	showcases with emissive lacquers or eggshell paint	showcases with E1 grade MDF
3000	showcases and cupboards made of wood or wood products	showcases with large areas of unsuitable lacquers or paints	showcases with large amounts of interior grade MDF or plywood
6000	poor quality cardboard boxes, paper envelopes	showcases with large areas of unsuitable lacquers or paints	not generally present at these concentrations unless highly emissive paints or lacquers

* Below detection limit of diffusion tube method in common use (40-140$\mu g/m^3$).

Table 5.1: Average ethanoica acid concentrations.

Ethanoic acid atmospheres were generated above the appropriate ethanoic acid solutions (Merck Analar) added to saturated magnesium chloride, magnesium nitrate hexahydrate and sodium chloride solutions to give relative humidity values of 33.1-33.6, 52-56 and 75.2-75.7% following the method developed by Tetrault et al (1998). The mixtures were prepared as KBr discs and analysed with FTIR and analysed with XRD.

5.2.3 Effect of sulphur dioxide and nitrogen dioxide

Sample were exposed in a Weiss WK111-180 pollution chamber. The tests were carried out at 23°C and 50% RH with 13350µgm^{-3} of sulfur dioxide and 9550µgm^{-3} of nitrogen dioxide.

5.2.4 Effect of chloride concentration

A series of iron and ferrous chloride powder mixtures were prepared with ratios of 1:3, 1:1 and 3:1. The mixtures were exposed to RH atmospheres of 15, 16, 17, 18, 20, 25, 30, 35, 40, 50 and 70%. After 12 months exposure the amount of akaganeite formed in the samples was determined using FTIR with the samples prepared as KBr discs.

5.2.5 Effect of species present in archaeological iron

A number of species were detected in close proximity to the akaganeite corrosion centres in Chapter 4. Several of these are reported to affect the oxidation or crystallisation of akaganeite.

The effect of copper (cuprous chloride 99.5%, Aldrich), humic acid (99% Aldrich), Goethite (99.98% Alfa), lepidocrite (99.98% Alfa) and magnetite (99.98% Alfa) on the relative humidity susceptibility of the formation reactions of akaganeite has been investigated.

Tests were undertaken, as described previously, with each compound added to produce a 1:1:1 mixture of the compound, iron and ferrous chloride powder. The mixtures were exposed to the same sets of relative humidity as previously, for the same time intervals and the amount of akaganeite determined using FTIR as KBr disc.

5.2.5.1 Akaganeite

The dramatic lowering of the critical RH for iron in the presence of akaganeite reported by Watkinson and Lewis (2005) has been investigated. The effect of the presence of akaganeite in corroding iron was examined by determining any akaganeite formed below 20% RH in mixture of iron, ferrous chloride and akaganeite powder. The potential effect of surface adsorbed chloride in iron was investigated with iron and akaganeite mixtures. A series of experiments were conducted with akaganeite samples removed from objects to elucidate the results.

5.2.5.1.1 Akaganeite and iron and ferrous chloride mixtures

The experiments in 4.2.1.1 produced akaganeite at different RHs. The products were analysed with thermogravimetry and thermo-magnetometry to determine the species present. In most instances no ferrous or ferric chloride remained. The amount of remaining elemental iron varied. Portions of the reacted material were mixed with fresh ferrous chloride and iron to produce a 1:1:1 ratio of akaganeite to ferrous chloride to iron mixture. This was ground to ensure thorough mixing as the akaganeite was cemented. A series of glycerol solutions were prepared to give 1% RH intervals between 10 and 20%. The powder mixtures were exposed in polyethylene caps above the glycerol soutions for a year. The mixtures were exposed in Escal bags and the oygen concentration measured every month with the GSS oxygen meter. At the end of the tests the powder mixtures were weighed and identified with FTIR as KBr discs, and quantified by TGA. FTIR was not thought sensitive enough to detect new akaganeite formed in the presence of the existing akaganeite.

5.2.5.1.2 Akaganeite and iron mixtures

Similar experiments were carried out with 1:1 mixtures of the akaganeite samples and iron powder.

5.2.5.1.3 Testing of akaganeite from archaeological iron objects.

There are no apparent differences in akaganeite formed at different RH values in FTIR, XRD or Raman so it has not been possible to discriminate between akaganeites formed on objects. The effects of akanageite from objects on the formation of further akaganeite was investigated. The samples are far too small for the tests described previously. Also, the detection of new akaganeite formed on top of the akaganeite originally present, is difficult. The oxygen depletion method was used. Each sample was mixed with 0.5mg of iron powder and 0.5mg of ferrous chloride in a small polyethylene cap. The cap, an oxygen SENSISPOT and 0.5ml of glycerol solution in another polethylene cap, were enclosed in an Escal bag that was double sealed with a impulse heat sealer. The oxygen concentration inside the bag was measured every seven days for two months.

5.2.5.5 Validation on artefacts

The complex nature of archaeological artefacts and the display environments means that there is always some uncertainty when applying experimental results in real situations. Hence the values were validated with object monitoring.

English Heritage has a large collection on display at over 130 sites around England. The many different building types, climates and variety of showcase designs present a range of different relative humidity environments. Many showcases have silica gel that is changed on a six monthly or annual cycle. The air exchange rate of the case, loading of silica gel and room environment determine the maximum relative humidity experienced. The case environments are monitored with a combination of Trendreader SR002 and Hanwell Humbug data-loggers and Meaco radiotelemetry sensors, all of which undergo annual three point relative humidity calibrations. Some cases have been continuously monitored for over twenty years.

Over 620 objects from display were closely examined for any signs of deterioration. The deterioration was roughly ranked into four categories;

i. apparently stable.
ii. slight deterioration: less than 1% of surface area showing corrosion
iii.` medium deterioration: between 1 and 5% surface area showing corrosion, no large areas of loss
iv. heavy deterioration: greater then 5% of surface showing corrosion or delamination or levering off of blisters

More detail on the assessment methodology is given in Chapter 2.1.2.3. A large number of these objects had been placed on display within the past seven years and were closely examined and conserved to remove any visible corrosion if required at that time. Hence in most instances any corrosion could be assumed to be newly formed. Many came from storage with dry silica gel. The showcases were divided into two categories, those with large exposed areas of wood or MDF (generally older) and generating relatively high ethanoic acid concentrations and those with no wood products or the wood products sealed with aluminised foils or incorporating activated charcoal absorbent which had much lower, but probably not zero ethanoic acid concentrations.

Where deterioration was observed samples were taken and analysed as described previously. The amount of damage was correlated against the environment in which the objects had been displayed.

5.3 Results

5.3.1 Effect of RH

5.3.1.1 Akaganeite formation

The amount of akaganeite formed in the exposed samples was determined with FTIR as KBr discs. Spectra after two years exposure at 15, 30 and 70% are shown in Figure 5.3.

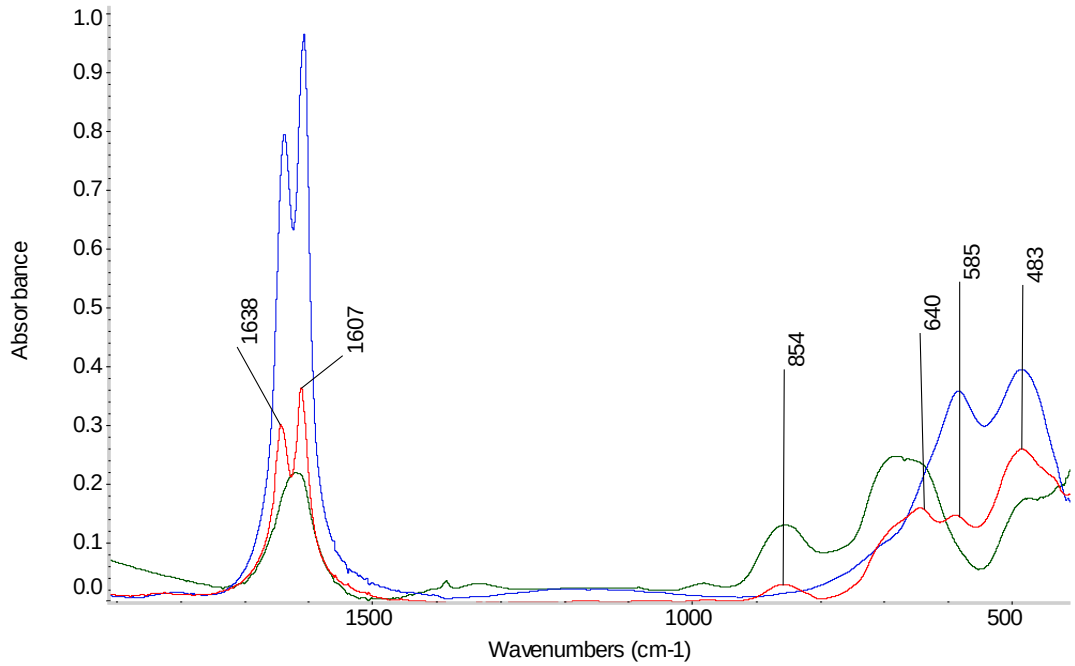

Figure 5.1 FTIR spectra of samples of iron and iron (II) chloride exposed to 15% (blue spectrum), 30% (red spectrum) and 70% RH (green spectrum) for two years.

The sample exposed to 15% relative humidity only shows absorptions due to iron (II) chloride at 483 and 585cm^{-1}. The water absorption is split into two absorptions at 1607 and 1638cm^{-1}. Ionic salts can split the water absorption, this behaviour is reported for iron phosphate (Parfitt and Smart, 1977). The sample exposed to 30% RH also shows the characteristic absorption bands of akaganeite at 640 and 854cm^{-1} (Murad and Bishop, 2000). The water absorption is split. After exposure to 70% for two years the iron (II) chloride absorption at 585cm^{-1} can no longer be observed and the water absorption appear as a single band at 1621cm^{-1}. There is still a very weak absorption at 483 cm^{-1}, possibly indicating a small amount of residual iron (II) chloride.

Representative thermogravimetry traces after two years exposure are shown in Figure 5.2.

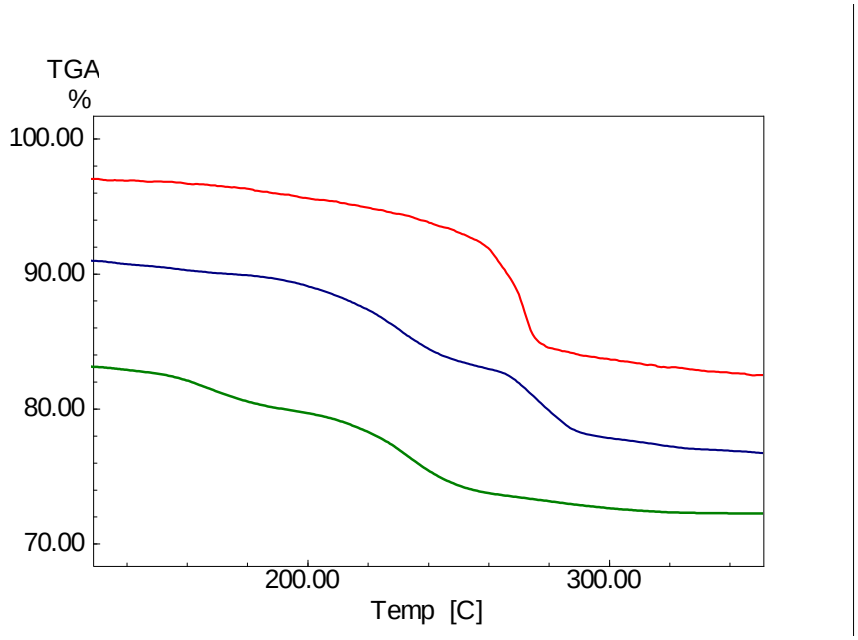

Figure 5.2 TG curves of samples if iron and iron (II) chloride exposed to 15% (lower green curve), 30% (middle blue curve) and 70% RH (upper red curve) for two years. The lowest curve (15% RH) shows no mass loss in the temperature region used for akaganeite characterization.

The initial mass loss with an onset just above 200ºC is due to iron (II) chloride remaining in the sample. Iron (II) chloride exists as the dihydrate at 15% RH, and the tetrahydrate at 30 and 70% RH. The waters of hydration are lost at lower temperatures. The sample exposed to 15% has the most residual Fe(II)Cl and this reduces in the sample exposed to 30% RH and is completely absent in the 50 and the sample exposed to 70% RH. The amount of akaganeite was calculated from the mass loss between 260 and 295ºC. The experiments show that no akaganeite was formed at 15% and a small amount formed already at 30% and a much larger amount is present in the sample exposed to 70% RH. The decomposition events for the akaganeites formed at 30 and 70% RH occur at different temperatures.

The amounts of akaganeite formed in the iron and ferrous chloride powder mixtures after 1, 3, 6, 12, 18, 24 and 48 months are shown in Figures 5.5 to 5.11. The amount of akaganeite formed is expressed as the proportion of the original iron available. Each test had elemental iron (15mg) and iron (II) chloride (15mg), giving 15+15*56/(56+2*35.5) = 21.61mg of iron. Full conversion would be equivalent to 36.70mg of akaganeite, using the latest chemical formula for akaganeite, $FeO_{0.833}(OH)_{1.167}Cl_{0.167}$ (Stahl et al, 2003). This value has been set to 100%.

Results for 1, 3 and 6 month exposures are shown in Figure 5.3.

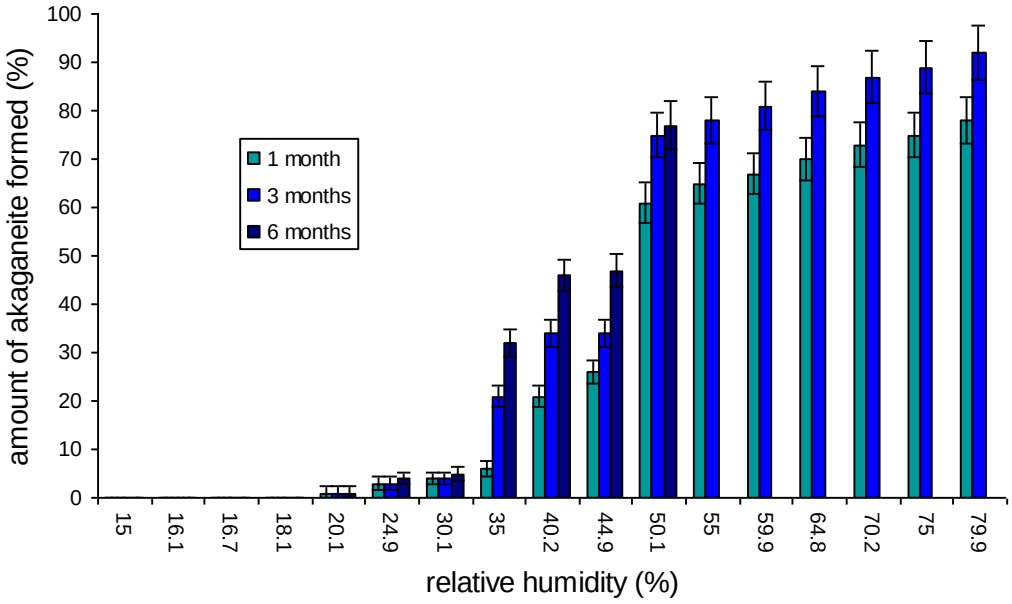

Figure 5.3 Amount of akaganeite formed from iron and ferrous chloride powders after 1 (pale blue), 3 (mid blue) and 6 (dark blue) months at various relative humidities by FTIR .

No detectable akaganeite was formed at 18.1%, but akaganeite was detected at 20% RH. After three months it becomes apparent that there is a significant increase in rate of akaganeite formation between 30 and 35% RH. In the early stages of the reaction (1 and 3 months) there is a second pronounced increase in rate of formation of akaganeite above 50% RH.

Results for the 12, 18, 24 and 48 month exposure tests are shown in Figure 5.4.

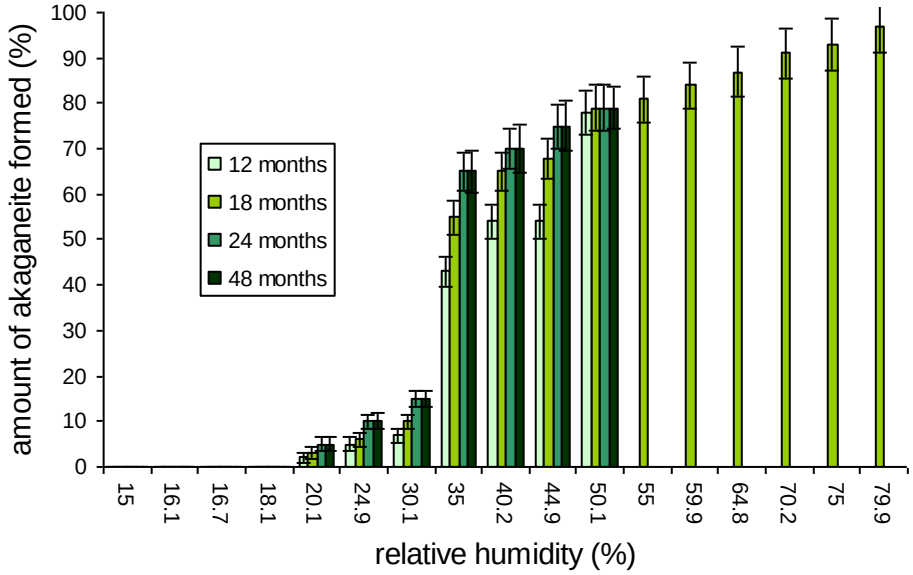

Figure 5.4 Amount of akaganeite formed from iron and ferrous chloride powders after 12 (pale green), 18 (yellow/green), 24 (mid green) and 48 (dark green) months at various relative humidities by FTIR.

The amounts of akaganeite formed increase, but the grouping of results is the same; no formation at 18.1%, a definite increase in formation rate between 30 and 35%RH with generally increasing rates above 35%.

Comparison of the recorded mass gains with the FTIR data after 24 months exposure shows some discrepancy, Figure 5.5. Both the amount of akaganeite and the mass gain were scaled as a percentage of the original mass of iron present in the sample for comparison.

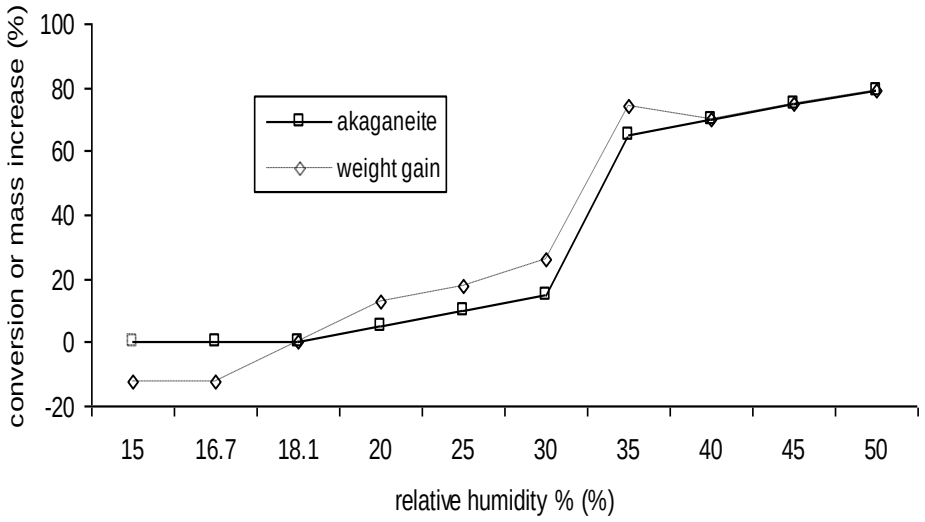

Figure 5.5 Amount of mass gain and akaganeite formed from iron and ferrous chloride powders after 24 months at various relative humidities.

There are quite large discrepancies between the two traces. Below 18% RH the powder lost approximately 12% mass. This is due to the previously recognised conversion of $FeCl_2.4H_2O$ to $Fe_2Cl_2.2H_2O$ [Turgoose, 1982b]. Between 20 and 40% the mass gain is somewhat higher than the amount of akaganeite detected by FTIR.

Table 5.2 shows the water content as measured by FTIR and TGA.

Relative humidity	Water content (% weight/weight of sample)		Difference between mass gain measured and that predicted from the amount of akaganeite (% weight/weight of sample)
	TGA	FTIR	
15%	10.0	10.0	0*
20%	22.1	22.3	8
25%	19.3	19.5	8
30%	14.3	14.5	11.2
35%	9.5	9.3	9
40%	1.1	0.8	1.0
50%	0.3	0.4	0.2
70%	0.2	0.1	0.1

* at 15% RH no akaganeite was detected, there was a mass loss of 12% due to dehydration of $FeCl_2.4H_2O$ to $FeCl_2.2H_2O$

Table 5.2: Water content of iron/ferrous chloride mixturesafter 24 months exposure to different RH values.This correlates well to the differences between the measured mass gain and the mass gain expected from the amount of akaganeite formed.

These values are the combined mass of water due to surface adsorption and waters of hydration in the ferrous chloride. At 15% RH, the powder mixture contained 10% water by mass, due to the two waters of hydration of $Fe_2Cl_2.2H_2O$. At 20% RH, $Fe_2Cl_2.2H_2O$ gains two extra waters of hydration to form $Fe_2Cl_2.4H_2O$, a small amount of akaganeite has formed. The mass of the sample has increased by 13%, 8% greater than is accounted for by the mass increase due to akaganeite. The discrepancy increases to a maximum at 30% RH and decreases to almost zero by 40%RH. At 35% there is a significant amount of akaganeite and no ferrous chloride

remaining. Almost all of the water content is due to adsorbed water at this RH and above.

The adsorbed water masks the increase in akaganeite formation between 30 and 35% RH in the mass data (Figure 5.7).

The powders expanded significantly during the higher RH experiments. Results after 24 months are shown in Figure 5.6. The volume increase is calculated from the height increase of the powder mixture.

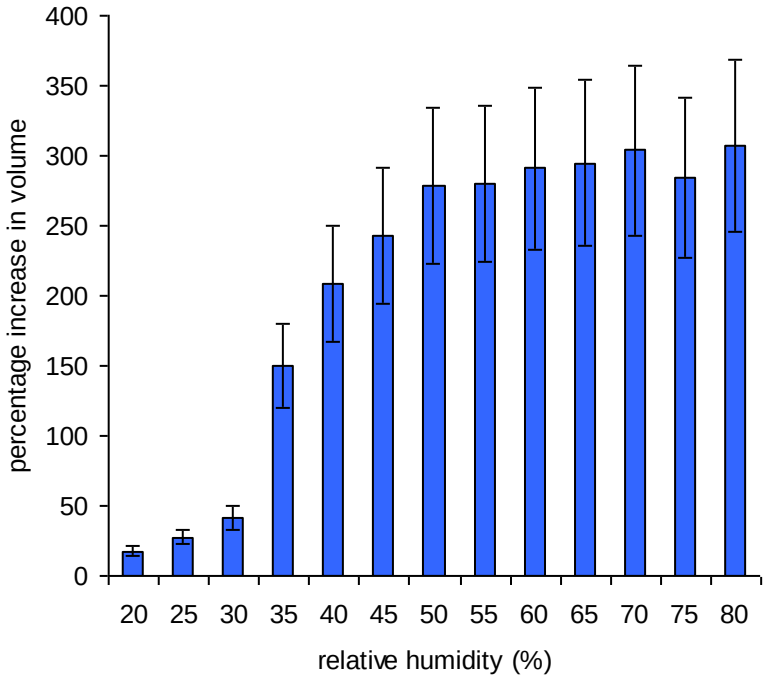

Figure 5.6 Increase in volume of iron and ferrous chloride powders after 24 months at various relative humidities.

There is a very dramatic increase in expansion between 30 and 35% RH, with some increase up to 50% and little increase above that value.

The transducer expansions recorded after 30 days are shown in Table 5.3.

RH the sample was exposed to (%)	height of mixture in container (µm)
30	234 ± 1.77
35	4765 ± 1.77
50	6720 ± 1.77
70	8658 ± 1.77

Table 5.3 Expansion of iron/iron(II)chloride mixtures when exposed to different RH atmospheres.

These results confirm that there is a dramatic increase in the pressure generated on formation of akaganeite between 30 and 35% relative humidity. Additionally they show that the increase in the relative humidity rising above 54% is not as dramatic as anticipated. The 70% relative humidity test was dehumidified to 50% after 30 days to ensure that the lower than anticipated pressure was not due to the mixture or components of it deliquescing. No additional expansion was detected.

5.3.1.2 Iron loss

A typical thermo-magnetometry curve for the mixture after exposure to 30% RH for 24 months is shown in Figure 5.7

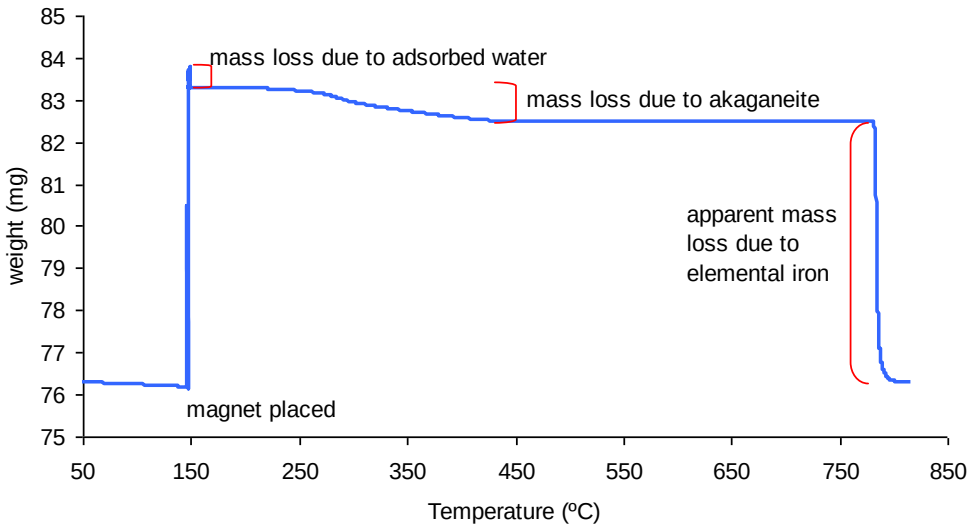

Figure 5.7 Thermo-magnetometry of iron/iron (II) chloride mixture after 24 months exposure to 30% RH.

The values for iron loss determined by thermo-magnetometry are plotted against RH in Figure 5.8. Measurements were taken after 24 months and 48 months.

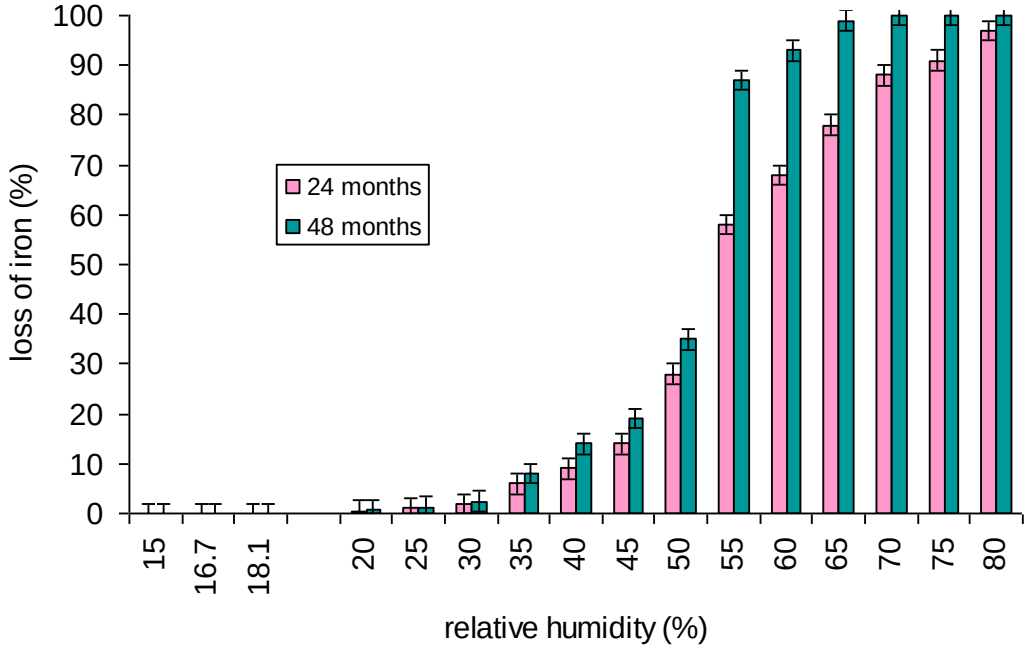

Figure 5.8 Loss of elemental iron from iron and ferrous chloride powders after 24 and 48 months at various relative humidities by thermo-magnetometry.

No iron loss was detected below 20%. Above 20% the losses increase and there is a large increase between 50 and 55%. After 48 months elemental iron has been totally lost from the 70, 75 and 80% tests.

5.3.1.3 Ferrous chloride deliquescence

The pseudo equilibrium RH values above saturated ferrous chloride slurry, as measured with a Rotronic A2 probe, are shown in Figure 5.9.

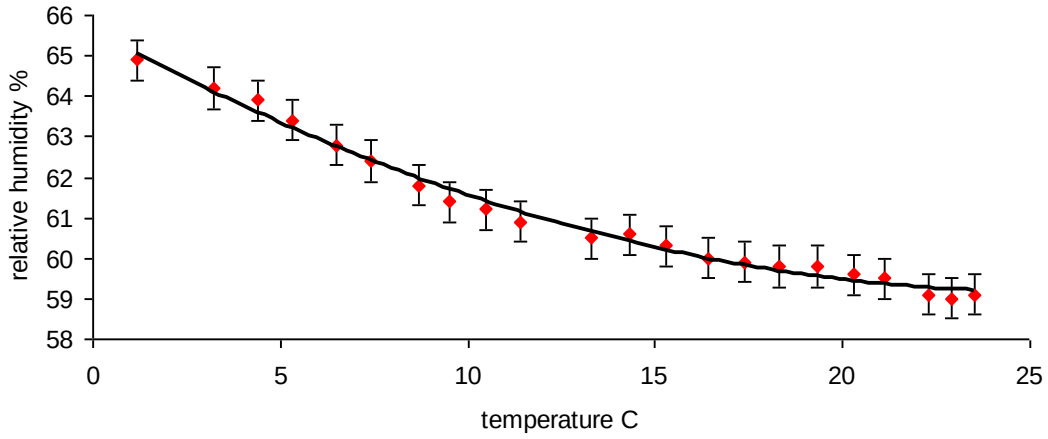

Figure 5.9 Relative humidity above saturated iron and ferrous chloride mixture as a function of temperature.

The deliquescent RH (which is the equilibrium RH) increases with decreasing temperature. Whilst the accuracy of the RH probe is very high (± 0.5% in the RH interval measured) and its response time is fast, the slow heating of the sample to room temperatures means a pseudo equilibrium is reached. The Escal bag was insulated with polystyrene pieces to reduce the heating rate as much as possible. The RH values at which deliquesceoccurs are about 10% higher than the RH at which iron loss increases. This effect may be due to adsorbed water increasing the ionic conductivity of the ferrous chloride to such an extent that the crystal can act as similarly to an electrolyte without being a solution. This effect has been reported for soluble salts on other metals (Yang et al, 2003).

5.3.2 Effect of carbonyl pollutants

The amounts of akaganeite formed on exposure to different ethanoic, methanoic and methanal atmospheres, expressed as a percentage of that formed with no acid present, is shown in Figures 5.10 to 5.12.

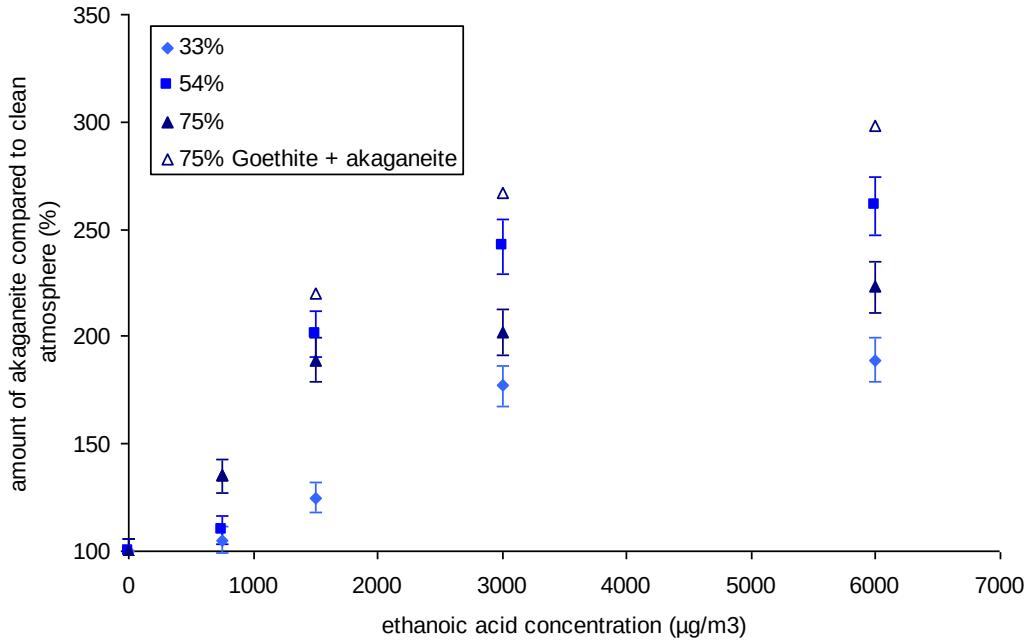

Figure 5.10 Amount of akaganeite formed in ethanoic acid atmospheres at different relative humidities. 75% Goethite+akaganeite is the combined amount of akaganeite and Goethite formed at 75% relative humidity as measured by FTIR.

The amount of akaganeite produced generally increased with increasing ethanoic acid concentration, with the exception of the 75% relative humidity tests at 3000 and 6000µg/m^3. Goethite was obvious in the infra-red spectrum at 3000µg/m^3 and 75% and was the major product at 6000µg/m^3, (Chapter 3.1.1.3). Close examination of the spectrum also revealed some goethite at 1500 µg/m^3. To take this into account samples were taken from the 75-76% tests and analysed with thermogravimetric analysis to quantify the amounts of akaganeite and Goethite that had been formed (see Chapter 2.2.5). These results are shown as 75% total in Figure 5.16. The formation of Goethite at 75% relative humidity and higher acid concentration is possibly due to the decreased pH during Fe(II)Cl oxidation ((Misawa et al., 1974). An alternative explanation could be initial formation of akaganeite, which is then

dissolved by the lower pH solution and re-precipitates as Goethite (Cornell and Schwertmann, 1986).

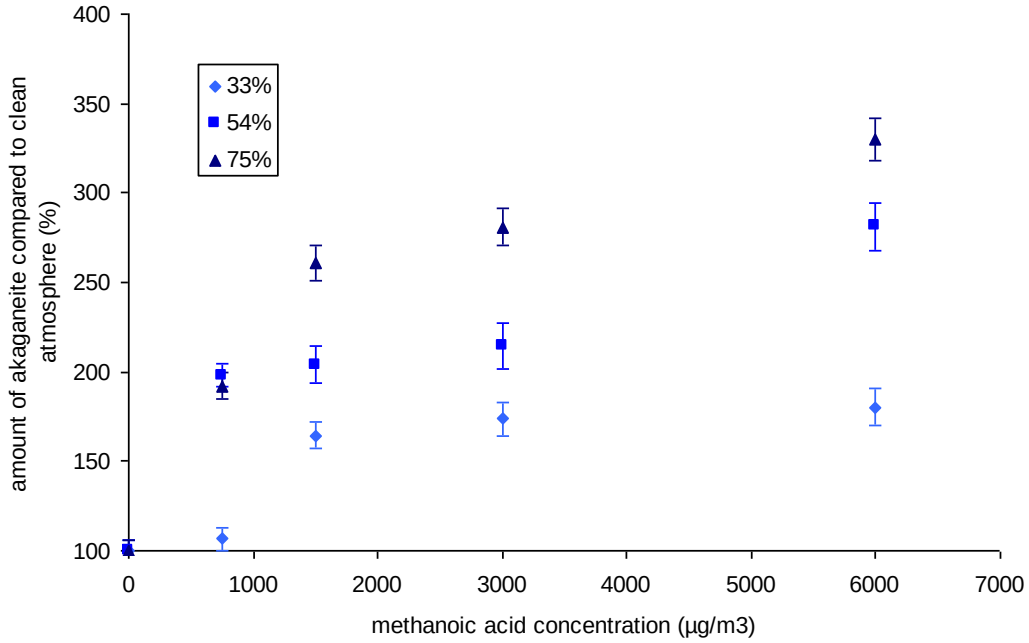

Figure 5.11 Amount of akaganeite formed in methanoic acid atmospheres at different relative humidities.

When exposed to methanoic acid, no Goethite was observed in any reaction. The amount of akaganeite increased with increasing methanoic acid concentration. The acceleration of the rate is generally greater at 750 and 1500ug/m^3 (with the exception of the 750ug/m^3 and 33% value) for methanoic than ethanoic acid. At higher methanoic acid concentrations the acceleration is less than with the same ethanoic acid concentrations.

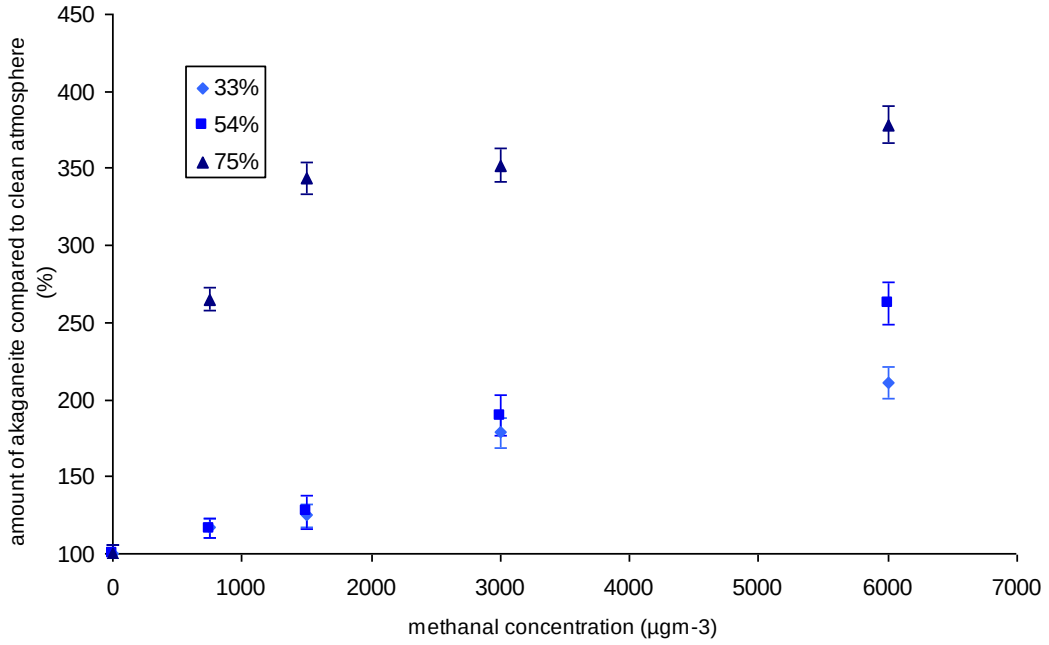

Figure 5.12 Amount of akaganeite formed in methanal acid atmospheres at different relative humidities.

When exposed to methanal, no Goethite was observed in any reaction. The amount of akaganeite increased with increasing methanal concentration. The 33 and 54% RH tests gave identical results (within the experimental errors) for 750, 1500 and 3000 ug/m^3 of methanal. The 75% test with methanal resulted in the greatest acceleration of the reaction compared to ethanoic and methanoic acid.

5.3.3 Effect of sulphur dioxide and nitrogen dioxide

Exposure of the iron and ferrous chloride powder mixture to 13350µgm^{-3} of sulfur dioxide and 9550µgm^{-3} of nitrogen dioxide at 50% RH generated an 30% increase in the amount of akaganeite formed, above that formed at 50% RH in clean air.

The accelerated aging used much higher concentrations of sulfur dioxide and nitrogen dioxide than those to which archaeological iron would be normally exposed. Measurements in typical showcases (Chapter 7) were 1.33µgm^{-3} for nitrogen dioxide and 1.335µgm^{-3} for sulfur dioxide at Portchester. The 30 day exposure in the

pollution chamber gives a dose equivalent to over 22 years exposure at these concentrations for nitrogen dioxide and almost 31 years for sulfur dioxide.

5.3.4 Effect of chloride concentration

The amounts of akaganeite determined in the powder mixtures with different amounts of chloride are shown below

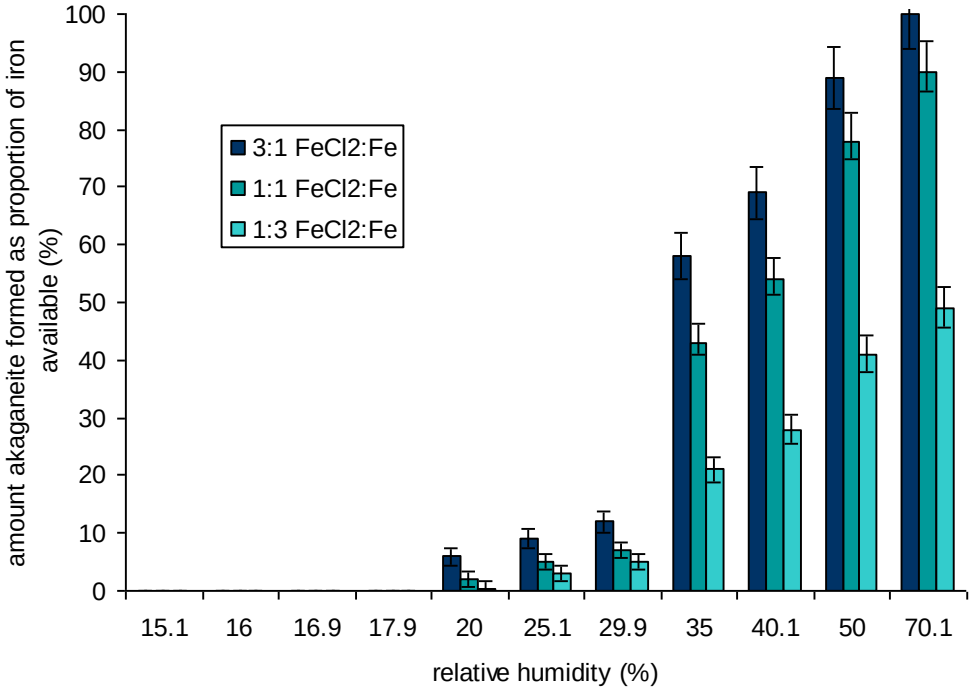

Figure 5.13 Amount of akaganeite formed from iron and ferrous chloride powders after 12 months at various relative humidities.

Increasing the chloride ratio, increases the amount of akaganeite formed. No akaganeite was formed below 18% RH, as was the case for the 1:1 mixture. There is a strong increase in the amount of akaganeite formed between 30 and 35% RH.

5.3.5 Effect of species present in archaeological iron

5.3.5.1 Copper chloride

Results from the mixture of iron, ferrous chloride and copper chloride are shown in Figure 5.16. The amount of akaganeite formed in mixtures of iron and ferrous chloride is included for reference.

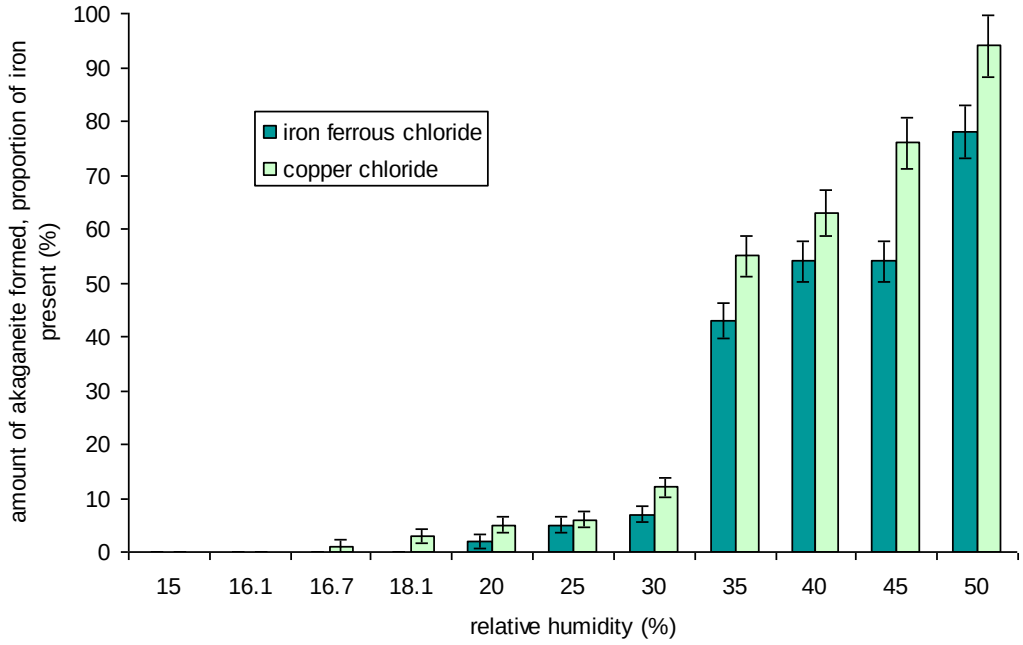

Figure 5.14 Amount of akaganeite formed in iron, ferrous chloride and cuprous chloride mixtures at different relative humidities after 12 months.

More akaganeite was formed when cuprous chloride was present. Akaganeite also formed at a lower RH (16.7%). This is probably due to the high affinity of cuprous chloride with water vapour. The overall shape of the response is maintained along with a large increase in akaganeite formation between 30 and 35%.

5.3.5.2 Humic acid

Results from the mixture of iron, ferrous chloride and humic acid are shown in Figure 5.15. The amount of akaganeite formed in mixtures of iron and ferrous chloride is included for reference.

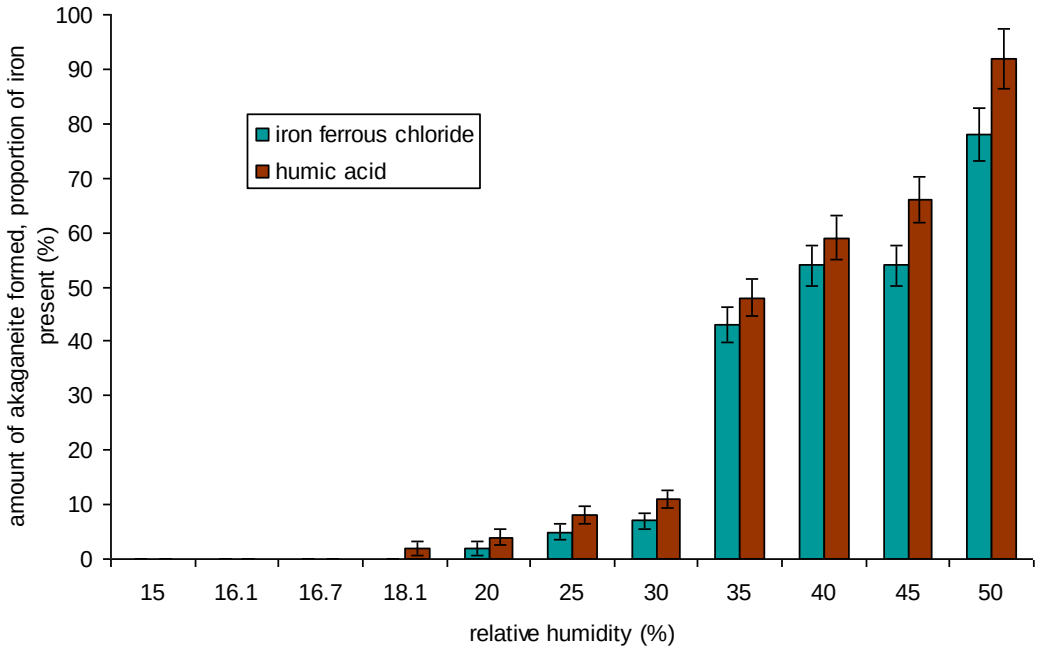

Figure 5.15 Amount of akaganeite formed in iron, ferrous chloride and humic acid mixtures at different relative humidities after 12 months.

Again more akaganeite was formed with humic acid present. Akaganeite did form at a lower RH. The increase in akaganeite between 30 and 35% is maintained.

5.3.5.3 Goethite

Results from the mixture of iron, ferrous chloride and Goethite are shown in Figure 5.16. The amount of akaganeite formed in mixtures of iron and ferrous chloride is included for reference.

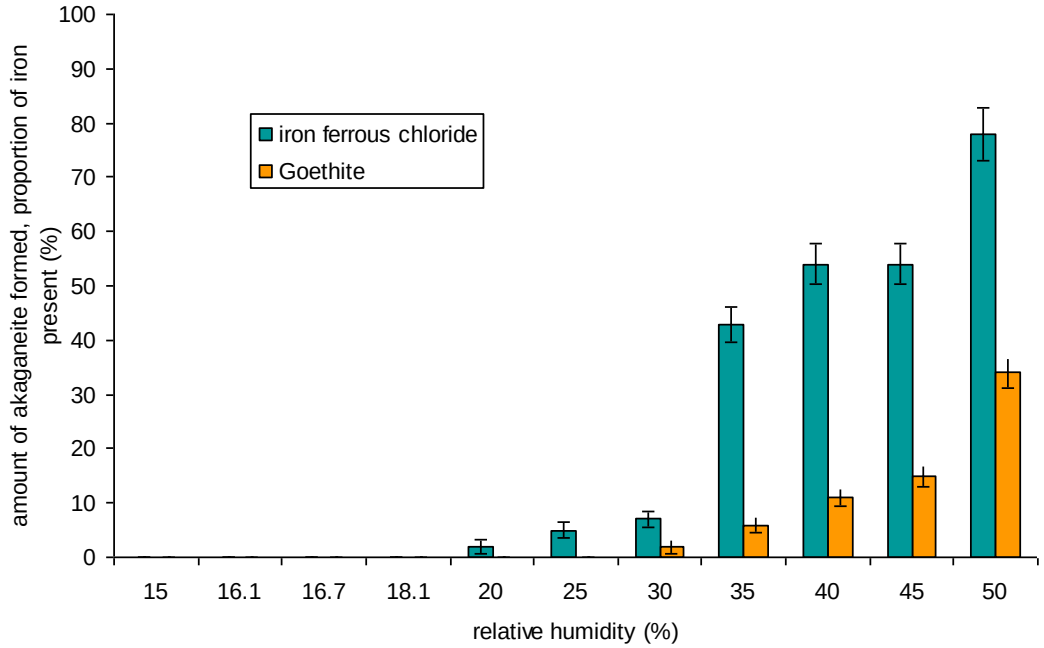

Figure 5.16 Amount of akaganeite formed in iron, ferrous chloride and Goethite mixtures at different relative humidities after 12 months.

Goethite has retarded akaganeite formation slightly at most RHs. There was no akaganeite formed at 20 and 25% and the akaganeite formation rate increases significantly between 35 and 40% and 45 and 50%.

5.3.5.4.1Akaganeite and iron and ferrous chloride mixtures

Results from the mixture of iron, ferrous chloride and akaganeite are shown in Figures 5.19 and 5.20. The oxygen loss is expressed as the reduction in oxygen concentration from 20.8%.

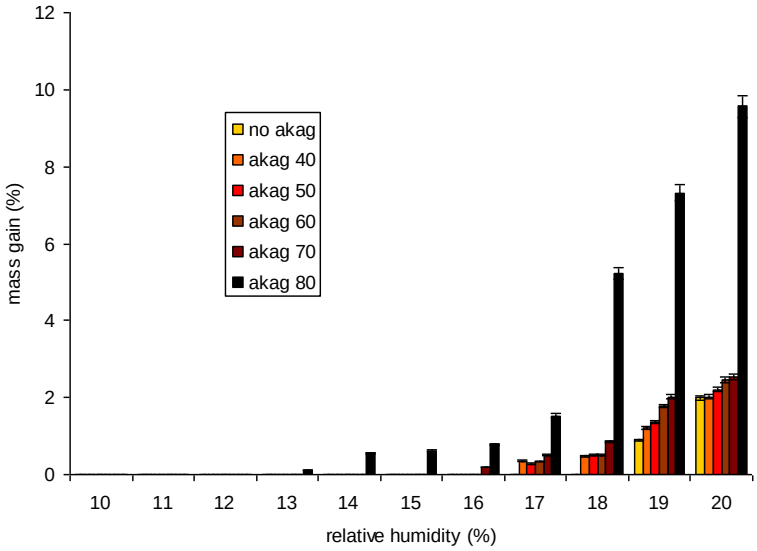

Figure 5.17 Mass gain of iron, ferrous chloride and akaganeite mixtures at different relative humidities.

There was no mass gain below 17% RH for the powder mixture with no akaganeite and with akaganeite formed at 40, 50, and 60%. Mass gains were observed at 16% RH with the powder mixture and akaganeites formed at 70 and 80%. Mass gains were observed as low as 13% with the akaganeite formed at 80%.

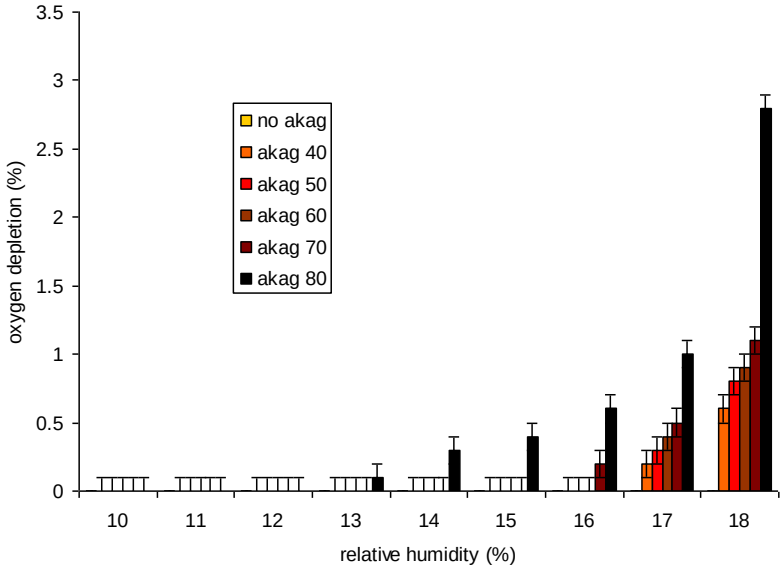

Figure 5.18 Oxygen depletion above iron, ferrous chloride and akaganeite mixtures at different relative humidities.

The oxygen depletion results agreed well with the mass gains. The instrument reads the percentage of oxygen in the air. As the volume of the enclosure was not controlled, full quantification was not possible. The volumes were very similar however, so some comparison can be done. Some depletion was observed at 13% RH with the akaganeite formed at 80%, at 16% RH with the akaganeite formed at 70% and at 17% RH with the remaining powder mixtures.

5.3.5.4.2 Akaganeite and iron mixtures

With no ferrous chloride present there was less reaction, Figure 5.21.

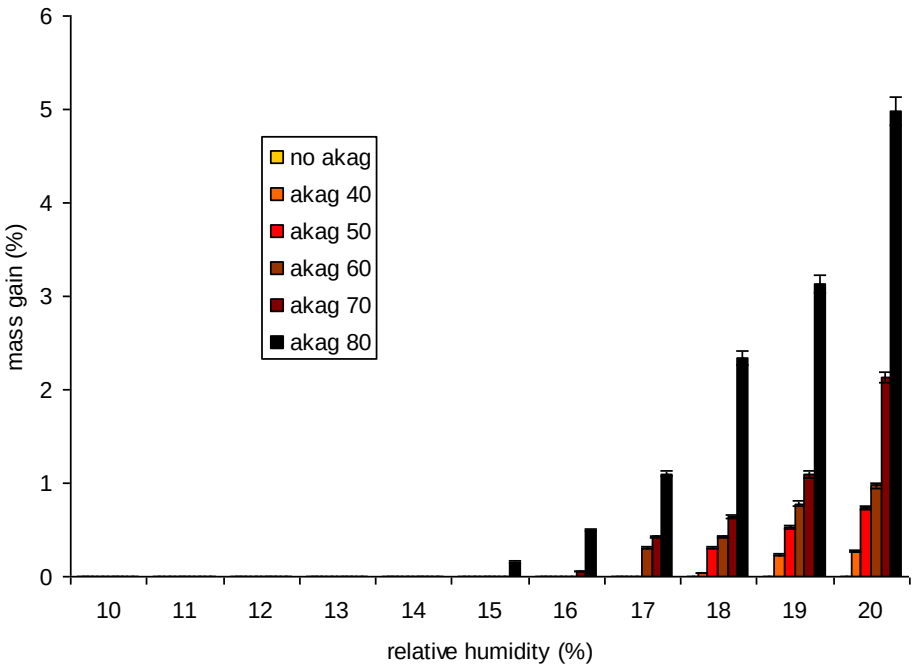

Figure 5.19 Mass gain of iron, and akaganeite mixtures at different relative humidities.

Mass gain was observed (presumably due to new akaganeite formation) at 15% RH with akaganeite originally formed at 80%. Mass gain was observed at 17% RH for akaganeites formed at 70 and 60% and at 18% for the rest of the akaganeite containing mixtures.

5.3.5.4.3 Testing of akaganeite from archaeological iron objects.

The mixtures of iron and ferrous chloride and akaganeite samples from objects did not show any detectable oxygen depletion at 16% RH.

5.3.6 Validation on artefacts

A small subset of the results from 620 objects on display are shown in Table 5.4. The collated results are shown in Figures 5.20 and 5.22. Figures 5.21 and 5.23 show the same data presented as percentages

Volume (m^3)	Amount silica gel (kg)	Air exchange rate (day^{-1})	Relative humidity over last four 6 month periods		Deterioration observed over a two year period	
			Averages	Maxima		
0.18	41.7	0.12	15.3-15.7	18-19	Stable	None
0.18	41.7	0.16	15.5-15.8	19-20	Stable	None
0.50	34.8	0.28	24.7-24.9	30-32	Slight	Some small losses
0.50	34.8	0.45	24.1-24.5	26-28	Stable	None
0.50	34.8	0.24	17.1-17.3	21-23	Stable	None
0.19	46	1.8	25.2-25.6	31-34	Slight	Some small losses
0.17	44	2.5	35.0-35.2	40-43	Medium	Obvious patches akaganeite
0.02	105	4.1	36.7-37.1	42-44	Heavy	Delamination on back
0.25	67.5	0.31	27.8-28.1	41-45	Medium	Large patches of akaganeite
0.23	75.6	0.28	29.2-29.4	41-44	Heavy	Large patches of akaganeite
0.50	0	1.9	46.2-61.6	74-84	Heavy	Large patches of akaganeite
3.1	0	2.1	50.3-68.3	76-88	Heavy	Delamination

Table 5.4 Results of object examination and relative humidity conditions.

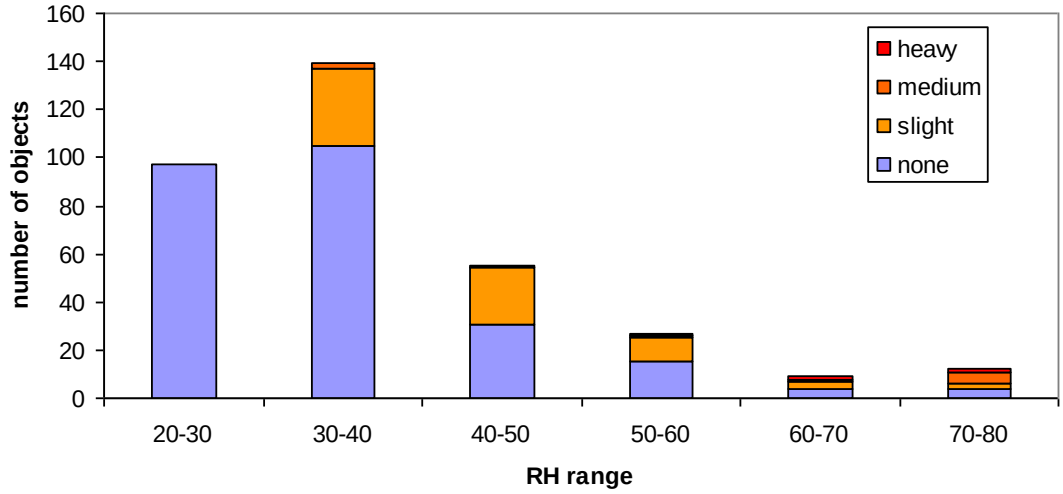

Figure 5.20 Assessment of condition of archaeological iron objects in showcases with different maximum relative humidities and low ethanoic acid concentrations (no wood products present).

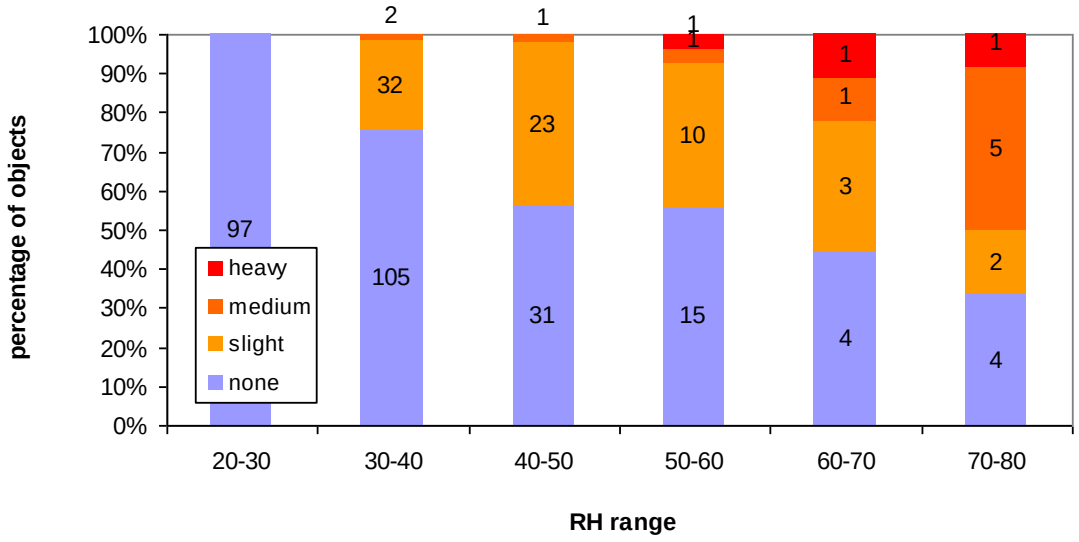

Figure 5.21 Normalised assessment of condition of archaeological iron objects in showcases with different maximum relative humidities and low ethanoic acid concentrations (no wood products present).

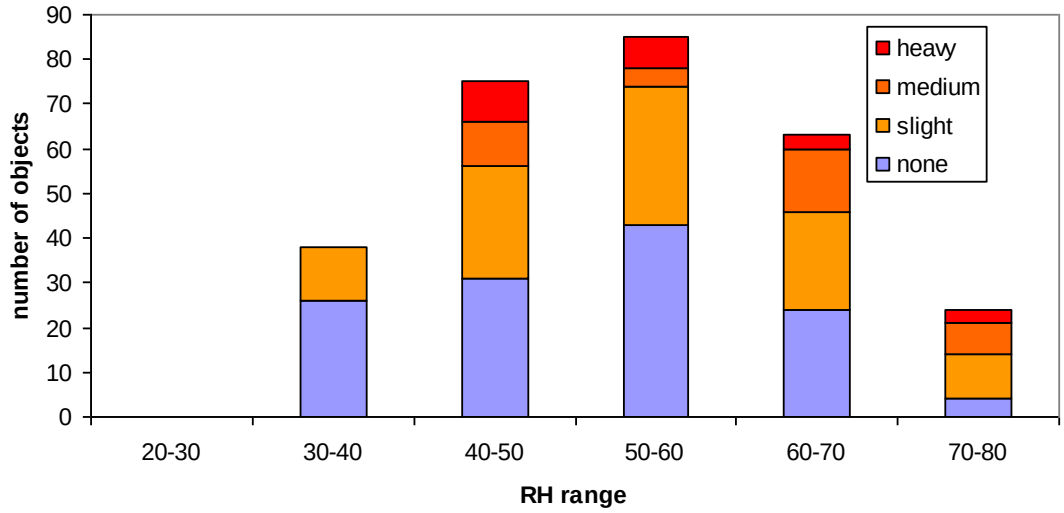

Figure 5.22 Assessment of condition of archaeological iron objects in showcases with different maximum relative humidities and high ethanoic acid concentrations from the presence of wood products.

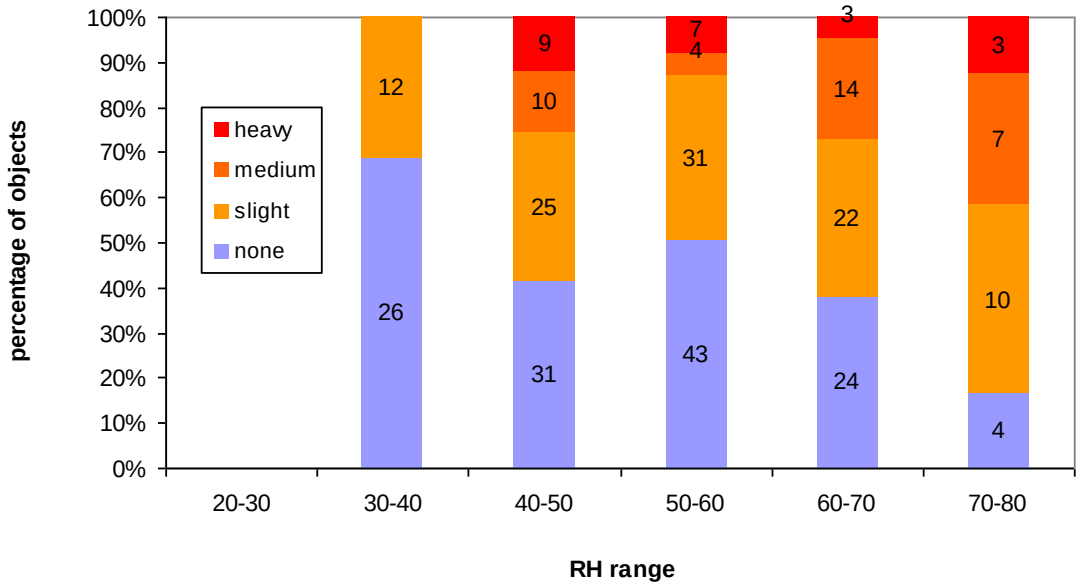

Figure 5.23 Normalised assessment of condition of archaeological iron objects in showcases with different maximum relative humidities and high ethanoic acid concentrations from the presence of wood products.

An extremely good correlation was observed between the condition of the objects and the relative humidity conditions in which they had been displayed in. No examples of new corrosion were observed, at least by visual assessment, in relative humidities below 30%. Display environments below 16% are extremely difficult to achieve, although this is relatively straight forward in storage situations. Heavy corrosion was only observed below 50% relative humidity in show-cases containing large areas of inadequately sealed wood products generating high ethanoic acid concentrations. Only limited instances of relative humidities above 50% were examined, as most cases have some form of silica gel or mechanical relative humidity control, albeit of limited efficiency in some instances. A proportion of objects showed increasing deterioration with increasing relative humidity. It was clear that only a proportion of the iron objects were unstable and many were apparently stable, even under high relative humidity conditions.

5.4 Discussion and Conclusions

The analyses in chapter 3 showed that over 85% of the instances of deterioration of archaeological iron examined were due to akaganeite formation. The risk of damage is probably best approximated by the amount of akaganeite formed. In actual objects the position and amount of akaganeite and morphology of the surrounding corrosion products will determine if damage does actually occur. For the Stonea and Uley objects, akaganeite can only crack the corrosion layer on top of the pits under the following conditions. There is enough ferrous chloride present at the base of the pit to generate a sufficient volume of akaganeite to fill the pit. The expansion is great enough to induce sufficient pressure on the overlying corrosion product layer to break it.

There are two obvious major changes in formation rate of akaganeite;

- No further akaganeite was formed: below 19%RH for most of the mixtures tested; below 16.7% when cuprous chloride was present and below 17% when akaganeite is present (it is unlikely that recently excavated objects will have been exposed to RHs above 50% in silica gel storage). As copper is often present in

burials with iron and many archaeological iron objects have akaganeite present from periods of RH above 16%, keeping the RH below 16% would be prudent, where feasible.

- The akaganeite formation rate increases between 30 and 35% (Figure 5.5 and 5.6). The step change or threshold is important for the display of archaeological iron, as 16% would be extremely expensive to maintain in a showcase on display. This threshold does not appear in short term experiments. The word "threshold" is used here to describe a change in reaction rate or step change in the English sense of the word. Only the 16% value is a threshold by the definiton in physics, below which the phenomena do not occur. The adsorption of water vapour at low RHs by ferrous chloride masked the 30% threshold when only mass gain was examined. These explain the fact that neither Turgoose or Watkinson identified this second threshold in their two week experiments measuring mass. The pressure generated by akaganeite formation increases dramatically between 30 and 35%.

At a RH between 50 and 60%, depending on the temperature (Figure 5.11), the electrochemical corrosion of iron becomes significant and there is a risk of loss of archaeometallurgical information retained in the remaining iron core. There is no apparent large increase in akaganeite formation or the pressure it generates when passing through these RH values. These values are approximately 10% lower than the deliquescent RH of ferrous chloride. This electrochemical corrosion, occurring before the salt is in solution is consistent with work on other soluble salts on metals (Yang et al, 2003).

As the RH approaches the deliquescence RH, soluble salts take in water vapour. This increases ionic and electron mobility in the solid salt. There is enough mobility for the salt to act as an electrolyte in the solid phase.

The other species present in archaeological iron do not change these thresholds. Some accelerate the akaganeite formation reactions and others slow these down, but the 16 and 30% thresholds remain constant.

Ethanoic acid accelerates the akaganeite formation reactions, even at 750µgm^{-3}, This level is present in almost all showcases with any wood products incorporated. Higher concentrations have been reported in metal and glass showcases when inappropriate lacquers are used (Schwieck, 2009 pp94-124). Concentrations of around 1000µgm^{-3} are reported to accelerate the corrosion of iron and would pose a risk to any remaining metal core of archaeological iron artefacts (Rance and Cole, 1958).

Methanoic acid causes less acceleration at the lower concentrations 750 and 1500 µgm^{-3}, which it typically occurs at in showcases. Some paints can emit very large concentrations of methanoic acid (Thickett, 2008c), at these higher (3000 and 6000 µgm^{-3}) concentrations it accelerates the formation of akaganeite more than ethanoic acid.

Methanal is more aggressive at 75% than either ethanoic or methanoic acid towards iron objects. At lower RH values it has a similar acceleration effect. (Figure 5.12, 5.13 and 5.14)

The industrial pollutants, sulfur dioxide and nitrogen dioxide were found to accelerate the akaganeite formation reactions (Table 5.3). The acceleration was quite slow compared to the effect of methanal and ethanoic and methanoic acids. Measurements inside showcases, reported in Chapter 7, indicate that the doses tested would be equivalent to almost 22 years exposure for nitrogen dioxide (much longer for sulfur dioxide). The tests with ethanoic acid were equivalent to 3 years exposure and produced 5 times more akaganeite. Tests with methanoic acid produced 9 times more and methanal, 6 times more akaganeite.

There was an extremely good correlation with these thresholds and the observed deterioration from objects on display. No environments with RH values below 16% were found. For the more modern showcases with low ethanoic acid concentrations and RH values below 30%, no deterioration was observed in five years of exposure. Above 30%, small amounts of deterioration began to be observed (slight degree of deterioration). The presence of high ethanoic acid concentrations increased the proportion and intensity of deterioration. The second 30% RH threshold appears to be correct for real situations.

Chapter 6 Transformation of Akaganeite

6.1 Introduction

Akaganeites formed on archaeological iron have been shown to contain between 6 and 15% of chloride, Chapter 4.3.1.3. If the akaganeite transforms to other iron corrosion products then the likely conversion products Goethite and hematite have much lower chloride concentrations (Turgoose, 1982). The excess chloride is likely to migrate in the corrosion layers and cause further corrosion when it reaches any remaining metal core. A recent review of the gaps in knowledge about archaeological iron highlighted as one of three key research needs, 'to characterize the stability of akaganeite to better determine when, under storage conditions, it can transform into Goethite or magnetite, release its chlorine as chloride ions, and stimulate on-going corrosion' (Selwyn, 2004). Four main conversion processes are reported in the literature.

- when akaganeite is immersed in acid aqueous solutions it slowly transforms to Goethite by a process of dissolution and precipitation (Cornell and Scwertmann, 2003 p366).

- when akaganeite is immersed in alkaline aqueous solutions it slowly transforms to hematite by a process of dissolution and precipitation (Cornell and Giovanoli, 1990).

- several of the iron oxyhydroxides, including akaganeite have been shown to react with ferrous ions or $Fe(OH)_2$ to form magnetite:

  $$Fe^{2+}_{(aq)} + 2FeOOH_{(s)} \rightarrow Fe_3O_{4\,(s)} + 2H^{+}_{(aq)} \qquad (6.1)$$

  or

  $$Fe(OH)_{2(s)} + 2FeOOH_{(S)} \rightarrow Fe_3O_{4(s)} + 2H_2O. \qquad (6.2)$$

  Laboratory studies have shown the order of reactivity is akaganeite>lepidocrite>Goethite (Ishikawa, 1998).

- akaganeite slowly transforms into the more stable hematite (Paterson et al, 1992; Naono et al, 1982).

The transformation of laboratory prepared akaganeite into hematite has been studied (Stahl et al, 2003). The authors concluded that although chloride was lost, this did not occur below 200ºC and no transformation of akaganeite occurred below this temperature.

The aim of this chapter is to investigate the transformation reactions of akaganeite particularly looking for evidence on archaeological iron artefacts. Both laboratory studies and analyses of akaganeites from archaeological objects have been undertaken. Over thirty akaganeite samples from objects with Goethite on their surfaces have been analysed and over 275 akaganeite samples analysed to determine if any hematite was present after long term storage.

6.2 Methods and Materials

Synthetic akaganeite was prepared by heating 500ml of 0.3M $FeCl_3$ at 70ºC in a sealed glass flask for 48 hours as described in chapter 3, (Schwertmann and Cornell, 1991). The precipitate was collected on a 0.45µm PTFE filter and then washed six times in a centrifuge, with fresh 18.2MΩ water each time. The chloride concentration of the wash waters was monitored with ion chromatography. It had dropped below 0.1ppm by the sixth wash. The samples were analysed with FTIR, Raman and XRD to confirm it was akaganeite.

6.2.1 Transformation of akaganeite into Goethite on objects

Akaganeite crystals from objects from four sites were observed to have a pale yellow layer on their surfaces. This has formed in three showcases at Portchester Castle; and cardboard storage boxes for materials from Lullingstone Castle stored at Fort Brockhurst and Stone and Uley stored in Blyth Road Store. Analysis (FTIR - ATR) reported in Chapter 4 identified the yellow material as Goethite in almost all instances and lepidocrite on just one object. This object had been treated with sodium hydroxide and white particles were observed on it under magnification (x40).

Akaganeite samples removed from the objects were carefully placed onto a PTFE sheet cleaned four times by immersion in 18.2MΩ water and allowed to air dry in a dessicator with dry silica gel. Moulds were placed around them and epoxy resin

(Struers EpoThin) cast so as to present a single face of the crystal, see below. When set the epoxy block was analysed using a Thermo Nicolet iS10 spectrometer with Continuum microscope with germanium ATR head. The microscope viewing system allowed the sample to be placed so only akaganeite was sampled. The analytical area was a square 20 by 20µm. The spectra were examined for any epoxy resin absorptions and repeated if any were observed.

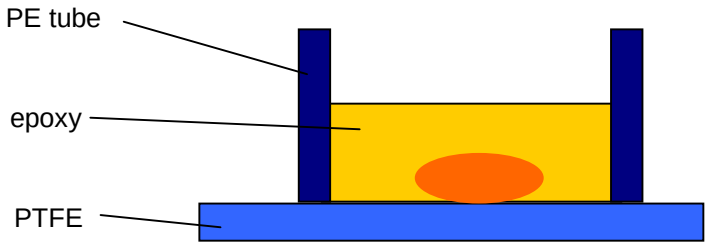

Figure 6.1 Sample Preparation for akaganeite samples for ATR-FTIR analyses.

This approach allowed the akaganeite sample to be accurately placed for analysis. The nature of the surface layer was determined. The peak ratio $802cm^{-1}/854cm^{-1}$ was determined to indicate the amount of Goethite present on top of akaganeite. The total information depth was calculated from equation 2.2 using published values for the refractive index of germanium (4.000) and Goethite (2.260). For the Goethite absorption used, $802cm^{-1}$ = 12.470µm wavelength. This gave a penentration depth of 1.038µm. The peak ratio was not converted into a layer depth due to the mathematical complexity of the conversion. The exponential decay of the evanescent wave, wavelength dependence and increased optical and dispersion effects in ATR lead Kwan (1998) to conclude 'the inherent features of internal reflection spectroscopy, render such a quantitative analysis very complicated'. As SEM-EDX analysis was planned this was not investigated further.

The sample was then cut down the epoxy cylinder with a cleaned Isomet diamond saw and an oil-based lubricant (Buehler ISOCUT). The surface was ground and polished down to a finish of 1µm using white spirit as the lubricating agent and cleaned abrasive disks. A few drops of Industrial Methylated Spirits (IMS) were used to clean the sample surface of any white spirit residues after polishing. All surfaces and solutions used were checked by swabbing with 18.2MΩ water and

analysis with ion chromatography. Chloride concentrations below 0.1ppm were detected in all samples. Some of the samples could not be polished as there was too much grain pull out. In these instances new epoxy was cast to encapsulate the remaining, unpolished half of the sample and the sample was ground and polished in the other direction. This produced a cross section, but not at the level analysed with ATR FTIR.

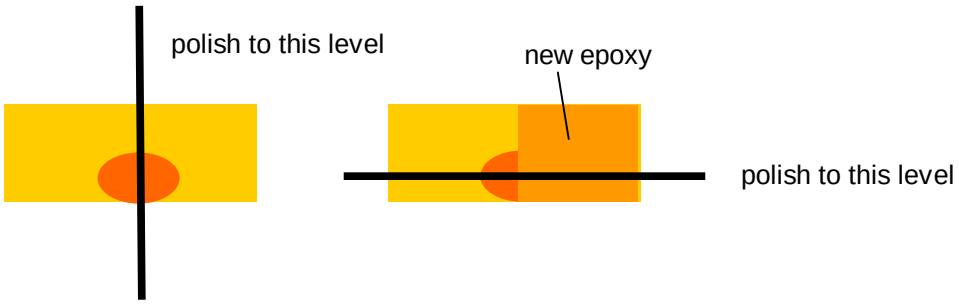

Figure 6.2 Sample Preparation for akaganeite samples for SEM-EDX analyses. Right hand side technique was used where possible to present samples including the part of the coating analysed by ATR-FTIR. If the sample could not be polished in this way, the sample was encapsulated with new epoxy and a perpendicular cross section produced.

The cross sections were carbon coated (400Å) and examined with scanning electron microscopy with energy dispersive x-ray analysis, SEM-EDX. This indicated that the orange akaganeite areas had between 6 and 8.5% chloride present, whilst the pale yellow coatings had very low chloride concentrations, less than 0.5%. The depth of layer was assumed to be the distance at which the chloride concentration decreased dramatically. Multiple line scans were carried out on the edges of each sample to determine the depth of the pale yellow layers. During all analyses the x-ray count rate was monitored and found to be constant. Any fluctuation in count rate could indicate a loss of chloride from the surface due to reaction with the electron beam.

6.2.1.1 Past environments

The environment under which the Goethite had formed from akaganeite is obviously of great interest. The old Portchester Castle display has calibrated monitoring with

dataloggers for their full fifteen year lifetime. The store rooms at Fort Brockhurst (Lullingstone) and Blyth Road (Uley and Stonea) had no contemporary environmental monitoring. Attempts were made to recreate the past environments.

A Meaco radiotelemetry logger was placed in the space at Fort Brockhurst for one full calendar year. No environmental monitoring records exist for the storage area at Blyth Road. Records for RH and temperature for the year 2000 are available from two of the Victoria and Albert Museum's stores on that site were obtained.

When the storage boxes containing deteriorating material were first brought into the Conservation laboratory, data-loggers (Hanwell Humbug 2 or Elsec 793) were placed inside the boxes to monitor the RH value to which they had equilibrated.

Analysis of the object surfaces (Raman micro-spectroscopy) indicated the presence of sodium hydrogen carbonate on several of the objects. This material was used as an abrasive for air abrasive cleaning and had penetrated many of the cracks and recesses of the artifacts as well as being present on the surfaces. Sodium hydrogen carbonate undergoes rapid conversion to sodium carbonate when in solution and the presence of carbonate on the surfaces could be readily detected by Raman micro-spectroscopy. In the atmosphere this conversion would be expected to occur predominantly when the sodium hydrogen carbonate deliquesces. This has been used as a marker to determine the maximum RH to which the objects have been exposed after conservation. The RH response of sodium hydrogen carbonate has been characterized (Ahlneck and Alderborn, 1989).

However, the conversion to carbonate is a much more complex process with a competing thermal reaction. Hence experiments were undertaken to measure this. Although some work has been undertaken the RHs used 48 and 75% were very widely spaced (Kuu et al, 1998). Analar sodium hydrogen carbonate (1.5g) was accurately weighed into a polyethylene container. Forty crystals were placed individually in polyethylene containers. The sodium hydrogen carbonate samples were then exposed to controlled RH atmospheres above glycerol solutions at 50, 60 and 70% and at 20, 30, 35 and 40˚C for 48 hours. The sodium hydrogen carbonate samples were the reweighed to measure any uptake of water. The bulk sample was analysed with XRD and the presence of any sodium carbonate determined from the diffraction patterns (5% detection limit). When sodium carbonate was detected with

XRD at one RH value, the individual crystal samples from the lower RH exposure were each analysed with Raman micro-spectroscopy to confirm no sodium carbonate was present.

Ethanoic and methanoic acid measurements were undertaken at Portchester Castle and in two of the storage boxes from the Blyth Road store. No measurements were carried out in the Lullingstone boxes before the objects were repacked into Stewart boxes. The original cardboard boxes were disposed. However, measurements have been carried out recently in similar cardboard boxes at the Dover store.

6.2.2 Tranformation of akaganeite into Goethite laboratory experiments

In order to facilitate analysis samples were prepared as pressed discs. This allowed pressure to be exerted for FTIR-ATR without the powder breaking up and aided the cross section preparation for SEM-EDX.

Small discs were pressed from both synthetic akaganeite powders and powdered akaganeite, the relatively pure sample from an object, a coffin clamp from Sutton Hoo, described in Chapter 4. The synthetic akaganeite discs were exposed to atmospheres above glycerol solutions similar to the experiments described previously, but with 16.7 and 18.4% excluded. The discs formed from the akaganeite sample from an object were exposed to 30, 50 and 70% RH due to the limited size of the sample. Further discs were immersed in 18.2MΩ water and water buffered to pH 8.5 with sodium carbonate and hydrogen carbonate. Portions of the disc were removed at one, two, three, six and twelve month intervals and analysed with FTIR with the Golden Gate and germanium ATR.

6.2.3 Transformation of akaganeite into hematite on objects

Hematite has only rarely been reported on iron from a non burnt context (Turgoose, 1982a). Hematite has a low sensitivity in both x-ray diffraction, which has been the predominant analytical method applied to iron corrosion and FTIR used in this study. Raman micro-spectroscopy has a much higher selectivity and hence sensitivity (Robinet and Thickett, 2005). Thermal conversion of akaganeite to hematite, via maghemite has been observed at moderate laser fluences and analyses where

undertaken using fluences below 64W/m^2 and the spectra from the early scans examined to ensure the sample was not reacting. Only five instances of hematite were observed on the corroded examples described previously. However, of the 200 instances of corrosion studied in that work, over 93% were from artefacts from low RH (less than 15% RH) storage, exposed for under three years. Hence it is unlikely that any detectable conversion to hematite would have occurred on these samples. To obtain a representative data set, 275 samples of akaganeite iron corrosion collected over the past thirty eight years for XRD analysis were re-examined with Raman microscopy. Samples over the past 13 years had been taken by the author and existing samples were also analysed. These samples were stored under ambient laboratory conditions (15-30ºC, 30-70%RH).

6.2.4 Transformation of akaganeite into hematite laboratory experiments

The thermal transformation of akaganeite into hematite was studied by heating synthetic akaganeite at a series of elevated temperatures. The rates of conversion to hematite were determined. Dried samples were accurately weighed (Oertling NA164 balance) and placed in 5cm^3 aluminium dishes. The dishes were placed in ovens at 60, 100, 140, 180ºC for three months. A control was kept at room temperature. After this time the samples were reweighed. Any new soluble chloride released from akaganeite transformation was assessed by extracting 100mg of the sample with 10ml of 18.2MΩ water and analysing the chloride concentration in the extract with ion chromatography. The samples were analysed with FTIR (KBr disc) and Raman.

Quantification with FTIR was difficult due to the broad akaganeite absorptions at either side of the 548cm^{-1} absorption of hematite and the raised baseline due to these peaks.

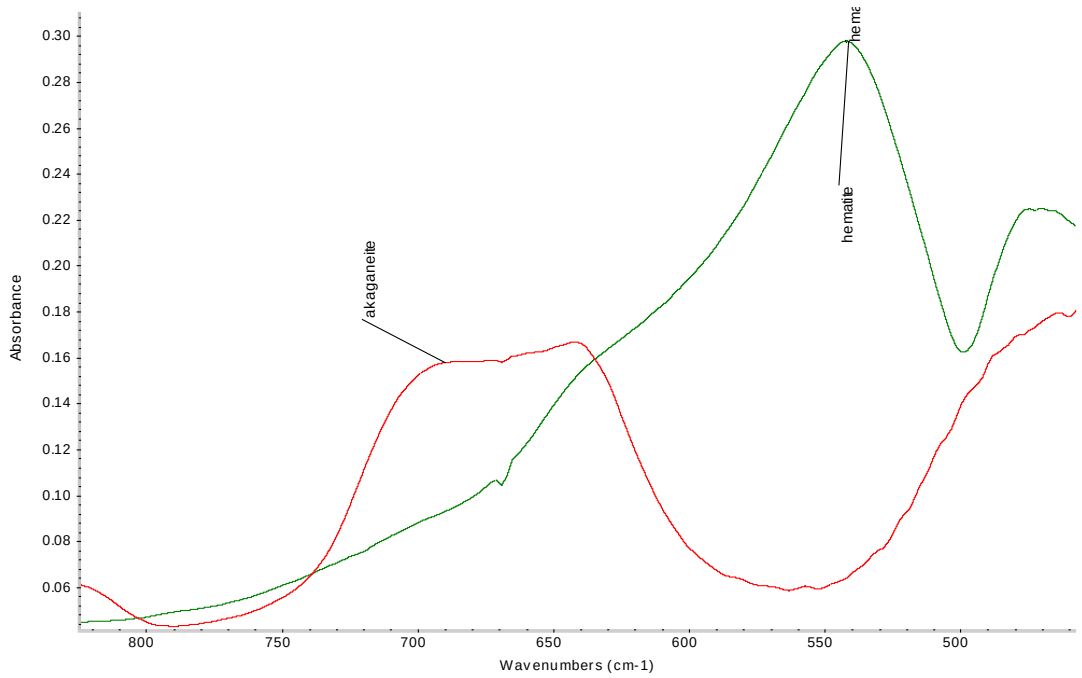

Figure 6.3 FTIR spectra of hematite (green) and akaganeite (red).

This was a particular issue with the lower concentrations of hematite produced at 60 and 100 ºC. Hematite was identified in all samples and no other minerals were observed with Raman. The mass losses were used to calculate the rate, assuming the equation

$$2FeOOH_{(s)} \rightarrow Fe_2O_{3(s)} + H_2O_{(g)} \quad \text{mass loss } 18\% \qquad (6.3)$$

The synthetic akaganeite contained 8.4% of chloride (determined by SEM-EDX on a prepared grain mount) and if any of this vaporised, the mass loss would overestimate the transformation. Hence the highest temperature experiment, 180ºC was repeated with a sodium hydroxide solution trap in the vent of the oven. The sodium hydroxide was analysed after three months to determine any chloride emitted.

This method required large amounts (100mg) of sample and there was not enough sample from objects available to attempt it.

A model free method using TGA data was investigated to see if kinetic modelling could be carried out with less sample. Synthetic akaganeite samples were analysed with a Perkin Elmer TGA7 in 60ml/min of nitrogen with different heating rates, between 1 and 20ºC/min. The TGA curves were processed with the AKTS software

developed from the ICTAC project (Roduit and Maciejewski, 1996; Roduit, 2000; Roduit, 2002).

6.2.5 Thermal analyses of differences between synthetic akaganeite and akaganeite from an archaeological object

Thermal analysis, TGA, DSC and thermo-gravimetry-mass spectrometry (TGA-MS) was undertaken to further characterise the synthetic akaganeite produced for these experiments. Akaganeite from the Sutton Hoo coffin clamp was also analysed with TGA and DSC for comparison. The TGA and DSC methods are described in Chapter 2. Thermo-gravimetry-mass spectrometry was undertaken by the Centre for Thermal Analysis at the University of Huddersfield. A Du Pont TG951 instrument with approximately 25mg of sample in a 70µl ceramic crucible was analysed in air and nitrogen, heated at 10ºC/min to 900 ºC. The evolved gas was analysed with a Prolab quadrupole mass spectrometer working in a mass range 1-100amu.

6.3 Results

6.3.1 Transformation of akaganeite to Goethite on objects

The depths of Goethite conversion layers determined by SEM-EDX line scans described previously are shown below.

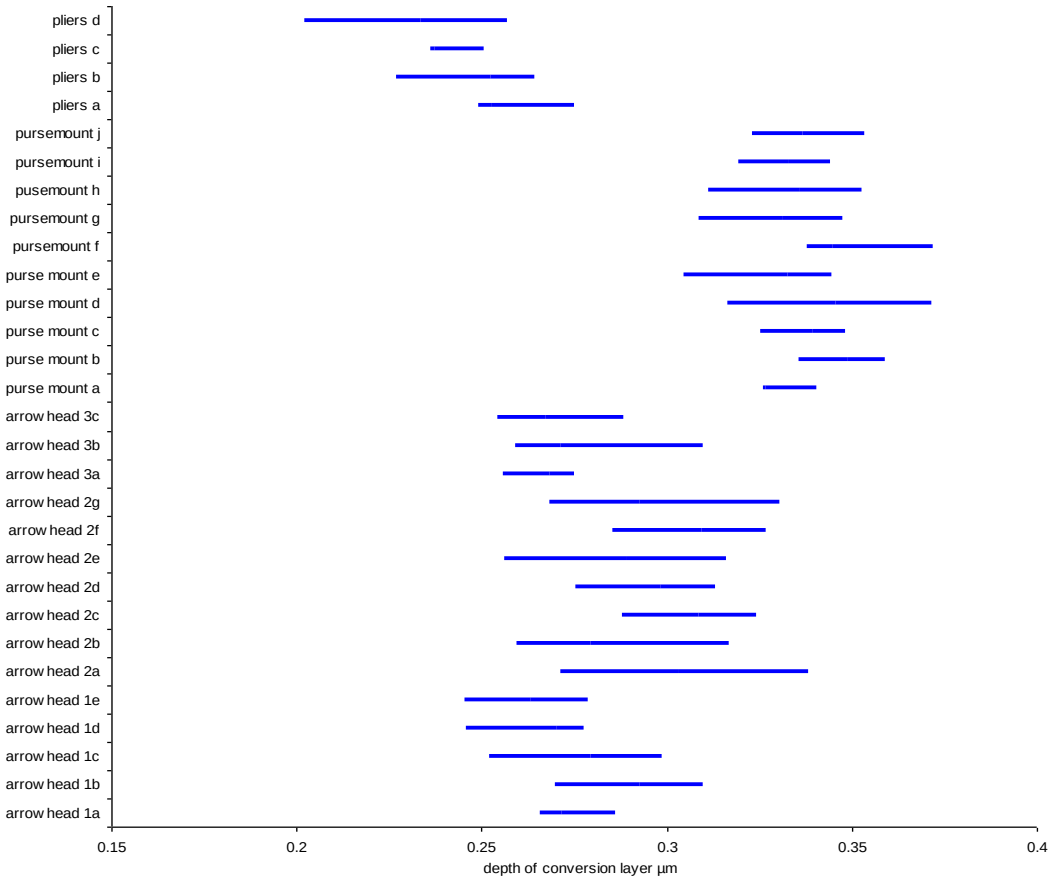

Figure 6.4Depth of Goethite transformation layers on samples from Portchester showcases determined by several SEM-EDX line-scans on a cross section of each sample.

Figure 6.5 shows the FTIR peak ratios for $802cm^{-1}/854cm^{-1}$.

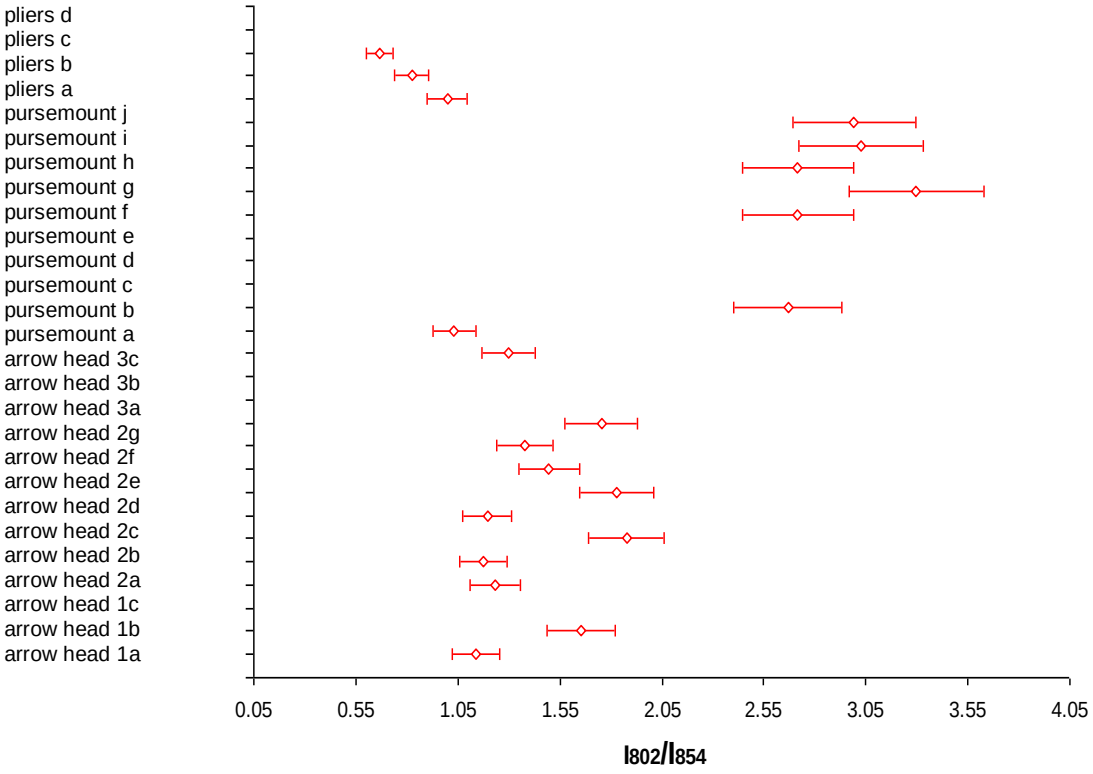

Figure 6.5 Peak ratios I_{802}/I_{854} for Goethite transformation layers on samples from Portchester by ATR FTIR.

There was good agreement between the FTIR and SEM-EDX data. The maximum Goethite depth detectable with the ATR head used was calculated to be 1.038µm, equation 2.2 so very little signal will be obtained from akaganeite beyond this depth of Goethite.

The purse mount from the Saxon case appears to be have thicker conversion layers than the other objects, although there is a slight overlap with the SEM-EDX line-scan data. The pliers in the Medieval case appear to have the shallowest conversion layer. Again there is overlap with the SEM-EDX line-scan data with the Roman case objects. Both Chi squared and t-tests indicated significant differences between the SEM-EDX line-scan data for objects in the three showcases at a 95% confidence level.

The depths of Goethite conversion layers determined by SEM-EDX line scans for the Uley, Stonea and Lullingstone objects are shown below.

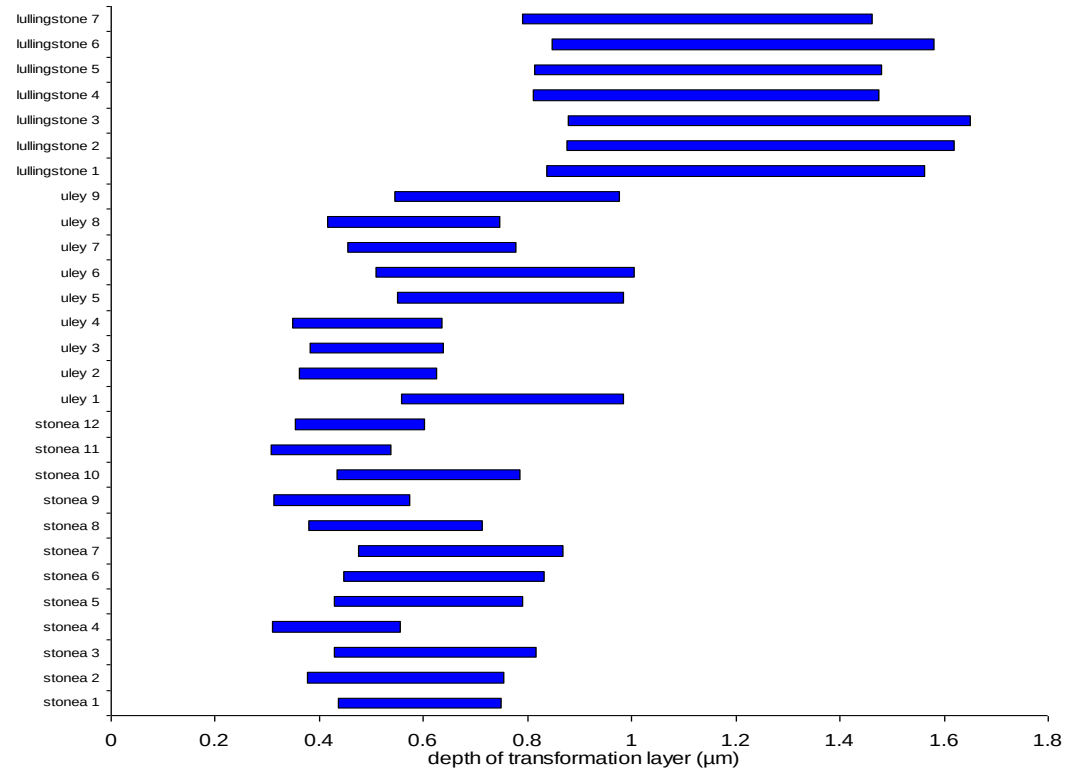

Figure 6.6 Depth of Goethite transformation layers on Uley, Stonea and Lullingstone objects from storage. Bars mark the minimum and maximum depths determined by several SEM-EDX line-scans on cross.

The akaganeites formed on the Lullingstone objects have thicker Goethite conversion layers than those from Uley and Stonea. Both Chi squared and t-tests indicated significant differences between the SEM-EDX line-scan data for objects from Lullingstone and those from Stonea and Uley at a 95% confidence level.

6.2.1.1 Past environments

The environment in the old display at Portchester Castle was by far the best characterised. The tabulated data is shown in Table 6.1.

Case	Maximum RH	Amount of time as a percentage in RH band									Carboxylic Acid Concentration µgm^{-3}	
		5-10%	10-15%	15-20%	20-25%	25-30%	30-35%	35-40%	40-45%	45-51%	ethanoic	methanoic
Roman	29-35	3	25	23	24	24	1	0	0	0	1189±64	124±26
Saxon	46-51	0	2	16	17	16	15	17	16	1	1835±87	206±31
Medieval	25-31	7	24	22	22	24	1	0	0	0	1243±64	128±26

Table 6.1 Environmental data from three showcases in old Portchester Castle display with archaeological iron.

The Saxon case experienced higher RH values than the Medieval and Roman cases. It also had higher ethanoic and methanoic acid concentrations, because ethanoic acid emission from wood is a strong function of RH (Thickett, 1998b).

The RH and temperature monitoring from the room used to store the Lullingstone material at Fort Brockhurst is shown in Figure 6.7.

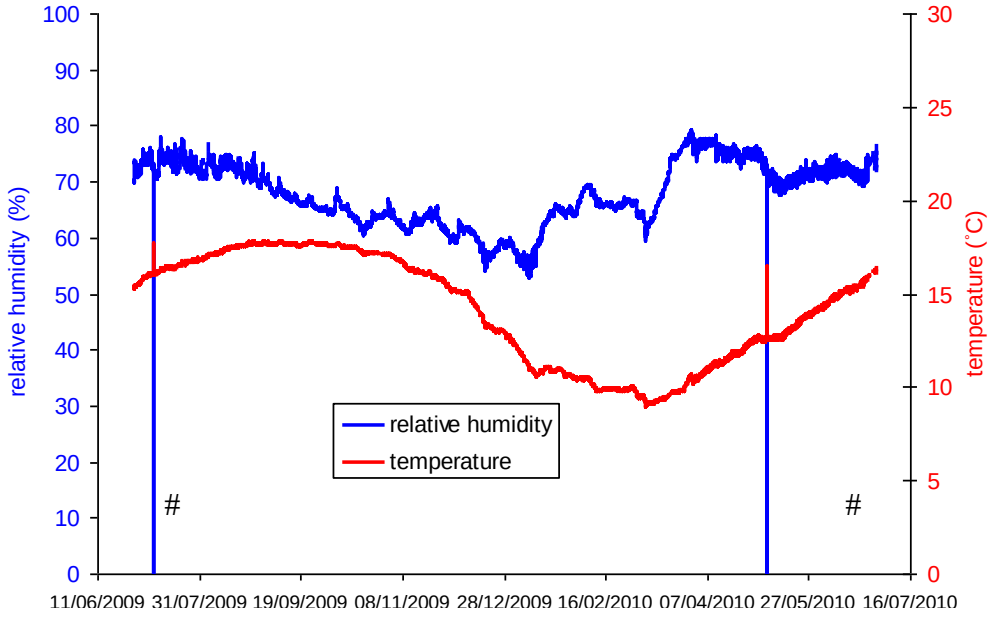

spike in data due to corruption through radio transmission

Figure 6.7 Environment in Fort Brockhurst store room used for Lullingstone material. The two sets of spikes in the data are due to anomalous radio transmission.

There is an annual cycle for temperature between 9 and 17ºC. The relative humidity is generally high and ranges between 55 and 78%. Ethanoic and methanoic acid concentrations of between 537 and 2394 and between 26 and 245 μgm^{-1} where measured in similar types of cardboard boxes in rooms in Dover stores with similar environments.

Environmental data from the adjacent room to the Blyth Road store room used for the Uley and Stonea material is shown in Figure 6.8. This data was kindly supplied by the Victoria and Albert Museum.

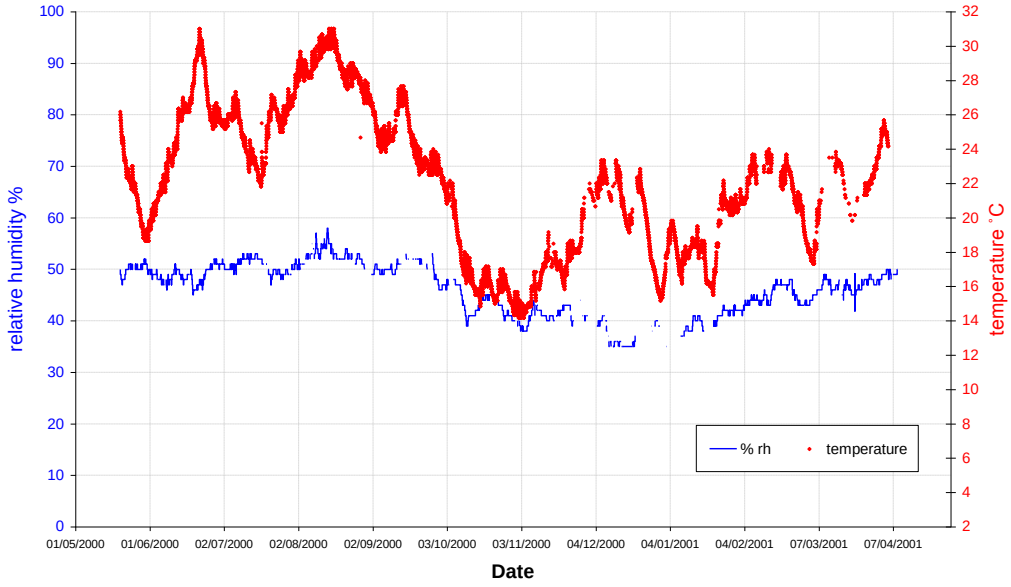

Figure 6.8 Temperature and RH in room adjacent to Blyth Road store room used for the Uley and Stonea material.

The Victoria and Albert Museum data showed temperatures ranging from 10 to 29˚C and relative humidities from 35 to 63% with means of 19 ˚C and 47%. The highest RH occurs in August and coincides with highest temperatures. It is likely that the iron store room conditions were not much different from these. The cardboard boxes would be expected to provide buffering of the RH, limiting the range, but keeping approximately the same mean. The equilibrated RH values measured in the boxes were between 48 and 51%. Unfortunately room conditions can vary widely due to differences in building fabric, building services, ventilation and aspect. Temperatures tend to be less variable than RHs and in these rooms the maximum temperatures

reach 26-31°C in late summer. This is generally accompanied by the maximum RHs experienced.

The presence of untransformed sodium hydrogen carbonate on the object surfaces can give an indication of the maximum RH experienced when combined with maximum temperature data. The results of the transformation tests on sodium hydrogen carbonate are shown in Figure 6.9.

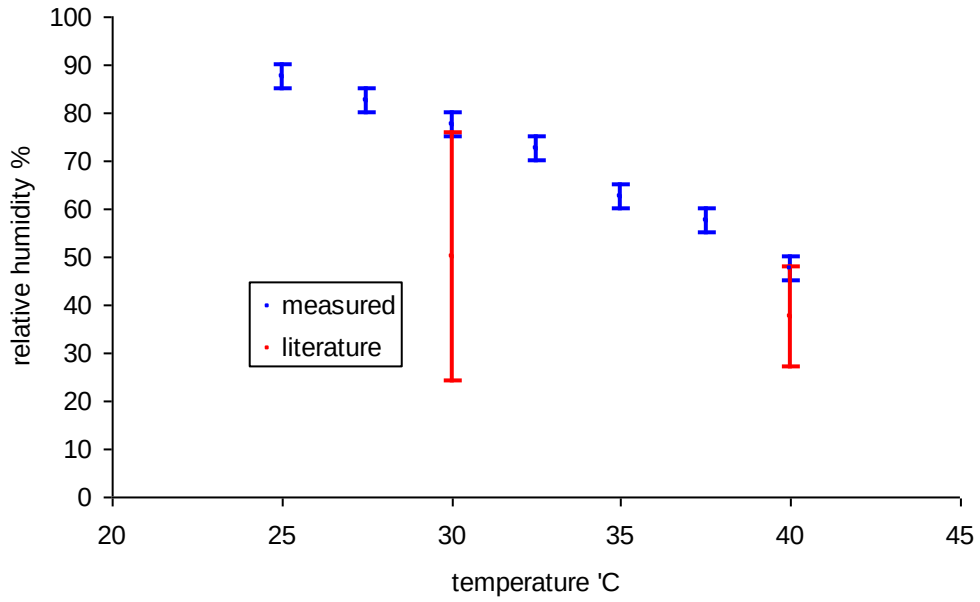

Figure 6.9 Transformation RH values for sodium hydrogen carbonate to sodium carbonate at different temperatures. Blue bars are measured ranges, red bars are literature values.

The critical RH values for the transformation to carbonate are between 75 and 80% at 30˚C. These are within the very wide range determined by Ahlneck and Aldeborn (1989).

Further tests were performed with 1% intervals between 75 and 80% relative humidity at 30ºC. These indicated that conversion had not occurred at 75%, but had occurred at 76%.

No sodium carbonate was detected on any of the iron surfaces indicating that the critical RH had not been exceeded since the air abrasive treatment was applied.

Ethanoic acid concentrations of 4758 ± 302 and 5630 ± 356 μgm^{-3} were measured in two of the Uley storage boxes. These values are relatively high compared with those measured in other display and storage situations, see Chapter 7.

6.3.2 Transformation of akaganeite into Goethite laboratory experiments

The results of the SEM-EDX line-scans are shown in Figure 6.10 and FTIR in Figure 6.11.

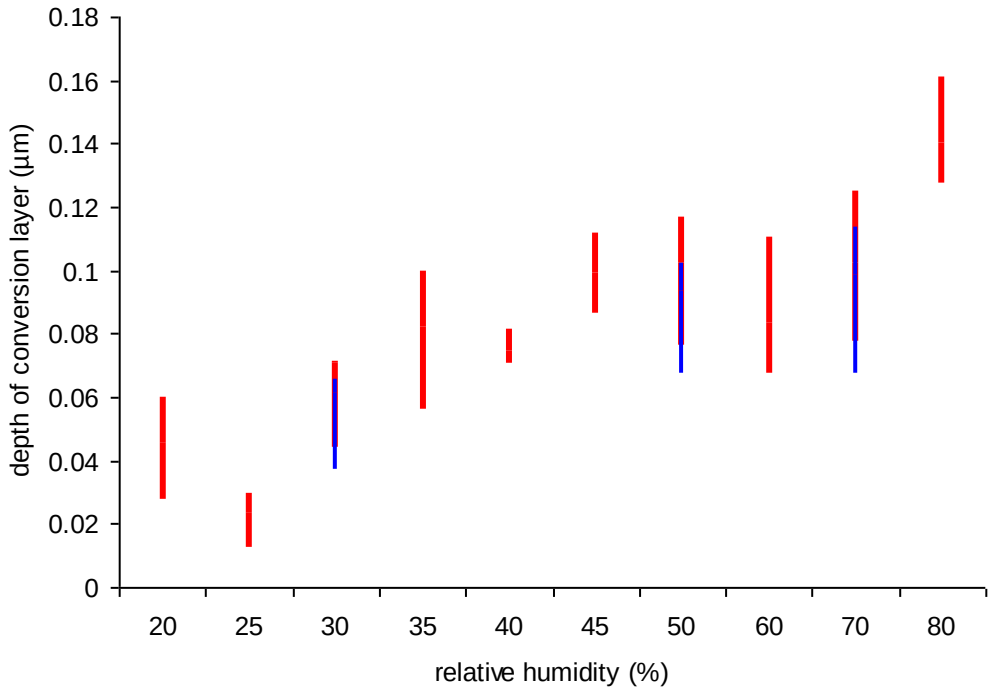

Figure 6.10 Depth of Goethite conversion layers formed on akaganeite after exposure to different relative humidities for 12 months. Red lines SEM-EDX line scans for synthetic akaganeite. Blue lines for akaganeite sample from archaeological iron objectiron object.

Figure 6.11 shows the ratio of FTIR peaks at 802 and 854 cm^{-1}.

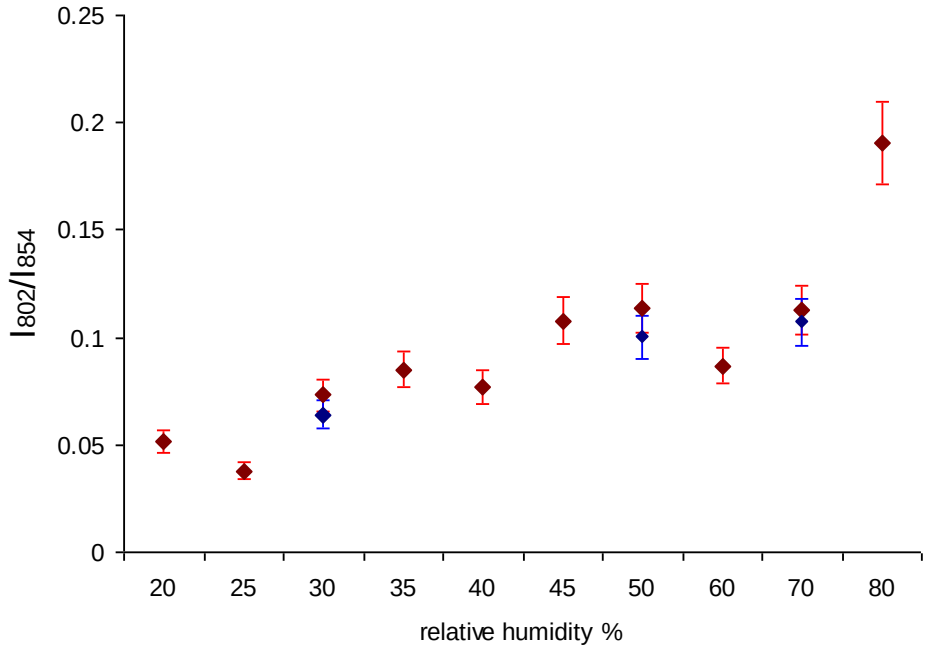

Figure 6.11 Peak ratios I_{802}/I_{854} for Goethite transformation layers on samples exposed to different relative humidities for 12 months. Red lozenges synthetic akaganeite. Blue lozenges for akaganeite sample from archaeological iron object.

The lower RH experiments produce very thin conversion layers. These thin layers are approaching the detection limit for both SEM-EDX and FTIR ATR. In SEM-EDX the sample epoxy interface can interfere with the line scans. Measurements below 300nm therefore have a large degree of uncertainty. The 25% RH experiment was below this figure and some caution should be exercised with the results. The experiment at 20% RH may also have been compromised by a lid not being fully tightened. The RH in the vessel was measured to be over 30% at the end of the experiment, well above the 20% aimed for. These results indicate a general increase in the rate of Goethite formation as the RH increases, but there is a lot of scatter in the data. The akaganeite sample from an object showed very similar behaviour to the synthetic akaganeite at 30, 50 and 70% RH. The data appear to show slightly less conversion, but this was not borne out by statistical chi squared and t-tests.

6.3.3 Transformation of akaganeite into hematite on objects

The instances of hematite identified with Raman micro-spectroscopy, are plotted against number of years since sampling in Figure 6.12. The number of samples and

percentage of samples with hematite observed is also included.

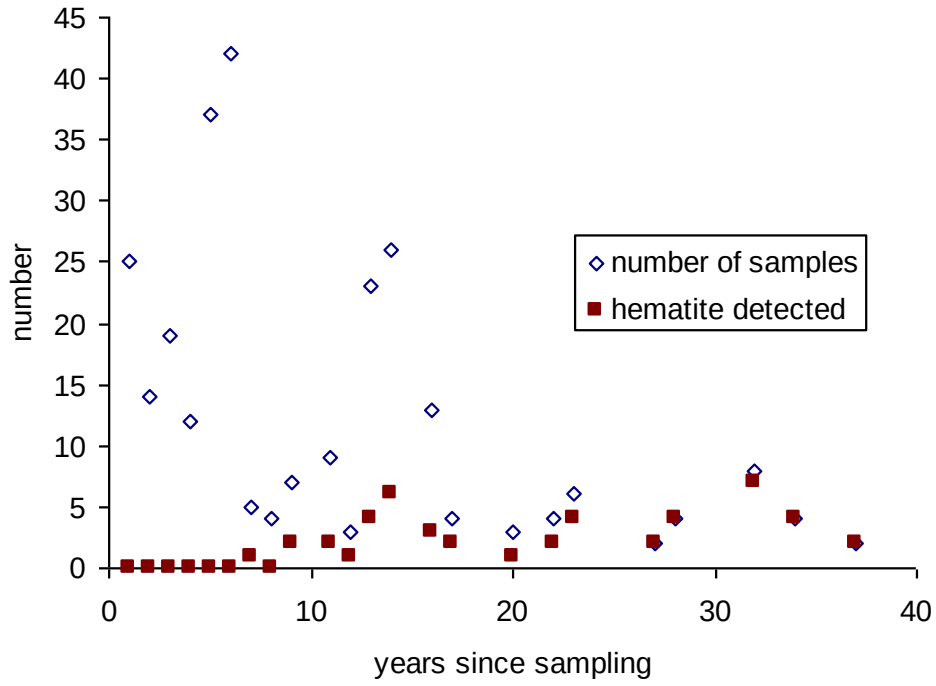

Figure 6.12 Hematite detected in old akaganeite sample from objects stored in the British Museum. As time progresses, more samples have hematite in them.

Although the sample size is still relatively small at the longer time periods, there appears to be an increasing occurrence of hematite associated with akaganeite with time. Hematite appears to be detectable with Raman microscopy (greater than approximately 10% mixed with akaganeite in a sampling volume of 100µm^3) after eight years storage under these ambient conditions and after thirty four years all of the samples had hematite present. Hematite has definitely been observed associated with akaganeite and it is highly likely that it is a conversion product of that akaganeite.

6.3.4 Transformation of akaganeite into hematite laboratory experiments

The mass losses from synthetic akaganeite and calculated rates are shown in Table 6.3. Additional surface chloride was detected from some of the experiments with ion chromatography and this is included in Table 6.2 also.

initial mass (mg)	Temperature (ºC)	90 days		120 days		reaction rate (% hematite converted in 3 months)
		Mass loss (mg)	chloride release (g)	mass loss (mg)	chloride release (mg)	
434.47	60	0.04	bd	0.10	bd	0.13
438.24	100	0.35	bd	0.70	bd	0.88
447.69	140	1.76	bd	3.44	bd	4.27
415.97	180	9.63	0.17	19.20	0.46	25.64

bd below detection limit 0.00002g, errors are $\pm$ 0.00001g on mass readings

Table 6.2 Mass losses and chloride released on heating akaganeite samples to different temperatures.

No significant chloride was detected in the extracts of the sodium hydroxide traps in the oven vents and it is therefore reasonable to calculate the conversion rates from the mass losses. The balance accuracy was $\pm$ 0.01mg.

An Arrhenius plot was constructed from the data and is shown in Figure 6.13.

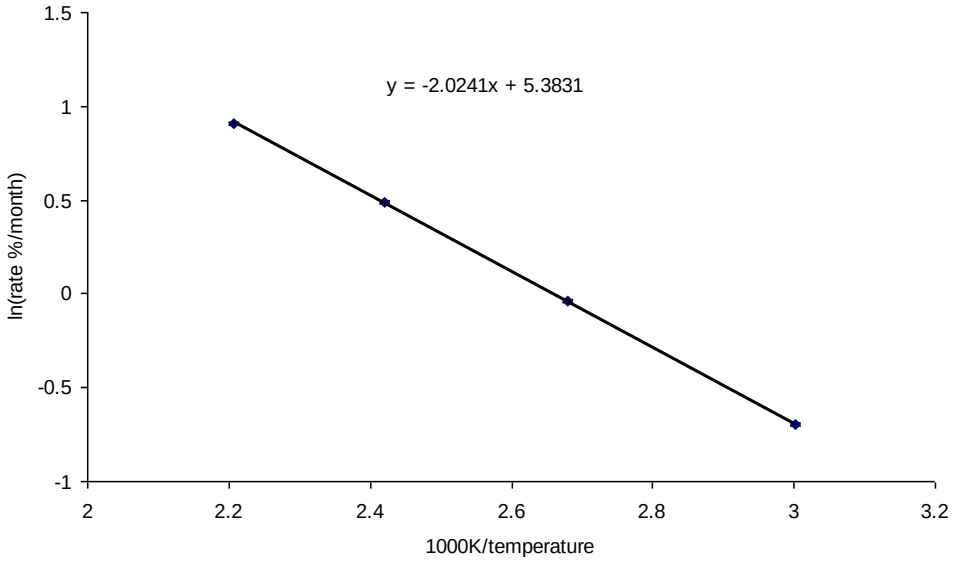

Figure 6.13 Arrhenius plot of akaganeite conversion to hematite.

The Arrhenius plot produced a good fit to a straight line. This was extrapolated to 20ºC to estimate the conversion rate at room temperature (ordinate value 3.411). This indicated a rate of 0.0081% in three months. Comparison with the analysed akaganeite samples in section 6.3.2 would give a conversion of 0.22% in the most recent samples on which hematite was detected (after 8 years). This value is consistent with the assumed detection limit of the analytical method used, Raman micro-spectroscopy.

Unfortunately this approach required large amounts of sample and could not be tried with akaganeite samples from objects. Attempts to model the conversion from TGA data were unsuccessful as a complex decomposition was observed with three peaks in the derivative TGA traces. It was not possible to determine which peak was due to transformation to hematite and the adjacent peaks made baseline correction and numerical fitting impossible.

6.2.5 Thermal analyses of differences between synthetic akaganeite and akaganeite from an archaeological object

The DSC curve for the synthetic akaganeite is shown in Figure 6.14.

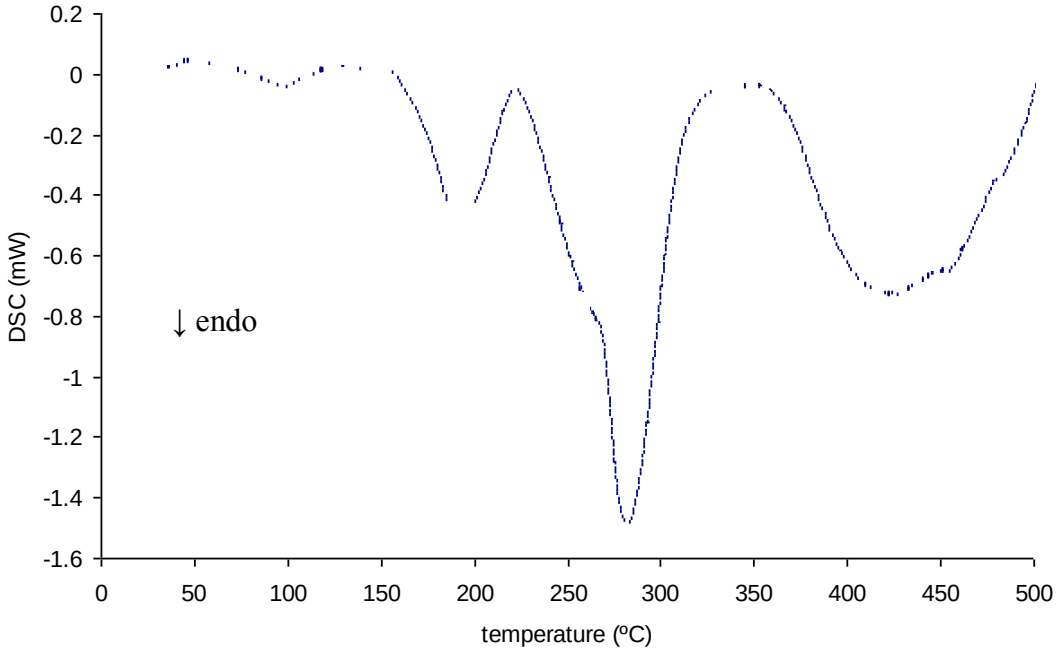

Figure 6.14 Synthetic akaganeite (first batch) analysed with DSC in nitrogen.

There is only a very small DSC peak below 100ºC and associated mass loss due to the very prolonged drying of the sample. The endotherms between 180 and 550ºC is reported to be loss of hydroxyl and chloride ions. Goni-Elizalde et al (1988) assigned the 241ºC DSC endotherm to dehydroxylation and the 292ºC DSC endotherm to chloride loss. An exothermic peak at 485ºC was assigned to crystallization to form hematite. This is not present on the DSC of the sample analysed.

The TGA curves and their first derivatives for the synthetic akaganeite on the DuPont TG951 are shown in Figure 6.15.

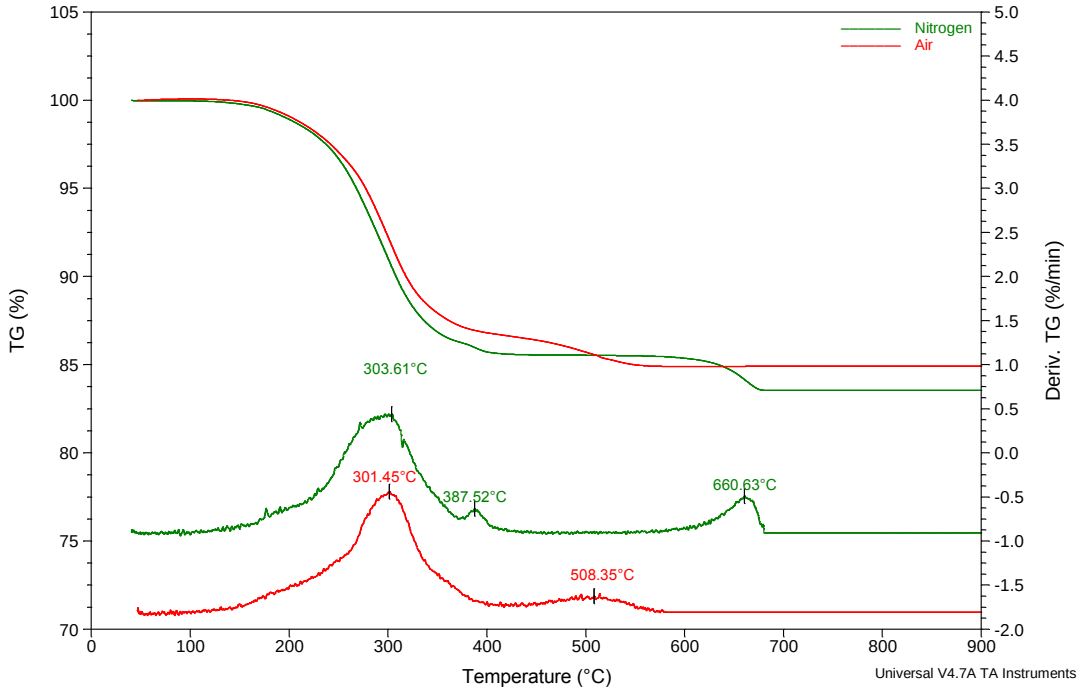

Figure 6.15 Synthetic akaganeite (fourth batch) analysed with TGA in air (red TGA and DTGA traces) and nitrogen (green TGA and DTGA traces).

In nitrogen the initial decomposition is at slightly lower temperature compared to the analysis in air (although the peak in DTGA is slightly higher 303ºC compared to 301ºC). In nitrogen there is a second effect (DTGA peak at 387 ºC). The second mass loss appears to be delayed in nitrogen compared to air (DTGA peak at 660 ºC compared to 508 ºC).

The curves are similar to those reported by Post et al (2003), Garcia et al (2008), Paterson et al (1982), Chitrakar et al (2009), Goni-Elizalde et al (1988), Music et al (2004) and MacKenzie (1970). They differ from that reported by Stahl et al (2003) in that the loss of mass is much more gradual. Stahl et al's analyses were carried out with air as a carrier gas, as were Goni-Elizalde et al and MacKenzie's.

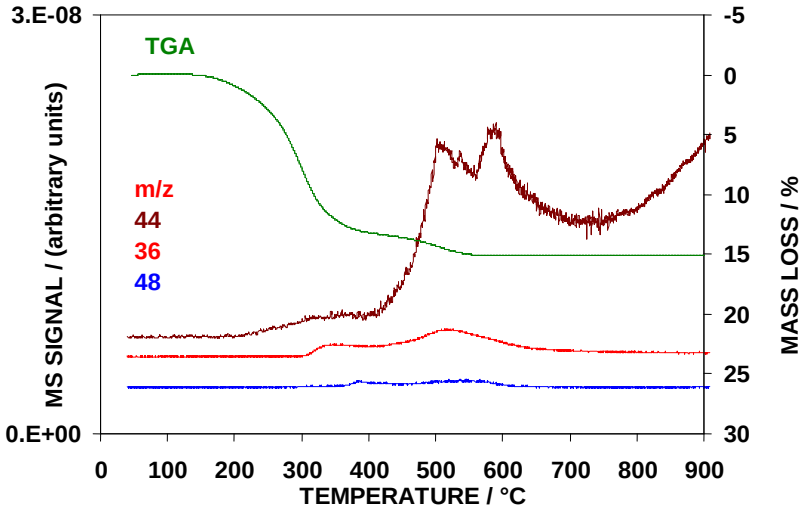

Figure 6.16 Synthetic akaganeite (fourth batch) analysed with TGA-MS in air.

Chloride (m/z = 36) is lost at 300 and 500ºC. Loss of carbon dioxide (m/z = 44), nitrogen dioxide (m/z = 48) were also observed. These species are most likely adsorbed on the akaganeite surfaces (Ishikawa and Inouye, 1973). The only reported TGA-MS analysis of akaganeite is by Stahl et al (2003). They report chloride loss determined by MS to correlate with the very abrupt mass loss they detected, as well as some water. Their analyses finished at 450 ºC. Ishikawa and Inouye (1976) reported that the chloride is lost as HCl from evolved gas analysis.

The DSC for the akaganeite sample from the Sutton Hoo coffin clamp is shown in Figure 6.17.

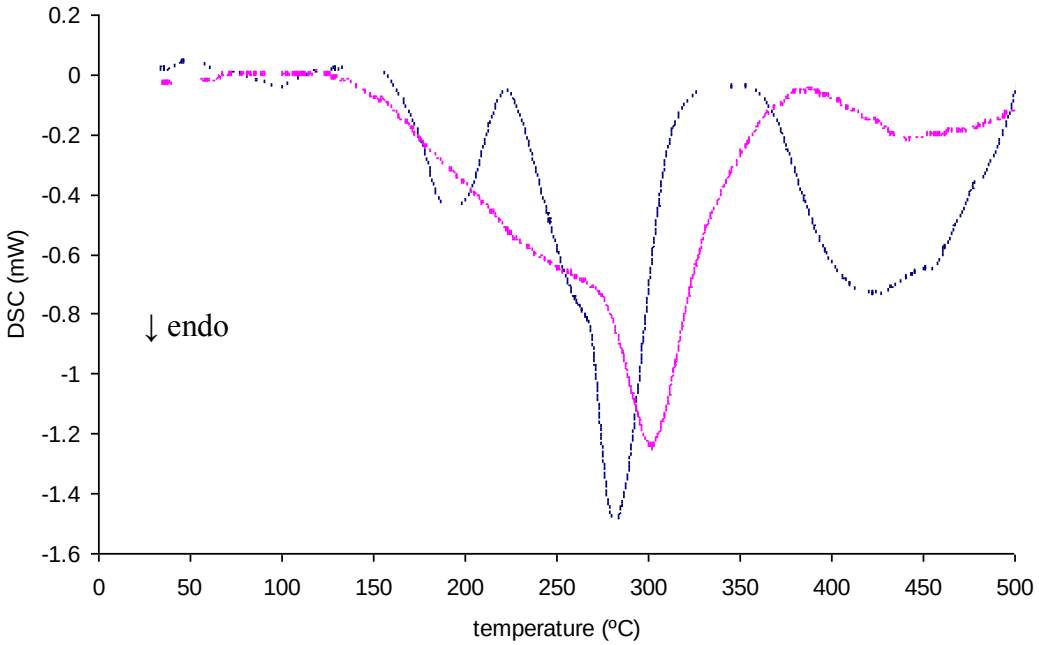

Figure 6.17 DSC of akaganeite from Sutton Hoo sample (purple trace), overlaid with synthetic akaganeite (blue) trace.

The DSC of the Sutton Hoo sample does not show endotherms at 100 and 180ºC, possibly due to it being stored above dry silica gel for several months prior to the DSC analyses. The shoulder peak at around 240 ºC is much broader than in the synthetic sample and the main endotherm is at a higher temperature 300ºC compared to 280ºC for the synthetic sample. This would be consistent with a more stable material. However, many factors can effect DSC results. For akaganeites the amount of chloride in the structure has been reported to affect thermal analysis. The crystallinity and morphology also affect thermal analysis. Low levels of impurities, as would be expected in archaeological iron samples can also change the DSC curves.

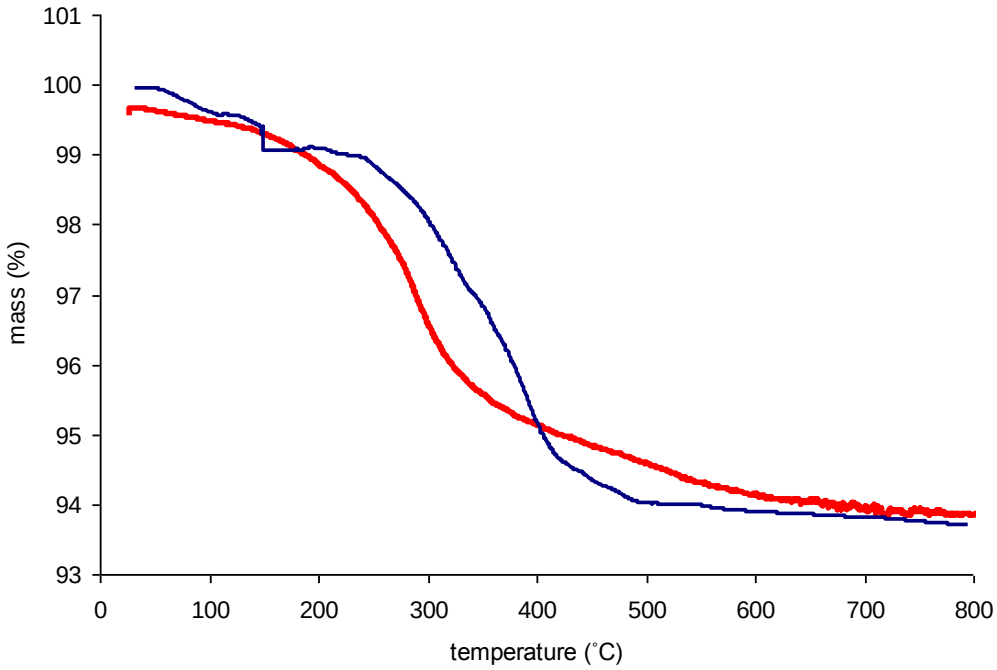

Figure 6.18 Akaganeite from Sutton Hoo coffin clamp analysed with TGA in nitrogen (blue trace). Apparent sudden drop at 150ºC is due to holding the run at this temperature for several minutes. Overlaid with synthetic akaganeite (red trace)

The TGA curve shows the same general shape as that for synthetic akaganeite but with the decomposition reaction occurring at slightly higher temperatures. This may indicate a more stable material. It is difficult to compare thermal analyses between materials as many factors can affect the traces. For akaganeites the amount of chloride in the structure has been reported to affect thermal analysis. The crystallinity and morphology also affect thermal analysis. Low levels of impurities, as would be expected in archaeological iron samples can also change the TGA curves. However thermal analysis is a sensitive probe of a materials structure and chemistry and may be able to distinguish between akaganeites where FTIR, XRD and Raman have failed to do so. MacKenzie (1970) has commented on the differening thermal analyses from different preparations of synthetic akaganeites.

6.4 Discussion and Conclusion

Two mechanisms of akaganeite conversion have been observed on object or akaganeite samples from objects. Conversion to form Goethite and hematite was observed for the first time on objects. No conversion to form magnetite was observed, probably because this reaction requires liquid water or the presence of $Fe(OH)_2$ adjacent to akaganeite. $Fe(OH)_2$ precipitates out of solution above pHs of 6, and hence again liquid water is required. The conversions to Goethite and hematite have also been studied in simple experiments.

A conversion to Goethite occurs at 35% RH and above. Conversion may occur at lower RHs, but the experimental method was not sensitive to very thin Goethite layers produced in the laboratory over 12 months. A single sample from an archaeological object showed very similar behaviour. There is evidence from the Portchester display that akaganeite conversion into Goethite does occur at RHs as low as 32%. All the showcases have high levels of ethanoic acid present and this may have increased the conversion rate. Results in chapter 5 showed Goethite production from ferrous chloride at acetic acid concentrations of 1500 μgm^{-3}, which is not greatly above the measured concentrations in the Roman and Saxon cases.

Conversion to hematite is much slower and could not be observed, even with Raman micro-spectroscopy within eight years. Laboratory experiments and Arrhenius calculations have indicated this is a very slow conversion.

Chapter 7 Display of Archaeological Iron

7.1 Introduction

This chapter considers what is needed to control the deterioration of archaeological iron on display and how that can be achieved via showcases. Archaeological iron is only very rarely displayed outside of showcases.

In this chapter the environmental requirements to control the deterioration rate of archaeological iron on display in showcases are summarised from the work in chapters 5 and 6. These are essentially maximum RHs , nitrogen dioxide, sulfur dioxide, ozone, ethanoic and methanoic acid concentrations and dust deposition rates. The design features and technologies used to ensure the creation of suitable environments in showcases are reviewed in 7.3. The methods used to measure showcase parameters and environments are described in 7.4. A tracer gas method to measure air exchange rates of showcases based on carbon dioxide had been developed. The performance of existing showcases was tested (7.5) to derive a new showcase specification (7.6). This involved measurements in over 100 showcases in English Heritage and the British Museum. An additional series of air exchange rate measurements was also undertaken in some of the showcases measured during the EC project MASTER to test models of pollutant ingress. Prototypes were built and extensively tested (7.7). The success of the new design has been assessed from installations across the English Heritage estate.

7.2 Environmental criteria for showcases for archaeological iron.

The preceding experiments and scientific literature allow specifications to be drawn for the performance of showcases. The high cost of new showcases means that, from a practical view, two specifications will be considered;

- New purpose built showcases when everything can be designed with optimum performance in mind

- existing showcases, where the architecture is fixed, but some re-fitting may be possible to improve performance. It is important that these criteria can form the basis for a prioritised program of initial re-fitting and eventual replacement as funds become available.

The specification must work within the limitations of English Heritage's estate and collections.

The discussion starts with new showcases as these can provide optimum attainable conditions for iron on display.

7.2.1 New purpose built showcases

Whilst the 16% RH threshold for no further change is desirable, it would be expensive to maintain in a dispersed collection such as English Heritage's. Mechanical dehumidification could achieve this with many designs, but has high installation costs and high running costs. Additionally many of the spaces used, or with potential for displays, do not have power, precluding this approach. Passive dehumidification is unlikely to maintain RHs below 16% in English Heritages damp estate without frequent changes of the absorbent. Many of the buildings have open doors, windows and chimneys. Issues with historic roofs, water goods and drainage often lead to waterlogged masonry in historic buildings. This generates RHs in many spaces exceeded 70% all year round and often rising into the 90s.

The second threshold at 30% seems a reasonable compromise for display, with the likely long term damage being of a minor nature and unlikely to compromise the object's archaeological research value.

Chapter 5 showed the importance of excluding ethanoic and methanoic acid and methanal from showcases. As emission testing of these gases from showcase materials is not normally undertaken, the best approach is to ensure all showcase materials have passed 'Oddy' tests with lead. Being rated as suitable for permanent use in these tests, (described later) mean the ethanoic and methanoic acid concentrations are very low and certainly below the no observable affect limits defined for lead, 600μgm^{-3} for ethanoic acid and 170μgm^{-3} for methanoic acid (Tetrault, 2005).

Whilst the effect of the industrial pollutant gas mixture on the akaganeite formation reactions was significantly less than that of ethanoic or methanoic acid, these gases are known to accelerate corrosion of iron and steel (Oesch, 1996). The low RH will control such corrosion to a significant degree. Hydrogen chloride has been reported to attack iron via a corrosion cycle (Askey et al, 1993). The concentrations at which this occurs have not been investigated.

Dust is reported to accelerate metal corrosion through the introduction of ions to the metal surface and crevice condensation (Thickett, 2008a; Vernon, 1935). It is now extremely rare to clean back to the existing metal core of iron artefacts, so increased condensation will be much less of a risk as the dust will not be in contact with the metal. The chloride ion is the most damaging both to iron corrosion and as it will also increase the rate of akaganeite formation by increasing the chloride to iron ratio. Chloride is also extremely mobile and can move from the surface of the object to the metal core. Many English Heritage properties are within 1km of the sea and have high sea salt aerosol concentrations. In polluted maritime environments nitrogen dioxides can react with sea salt aerosol to generate hydrochloric acid in the gas phase (Robinset 1956, Finlaysan 1989). This is more problematic as the gas penetrates showcases to a greater degree than the sea salt aerosol.

7.2.3 Existing showcases

There are over two hundred showcases containing archaeological iron in English Heritage's displays. It would be prohibitively expensive (over £2,000,000) to replace all of these showcases. The cost to replace all the presentation aspects of the cases is likely to be triple that figure. Many of the existing showcases are made from wood and even the more modern metal framed ones contain significant amounts of MDF as base and backboards and display furniture. Where silica gel facilities are present they often only allow for a relatively small amount of gel, with a maximum of $1kgm^{-3}$ in most instances.

It is unlikely that 30% RH will be achievable in the majority of these showcases. The third threshold, with a minimum of 50%, will retain some degree of control of the deterioration rate and should retain much of the archaeological research value of the objects over the next ten years, whilst replacement can be considered. This

approach needs to run alongside a program of determining the deterioration rates and removing the more rapidly deteriorating objects from display, back into dry storage.

At 33 and 54%, 750μgm^{-3} of ethanoic acid increases the akaganeite formation rate by approximately 10% after 3 months exposure. This concentration can be achieved through replacement of MDF base boards and back boards, blocking of wooden frame emissions with aluminium foil or tape or the incorporation of chemical adsorbents such as activated charcoal cloth or corrosion intercept (Thickett and Short-Traxler, 2011; Thickett et al., 2008d).

7.3 Creating suitable environments in showcases – present state of knowledge

7.3.1 Air exchange rate

The air exchange rate of a showcase is fundamental in its response to external RHs (and performance of any control method for RH), its concentration of any internally generated pollutants, such as ethanoic and methanoic acid and the degree of protection it offers against external pollutants and dust.

There are three possible mechanisms for air exchange; permeation, diffusion and infiltration (Michalski, 1994; Padfield, 1966).

- permeation is the passage of gases through a material. It depends on the gas and the material. Water vapour, sulfur dioxide, nitrogen dioxide and ozone would generally permeate at different rates through the same material. The metal and glass construction of modern showcases is essentially impermeable. Although permeation will occur through the adhesives and seals, the rate is likely to be much lower than those of diffusion and infiltration through gaps (Michalski, 1994). Wood and acrylic are both permeable.

- diffusion through gaps in the showcase fabric is governed by Ficks Law.

$$J = -D \partial N / \partial z \qquad (7.1)$$

Where J is the flux in m^{-2}s^{-1}

D is the diffusion co-efficient in m^{2}s^{-1}

N is the number density of particles in m^{-3}

Z is the length in one dimension in m

It depends on relative molecular masses and the relative rates of diffusion of two gases is given by

$$r_1 / r_2 = \sqrt{M_2 / M_1} \qquad (7.2)$$

Where r_1 is rate of gas one

r_2 is rate of gas two

M_1 is relative molecular weight of gas 1

M_2 is relative molecular weight of gas 2

Therefore diffusion is fastest for water vapour of the gases of interest.

- infiltration will dominate air exchange rate in most showcases. This is the movement of air driven by pressure differences. The movement carries other gases with it. Pressure differences arise from four causes.

    - changes in atmospheric barometric pressure that transmit into showrooms. Many historic properties have little resistance due to their public nature and hence open doors, poorly sealed windows and the presence of chimneys. These determine the practical limit for air tightness of a showcase, but in practise the differences from other cause dominate (Michalski, 1994)

    - temperature differences between the showcase and room generate pressure differences. Internal heat sources include lighting and room lighting or sunlight through blinds can heat cases significantly.

    - Relative humidity differences also generate pressure differences but generally to a much lesser degree than temperature differences. For a $1m^3$ case with 5mm diameter circular holes in the top and bottom, a 1ºC temperature difference causes as much increase in air exchange rate as 40% RH difference (Ankersmit, 2000).

- often the main driver of infiltration is the stack pressure. This originates from pressure differences between a column of air inside the showcase at one temperature and RH, and the corresponding column of air just outside the case at a different temperature and RH. For temperatures between 10 and 30ºC this pressure can be approximated by (Michalski, 1994);

$$Ps \approx h(0.040\Delta T + 0.100\Delta RH) \qquad (7.3)$$

where h is the height of the stack, in practice this is defined as the vertical distance between two significant cracks or holes;

ΔT is the temperature difference in ºC;

ΔRH is the decimal difference in RH, ie a 40% difference in RH is 0.4

This means that temperature differences tend to be more important .

In order to achieve a low air exchange rate it is desirable to construct showcases using impermeable materials such as glass and metals and essential to take great care to exclude gaps. Suitable door closing and sealing mechanisms are essential for this. As it is impossible to have no gaps whatsoever, design is essential to minimise the effects on air exchange rate. As described previously, vertically separated gaps have most influence and doors will inevitable have some gaps. A low height showcase will minimise the vertical separation of gaps and a lower hinged desktop design will have a single level seal. This design is suitable for the small scale of archaeological iron from a display design point of view.

7.3.2 Controlling RH

7.3.2.1 Adsorbents

A variety of materials adsorb water vapour and can be used to generate a low RH atmosphere inside showcases.

Silica gel is composed of randomly linked spherical polymerised silicate particles. Modern production is exclusively from sulphuric acid and sodium silicate (Grace, 2012). Mixing under controlled conditions creates primary particles of the desired size. These polymerise to form the raw gel, which is then washed and dried. By controlling the primary particle size, the washing, aging and drying conditions different pore size distributions can be fabricated (Greenwood and Earnshaw, 1997). The isotherm of the gel depends on the pore size distribution. Regular density (RD) silica gels adsorb large amounts of water vapour below 40% RH and are suitable for drying (Weintraub 2002).

Zeolites are naturally occurring alumino silicate minerals with three dimensional structures. They have an open structural form which has internal cavities, in which molecules of various sizes can be trapped. These internal voids can be engineered to have specific opening sizes and hence trap specific molecules including water vapour. Zeolite 4A adsorbs water vapour faster than RD silica gel due to its higher specific area. However, once the voids are full, the zeolite has very little further buffering capacity and the RH will increase much more rapidly than with RD silica gel. In a dispersed collection with limited conservation time, this is a drawback as the RH will rise higher than with RD silica gel if the adsorbent is not replaced in time.

Bentonite is an aluminium phyllosilicate impure clay, generally consisting mainly of montromillonite. Water can substitute between the silicate layers of the clay structure. Commercial bentonites have a similar adsorption capacity as RD silica gel below 40% RH, but much less capacity above 40% (Waller 2011). Although RD silica gel actually has a higher density (700 kgm^{-3}) than clays (593kgm^{-3}), its packing density is somewhat lower as it is generally formulated in large granules whilst the clay exists as a very fine powder. Practically this means a 1kg bag of bentonite has half the height of a 1kg bag of silica gel. This property is especially useful for use in old showcases with inadequate silica gel facilities.

Regular density silica gel remains the most cost effective adsorbent for new showcases. When there is limited facility volume for silica gel, Bentonite will allow a greater mass of adsorbent and better RH control.

7.3.2.2 Dehumidifiers

When power is available, and resources allow, dehumidifiers can control much larger showcases and higher air exchange rate than adsorbents (Thickett, 2008b). They can control within a 5% RH band to any value lower than the room RH. This is a major advantage when archaeological iron and RH-vulnerable organic materials are displayed in the same showcase. Both wood and bone often occur in iron objects and are susceptible to cracking below 30% RH. Dry silica gel has an RH of approximately 5% and will reduce the showcase RH to below 10% when fresh gel is added.

Two main types of dehumidifiers are available;

Condensing dehumidifiers have a chilled surface on which that water vapour condenses on. The water needs to be removed periodically and this can be several times a day, which is difficult to resource. Drainage can be supplied, but this can be difficult in an historic building. As the dehumidification is based on condensation, these units become less efficient at lower temperatures, and most essentially stop working at 5°C. The efficiency of a commercial unit was measured. The unit runs in a large brick lined underground casemate. A mass transducer was attached to the condensed water container and the mass of water measured and recorded on an Signatrol SR007 logger every 30 minutes. This combination gave a sensitivity of 1.1g and range of 12 kg. The temperature and RH in the room was recorded. The RH varied between 60 and 90%. The mass of water condensed is plotted against temperature.

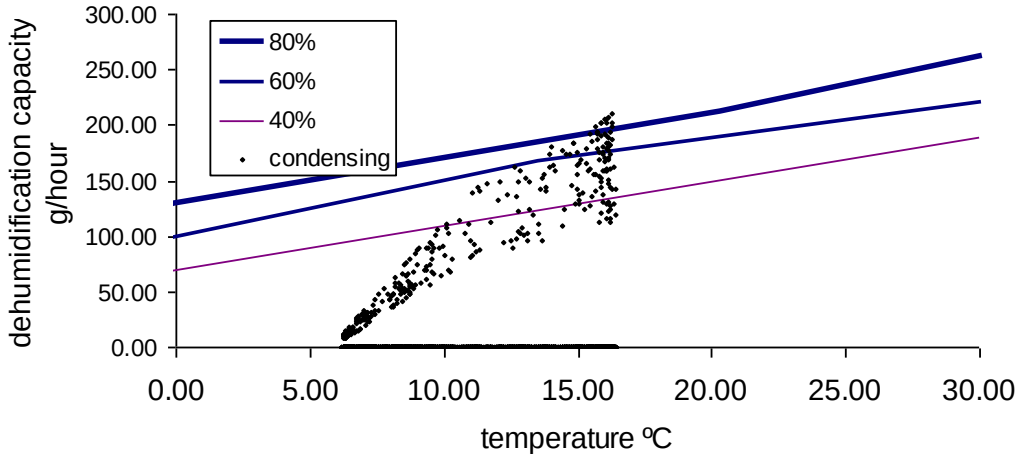

Figure 7.1; Dehumidification capacity of Munters MG50 drying wheel and condensing dehumidifier measured at Fort Brockhurst

The dehumidification capacity drops to zero at 7°C and reduces sharply around 10°C. This limits the use of this type of unit, as many English Heritage displays are unheated.

Drying wheel dehumidifiers use an adsorbent wheel which passes through two air streams. One air stream is dried and produces a flow of dry air which can be ducted into showcases. The second air stream feeds heated dry air over the wheel to remove the moisture. An exhaust of warm damp air needs to be expelled from the unit. Such units maintain their drying capacity much better at lower temperatures. The manufacturers capacity data given for a Munters MG50 drying wheel dehumidifier is included on Figure 7.1.

7.3.2.3 Membrane driers

Membrane driers apply a direct current across a polymer electrolyte membrane. The anodic side of the membrane is on the inside of the showcase. At this surface water vapour dissociates into oxygen and hydrogen ions. Hydrogen ions migrate through the polymer membrane and react with oxygen at the cathodic side, forming water vapour outside the showcase. This technology is attractive due to the simplicity of the system and low cost. However, the present commercial units also generate ozone inside the showcase (Maish, 2005).

As many English Heritage properties have no power adsorbents have to be used in many instances. Regular density silica gel provides the best compromise between performance and cost.

Equations have been developed to quantify the buffering effect of silica gel (Thomsen, 1977).

$$T_{1/2} = 4MB/n \qquad (7.4)$$

Where $T_{1/2}$ is the hygrometric half life, the time taken for the RH inside the case to move half way to the value of the RH outside the case in days

B is the loading of buffer material in kg/m^3

M is the specific reserve of the buffer, the amount of water vapour adsorbed for a 1% increase in RH in g/kg, for most materials this is a function of RH and a single value cannot be used over wide RH ranges

n is the air exchange rate, day^{-1}

The RH inside a showcase can be calculated from the room RH and hygrometric half life in an iterative approach using a spreadsheet. For each time segment (1 hour in Table 7.1), the RH, RH_t is calculated from the previous RH value, RH_{t-1} and the room RH, RH_{room} using the following equation

$$RH_t = RH_{t-1}+(RH_{room}-RH_{t-1})\exp(-\ln 2/T_{½}) \qquad (7.5)$$

data user enters		length	1	m
data from data logger		width	0.6	m
calculated data		height	0.3	m
		volume	0.18	m3
		mass of silica gel	1	kg
		loading	5.555556	
		air exchange rate	1	
		half life	2133.333	hours
	----------room data----------		showcase relative humidity	
date time	temperature	relative humidity	5	< starting relative humidity
01/01/2008 00:00	19.2	35	5.009746	
01/01/2008 01:00	19.1	35	5.019488	
01/01/2008 02:00	19.1	39	5.030527	
01/01/2008 03:00	19	40	5.041888	
01/01/2008 04:00	19	43	5.054219	
01/01/2008 05:00	18.9	42	5.066221	
01/01/2008 06:00	18.8	41	5.077894	
01/01/2008 07:00	18.7	40	5.089239	
01/01/2008 08:00	18.7	40	5.10058	

Table 7.1 part of spreadsheet used to calculate enclosure RH from room RH and equation 7.4

Annual RH data from a number of rooms proposed for displays, was assessed. Portchester castle had the highest RHs and this was used to model the internal RH of a case with different hygrometric half lives.

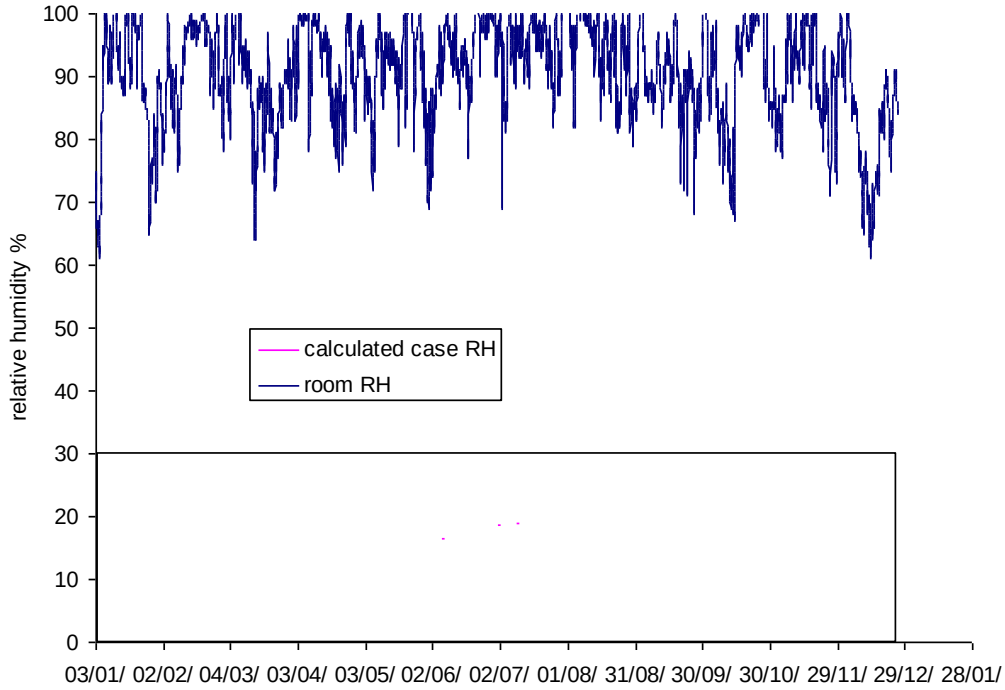

Figure 7.2 Internal RH in 0.15m^3 showcase with hygromentric half life of 367 days at Portchester Castle, calculated from Thomsen equation

To achieve twelve months between silica gel changes, a half life of 367 days is needed

7.3.3 Internal pollutant concentration

The low air exchange rate of showcases (anything below approximately 20day^{-1}) concentrates any emissions of volatile organic compounds from the showcase construction and dressing (fabrics, paints back board, baseboards etc) materials and the objects themselves. Concentrations of several thousand µgm^{-3} can be generated in this way (Grywacs and Tennent, 1994). A wide range of VOCs have been reported in showcases (Schieweck, 2009). Ethanoic and methanoic acid have been identified as the major corrosive species towards metals and were shown to accelerate the akaganeite formation reactions in chapter 4. Methanal was reported to be a major problem in the 1980s (Hatchfield and Carpenter, 1987), but further research concluded its effect was due to formation of methanoic acid, which only occurred at high RH and in the presence of strong oxidising reagents (Raychaudhuri and Brimblecombe, 2000; Tetreault et al., 2003; Thickett, 1998b). Testing of showcase materials was developed in the 1970s in conservation (Oddy, 1973) and

has undergone continuous development (Bamberger et al., 1999; Green and Thickett, 1995; Robinet and Thickett, 2004).

7.3.3.1 Testing materials

A simple accelerated corrosion test was developed in the early 1970s (Oddy, 1973). It involved cleaning coupons of three metals (silver, copper and lead – the major metals of antiquity that had been found to be susceptible to such corrosion). The coupons were enclosed in a glass tube with the material to be tested and some water to provide a near 100% relative humidity, RH atmosphere. The sealed tube was aged at 60°C for twenty eight days and the degree of corrosion on the coupon used to assess the suitability of the material for use in display and storage enclosures. The test accelerates the degradation of the material being tested and the corrosive gases are mainly degradation or secondary products. Several tests have had no visible corrosion after twenty one days, only to cause corrosion before the end of the test; highlighting the necessity for the full twenty eight day testing period (British Museum 1996). It also accelerates the corrosion of the metals in the atmosphere generated. Initially this was a simple pass or fail test, but the large number of short term exhibitions led to the introduction of a temporary (for up to six months) classification. The variability in results reported between different users was assessed in 1992 (Green, 1992), and photos and descriptions were disseminated to help standardise the visual assessment of coupons and a second standard method published. An improved method, that takes less time to set up the tests was published in 2003 (Robinet and Thickett, 2004). Alternative methodologies have been published (Bamberger et al., 1999). The Oddy test is not normally undertaken with ferrous metals as the high RH induces significant corrosion without any test material. It is often impossible to distinguish a greater effect from a test material by eye than from the blank control test which is always run alongside. The corrosion can be quantified, by chemical stripping (ASTM, 1999) and corrosive materials can be identified and excluded from use. To assess the effects on akaganeite formation, the test has been modified to use an iron and iron (II) chloride powder mixture instead of the metal coupons. The mixture (3mg) is placed in a polyethylene cap for

the test and analysed as a KBr disc with FTIR to quantify the conversion to akaganeite after accelerated aging.

The Oddy test has protected metals on display and in storage for over forty years and where it has been used, there have been no corrosion issues. Results are often extrapolated to other materials. A material that has passed the Oddy test with lead will certainly emit only very low levels of acetic acid, formic acid and formaldehyde. The concentrations developing in normal situations will be well below the no observable adverse effect levels collated by Tetrault and elucidated further in recent research (Robinet, 2006; Tetrault, 2005).

7.3.3.2 Ethanoic and methanoic acid concentration

The internal concentration of a gas inside a showcase can be described by the mass balance equation developed by Weschler and Shields (Weschler et al., 1989).

$$I = {nO}/{(n+K_s)} + {(G/V)}/{(n+K_s)} \qquad (7.6)$$

Where I is the internal concentration (ppb or μgm^{-3}),

N is the air exchange rate (day^{-1})

O is external concentration, n is air exchange rate (day^{-1}),

Ks is the surface removal rate (ppb or µg per day),

G is the generation rate of pollutant (ppb or µg per day) and

V is the showcase volume (m^3)

The concentration of ethanoic and methanoic acid in rooms is almost always zero, and with the external concentration O being zero, the equation reduces to

$$I = {(G/V)}/{(n+K_s)} \qquad (7.7)$$

The surface generation rates of ethanoic acid from 'sealed' MDF boards and of methanoic acid from Dulux 103Y have been measured (Thickett, 1998c). Surface

generation rates of ethanoic and formic acid from a variety of other materials are also available (ECA, 1997). No values for Ks, the surface removal rates have been published. Calculations were undertaken using a range of Ks values from 0.0, no removal (glass) to 2.0, probably a reasonably strong removal rate for the weak acids. For the reactive gas ozone, Ks have been reported between 1 and 4 in offices (Weschler et al., 1989) and between 2 and 3 for museum storage (Ryhl-Svendsen and Claussen, 2009). Results are shown in Figures 7.3 and 7.4

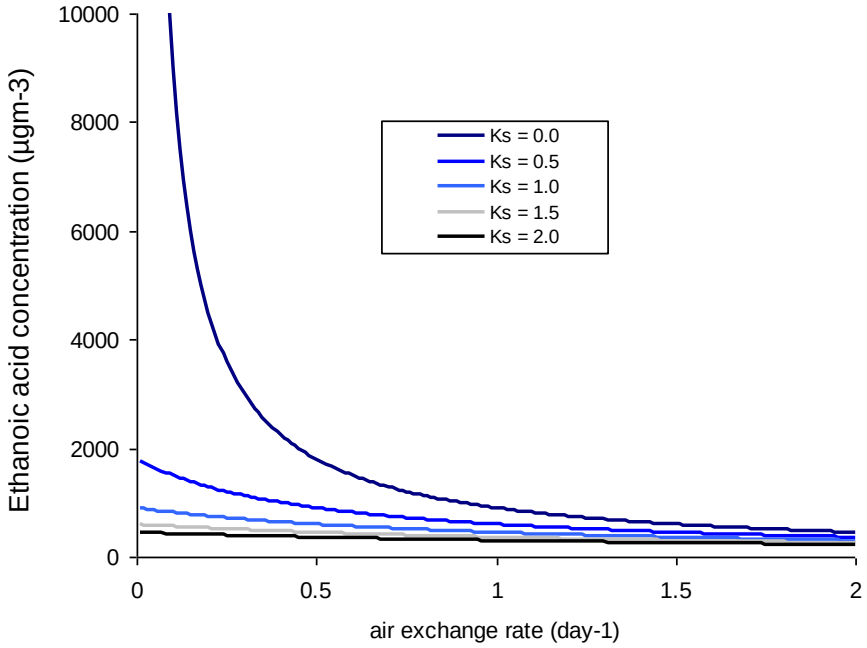

Figure 7.3 Calculated ethanoic concentrations inside a showcase with Moistop taped MDF baseboard with an ethanoic acid emission rate of 900µg/day

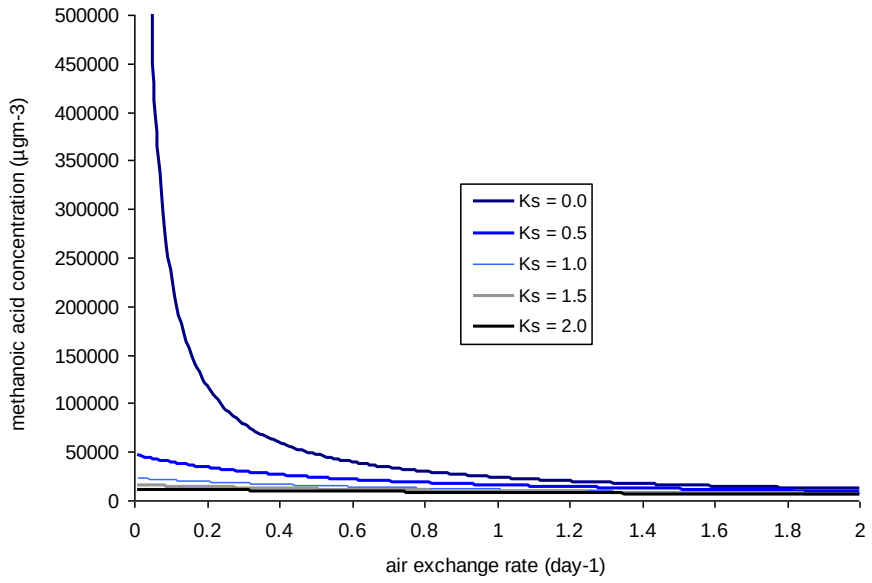

Figure 7.4 Calculated methanoic acid concentrations inside a showcase with eggshell painted panels with a methanoic acid emission rate of 23700µg/day

Both the ethanoic and methanoic acid concentrations increase dramatically as the air exchange rate drops below 1 day^{-1}. This is especially dramatic at low Ks values such as would be expected with modern glass and steel showcases.

7.3.4 Controlling pollutant ingress

7.3.4.1 Chemical pollution

Industrial pollutants, mainly from traffic, are increasing in many urban centres that house museums and historic houses. The key damaging pollutants for collections are nitrogen dioxide, ozone, sulfur dioxide, hydrogen sulfide and carbonyl sulfide, with dimethyl sulfide present in maritime locations and hydrogen chloride present in polluted maritime locations. There is some effect for sulfur dioxide and nitrogen dioxide on the akaganeite formation reactions and both gases would be expected to corrode iron. Hydrogen chloride has been reported to attack iron as well. The concentrations of these pollutants inside showcases are reduced from room levels by a combination of air exchange rate and deposition onto the internal showcase

surfaces. For steady state conditions, this reduction is also described by equation 7.6.

$$I = \frac{nO}{(n + K_s)} + \frac{\left(\frac{G}{V}\right)}{(n + K_s)} \qquad (7.6)$$

Where I is the internal concentration (ppb or μgm^{-3}),

O is external concentration,

n is air exchange rate (day^{-1}),

Ks is the surface removal rate (ppb or µg per day),

G is the generation rate of pollutant (ppb or µg per day) and

V is the showcase volume (m^3)

as

$$K_s = v_{dep}\left(\frac{A}{V}\right) \qquad (7.8)$$

Where v_{dep} is the deposition velocity of the surface materials inside the showcase (ms^{-1}) this is a function of both temperature and RH

A is the area of material (m^2)

As the internal generation rate for ozone is zero, this reduces to the well known equation for ozone by Weschler

$$I/O = \frac{n}{\left(v_{dep}\left(\frac{S}{V}\right) + n\right.} \qquad (7.9)$$

Reducing the air exchange rate of the showcase will reduce the inside concentration for a given room concentration.

The IMPACT project researched the information required to apply the Weschler equation in heritage buildings. It measured the deposition rates of sulfur dioxide, nitrogen dioxide and ozone onto a series of common building materials as a function of temperature and RH. Fortunately this included many of the common materials used to fabricate showcases. The project also developed a web based application to

easily apply the Weschler model without numerous calculations (Blades et al., 2002). The screen showing the inputs required is included as Figure 7.5.

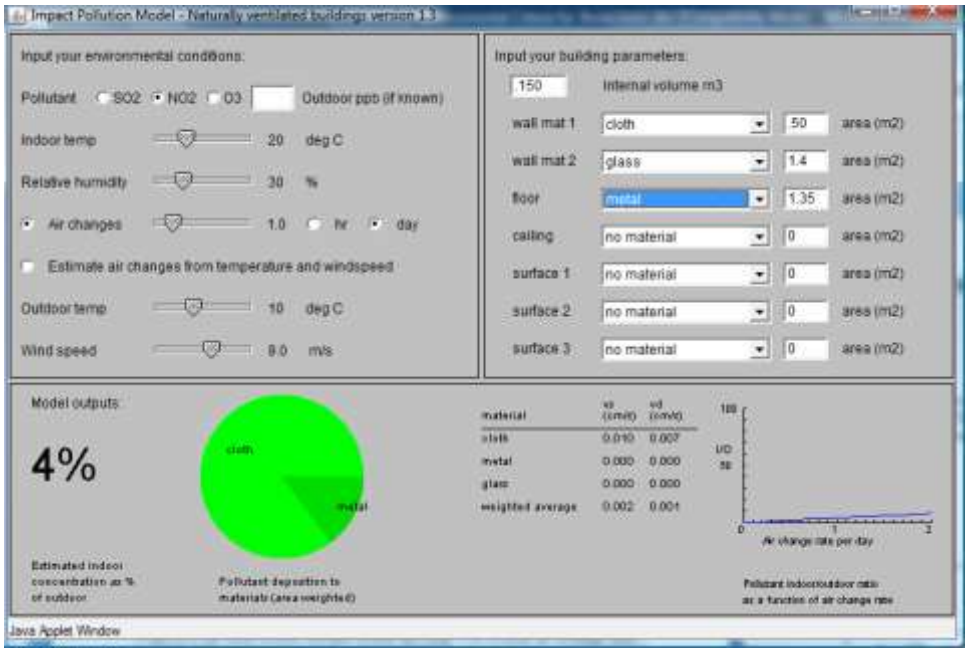

Figure 7.5 Impact applet. Environmental conditions are on left, showcase dimensions and materials are on right and calculated ingress and deposition is in bottom section.

Calculations were carried out for the standard case design (see later section) using pollution data from Porchester Castle, at 30% RH and 10 and 20ºC for sulfur dioxide, nitrogen dioxide and ozone with different air exchange rates. Results are shown in Figure 7.6.

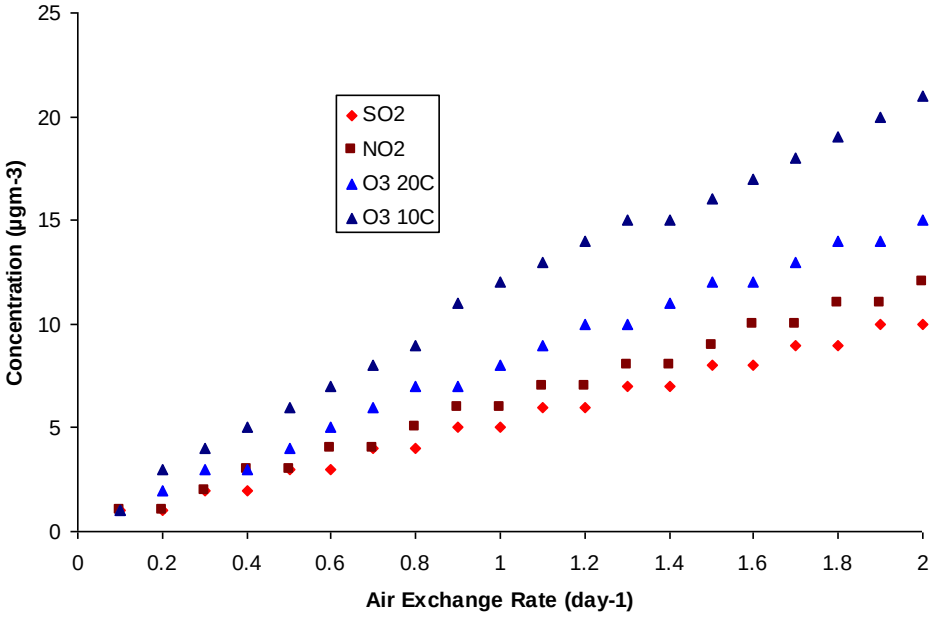

Figure 7.6 Calculated pollutant ingress into 0.15m^3 glass and metal showcase with fabric wrapped metal baseboard at different air exchange rates.

There was no difference in the calculated concentrations at 10ºC and 20ºC for sulfur dioxide and nitrogen dioxide.

7.3.4.2 Dust

Whilst several studies have been reported into the amounts and composition of dust in heritage buildings and museums (Adams and Ford, 1999; Worobiec et al, 2007; Kontozona-Deutsch et al, 2008; Howell et al, 2002; Gysels et al, 2004), no work has been published into dust inside showcases.

7.4 Methods

7.4.1 Air exchange rate testing

Air exchange rates were measured with the method developed in chapter 3.4. The Vaisala carbon dioxide logger was placed at the bottom of showcases in the middle of the baseboard when objects allowed. The carbon dioxide was injected either mid

way up for tall showcases with side opening doors or at the base in the middle for desktop type showcases.

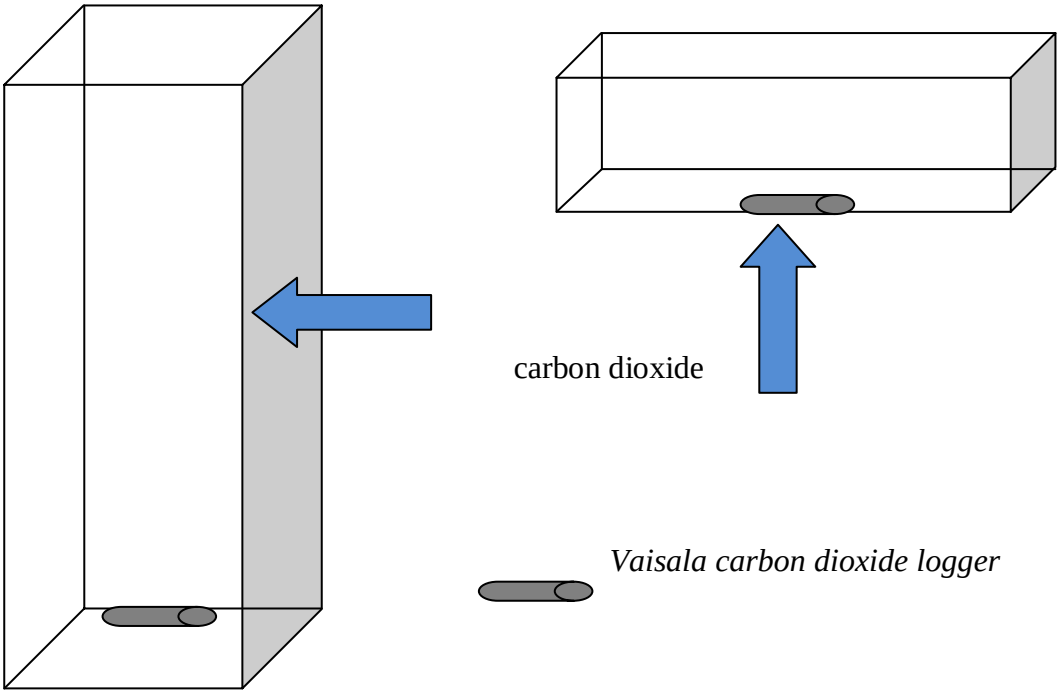

Figure 7.7: Logger and carbon dioxide injection positions.

All showcases were tested running under their normal operating conditions. All lighting and electrics were on during the day and doors and windows to the room in their normal positions.

7.4.2 Leakage testing

Testing to find leakage paths involved injecting compressed air from a commercial air duster (Maplin dustoff) into the case, and closing the door. An Inficon CFC leak detector was run down any joints or over surfaces to detect the propellant from the air duster.

7.4.3 Temperature and RH monitoring

Temperatures and RHs were recorded with a variety of data loggers. The loggers and their specifications are shown in Table 7.2.

Manufacturer	Type	Temperature accuracy (ºC)	RH accuracy (%)
Signatrol	SR002	± 0.02	± 3
Hanwell	Humbug II	± 0.03	± 3
Rotronic	Hygrolog	± 0.02	± 1
Meaco	Hygroclip	± 0.02	± 1
Eltec	GD310	± 0.5	± 3

Table 7.2 Temperature and RH sensor characteristics

All sensors were calibrated annually with salt pots with National Accreditation Measurement Service certification. All calibrations were at three points; 11, 33, 54 for showcases with silica gel and 33, 54 and 75% for rooms or unconditioned showcases.

7.4.4 Gas Analysis

7.4.4.1 Ethanoic and methanoic acids

The airborne concentration of carboxylic acids was analysed using diffusion tubes following the methodology developed by Gibson et al (Gibson et al., 1997b) described in 2.2.9. Each measurement involved exposing four diffusion tubes for approximately twenty eight days.

7.4.4.2 Sulfur dioxide, nitrogen dioxide, hydrogen chloride

The airborne concentrations were analysed using a modification of the diffusion tube method (2.2.9).

7.4.4.3 Ozone

All ozone measurements were carried out with diffusion tubes supplied and analysed by Gradko International Ltd.

7.4.5 Dust analysis

Dust was collected on glass slides exposed for twenty eight days. The surface coverage of deposited dust was analysed using microscopy and image analysis (Howell et al, 2002). The analysis measures 50 approximately 1mm by 1mm areas on the slide surface. The light intensity of the microscope was set using the image processing routine on a graticule standard from the National Physical Laboratory. Particle size distributions were calculated from the areas of each particle detected, by assuming the particles were circular.

In some instances the dust was extracted with 18.2MΩ water and the extracts analysed with ion chromatography to determine the chloride deposition rate.

7.4.6 Modified Oddy tests

The commonly applied accelerated corrosion test used in conservation the 'Oddy' test has been modified to determine the effects of any off-gassing from showcase materials on the akaganeite formation reactions. Instead of metal coupons a mixture of iron and ferrous chloride powder was used. The RH inside the 50ml conical flask reaction vessel at 60°C was controlled to 42.6% with saturated magnesium nitrate. This RH was selected to be high enough to allow the reaction to progress without being so fast that all the iron and ferrous chloride would be consumed within the 28 days of the test. After the test the amount of akaganeite formed was determined with FTIR KBr (3.1.1.2).

7.5 Testing Existing Showcases

Existing showcases were measured to examine the feasibility of low RH control with silica gel and elucidate the design features required to achieve the criteria. A number

of other factors became apparent that influenced performance. The pollution in a series of showcases was measured to confirm the Weschler ethanoic and methanoic acid concentration models described in 7.3.3.2 and the pollution ingress modelled with IMPACT, 7.3.4.1.

Approximately thirty desktop type showcases had been installed in a range of English Heritage properties over the previous five years. The performance of these cases was monitored (Temperate and RH, air exchange rate, AER, dust and pollutant ingress) and the cases were examined. The locations and physical characteristics of the cases examined were;

Site	Number of cases	Type	Showcase materials		AERs	Silica gel loading	Max RH
			Carcass	Interior			
Helmsley Castle	4	B	Steel	MDF	0.31-0.76	56	50-58
Chesters Roman Fort,	8	C	lacquered wood	painted hardboard	1.05-2.31	50	53-65
Castle Acre Abbey	3	D	melamine coated particle board	melamine coated particle board	0.91-1.8	15	61-68
Portchester Castle	2	C	Plywood	melamine coated particle board	0.67-1.56	55-110	28-45
St Augustines Abbey	3	A	Steel	melamine coated particle board	0.21-0.32	20	15-19
Dover Castle	1	A	Steel	Moistop	0.81	28	59

				wrapped MDF			
Jewel Tower	1	C	Brass	hardboard	1.45	25	62
Lullingstone	1	A	Steel	particle board	0.68	83	31
Fort Brockhurst	3	C	Wood	wood, fabric	0.23-1.45	33	45-61
Richborough	3	C	Wood	painted wood	0.56-1.21	33	57-68
Stoksay	1	C	Wood	Wood	1.24	22	69
Down House	3	A	Steel	Dacrylate 103Y coated MDF fabric	2.98-3.87	42	45-61

Type A

Type B

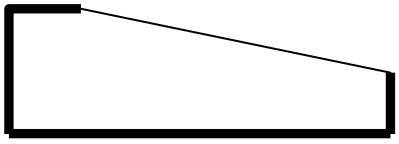

Type C

Type D

Table 7.3 Tabletop type showcases investigated

A number of issues were identified which limit their ability to maintain low RH environments.

7.5.1 Leaks in showcases

Gaps in cases and their seals are often not visible, but the resulting leaks can dramatically increase the AER. These can result from problems during manufacture or as a result of inadequate sealing of joints when the cases are installed on site. A D-Tek chloro fluoro carbon (CFC) leak detector was used to locate any hidden gaps. Top hinged cases often showed large leakage through this hinge and had high air exchange rates. The type A showcases with seals at a single level generally had much lower air exchange rates. Down House was an exception as the small cases each had four unfilled 12mm mounting holes in them.

7.5.2 Medium density fibreboard (MDF)

All of the display cases included the wood product, MDF, as baseboards and mounts. To prevent organic acid emissions these were sealed with Dacrylate, however this has been shown to be ineffective against acetic and formic acids (Thickett, 1998a). At Helmsley Castle two cases with MDF inserts were monitored, Figure 7.2. The buffering effect introduced by the MDF, caused a slow drying of the internal RH. A minimum of above 25% was reached and the RH then increased back above 30% within 45 days. To maintain the desired low humidity the silica gel would need to be replaced this often.

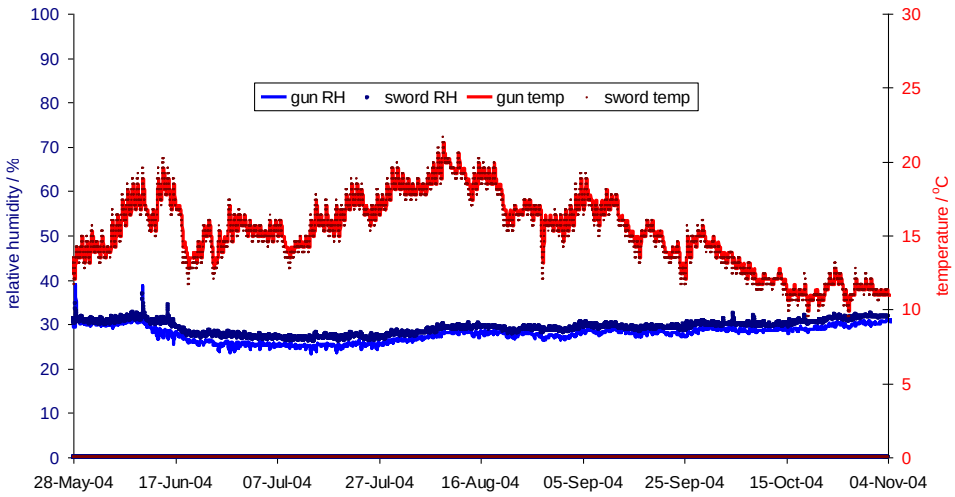

Figure 7.8 Relative humidity (blue traces) and temperature (red traces) conditions inside two showcases with MDF at Helmsley Castle

7.5.3 Air movement between the silica gel compartment and display volume

Environmental monitoring of a commercial showcase design demonstrated a large, long term significant RH difference between the silica gel compartment and the display volume, Figure 7.9. This completely compromised the performance of the cases, with the objects being exposed to RHs above 50%. It was possibly caused by a combination of stratification in the 30 cm chimney between the silica gel tray and the display volume and insufficient air pathways (approximately 8mm gap around the edges of the MDF baseboard) between the two.

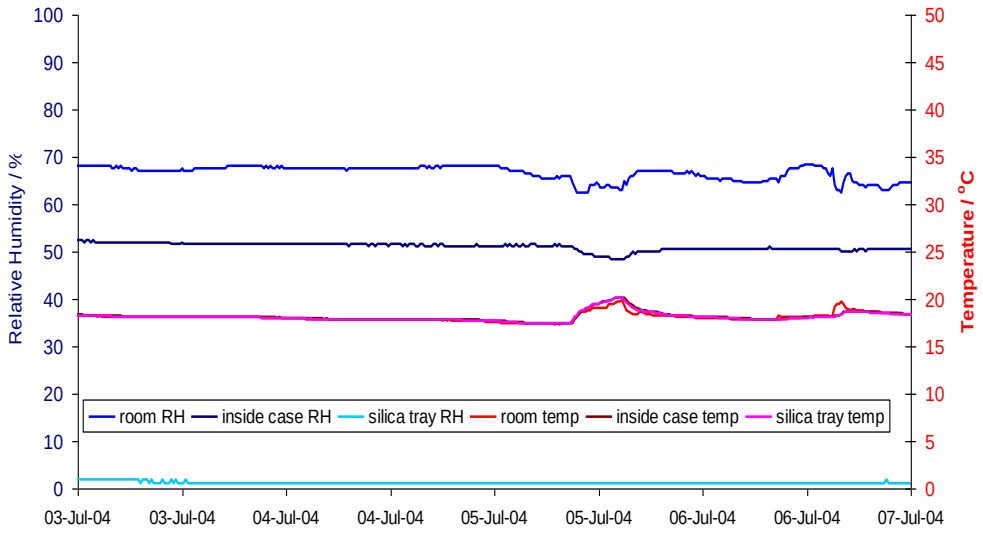

Figure 7.9 Condition in various compartments of commercial showcase at Dover Castle. Pale blue trace is RH in silica gel compartment, red traces are temperatures, dark blue trace is the showcase RH and mid blue trace is the room RH.

7.5.4 Access

Three cases installed in an exhibition at St Augustine's Abbey in 2000 were found to be performing very well keeping the RH below 13%. They had relatively low air exchange rates.

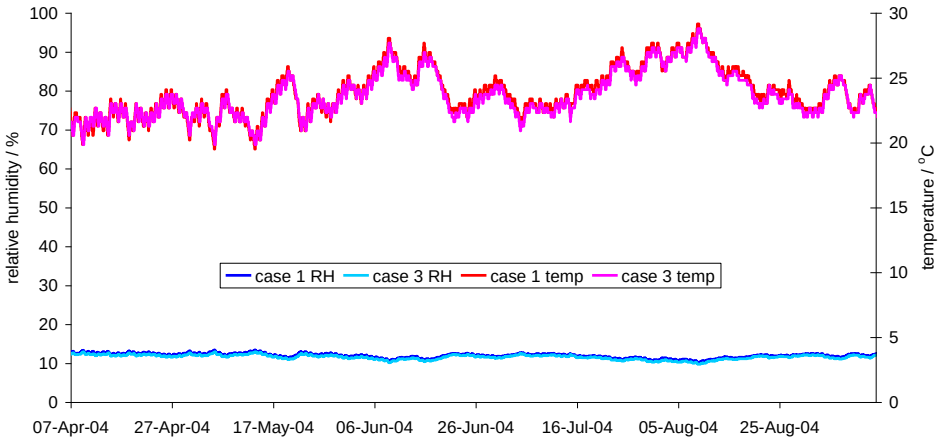

Figure 7.10 Relative humidity (blue traces) and temperature (red traces) conditions inside two of the three showcases at St Augustines Abbey

However, the silica gel is within the display volume and requires the case to be opened in order to replace the silica gel. The glass lids are heavy and difficult to remove requiring a minimum of four people to be present. The amount of RD silica gel required is also substantial, 35 kg per case.

7.5.5 Ethanoic and Methanoic Acid Concentration

The ethanoic acid and methanoic acid concentrations in a wide range of showcases and some storage locations were measured. Five basic situations were encountered;

A Showcase frames of inert materials, metals and glasses with 'sealed' MDF baseboards and backboards.

B Showcase frames of inert materials, metals and glasses with plywood or hardboard baseboards and backboards.

C Showcase frames made from wood.

D Wooden cupboards or drawers.

E Cardboard boxes.

Figure 7.11 shows the results of the analyses. The points are the medium values, the boxes the interquartile ranges and the bars the full range of values.

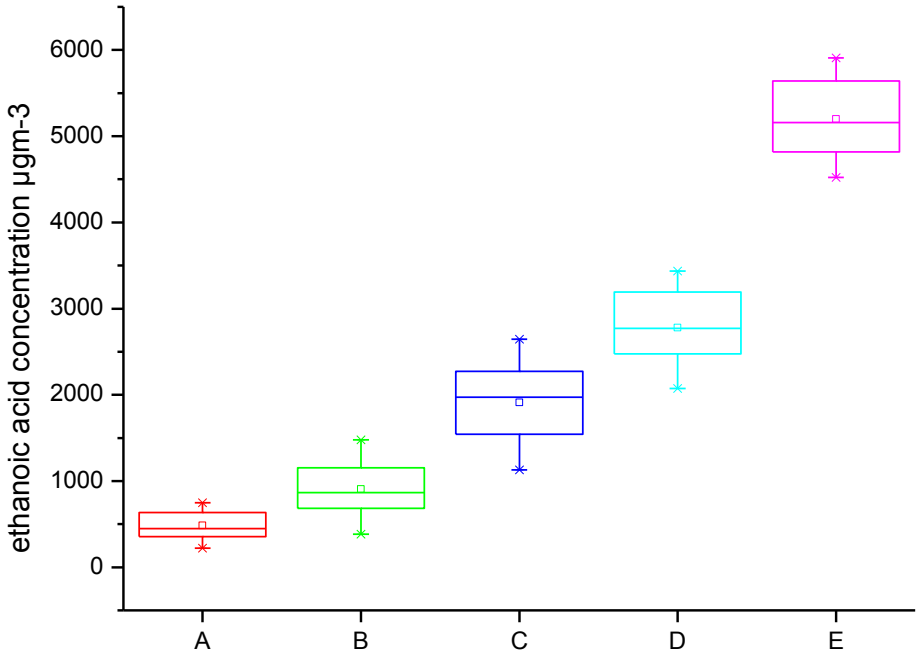

Figure 7.11 Ethanoic acid concentrations in different types of showcases and storage at the British Museum

The amount of wood product and degree of sealing determines the ethanoic acid concentration in the enclosures.

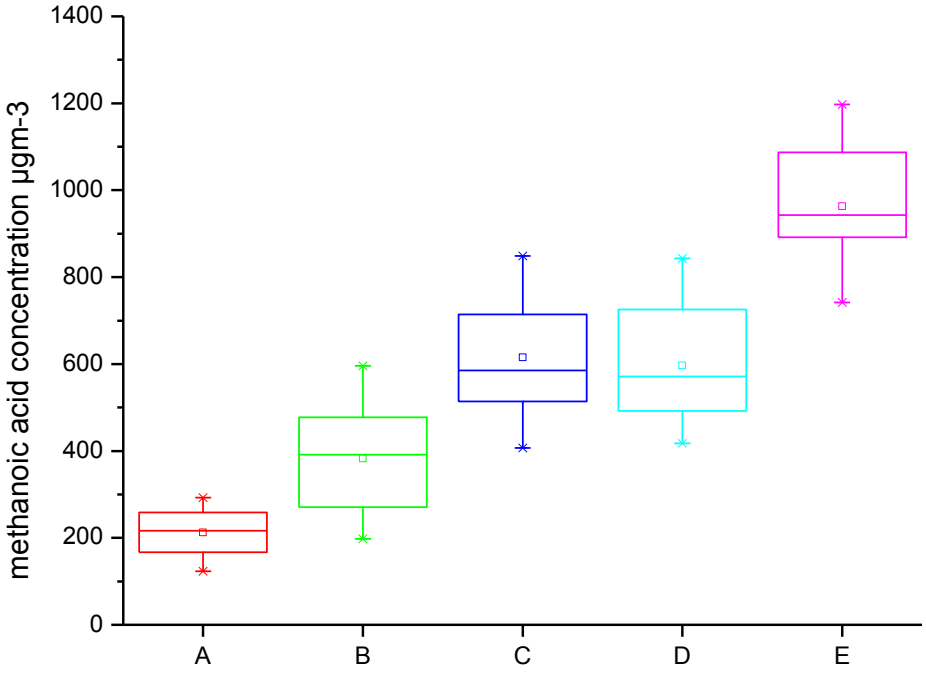

Figure 7.12 Methanoic acid concentrations in different types of showcases and storage at the British Museum

In order to apply equation 7.6 ethanoic and methanoic acid generation and surface removal rates are required.

Specific methanoic acid generation rates from Dulux 103Y paint have been measured. Experiments to improve the environment inside a series of showcases at Kenwood House, London had systematically increased their air exchange rates. The measured methanoic acid concentrations and air exchange rates were used to calculated the surface removal rate for each showcase.

Specific generation rates of ethanoic acid (rate per surface area) had been measured for the materials in a series of showcases at The British Museum with taped aluminium foil wrapped MDF baseboards. As the baseboards are approximately the same size in each showcase then the generation rates are equal. The measured ethanoic acid concentrations and air exchange rates were used to estimate the surface removal rates. Equation 7.7 can be rearranged to give

$$K_s = \left(G/V - nI \right) / I \qquad (7.11)$$

Hence Ks can be calculated from the generation rate, air exchange rate and ethanoic acid concentrations for each showcase.

A series of wooden cases at Kenwood House, London caused dramatic corrosion of jewellery solder. A series of carboxylic acid measurements confirmed that emission of methanoic acid was causing the corrosion, which had been identified as a lead methanoate by x-ray diffraction. A series of refits, to increase the air exchange rate, was undertaken by drilling holes initially in the tops and then in the tops and bottoms, of two cases to try to reduce the methanoic acid concentration. A case with similar initial concentration was measured as a control through-out this work. Methanoic acid emission from paints is likely to be a strong function of temperature and a control was needed to quantify this effect (Tetreault, 1999). The major source of the methanoic acid was a Dulux eggshell paint used inside the showcases. This paint was intensively studied at the British Museum as it had caused similar lead corrosion in a showcase there. The emission rate was measured, by placing dried samples on Melinex in a closed glass dessicator above water. The methanoic acid concentration was measured with ion chromatography and the emission rate calculated. A series of samples were naturally aged (three years) and artificially aged (60ºC for 28, 56 and 72 hours). The emission rate was measured from the aged samples to determine any drop in emission (Tetreault, 1999).

The Ks values were calculated from the three air exchange rates; unaltered, with one set of holes and with two sets of holes.

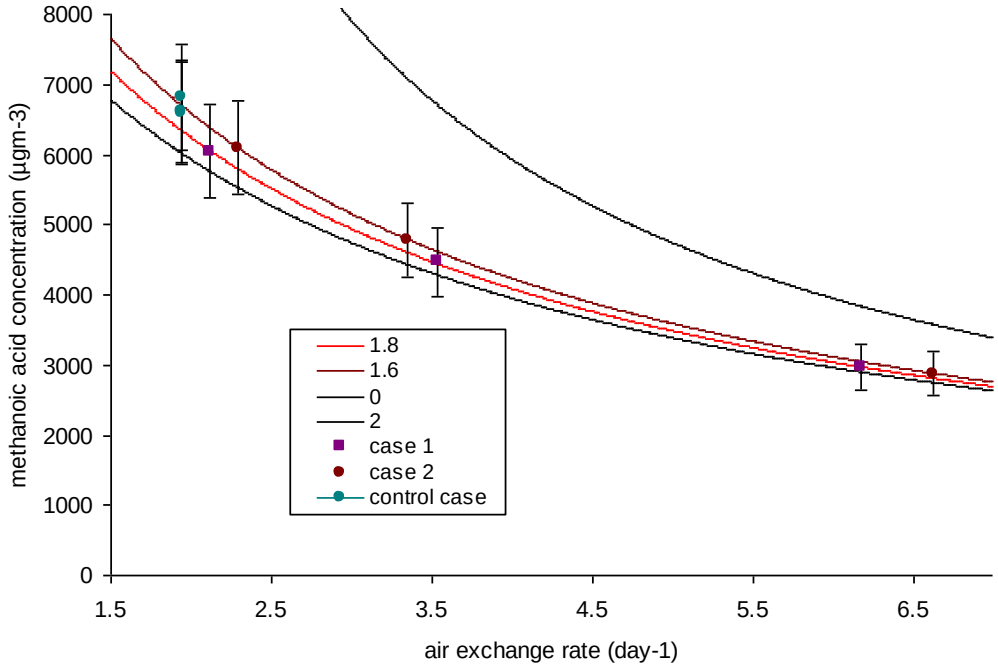

Figure 7.13 Methanoic acid concentrations inside painted wooden showcases at Kenwood House

The three data points for each showcase fall between the Ks lines for 1.6 and 1.8day^{-1}. The three repeat control tests confirmed the emission rate was very similar for the three July measurement periods.

A set of six showcases at the British Museum constructed between 1995 and 1999, using similar designs and materials, was selected to give a range of air exchange rates. Cases without objects that could be sources of carboxylic acids were selected and the surface area of an internal source (Moistop sealed MDF base and back boards) was measured. The emission rate of ethanoic acid from this type of sealed board had been measured previously (Thickett, 1998c). All other materials in the showcases had undergone and passed accelerated corrosion tests with lead, indicating an extremely low emission rate of carboxylic acids. All the showcases investigated were approximately 2m high, 1m deep and 2 m wide, with 'pull and slide' doors as the front face.

The air exchange rate of each case was measured twice. Carboxylic acid concentrations inside showcases were measured using diffusion tubes exposed for twenty eight days and analysis by ion chromatography. Measurements were made

every three months to account for the large seasonal variation in carboxylic acid concentrations in showcases containing wood products in naturally conditioned buildings. This is because large seasonal variations in temperature and RH dramatically influence carboxylic acid emissions from wood products and paints. The generation rates, ethanoic acid concentrations and air exchange rates were used to calculate Ks, results are shown in Table 7.4, equations were then solved for pairs of equations giving 15 values for Ks. The ethanoic acid concentrations and air exchange rates are shown in Table 7.4.

case	AER day^{-1}	ethanoic acid concentration μgm^{-3}	Ks calculated day^{-1}
1	0.08	4736	0.110
2	0.10	3600	0.150
3	0.40	1640	0.149
4	0.44	1636	0.110
5	1.40	600	0.100
6	1.74	476	0.151

Table 7.4 Calculated Ks values in 4m^3 glass and metal showcases with taped Moistop MDF baseboards

The ethanoic acid concentrations are also plotted against air exchange rate in Figure 7.14. The boundary Ks values are shown on Figure 7.14. Lines for Ks =0, no surface deposition and Ks=2, a relatively high value are also plotted.

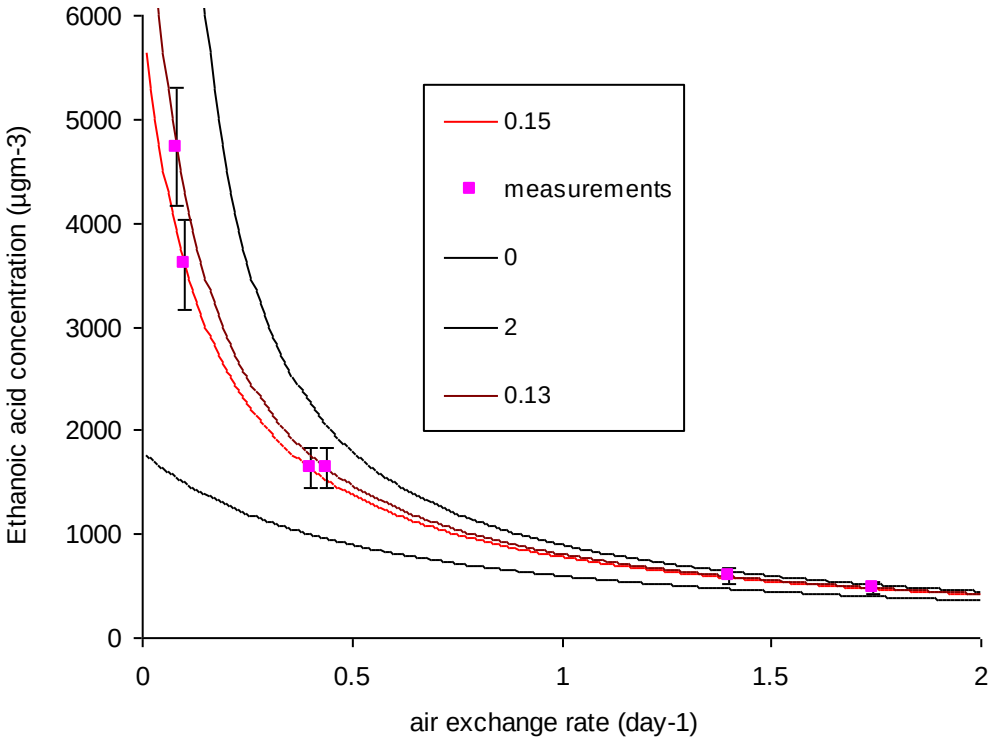

Figure 7.14 Ethanoic acid concentrations inside glass and steel showcases with MDF at the British Museum

The showcases measured only had MDF baseboards and these were 'sealed' to reduce emissions. It is interesting that for a given emission rate, the low surface deposition resulting from the majority of the case surfaces being glass or powder coated steel, means the ethanoic acid concentration increases sharply as air exchange rate reduces. Practically, this means there is a pseudo threshold for air exchange rate, above which the ethanoic acid concentration is low (below 750µgm^{-3}) and below which it is over 1500µgm^{-3}.

7.5.5 Pollution Ingress

A series of measurements have been undertaken in showcases to test the validity of the Weschler equation and IMPACT model.

7.5.5.1 Showcase measurements and IMPACT calculations in the British Museum

Eight showcases in the British Museum, built between 1995 and 1999, were measured over twelve months in eight showcases. The air exchange rates were measured twice in that period. Sulfur dioxide and nitrogen dioxide concentrations inside the showcases and the rooms were measured with diffusion tubes. Each measurement was for 28 days and a measurement was carried out every three months. The showcase dimensions and surface areas of each material present were measured. All the data and the room concentration was fed into the IMPACT application to calculate the internal concentration. This was compared with the measured internal concentration. Errors were calculated from the errors in the diffusion tube measurements. The errors on the IMPACT calculations were calculated by inputting the top end of the measurement, value + error, the bottom end of the air exchange rate measurement, value – error and the bottom end of the room pollutant measurement and top end of the air exchange rate. This gave the maximum and minimum concentration inside the showcase. Results are shown in Figure 7.15 and 7.16.

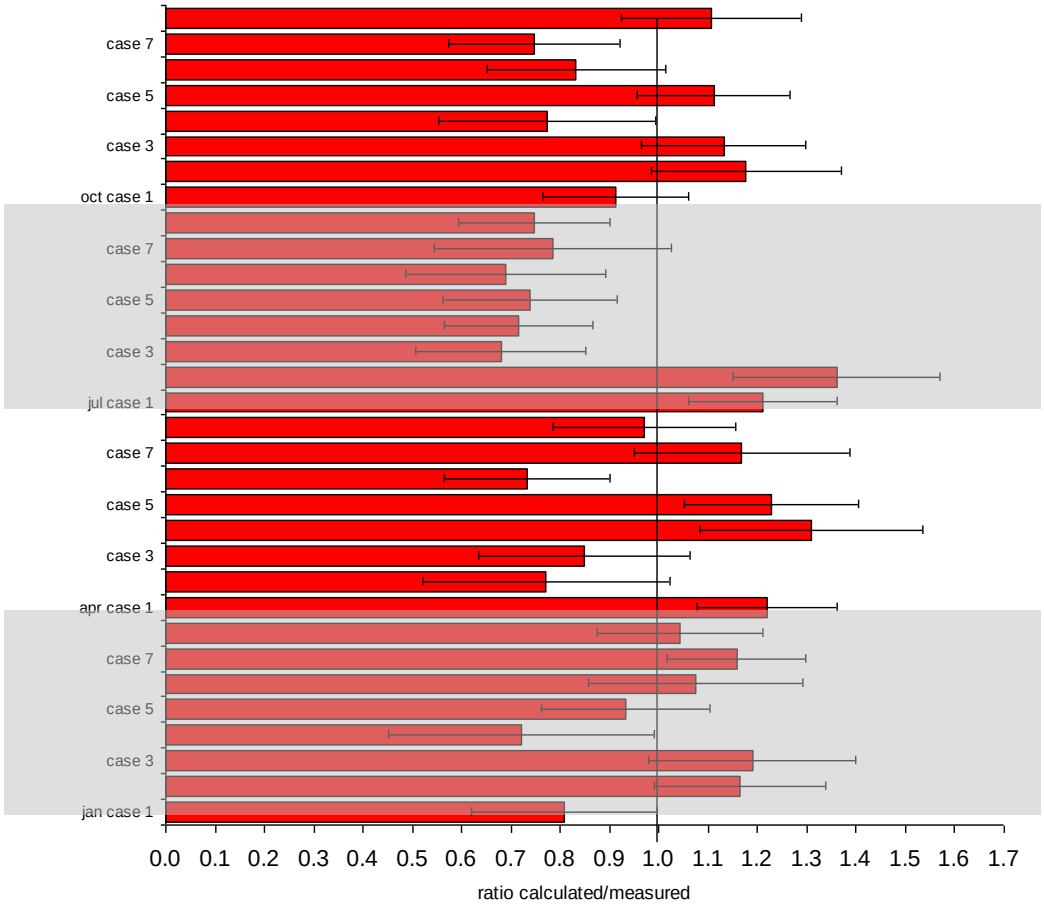

Figure 7.15 Nitrogen dioxide calculations using the IMPACT model and measurements in 4m^3 showcases at the British Museum

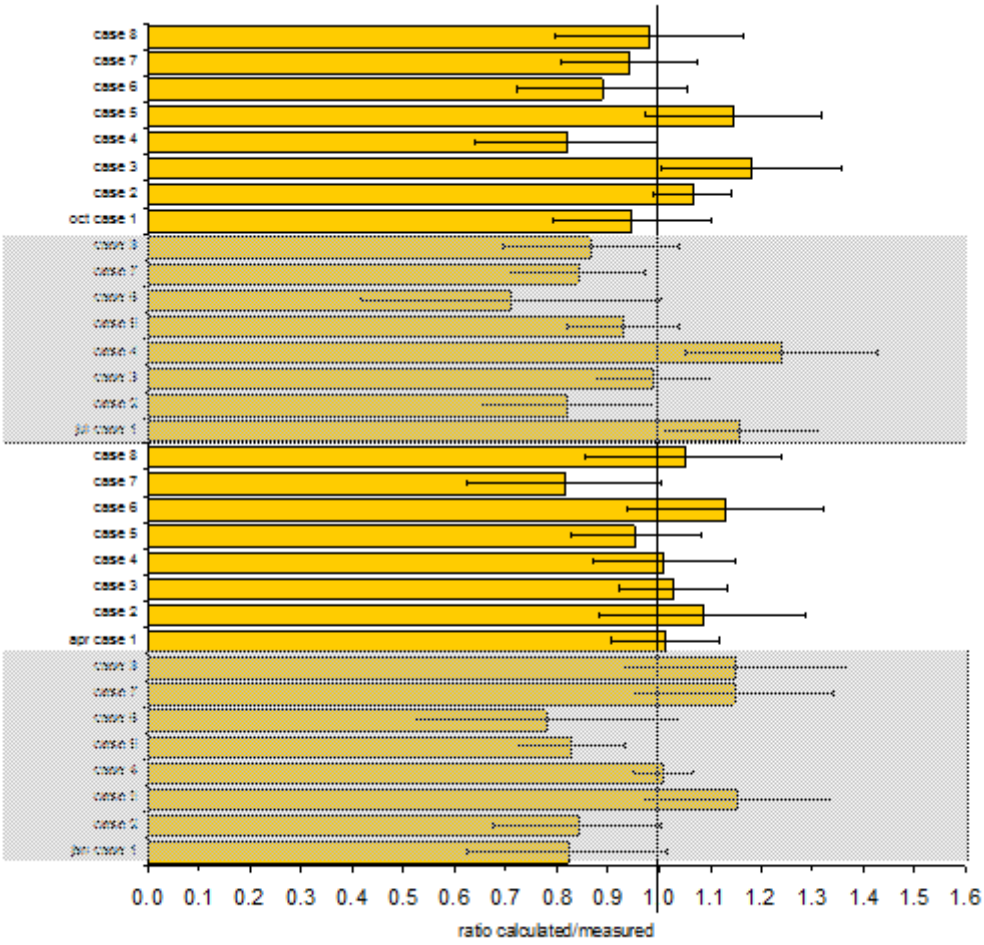

Figure 7.16 Sulfur dioxide calculations using the IMPACT model and measurements in 4m^3 showcases at the British Museum

The measured concentrations were in reasonable agreement with the values calculated from IMPACT considering the errors in the inputs. The errors in diffusion tube concentration measurements were assessed to be approximately 15% depending on the concentration value. The estimated errors in the air exchange rate measurements were 17%. The temperature and RH inside the showcases and their volumes and surface area of each material were all measured relatively accurately, (RH $\pm$2%, temperature $\pm$ 0.2°C, all dimensions $\pm$ 3mm).

Almost all of the measurements (27 out of 32) were within the calculated errors for sulfur dioxide, i.e. a ratio of calculated to measured concentration of 1.0 fell within

the error bars. The nitrogen dioxide concentrations showed much less agreement (13 out of 32) between the measurements and the IMPACT calculated values. The higher disagreement in the nitrogen dioxide values than the sulfur dioxide values may be due to nitrogen dioxide being re-emitted from surfaces. The model assumes that once a gas has reacted at a surface it will not be re-emitted. Nitrogen dioxide can convert into nitrous acid which will be re-emitted (deSantis et al., 1996; Spicer et al., 1993). However, this could only account for negative deviations (Rcalculated/measured <1). The majority of the nitrogen dioxide values that did not agree were in April and June. This may be due to homogenous reactions in the gas phase, which the model neglects. Such reactions are driven by light and light levels were highest during these months (Svendby and Henriksen, 2004).

7.5.5.2 Air exchange rate measurements and IMPACT calculations in showcases in other locations from the MASTER project

In order to widen the testing, showcases measured in the MASTER project were assessed. The project measured pollutant gas concentrations in ten show cases and rooms across Europe for monthly periods for a year, along with temperature and RH. No air exchange rates were measured as part of the project. Selected showcase air exchange rates were measured and the surface areas of the different materials measured. The internal concentrations were calculated as before for each of the twelve periods and compared to the measured values.

Four showcases were selected from the room and showcase pollutant concentration data. The full set of data is shown in Figures 1 to 6 in the Appendix 2. The instances were selected to give a good coverage of the data.

The showcase air exchange rate was measured and internal dimensions and material types recorded to allow the IMPACT calculations. The measurements in Malta, Crete and Germany where undertaken by Jenny Studer, with those in Malta and Crete generously funded as short term scientific missions under the COST action D42. In the MASTER project duplicate measurements were made for each pollutant. As there were a large number of measurements the errors have been treated

differently to reduce the computational requirement. Equation 6.8 gives the relationship between the showcase concentration and the room concentration.

As discussed earlier the variance of the measured concentrations and air exchange rate is much greater than that of the deposition velocity, volume and surface area. Hence the errors can be approximated to;

$$\left(\frac{s_I}{I}\right)^2 = \left(\frac{s_n}{n}\right)^2 + \left(\frac{s_O}{O}\right)^2 + \left(\frac{s_n}{n}\right)^2 = 2\left(\frac{s_n}{n}\right)^2 + \left(\frac{s_O}{O}\right)^2 \qquad (7.12)$$

the air exchange rate variance was estimated at 0.2 to take into account the variety of closure mechanisms for the MASTER showcases.

For each calculated and measured value a ratio was then calculated as before, 1 indicates perfect agreement. The ratios of the calculated to measured concentrations are shown in Figures 7.17 to 7.19.

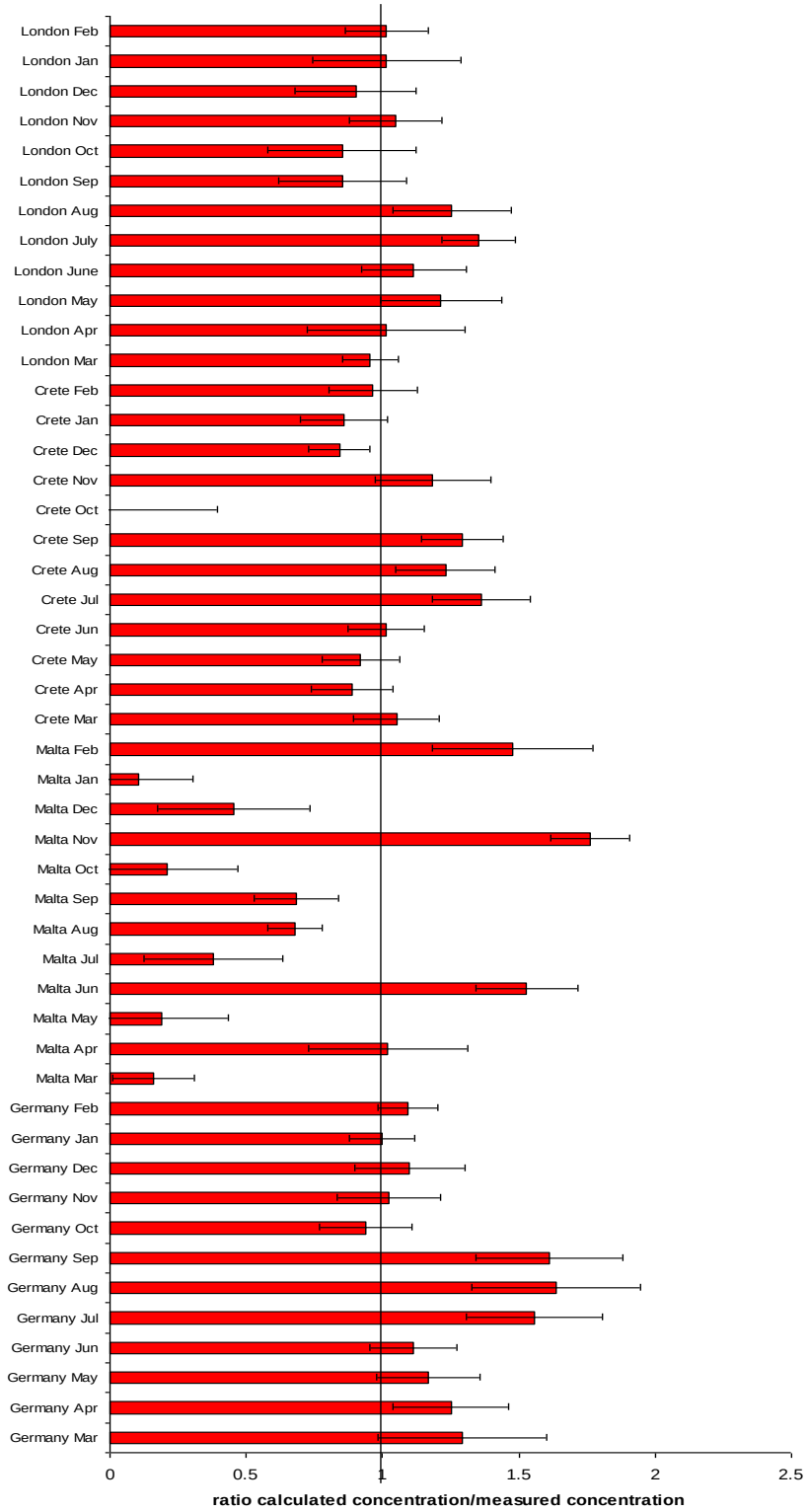

Figure 7.17 Ratio of nitrogen dioxide concentration calculated from the IMPACT model in four MASTER showcases to measured concentration

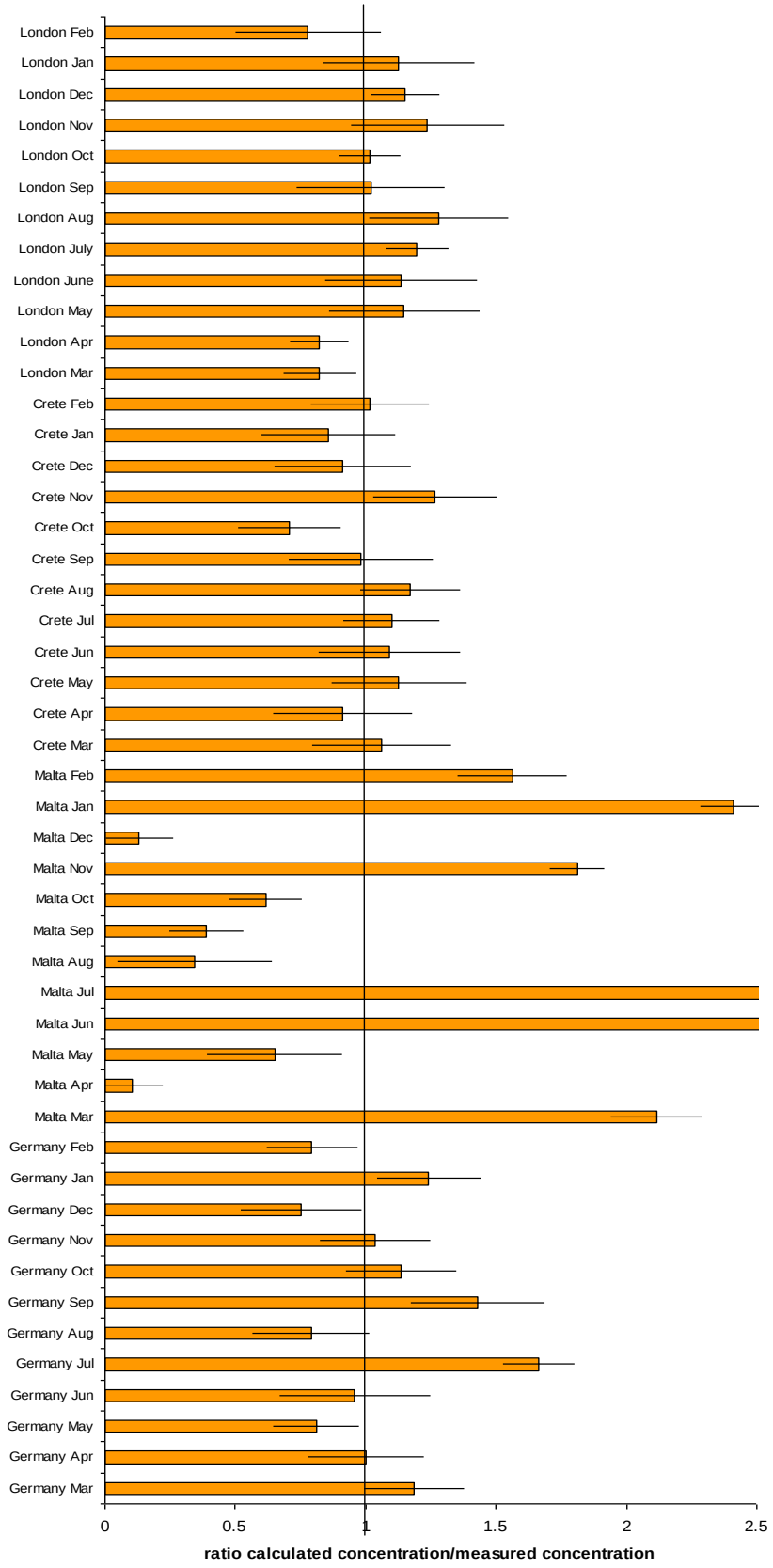

Figure 7.18 Ratio of sulfur dioxide concentration calculated from the IMPACT model in four MASTER showcases to measured concentration

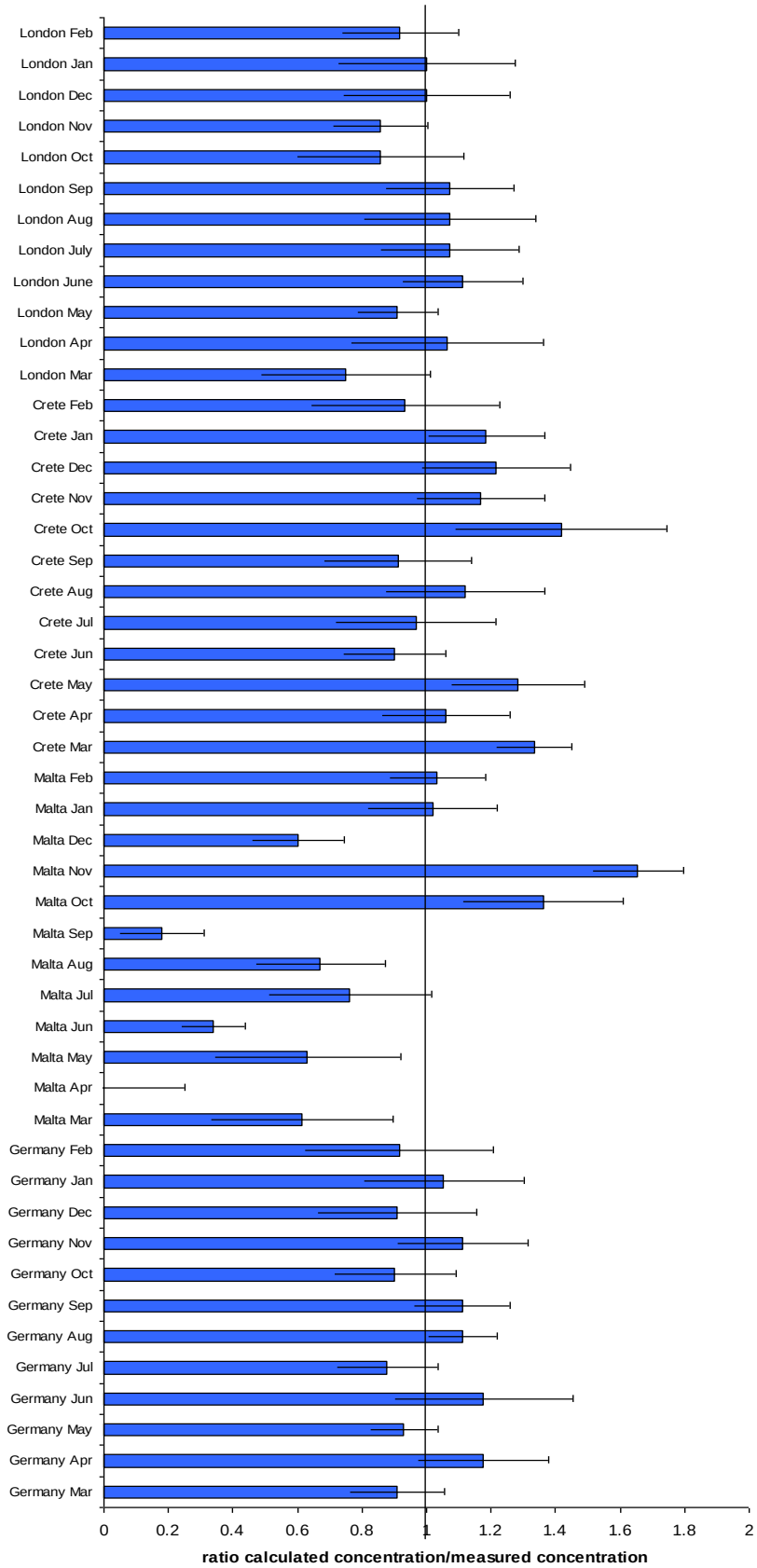

Figure 7.19 Ratio of ozone concentration calculated from the IMPACT model in four MASTER showcases to measured concentration

The calculated results from the Malta showcases show very poor agreement with the measured pollutant gas concentrations. The showcases at Malta were poorly constructed and the warped wooden doors closed quite differently each time. The measured air exchange rates are likely to differ from those for each monthly period of measurement for gases. This is the likely cause of the much worse fit for this data. The values from Crete, London and Germany are much better. For nitrogen dioxide higher calculated values were observed in some summer months in Crete and Germany, but not the UK. The Tower of London site was in a dark room, whereas both the German and Cretan sites had natural daylight. This appears to have driven homogeneous reactions in the gas phase. The October measurement for Crete had a nitrogen dioxide concentration 15 times greater inside the showcase than the room. Although showcase concentrations can be higher than room concentrations through the delay brought about by air exchange, this value was considered highly unlikely and the data excluded. Excluding these effects all bar two of the calculated concentrations are equal to the measured concentrations within the experimental errors. Considering sulfur dioxide, no seasonal effects were observed. All except six of the thirty six calculated concentrations are equal to the measured concentrations within the experimental errors. For ozone all but two of the thirty six calculated concentrations are equal to the measured concentrations within the experimental errors and no seasonal effects were apparent in the data.

7.5.6 Dust

A series of eight showcases at Rangers House, London were examined. Dust deposition rates were measured using the method described in 2.2.12. Glass slides were placed inside each showcase and on nearby horizontal surfaces at 2m height. Air exchange rates were measured of each showcase. Results are shown below.

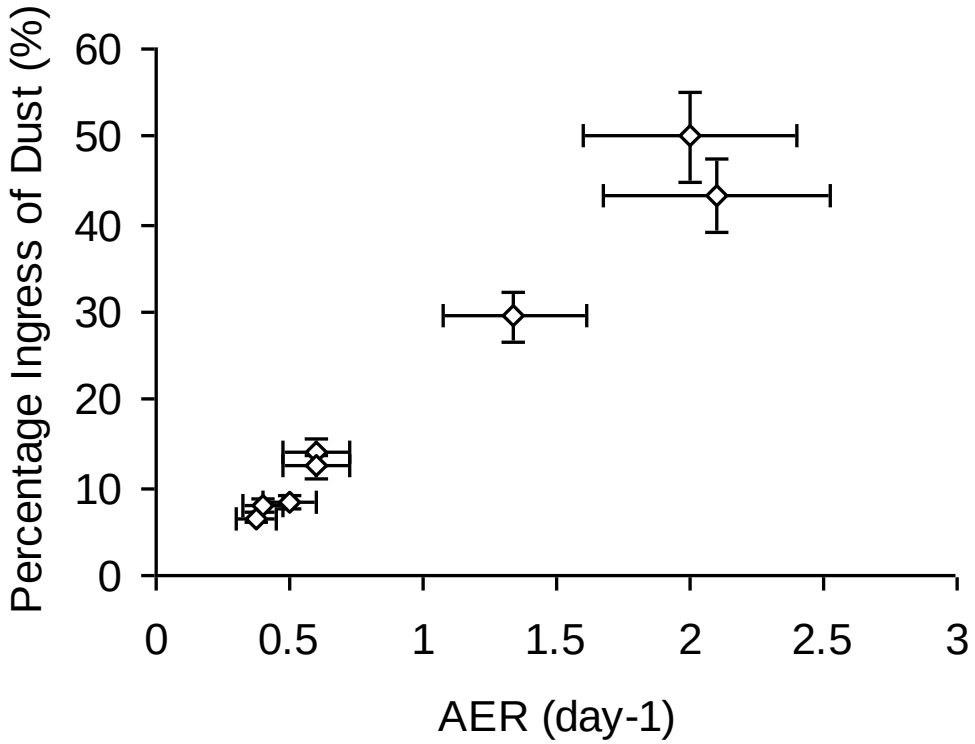

Figure 7.20 Dust ingress into showcases at Rangers House plotted against the showcase air exchange rate

The proportion of dust entering the showcase decreases with the air exchange rate.

Dust ingress was also measured into three showcases in two rooms in a maritime location, Portchester Castle. Glass slides were exposed for twenty days to collect dust and analysed with microscopy and image analysis. After image analysis the soluble anion content of the dust was measured by extracting in water and ion chromatography. The sea salt aerosol and hence chloride concentration in dust is a strong function of wind speed and direction. It would be expected to vary greatly over time and a twenty eight day measurement may not be very representative of the long term deposition rate. As these showcases were replaced samples of the showcase fabric were available. These were weighed, extracted with 18.2MΩ water and the chloride concentration and long term (twenty eight years) deposition rate calculated. Results are shown in Table 7.5.

Case	Air Exchange Rate	Dust coverage in 30 days %	Chloride deposition rate µg/m^2/day	Long term chloride deposition rate mg/m^2
Room 1		0.98	238	
Case 1	1.8	0.53	124	75
Case 2	3.9	0.67	41	33
Room 2		1.23	335	
Case	2.1	0.76	61	41

Table 7.5 Dust and chloride ingress into three showcases at Portchester Castle

The dust ingress reduces with air exchange rate, as do the amounts of deposited ions, but to different degrees.

Figure 7.21 shows the particles size distributions of dust deposited in showcases and the rooms they are in. Room 1 contains showcases A and B, Room 2 contains a single showcase. The particle size distributions were extracted by image analysis.

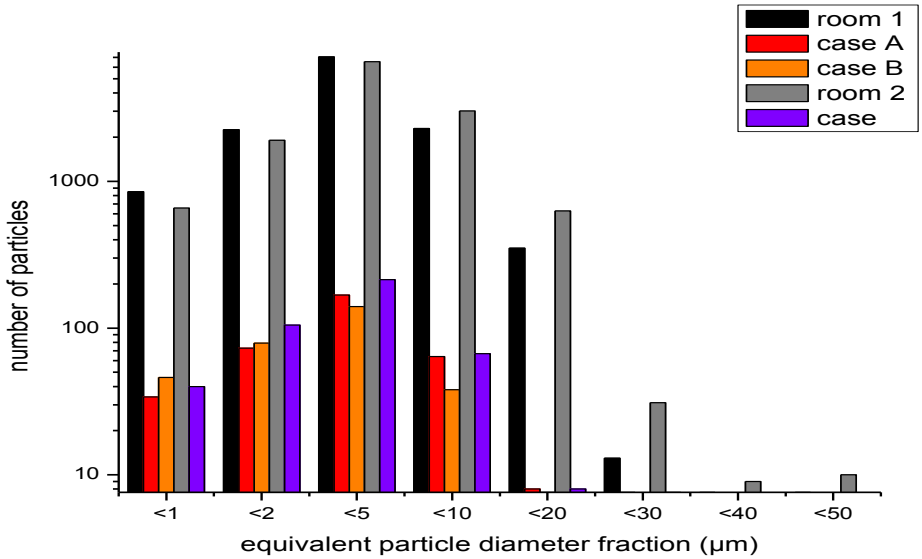

Figure 7.2 1 Particle size distribution of dust in showcases

The coarser dust does not ingress into the showcases and finer particles tend to penetrate showcases preferentially. Figure 7.22 shows the same data with the percentage of number of particles at each size fraction calculated compared to the room.

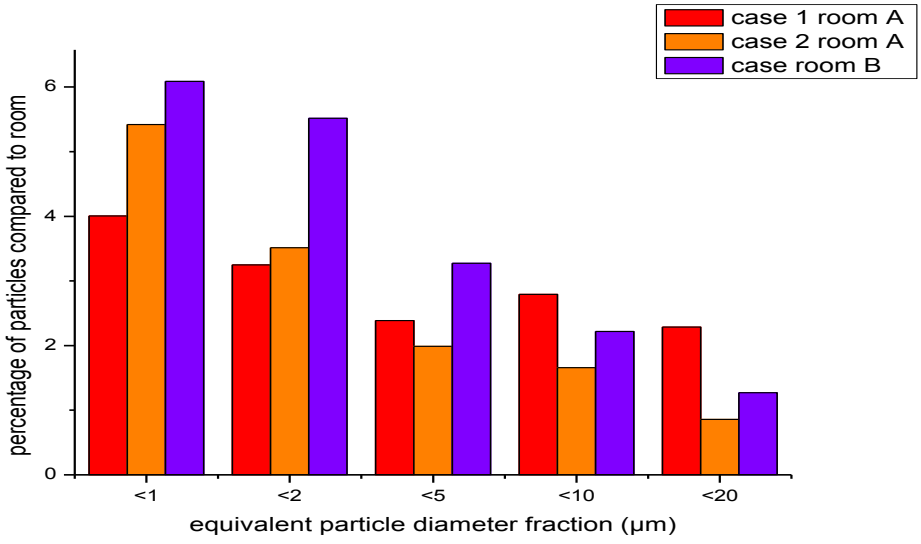

Figure 7.22 Percentage of dust ingressing at each size fraction compared to room

A greater proportion of finer particles ingress the showcases. Each case shows a different distribution due to different crack sizes and geometries.

7.6 New Showcase Specification

The specification was developed from the conclusions of the assessment of current cases. A desktop case was chosen, as a single level seal can produce a low air exchange rate. The major mechanism of air ingress in many cases is the stack effect, with the mass of a column of air pushing air through vertically separated horizontal gaps. Table cases, rather than plinth bases were chosen to allow greater disabled access. A number of further features were required to maintain low RH.

7.6.1 Low air exchange rate

A low air exchange rate (AER) is essential. This will increase the length of time the silica gel is effective for and reduce the number of visits for maintenance. To achieve six months between silica gel changes a half life of 226 days is needed, requiring an AER below 0.4 changes per day (day^{-1}), preferably lower. A desktop case with a well sealed, five sided glass lid, hinged along the lower back edge, was selected as most likely to meet the criteria. The weight of the lid and an overlapping metal flange also help the compression seal to function efficiently.

7.6.2 No wood products

Wood products are known to emit organic acids, and in sealed environments, these will concentrate. A further problem in trying to create low humidity environments in display cases is the moisture released by organic materials in the case, most often MDF baseboards. Buffering by wood products affects the creation and maintenance of low RH environments suitable for the display of archaeological iron objects. As metal baseboards and acrylic mounts are inert, and available for a similar cost to wooden materials, these should be used instead.

7.6.3 High silica gel volume

In order to have a sustainable maintenance programme a minimum hygrometric half life of 226 days was required. If the AER of 0.4 day^{-1} was met for a $1m^3$ case then Thomson predicts 5.65 kg of silica gel would be required.

7.6.4 Silica gel tray close to the display area

The air exchange between the silica gel tray and the display area has been found to be a critical factor in the effectiveness of maintaining a dry environment. Additionally easy access required to a silica gel compartment can compromise its sealing. The closer this opening is to the horizontal seal of the display volume, the less the potential stack effect will be and thereby the lower the AER with the same gaps.

7.6.4 Baseboards

It can be difficult to ensure sufficient gaps around solid baseboards to give adequate air exchange between the silica gel compartment and display volume. A minimum of 15mm has been recommended by the Canadian Conservation Institute (Tetreault, 1999). The specification included a perforated baseboard, with holes of at least 15mm diameter covering 50% of the area. Sealing a wood product baseboard with such holes is unlikely to be effective, resulting in emitted organic acids and buffering. Hence metals baseboards were specified.

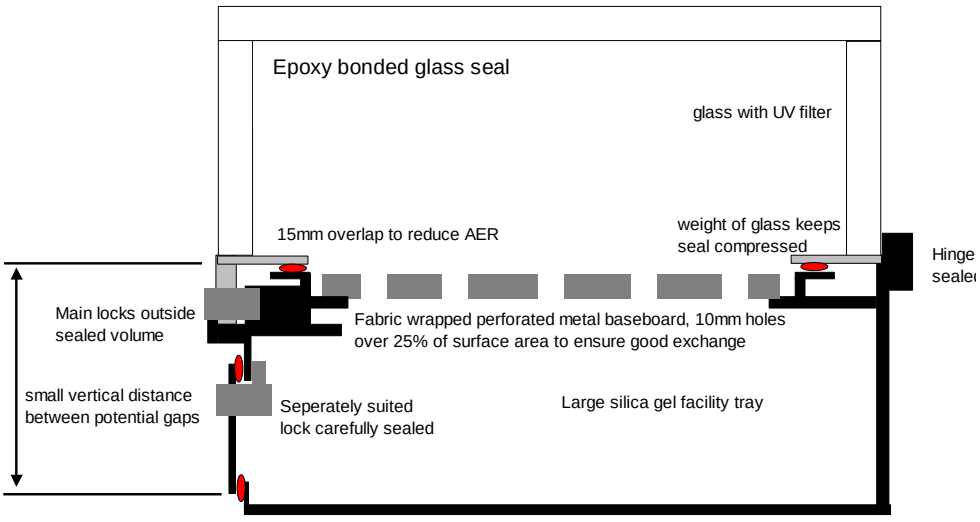

Figure 7.23 Showcase schematic

7.7 Trials of Prototypes

Two companies produced cases to the modified design, which were installed in spring 2005. Some differences were evident immediately. A panel placed over the front of the silica gel tray for one design, minimised the possibility of wheelchair access by reducing the height of the table. The same manufacturer had also produced a metal baseboard with smaller holes than specified, although the number of holes was greater. When initially testing the cases for leaks, more gaps were found with this manufacturer's design and the AER, measured during the installation, also showed this case did not meet the specification. During the installation it was also noted that the locks were difficult to close and some have since needed to be replaced. Monitoring has taken place since installation and the results are described below.

7.7.1 Temperature and RH

The four prototype cases were installed at Portchester Castle where the room environment varies between 60 and 90% RH. The silica gel was changed around 6 months after installation, the RH is shown in figure 3. For Manufacturer 1's case the RH had crept up above 30% during the first 6 months, however the silica gel used was not completely dry when inserted (12% compared with 5% RH). After the silica gel was changed the RH was reduced below 25%. During the second 6 month period the RH gradually increased but is still under 30%. Manufacturer 2's case showed a smaller increase in RH during the first 6 months, with the RH around 15% when the silica gel was changed. The RH decreased to 10% and has since risen slowly. It is currently just under 15% RH. Plotting a regression line of the second period of data shows the RH would reach 20% after a further 9 months. This demonstrates the case could be passively controlled below 20% RH with an annual change of dry silica gel. As a result it will be possible to control the case below 30% RH with an annual change of silica gel.

In fact the two cases from manufacturer 2 held an RH below 20% for over twelve months. The RH in the showcases from manufacturer 1 was observed to rise above 30% in some of the six month periods over the past three years since installation. Fresh corrosion, identified as akaganeite by FTIR, was observed on archaeological iron objects in those cases. No corrosion was observed in the cases from manufacturer 2, where the RH stayed below 22%, despite having similar objects that

had shown similar potential for corrosion when displayed previously (Thickett, 2010).

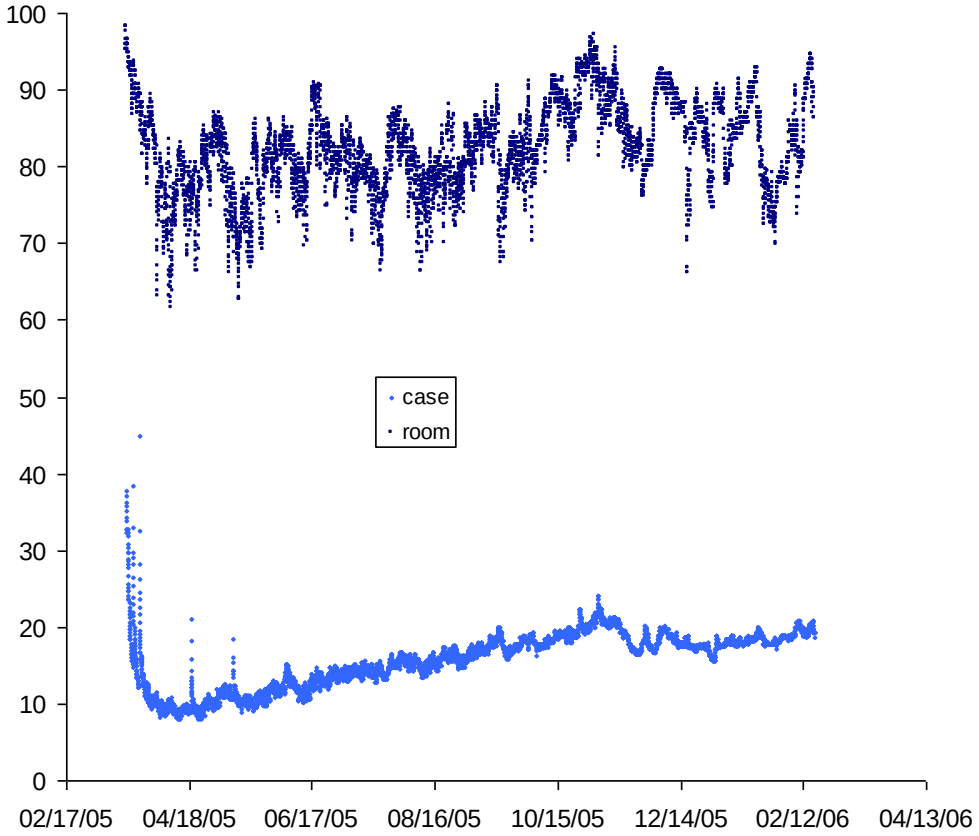

Figure 7.24 Relative humidity in room (dark blue trace) and showcase (pale blue trace) for trial showcase at Pevensey Castle

Two cases from Manufacturer 2 were installed at Pevensey Castle during spring 2005. Monitoring of the environmental conditions in the display room show the humidity varies between 65 and 95% RH annually. After 11 months monitoring both the cases were still below 30% RH, however the silica gel was not changed during this period. Air exchange rates have not been measured but the cases came from the same batch as those at Portchester Castle. This demonstrates that the chosen, modified case design is performing not only as desired but better than expected.

The results of monitoring in the showcase and silica gel facility tray for one of the showcases, by manufacturer 1 is shown in Figure 7.25.

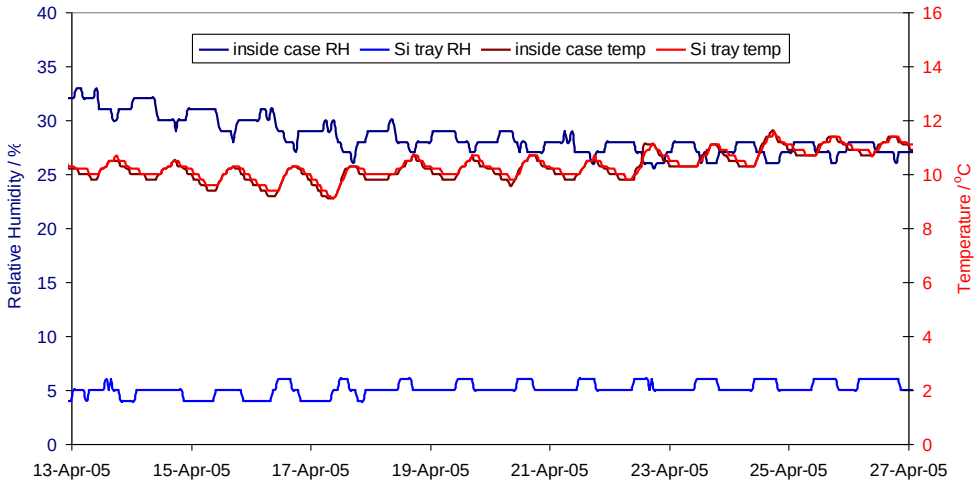

Figure 7.25 RHs inside trials showcase from manufacturer 1 at Portchester Castle showing different RH in silica gel and display volumes

The temperatures are very similar. Whilst the RH in the silica gel tray is low, around 5%, that in the display volume is much higher, still above 25% after two weeks. This indicates poor exchange between the silica gel tray and display volume. The baseboard had 5mm diameter holes.

Monitoring from a case by manufacturer 2 is shown in Figure 7.26.

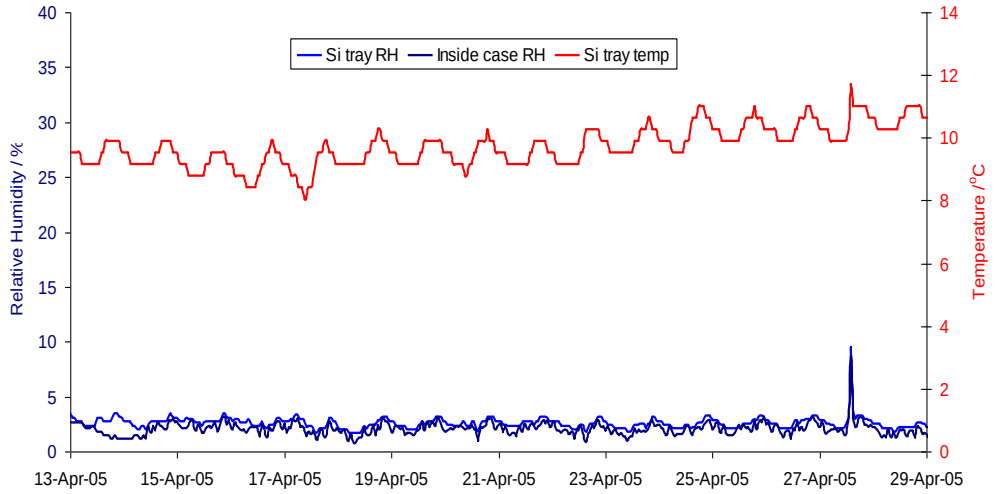

Figure 7.26 RHs inside trial showcase from manufacturer 2 at Portchester Castle showing RH equilibration between silica gel and display volumes

In this instance the silica gel facility tray RH is very slightly lower than the display volume, (less than 2% difference). The baseboard in this case has 8mm diameter holes.

7.7.2 Pollution

Pollution monitoring with diffusion tubes has been undertaken at Portchester Castle in the case from manufacturer 2 with the highest measured air exchange rate. Tubes were exposed for four week periods with three measurements being taken, equally spread over a year.

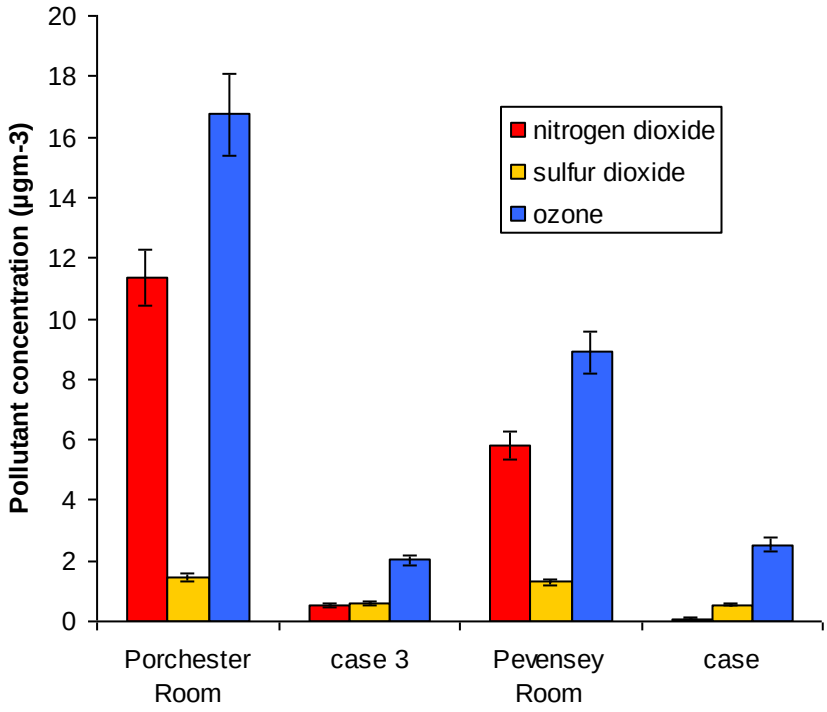

Figure 7.27 Industrial pollutant gas concentrations inside trial showcases at Portchester Castle

Hydrogen chloride concentrations were also measured because Portchester is in a marine environment with medium concentrations of industrial pollutants, which are reported to react with sea salt aerosol to generate hydrogen chloride.

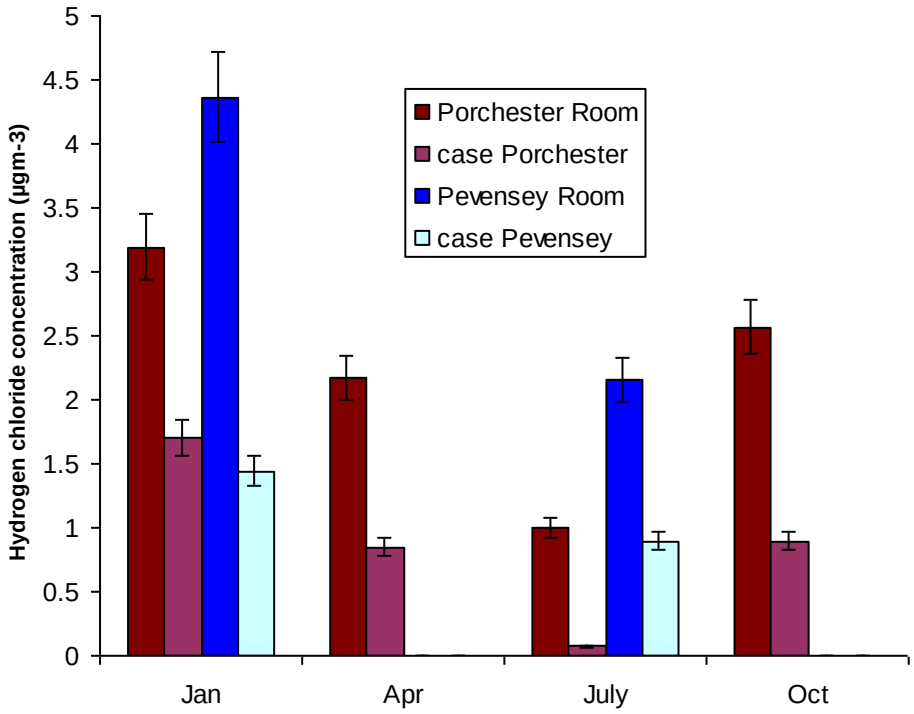

Figure 7.28 Hydrogen chloride concentrations inside trial showcases at Portchester and Pevensey Castles

Dust deposition was monitored in the room and all four cases by exposing glass slides and then undertaking image analysis. The dust was then extracted with water and the chloride concentration determined with ion chromatography, to calculate a chloride deposition rate from sea salt aerosol. Results are shown below.

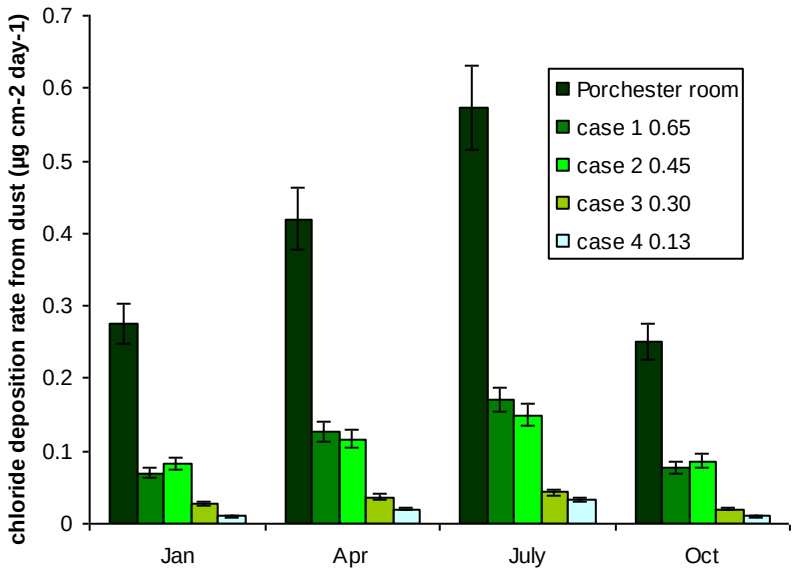

Figure 7.29 Chloride deposition as dust inside trial showcases at Portchester Castle

The degree of pollution protection demonstrated and utility of the case is also markedly superior.

7.8 Installation of new showcase design

Thirty six showcases of the new design have been installed in seventeen properties in the past five years. The cases were supplied by three different manufacturers. Air exchange rates were tested for each case on installation, and refits made by the manufacturers if the 0.4day^{-1} specification was exceeded. This was required for just over 20% of the cases. In all instances continuous RH monitoring was installed in the showcases. All were found to be able to hold less than 30% RH for twelve months with dry silica gel. Many of the showcases kept the RH below 20% for twelve months.

7.8.1 Assessment of Thomsen equation for internal relative humidity

The new showcases have very little hygroscopic material present apart from the silica gel and most have continuous RH monitoring and their air exchange rates are known. This makes them ideal to assess the iterative approach to the Thomsen equation described in 6.3.2. The calculated time for the showcases to increase an

initial RH of 5% to 30% is tabulated in Table 7. For most of the showcases it was calculated that the RH would only reach 30% some while after 365 days. Conservators visit English Heritage sites annually to perform condition checks and maintenance and the silica gel is replaced with freshly conditioned gel at this time. The room data was used to calculate what RH would be expected inside the showcase 365 days after the additions of silica gel conditioned to 5%RH.

Location	Number of showcases	Number of days for RH to increase from 5 to 30%	RH 365 days after installation of silica gel conditioned to 5%	
		calculated	calculated	Measured
Portchester	2	512	22	21
Pevensey	2	593	18	16
Lullingstone	4	623	17	18
Goodrich#	1	381	29	27
Osbourne	1	703	15	13
Jewel Tower	1	610	16	16
Chesters*	6	418	25	26

* Not a standard case design, top back hinged – type B in Table 2

Table 7.6 Measured and calculated performance of new design showcases

The measured values are in good agreement (2%) with the calculated values.

7.8.2 Assessment of efficiency

Prior to the installation of the new showcases, sites with archaeological iron had the silica gel changed every six months. Data has been collected for sites in the South East Territory assessing the time and travel required to service the sites with silica gel. The mileage figures were converted to carbon equivalents using the Carbon Trust website.

Site	old cases			new cases	
	days	miles	CO_2 (kg)	days	CO_2
Portchester	4	80	3.2	2	1.60
Pevensey	4	312	12.48	2	6.28
Battle Abbey	4	288	9.12	4	9.12
St Augustines Abbey	4	72	2.88	4*	2.28
Lullingstone*	4	388	15.52	2	7.76
Richborough	4	56	2.24	4*	2.24
TOTAL	24	1136	45.49	18	29.2

* showcases have not been replaced with new design yet

Table 7.7 Time and carbon footprint to maintain low RH environments in showcases in English Heritage South East Region before and after partial replacement with new design showcases

There is a very significant saving in both staff time and carbon footprint from using the new showcase designs compared to those used previously.

7.9 Conclusions

Models have been tested to determine the RH, ethanoic acid, methanoic acid, sulfur dioxide, nitrogen dioxide and ozone concentrations inside showcases from room data and showcase parameters. The models have been found to perform adequately for their application to showcases. The ability to model these factors has allowed design of showcases to meet RH, ethanoic acid, methanoic acid, sulfur dioxide, nitrogen dioxide criteria to preserve archaeological iron artefacts. Examination of existing showcases of appropriate designs has elucidated the design features required to achieve these criteria. A low air exchange rate and correct design of baseboards to allow dry air from silica gel to condition the showcase, were found to be critical to performance. The new showcase design has been developed and tested against these criteria and found to perform well. Measurements of dust and its chloride content and hydrogen chloride ingress into showcases have been made. The criteria and measurements have provided the framework to assess English Heritages existing showcases for archaeological iron and prioritize refitting and replacement.

Chapter 8 Storage of Archaeological Iron

8.1 Introduction

Storing the large volumes of archaeological iron accessioned in many institutions is a significant management challenge. English Heritage has well over 1000 boxes containing archaeological iron stored in 14 sites. Present guidelines do not fully agree, but many recommend storage at 10% RH or below (Watkinson, 1987; UKIC, 1983; Brown, 2007). The studies presented in chapters 5 and 6 indicate 16% as a reasonable target RH. In the UK, low relative humidities are normally achieved with silica gel in Stewart boxes. These were formed from polyethylene, but in 1997 the material was changed to polypropylene. Indicating cards based on cobalt chloride are normally added. Whilst these have very limited precision, (normally 5%), the large number of boxes precludes more precise measurement methods for economic reasons.

Figure 8.1 Stewart box with silica gel, indicator card and iron and a typical archaeological iron store at Dover Castle.

The silica gel requires reconditioning periodically, and checking the boxes and replacing the gel takes a significant amount of staff time, and is often neglected (Harder, 2010). A number of aspects were investigated;

- the accuracy of the cobalt chloride indicators used in English Heritage.
- the feasibility of modelling the internal RH inside boxes to produce a silica gel change schedule for individual storage areas.
- the economics and sustainability of dehumidifying the major store rooms with archaeological iron were assessed.
- the performance of the present Stewart boxes in use (the old (pre 1995) style polyethylene and two newer (post 1995) styles made of polypropylene).
- whether there are significant changes in the properties of these boxes, affecting their performance.
- the boxes presently commercially available were assessed and compared.

The Stewart box changed in approximately 1995 from a polyethylene box to one made from polypropylene. The design of the lids changed after public complaints about difficulty in closing the boxes.

A wide range of volatile organic pollutants has been reported from Stewart boxes (Larkin et al., 2000). Other authors have also commented on the potential for emission of an airborne chloride from polypropylene (Larkin et al., 1998). Tenax absorption and gas chromatography–mass spectroscopy (GC-MS) analysis by Larkin *et al.* did not quantify ethanoic acid, although three failed accelerated corrosion tests with lead were reported, which may indicate ethanoic acid emission from the boxes. The effects of acetic acid on iron and steel corrosion are well known (Oesch, 1996) and Chapter 5 has shown that ethanoic acid concentrations of 1500 μgm^{-3} can accelerate the oxidation of ferrous chloride and iron mixtures to akaganeite by up to a factor of four. Accelerated corrosion tests (Robinet and Thickett, 2004) were undertaken on 24 samples (20 from old-style polyethylene, 4 from new-style polypropylene) from Stewart boxes purchased over the past 15 years. Approximately half of the tests being undertaken at the time the boxes were purchased. None of

these tests showed any corrosion on the lead coupons. Eremin and Wilthew (1996) undertook diffusion tube analyses inside Stewart boxes. The ethanoic acid concentrations were below the detection limit for the method, which is approximately 100 μgm^{-3} (Gibson et al., 1997a; Gibson, 2005). Almost all of the compounds identified by (Larkin et al., 2000) are known to be inert toward lead. Styrene, vinyl benzene is reported to cause lead corrosion but only at levels much greater than those detected. However, the extreme conditions of the accelerated corrosion tests may have caused higher levels of styrene release.

8.2 Methods and materials

8.2.1 Assessment of indicator cards to measure RH inside boxes

Several humidity indicator cards have been used in storage boxes. The short term accuracy of these cards has been assessed (Daniels and Wilthew, 1982). In the present study, the long-term accuracy was assessed by comparison with calibrated dataloggers inside storage boxes. Atcham store contains the archaeological archive from Wroxeter Roman City (Viroconium). The archaeological iron is stored in boxes in a dehumidified shipping container. The steel containers have desiccant drying wheel type dehumidifiers installed to reduce RH. This reduces the RH, to below 55%, whilst the main store building experiences RH values up to 90% through the winter. The artifact material has been repacked in various phases over the past 30 years with no silica gel being changed in this period. All the boxes have Humidial Corporation type 6203-BB RH indicating cards incorporated within them, Figure 8.2.

Figure 8.2 Humidial Corporation type 6203-BB RH indicating card

The silica gel has not been changed since the objects were boxed and hence it is reasonable to assume the cards have not been changed either. Humbug II dataloggers were calibrated with NAMAS certified magnesium chloride (33%), magnesium nitrate hexahydrate (54%), and sodium chloride (75%). Low RH calibration checks were undertaken with zeolites (<0.5% RH), lithium chloride (15%) and potassium acetate (20% NAMAS certified) saturated salt solutions. The zeolite was heated at 150°C and the water content of small powdered samples checked with thermogravimetic analysis (Perkin Elmer TGA7). Examination of the published isotherm for the zeolite indicated that a water content of less than 0.1% corresponded to less than 0.5% RH (Huang et al., 2007).

The dataloggers were placed in boxes packed eight, six, four, and two years before the measurements were made. The RH recorded was compared to that read from the indicator card. The calibration of eight of the RH indicating cards, two from each packaging campaign, was checked. Reading the RH from the indicator card is subjective and relies on discriminating the pink and blue RH panels. Colorimetery

was undertaken on the cards with a Minolta 2600D reflectance visible spectrometer. Reflectance spectra were collected of the six RH indicating circles. The spectra were converted into CIE Lab co-ordinates (CIE, 2004). The change from pink to blue of the RH indicating circles generate a large colour change, ΔE_{76} value. The lower RH circle were this large change in colour was observed, was considered the correct RH reading.

8.2.2 Modelling methods for internal RH

A number of equations have been developed to determine the RH inside an enclosure from the external conditions and the amount of buffering material (Thomsen, 1977; Tetreault, 2003; Lehto and Lankinen, 2004; DiPietro and Ligterink, 1999). Four RH models were investigated in two Stewart boxes by monitoring the RH increase inside the boxes with 2g of dry (5% RH) regular density silica gel in a 75% RH atmosphere. Monitoring was done with calibrated Humbug II data-loggers. The time taken to reach 16% RH in the box was compared to that predicted by the model. Details of the models and how they were applied are included as Appendix 3.

The best two performing models were then checked by measuring the RH inside over 30 Stewart boxes in four buildings used for iron storage.

Four sites with large iron stores were selected to test the modelling of RH values inside the boxes from air exchange rate, silica gel amount and room RH data. The rooms were of different construction types and had very different environments.

Site	construction roof	date built	storage	RH range	Pollution	pollution source distance	distance from sea
Dover	stone, slate	1912	room	43-81%	very high	ferry port 200m	200m
Fort Brockhurst	brick, brick and earth	1850-1870	casemate	41-97%	Medium		750m sheltered harbour 3km
Atcham	aluminium, aluminium	1970s	shipping container	45-55%	Low		80km
Corbridge	concrete, slate	1983-1985	basement	35-58%	Medium	MDF factory 5km	30km

Table 8.1 Locations selected to test RH modelling. These encompass a range of building types with a variety of nearby pollution sources including industrial and marine pollution

Calibrated RH sensors were placed in a number of Stewart boxes for one year. Humbug II and Smartreader 2 dataloggers and Meaco radiotelemetry sensors were used. The modelled data was compared to the recorded data. The mean square difference (MSD) between the modelled and actual RH data was calculated. The model with the lowest MSD gave the best fit to the measured data.

Once validated, the modelling was applied to the, presently uncontrolled, rooms at Dover and Fort Brockhurst and the present performance compared with an assumed maximum RH of 55%, such as would be achieved with a suitable dehumidifier. The conditioned store rooms at Dover and Fort Brockhurst already achieve a maximum RH of 55% with the dehumidifiers installed.

8.2.3 Stewart polyethylene and polyproylene boxes presently used

The performance of the Stewart boxes in present use was assessed in a number of ways.

8.2.3.1 Pollution Ingress

The degree of protection against pollution ingress was assessed by exposing diffusion tubes, followed by ion chromatography, (2.2.8.3). The measurements were undertaken at Dover Castle store as this had the highest pollution and sea salt aerosol concentrations of the four sites investigated. Only one set of diffusion tubes was deployed. The deployment period was determined by IMPACT model assessment of the likely sulphur dioxide concentrations in the store room (7.3.4.1). External sulfur dioxide concentrations readily available from the Port Authority automated monitoring site on the cliff. Nitrogen dioxide concentrations are generally much higher in the UK, but such data was not available. The air exchange rate of the room was measured with the carbon dioxide tracer gas method (3.4). Results are shown in Figure 8.3.

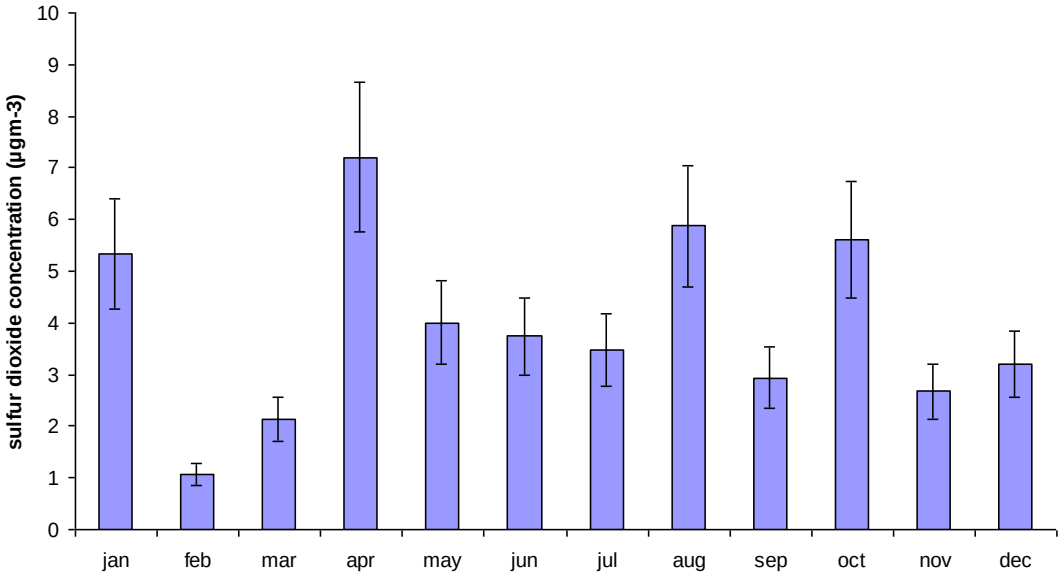

Figure 8.3 Calculated monthly sulfur dioxide concentrations in Dover Castle store room for 2005. Values calculated from sulfur dioxide concentration data on the adjacent cliff face, air exchange rate and internal and external temperature and RH values.

The highest concentration was in April. Examination of the associated wind direction data also showed a greater amount of time when the wind direction would blow pollution from the ferry port towards the store building in April, than in the other high sulphur dioxide months, (January, August and October). The diffusion tubes were exposed in an old type Stewart box, a new type Stewart box and in the store room in April. The boxes had almost identical volumes and the same loading of silica gel.

8.2.3.2 Deterioration of the boxes

Deterioration of the polyethylene and polypropylene Stewart boxes was measured with Fourier transform infra-red (FTIR) spectroscopy and differential scanning calorimetry (DSC). The enthalpy of the melting peak in DSC was compared to published values of 100% crystalline polyethylene and polypropylene to determine the degree of crystallinity (Wunderlich, 1990). The permeability of both polyethylenes and polypropylenes increases as the number and size of amorphous regimes increases, ie the degree of crystallinity decreases. The free-radical-initiated oxidation of polypropylene and polyethylene generates carbonyl and carboxylic acid containing moities that are readily observed with infra-red spectroscopy (Bohm, 2003). The ratio of the absorption band at peak around 1741cm^{-1} to that at 1471cm^{-1} was used to calculate a carbonyl index. Two small samples were removed from the lips of each box with a scalpel. One sample was removed from the side illuminated with daylight or artificial lighting and a second from the sheltered side. The exterior and interior face of each sample was analyzed with ATR FTIR (2.2.1.3).

In one casemate (brick built tunnel) in the Fort Brockhurst store, one set of windows was not blocked out and had no UV filter. This exposed some boxes to up to 200 mW/m^2 of UV radiation. To elucidate the situation, twelve of the samples were exposed to intense UV radiation from a UVL lamp (366 nm, 15268 mW/m^2) for seven days. All of the samples, polyethylene and polypropylene, were analyzed with differential scanning calorimetry (2.2.7). Samples of approximately 200 μg were removed through the thickness of the original scrapings. The degree of crystallinity was determined by measuring the enthalpy of the melting endotherm and comparing with published values for 100% crystalline polyethylene and polypropylene.

The most deteriorated boxes, as determined by FTIR and DSC, were selected for air exchange rate and water vapour transfer testing. Air exchange rates were measured with carbon dioxide tracer gas (3.4). To investigate the relative proportion of the air exchange (due to leakage at the seal versus due to permeation through the walls), the inside of the boxes were masked with aluminized film (Moistop 622) taped with aluminium tape (3M 425) so that almost all the walls were coated, leaving predominantly only the seal for gas exchange. Test were also undertaken with two boxes filled with iron stacked on top of a box. Such stacking of boxes is common in archaeological storage.

The newer (post 1995) Stewart polypropylene boxes used were tested in the same way. Additional information about the degree of crystallinity was extracted from the FTIR spectra using peak ratios (2.2.1.3).

8.2.3.3 Internal pollution generated by the boxes

In the present study, two modified accelerated corrosion tests were undertaken to test the effects on iron of emissions from old and new Stewart boxes. One test used iron sheet coupons and the other used mixed ferrous chloride and iron powder. Accelerated corrosion tests are not normally undertaken with iron sheet, as the control coupon produces significant corrosion, and any additional corrosion on the test coupon can be hard to determine. In this analysis, the amounts of corrosion on the control and exposed coupons were assessed by cathodic stripping in 1M sodium hydroxide solution using a Uniscan PG580 potentiostat (ASTM G1, 1999).

In the second test type, a model system of mixed ferrous chloride and iron powder was exposed inside Stewart boxes with silica gel conditioned to 40% RH. The model mixture was also exposed to an additional environment within these boxes: inside a glass jar with activated charcoal cloth over the jar opening to eliminate or reduce any corrosive gases. The efficacy of activated charcoal cloth was demonstrated during similar tests with iron sheet as described in the previous paragraph. The Stewart boxes were placed in an oven for 28 days at 60°C; the RH inside the Stewart boxes and inside the jars was measured continuously with Smartreader 2 dataloggers. After

the tests, the amount of akaganeite present was determined by FTIR spectroscopy (3.1.1.2). Each test was done in triplicate.

8.2.4 Box types commercially available

Stewart polyethylene containers were chosen following comparative trials (UKIC 1983; Watkinson and Neal 1987). Several containers are now available that promise better performance and incorporate compression seals and 'locking' systems. Those from major manufacturers that are likely to be available for an extended period of time and are available in a range of sizes were selected for trials. Boxes of similar sizes were used for comparison.

Manufacturer	Type	Dimensions (mm)			Cost GBP
		Length	Width	Height	
Lakeland	Store and Save	190	120	70	1.69
	Lock and Lock	260	180	90	2.99
Stewart	SealFresh	220	160	70	3.69
Tu		170	100	70	2.50

Table 8.2 Physical characteristics of box types tested

The ability of each box to retard RH change was tested. Dried silica gel (2 $\pm$ 0.01g) was placed inside each box along with a calibrated Meaco radio telemetry transmitter with Rotronic hygroclip II sensor. The initial RH was 5%. The boxes were carefully sealed and placed in a chamber at 70% RH. The RH was measured every 30 minutes though-out the experiment and the time to reach 16% determined.

Each box was tested with accelerated corrosion tests described in 8.2.3.3. Each of the aged boxes (60°C, 28 days) was retested as above for the time for the internal RH to reach 16%.

Air exchange rate measurements were not undertaken as the tight sealing of these boxes is likely to mean that a significant proportion of the air exchange occurs via

permeation through the plastic of the boxes. The tracer gas method is not suitable to determine air exchange through permeation. The permeation rates through plastics are strongly dependant on the gas and water vapour is unlikely to behave in a similar manner to carbon dioxide.

Measurements of the box materials were undertaken with ATR FTIR and DSC. Small samples were analysed with a Shimadzu DSC50 in L5116 aluminium crucible (0.1mm thick) from 20 to 500ºC at 10ºC per minute in air (50cm^3/min).

8.3 Results

8.3.1 Assessment of RH indicating cards

Figure 8.4 shows the RH readings from the indicator cards plotted against the readings from calibrated Humbug 2 data loggers.

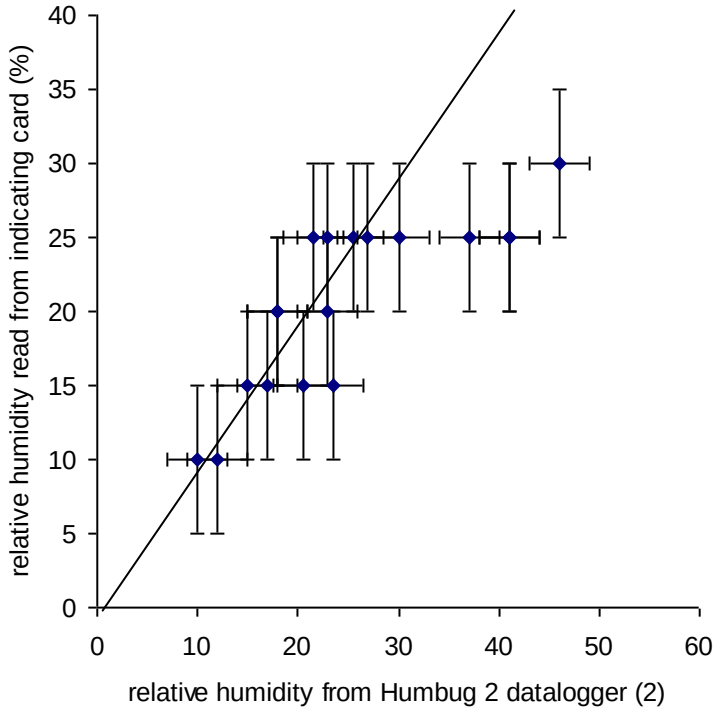

Figure 8.4 RH read from indicator card against that determined by placing a data-logger into the Stewart box.

The cards appear to be reading too low in some instances, even taking their low precision into account.

A number of cards placed at known dates were assessed similarly. The indicator cards were also determined by colorimetry to remove operator bias in the reading.

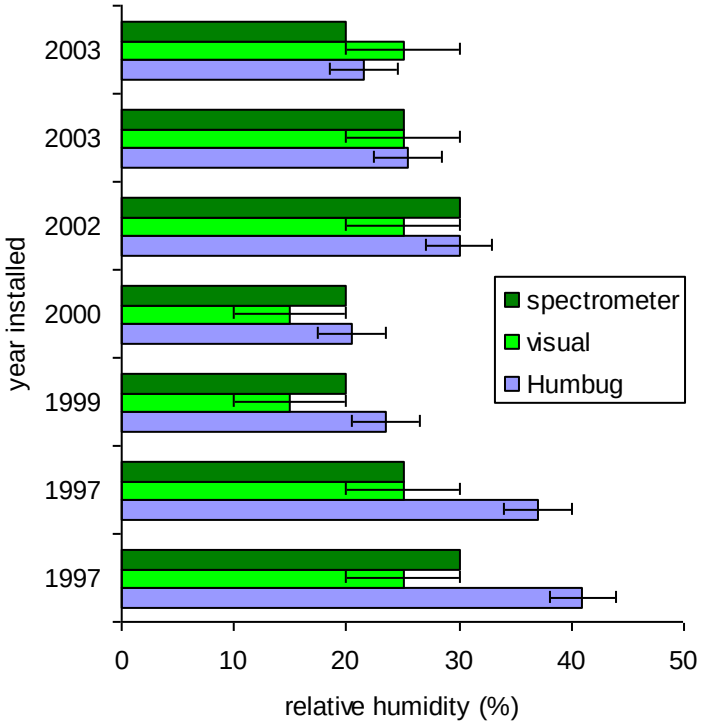

Figure 8.5 RH read from indicator cards with known installation dates against that determined by colorimetry and by placing a data-logger into the Stewart box.

The cards appear to read correctly, up to around seven years, after which time they read too low, which is obviously problematic. The loss of accuracy may be caused by slow sublimation of the salts added to modify the RH at which the cobalt chloride indicator changes colour.

8.3.2 Results of modelling internal RH

The measured and predicted number of days required to reach the 16% RH threshold from dried silica gel (5% RH) with 1g in a 0.235m^3 Stewart box in a space at 75% RH was calculated for two Stewart boxes with known air exchange rates are shown in Table 8.3.

Model	Air Exchange Rate (/day)	Time to 16% (days)	
		Predicted	Measured
Thomsen	0.35	7.29	7.31
	0.65	3.90	3.88
Weintraub	0.35	7.29	7.31
	0.65	3.92	3.88
Di Pietro	0.35	8.94	7.31
	0.65	4.53	3.88
Lehto	0.35	8.56	7.31
	0.65	4.47	3.88

Table 8.3 Predicted and measured break through times to 16% RH for 1g of silica gel in 0.235m3 boxes at 75%

As can be seen, the first two models predicted much shorter times before 16% RH was exceeded. Both of these models include leakage through the seal, whilst the latter two models only consider permeability through the polyethylene, see Appendix 3. The measured times are in better agreement with the first two models.

The results of two best performing equations Thomsen's and Weintraub and Tetrault's used iteratively for the real data from the four properties are shown in Table 8.4. The mean square difference between the modelled and actual RH data was calculated and the model with the lowest difference gives the best fit. Results for four of the thirty six boxes tested are shown in Table 8.4.

Location	Volume (m^3)	AER (day^{-1})	Silica gel loading (kg/m^{-3})	Model	MSD
Dover	0.0135	0.32	10	Thomsen	0.0105
				Weintraub	0.0072
Fort Brockhurst	0.0135	0.35	5	Thomsen	0.0102
				Weintraub	0.0132
Atcham	0.0042	0.41	2.96	Thomsen	0.0253
				Weintraub	0.0231
Corbridge	0.0042	0.43	5.92	Thomsen	0.0052
				Weintraub	0.0083

Table 8.4: Comparison of modelled data to monitoring in four boxes in four stores

The average results for the MSDs for each store and model are shown in Table 8.5.

Location	Number of boxes tested	Model	Average MSD
Dover	11	Thomsen	0.0098
		Weintraub	0.0075
Fort Brockhurst	6	Thomsen	0.0101
		Weintraub	0.0129
Atcham	10	Thomsen	0.0251
		Weintraub	0.0229
Corbridge	9	Thomsen	0.0059
		Weintraub	0.0087

Table 8.5 Overall results of modelling of RH inside Stewart boxes from RH values in archaeological four stores

The different buildings have very different properties leading to very stable temperatures in some of them and much more fluctuating temperatures in others. The

models appear to have differing efficacies in these two situations. In two instances (Fort Brockhurst and Corbridge) the Thomsen model performs better, whilst at Dover and Atcham the Weintraub model gives better results. Thomsen's approach assumes isothermal conditions and both Fort Brockhurst and Corbridge have very stable temperatures due to large thermal masses of the stores. Atcham experiences very dramatic daily temperature variations due to its lightweight construction. Dover also has a much larger daily range than either Fort Brockhurst or Corbridge. Whilst the temperature inside the Stewart boxes follows the room temperature, there is some lag and there will be differences for periods at Dover. It is likely there will be more difference at Atcham, due to a greater rate of temperature increase. The Weintraub model responds to water vapour equilibrium concentrations and appears to better model these situations.

The results from the modelling of the addition to dehumidifiers to stores at Dover and Fort Brockhurst are shown in Table 8.6

Site	Room	Number of days to reach 16% RH for Stewart Box type, dimensions, mass of silica gel		
		Old 8"x6"x4" 1kg	Old 12"x12"x4" 2kg	New 12"x12"x4" 2kg
Dover	F	807	1108	566
	F dehumidified	1106	1547	733
Fort Brockhurst	26	516	837	414
	26 dehumidified	1109	1509	749
	28	1159	851	300
	28 dehumidified	1494	1090	402
	31	2564	1031	400
	31 dehumidified	3669	1488	963

Table 8.6 Predicted times for dry silica gel to reach 16% RH in a variety of box types in store rooms and those same rooms if they were dehumidified to 50% RH.

Large benefits would be expected from adding dehumidifiers to the Dover metal store and rooms 26 and 31 at Fort Brockhurst. Room 28 at Fort Brockhurst showed little benefit as the RH values rarely exceed 50%.

8.3.3 Results of testing Stewart polyethylene and polypropylene boxes

8.3.3.1 Pollution ingress

The measured pollutant concentrations are shown in Figure 8.6.

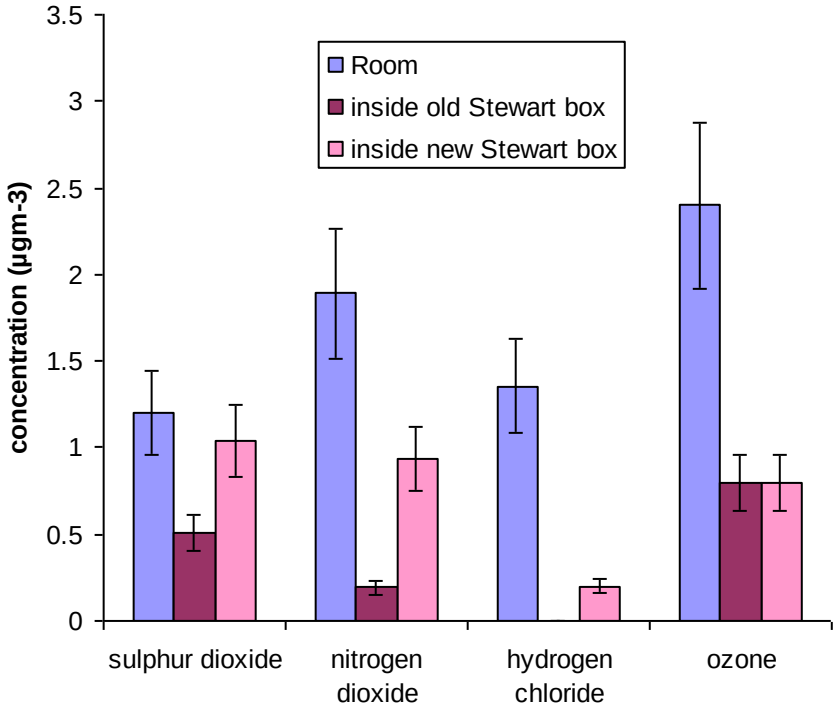

Figure 8.6 Pollutant gas concentrations measured inside old and new style Stewart boxes.

The pollutant concentrations in the room are low, below 3µgm^{-3}. The sulfur dioxide is relatively high due to the nearby ferry emissions. Hydrogen chloride is present as a reaction product between sea salt aerosol and sulfur dioxide or nitrogen dioxide (Robinset, 1956; Finlaysan, 1989). The old Stewart boxes are providing a good degree of protection against all pollutant gases. They have more effect against nitrogen dioxide and hydrogen chloride than against ozone and sulfur dioxide. The new Stewart boxes provide less protection. They seem to have no significant effect

against sulfur dioxide, some reduction in concentration of nitrogen dioxide, similar reductions to the old style Stewart boxes for ozone and less but good protection against hydrogen chloride.

8.3.3.2 Deterioration of the boxes

The degree of degradation as measured by the carbonyl index by FTIR-ATR and the degree of crystallinity measured with DSC for a series of boxes is shown in Table 8.7. The measured air exchange rates are also included.

Box	Location	ATR FTIR	DSC	Air Exchange Rate (/day)
		Ratio 1741/1471	Degree of crystallinity (%)	
Armour	Dover	0.081*	33	0.32
Nails	Dover	0.038	36	0.34
92,29	Dover	0.052	30	0.39
12,11	Dover	0.017	31	0.41
1003	Fort Brockhurst	0.048	41	0.33
Car2	Fort Brockhurst	0.176*	35	0.29
Car3	Fort Brockhurst	0.218*	37	0.33
996	Fort Brockhurst	0.021	35	0.35
14,5	Atcham (7)	0.053	40	0.41
18,1	Atcham (15)	0.071	43	0.37
29,5	Atcham (2)	0.081	45	0.40
	Stored 5°C since 1995	0.017	29	0.32
	" , Moistop	-	-	0.26
	" , weighted	-	-	0.27

Table 8.7 Carbonyl indices (by FTIR), degree of crystallinity (by DSC) and air exchange rates of polyethylene Stewart boxes

A wide range of values were analysed for both the carbonyl deterioration and degree of crystallinity. There is some correlation between the carbonyl indices and degrees of crystallinity for particular boxes. Both are measures of deterioration. However, the carbonyl indices measured with ATR FTIR are from the first micron or so of the

plastic surface, whilst the DSC is measuring the bulk property of the samples. No systematic relationship was observed between either the carbonyl index or degree of crystallinity and air exchange rate. Blocking permeation through the polyethylene, by adding Moistop, reduced the air exchange rate by approximately 19%, indicated that the majority of air exchange was occurring through the seal of the boxes.

The ATR-FTIR, DSC and air exchange rate results for the new style polypropylene boxes are shown in Table 9.7. The results of the tests with permeation through the polypropylene and with stacked boxes are also included in Table 8.8.

Box	Location	ATR FTIR		DSC	
		Ratio 1741/1471	Degree of crystallinity (%)	Degree of crystallinity (%)	Air Exchange Rate (/day)
St Aug	Dover	0.024	45	42	0.54
N Leigh	Fort Brockhurst	0.109	65	48	0.41
	Corbridge	0.010	49	43	0.44
New	Unused	0.010	40	39	0.60
New	Unused, Moistop	-	-	-	0.47
New	Unused, weighted	-	-	-	1.43

Table 8.8 Carbonyl indices (by FTIR), degree of crystallinity (by FTIR and DSC) and air exchange rates of polypropylene Stewart boxes

The degree of crystallinity values for two boxes were in reasonable accord, whereas for another two they were very different. This is likely to be due to the surface nature of the FTIR analyses and the bulk nature of the DSC.

Again there is no correlation between the carbonyl index or degree of crystallinity with the air exchange rate.

Only 20% of the measured air exchange rate appears to be due to permeation through the polypropylene. This explains why the air exchange rate does not increase as the polypropylene ages. Placing a full box on top of the polypropylene box dramatically affected the lid seal and the air exchange rate more than doubled.

8.3.3.3 Internal pollution generated by the boxes

Results of the two types of corrosion tests are shown in Table 8.9.

Test	Iron corrosion (mg cm^{-2})	Akaganeite formed from Fe/Fe(II)Cl (mg)
Control, no box material	0.95	6.0
Old style polyethylene	5.05	5.8
New style polypropylene	4.96	5.9

Table 8.9 Iron corrosion and akaganeite formation tests on Stewart brand boxes

Both the polyethylene and polypropylene box materials increased corrosion of iron above that formed on the control test. The tests with iron and iron (II) chloride powder mixtures showed no increase in akaganeite formation, compared to the control test for either box.

8.3.4 Box types now available

The number of days to reach 16% before and after ageing are tabulated in Table 8.10

manufacturer	materials determined by FTIR body, lid, seal	time to reach 16% (days)		Iron corrosion (mg/cm^2)	Akaganeite formed from Fe/Fe(II)Cl (mg)
		as received	after ageing		
Lakeland	PP, PP, Si	27.44	22.21	6.43	5.84
Lock and Lock	PP, PP, Si	31.73	31.78	4.98	5.87
Stewart	PP, PP	15.32	15.21	5.05	5.84
Tu	PP, PP, Si	12.13	10.32	7.83	5.82
control		-	-	0.95	5.87

PP polypropylene, Si silicone

Table 8.10 Results of materials testing and RH Box types tested

The Lakeland and Tu boxes appeared to become less well sealed after the 60ºC aging. This could be due to increased permeability or a less efficient seal. The Lock and Lock and Stewart boxes retained their properties.

All of the boxes caused some additional corrosion of iron, but no acceleration of the akaganeite formation reactions.

DSC analyses of the Tu and Lakeland boxes indicated that the box bodies were not pure polypropylene, but were mixtures with another polymer. The melting endotherm, at around 120°C, was not a single peak, but two overlapping peaks. The FTIR spectra of these materials did not show any additional peaks beyond those of polypropylene. This indicated the other polymer was present in a relatively low concentration, perhaps below 10%.

8.4 Discussion and Conclusion

A systematic error has been observed in one brand of humidity indicating card. This appears to begin after several years use and may be related to changes in the cobalt to chloride ratio of the indicator. This error is particularly troubling as it causes the card to 'read' a lower RH and could result in archaeological iron being exposed to higher RH values than thought.

Modelling the internal box RH from room data appears to produce results of sufficient accuracy to predict the lifetime of silica gel in Stewart boxes and to produce replacement schedules. The two equations tested appeared to produce similar results, with that derived by Thomsen, being less computationally complex.

Both types of Stewart boxes appear to give good protection against most pollutants. The new polypropylene boxes offer less protection against sulfur dioxide, but concentrations in the UK are now generally so low indoors to pose little risk. Dover is a notable exception due to the high volume of ferry traffic using less regulated marine oil.

A range of air exchange rates was measured for different sizes of Stewart boxes. The newer style boxes appear to be less air tight than the old boxes and are very susceptible to stacking increasing this further. For both types of boxes in present use, the majority of the air exchange takes place through the seal, with only a small amount due to permeation through the box materials.

Surface degradation caused by light and UV exposure (measured by ATR/FTIR) was observed, as were changes in the bulk crystallinity (DSC). The degradation appears to be limited to the surface of the boxes, with the interior samples showing no degradation. Neither of these effects appear to have increased the air exchange rate of the boxes. This is probably due to over 70% of the air exchange occurring through the seals for the Stewart boxes. Hence changes to degree of crystallinity and probably permeability have little effect.

Both polyethylene and polypropylene box materials accelerated the corrosion of iron at near 100% RH. Neither material accelerated the formation of akaganeite at 40% RH. Considering the low RH values inside the boxes they should not cause any

acceleration of the main deterioration reactions of archaeological iron, provided the silica gel is changed regularly.

The new locking type polypropylene boxes, especially the Lock and Lock brand, appear to hold low RH for longer, whilst posing no additional risk to archaeological iron and are suitable replacements for Stewart boxes.

Chapter 9 Conclusions

The intimate association between akaganeite and the physical deterioration of archaeological iron objects has been confirmed. Akaganeite was present as crystals in the centre of pits, causing delamination or in powdering areas in most of the objects examined. It was the main cause of damage in over 78% of the 284 deteriorating objects examined and analysed , Chapter 4. Goethite was present in a further 8.5% of instances, all powdering. Overall approximately 62% of the iron objects surveyed had no obvious signs of deterioration over a five year period. Of the remainder, approximately 27% only showed signs of slight deterioration, with less than 2% of their surface area showing any signs of change.

Iron(II) chloride has been observed at the base of pits on freshly excavated iron objects. This was observed to transform into akaganeite via iron (III) chloride. This confirms the mechanism suggested by Turgoose (1982a) for the deterioration of archaeological iron, at least in some instances. Iron and iron(II) powder mixtures therefore appear to be suitable starting points to model akaganeite formation reactions occurring in archaeological iron objects on excavation.

Goethite, magnetite, copper species and organic compounds, probably including humic acid have been found in close association with akaganeite and could potentially modify its formation in archaeological iron objects.

At low RH values, conversion of iron and iron (II) chloride present in or at the surface of the object is the major deterioration mechanism. As a first approximation the risk posed to the archaeological information in the objects can be assumed to be proportional to the amount of akaganeite formed. Whether material will be lost will of course depend on the exact morphology of the object and location of the iron(II) chloride. For pitted objects, is there enough iron (II) chloride present at the base of the pit to form sufficient akaganeite to break and lever the layer of corrosion products at the top of the pit? For delamination, is there enough iron (II) chloride present to form sufficient akaganeite to lever apart the iron corrosion product layers? At higher RH values iron is also lost from any remaining metal core, potentially destroying metallurgical information.

A series of thresholds, where the reaction rate increases, have been determined from experiments with powders replicating the chemistry observed in archaeological iron.

If akaganeite has formed in the sample at RH values above 70%, no reaction occurs below 11%.If the object was kept below 70% after excavation or was washed and then kept below 70%, no reaction occurs below 16%. Between 30 and 35% the akaganeite formation reactions accelerate. Between 50 and 60%, depending on the temperature, iron loss becomes significant. This appears to be associated with the deliquescence of iron (II) chloride. The iron loss accelerates at approximately 10% below the deliquescent point. This is possibly due to the iron(II) chloride crystals having enough water in their structure to act as a solid state electrolyte.

The presence of ethanoic acid can accelerate the formation reactions for akaganeite by a factor of three, depending on the RH. Goethite is formed, as well as akaganeite, at higher ethanoic acid concentrations ($1500 \mu g m^{-3}$ and higher) and RH values.

No Goethite was formed with methanoic acid or methanal. Methanoic acid was found to be more aggressive (but generally present in lower concentrations e.g in practice). Methanal was found to accelerate the deterioration reaction the most at high relative humidity values, 75%.

Nitrogen dioxide and sulfur dioxide do not have a great accelerating effect on the akaganeite formation reactions. They have much less of an effect, when considering likely dose exposures than the volatile carbonyl compounds. The effects of nitrogen dioxide and sulfur dioxide on the corrosion of iron are well researched (Oesch, 1996). The concentrations likely to be present in most showcases and storage boxes mean their effect is likely to be very low.

Both synthetic akaganeite and akaganeite samples from objects have been observed to transform into Goethite slowly in laboratory experiments. The transformation increased with increasing RH values. Thin surface Goethite layers have been observed on the surface of akaganeite on archaeological iron objects from three sites. The amount of Goethite was found to correlate with the RH the iron had been exposed to over the past fifteen years. Higher ethanoic acid atmospheres appeared to have thicker Goethite layers on the akaganeite surface. This appears to be evidence for akaganeite transforming into Goethite. This transformation releases chloride ions

from the akaganeite back into the object. The akaganeite chloride concentrations were between 8 and 12%, the Goethite had less than 0.5% chloride present. This is the first evidence of this transformation occurring on archaeological iron objects. A relative risk assessment for this process could be constructed, comparing the rate of chloride release with chloride deposition rate from the atmosphere. There is a shortage of reported data for chloride deposition rates indoors and these have been measured in several showcases and storage boxes, Chapters 7 and 8.

Synthetic akaganeite has been observed to transform into hematite releasing chloride at slightly elevated temperatures (60°C and above, Chapter 6). This was detected with mass loss and FTIR. Chloride release was detected at higher temperatures. Calculations using simple Arrhenius type assumptions indicate a very slow, but non negligible transformation rate at room temperatures. This contradicts the work published by Stahl et al (2003), who predicted no release of chloride from akaganeite below 200°C. Analysis of red spots formed on akaganeite samples removed from objects over the past 38 years indicates that they are hematite. No red spots were observed on samples removed in the previous eight years before analysis. The incidence of hematite increased with increasing time since sampling, rising to 100% after 32 years. This appears to suggest that some of the akaganeite in the samples had transformed to hematite. The samples were initially analysed with XRD, which would be insensitive to small concentrations of hematite, but contemporaneous notes make no mention of red spots on the samples, all of which were examined under magnification. Whilst not uncontroversial, this is strong evidence that akaganeite did transform into hematite on these samples.

For display of archaeological iron objects a RH limit of 30% seems a reasonable compromise between the risk of damage and the cost of providing the low RH environment. The carbon dioxide tracer gas method has been assessed for showcase testing and the methodology developed and errors determined. The factors in showcase design critical to maintaining a low RH and low carbonyl compound environment have been elucidated. A showcase specification of $0.4 day^{-1}$ air exchange rate was derived. Models for showcase RH derived from room RH data have been validated and used to design showcases. The ingress of dust, and particularly chloride-containing dust, has been measured. Standard showcase designs for archaeological iron objects have been developed and tested in very

aggressive historic building environments. Showcases with air exchange rates below $0.4day^{-1}$ have been reliably produced. The size of holes in the metal baseboard, between the silica gel and display volumes have been found to be critical in showcase performance. Actively desiccated showcases have also been investigated using drying wheel dehumidifiers. The carbon footprint of both methods has been compared for English Heritages Estate, with over 40% savings in all areas.

For storage of archaeological iron objects, a RH limit of 16% is reasonably practicable. For material left at over 70% after excavation a RH of 11% would be required to totally halt deterioration. However, this is likely to be a small portion of the archaeological archive and deterioration rates at 16% for this material would still be very low. Maintaining 11% RH would mean frequent silica gel changes in many environments. The present main system in use, silica gel in polyethylene/polypropylene (Stewart) boxes with cobalt chloride indicators has been assessed. The cobalt chloride indicators are a weak point with insufficient precision and some evidence of drift in readings after several years. A system of modelling the RH inside the box from room RH data has been used to construct silica gel changing schedules to remove the reliance on manual checking of the cobalt chloride indicators. Although evidence of deterioration of the polyethylene and polypropylene boxes was found, this has not reduced their performance in holding low RH values. Tests have shown accelerated iron corrosion in the boxes at near 100% RH and accelerated akaganeite formation at 50% RH. This emphasizes the importance of regularly maintaining the silica gel. A series of alternative boxes has been tested. Several proved to be more air tight and maintain low RH values longer than the boxes presently in use.

Chapter 10 Areas for Further Study

Differences in behavior in akaganeites formed at different RH values have been observed in experiments in Chapters 5 and 6. No differences could be detected in XRD, Raman and FTIR spectra of these akaganeites. The differences should be studied further as a reliable analytical discriminator would allow setting a RH threshold of 11 or 16%. Additionally synthetic akaganeite is routinely used to test investigate several aspects of preventive and interventive conservation. Significant differences in properties were found for akaganeites synthesized by different methods and even repeats of the same method. The thermograviemtric data published by Stahl et al (2003) differs from those published by several other authors (Post et al., 2003; Garcia et al., 2008; Paterson et al., 1982; Chitrakar et al., 2009; Goni-Elizalde et al., 1988; Music et al., 2004; MacKenzie, 1970). There is a difference in reduction in critical RH cased by akaganeites formed at different RH values. These differences require elucidation before synthetic akaganeite can be reliably used to understand the behavior of akaganeite on archaeological artefacts. Thermal analysis is a promising method and appears to be sensitive to differences. The large sample size has limited its use on akaganeite from objects, but micro and nano thermoanalytical methods are now available which can work with much smaller sample sizes.

Basic modelling of akaganeite transformations has been undertaken in this thesis (based on the Arrhenius equation, Chapter 6). More advanced modeling could yield useful results to further assess the relative importance of these processes in the preservation of archaeological iron collections. Recent developments in flash DSC and micro thermal analysis could allow much smaller sample sizes (10µg) and allow analysis of different types of akaganeite formed. At present it is difficult to be certain which of the thirty or so methods of synthesizing akaganeite best represents that formed on archaeological iron objects. Or indeed if there are differences between the akaganeites formed on different objects.

The effects of the volatile carbonyl compounds present in many display and storage environments on the transformation of akaganeite should be studied. There is some

circumstantial evidence for an effect from the object analyses and characterization of the environments in which they have been. Determination of the levels at different ethanoic and methanoic acid and methanol concentrations and RH values would allow an informed risk assessment. Difficulties were encountered in measuring the amount of Goethite present in the presence of akaganeite. Quantification from the FTIR peak ratios could provide a rapid method for this. The exotherm (crystallization) exhibited by akaganeite and not Goethite in DSC could also be used to quantify the akaganeite in a bulk sample (1-5mg). The combined amount of akaganeite and Goethite could be measured with TGA (the two decompositions are too close to resolve with TGA but advanced TGA using controlled rate could be attempted.

The effect of ozone on the formation reactions of akaganeite has not been studied. The effect of nitrogen dioxide, which is generally present in museum exhibition and store areas at approximately thirty times the ozone concentration, has been studied. The likely nitrogen dioxide doses had a small acceleration effect on the formation of akaganeite. The effects of the carbonyl compounds were approximately 5 times greater at a dose equivalent to three months exposure, whilst the equivalent dose for nitrogen dioxide was 27 years.

Further work on hydrogen chloride concentrations and chloride deposition rates from dust would extend the corpus of measurements undertaken in this thesis. Direct damage caused to objects from dust deposition is an under-researched area for conservation science. Very few HCl measurements have been published, although damage from enhanced concentrations from incinerators has been cited in the literature.

Testing for object instability or reactivity with oxygen depletion has great potential of archaeological iron and probably copper alloy objects. Only a portion of objects appear susceptible to the reactions described in this thesis. This is probably due to the amount of chloride present in the object on excavation and its distributions (Rimmer 2010). Objects with high chloride content have been observed to deteriorate. Provision of dry environments, (and interventive conservation treatments) are expensive in staff resources, electricity and carbon footprint. Only providing dry environments for those objects at risk of deterioration would lead to

considerable resource savings. Most archaeological displays contain mixed media. The RH levels recommended for archaeological iron pose some risk to many rigid organic materials. Additionally using silica gel (or zeolites or clays) inevitably exposes the objects to RH levels somewhat below 30% when the dried gel is added. Identifying those archaeological iron objects at risk will allow a better informed assessment and balancing of the relative risks when arranging exhibitions.

References

Adams S. and Ford D. 1999 Deposition rates of particulate matter in the internal environment of two London museums, *Atmospheric Environment* 33, 4901-4907.

Ahlneck C. and Alderborn G., 1989. Moisture adsorption and tabletting. I. Effect on volume reduction properties and tablet strength for some crystalline materials. *International Journal of Pharmaceutics* 54, 131–141.

Ahmed I.A.M., Benning L.G., Kakonyi G., Sumoondur A.D., Terrill N.J. and Shaw S., 2010. Formation of green rust sulphate. *Langmuir*, 26(9), 6593-6603.

Al-Zahrani A.A., 1999. *Chloride ion removal from archaeological iron and β-FeOOH*, PhD Thesis Cardiff University.

American Society for Testing Materials, 2001. *ASTM E741-00: 2001 Standard Test Method for Determining Air Change in a Single Zone by Means of a Tracer Gas Dilution*. Conchohoken, PA, USA: ASTM.

American Society for Testing Materials, 1999. *ASTM G1-90: 1999 Standard practice for preparing, cleaning and evaluating corrosion test specimens*. Conshohocken, PA, USA: ASTM.

Amaroli T., Becue T. and Gautier S., 2004. Diffuse reflection infrared spectroscopy (DRIFTS): Application to the *in situ* analysis of catalysts. *Oil and Gas Science and Technology –Rev. IFP*, 59(2), 215-238.

Ankersmit, B. 2005, personal communication.

Archaeological Archives Forum, 2007. *Transfer and Curation,* [online] London. Available at < http://www.archaeologists.net/modules/icontent/index.php> [Accessed on 23 July 2011].

Arni P.G., Cochrane G. C. and Gray J. D, 1965. The emission of corrosive vapours by wood, II. The analysis of the vapours emitted by certain freshly felled hardwoods and softwoods by gas chromatography and spectrophotometry, *Journal of Applied Chemistry*, 15**,** 463–468.

Arroyave C. and Morcillo M., 1995. The effect of nitrogen oxides in atmospheric corrosion of metals. *Corrosion Science*, 37(2), 293-305.

Askey A., Lyon S.B.,. Thompson J.B., Wood J.C., Cooke M. and Sage P., 1993. The corrosion of iron and zinc by atmospheric hydrogen chloride. *Corrosion Science*, 43, 233-247.

Atkins P.W., 2000. *Physical Chemistry*, Oxford: Oxford University Press, 766-784.

Bak J. and Kindl B., 1997. Quantitive analysis of mineral powders by DRIFTS, *Applied Spectroscopy* 51(11), 1730-1737.

Bak J., 2002. Measurements of impurities in strongly absorbing powdery materials by DRIFTS, *Internet Journal of Vibrational Spectroscopy* 2(4), 1-7.

Bamberger, J. A., Howe E.G. and Wheeler G. 1999 A variant Oddy test procedure for evaluating materials used in storage and display cases. *Studies in Conservation* 44, 86-90.

Baranski, A., Dutka D., Dziembaj R., Konieczna-Molenda A. and Lagan J. M., 2004, Effect of relative humidity of the degradation rate of cellulose: *Restaurator,* 25, 68-74.

Beattie, I.R. and Gilson, T.R., 1970. The single crystal Raman spectra of nearly opaque materials. Iron (II) oxide and chromium (III) oxide. *Journal of the Chemical Society*, A, 92, 980.

Bellot-Gurlet L., Neff D., Reguer S., Monnier J., Saheb M. and Dillman P., 2009. Raman studies of corrosion layers formed on archaeological irons in various media, *Journal of Nano Research,* 8, 147-156.

Berthalon R., 2000. *La Limite de la Surface d'origine des Object Metalliques Archaeologiques*, Ph.D. Universite Paris 1 – Pantheon-Sorbonne.

Blades, N., Kruppa D. and Cassar M., 2002. Development of a web based software tool for predicting the occurrence and the effects of air pollution inside museum buildings. *13th Triennial Meeting of ICOM-CC*, Rio de Janeiro, 22-27 September 2002, London, James and James, 9-14.

Bland, P. A., Kelley S. P., Berry F. J., Cadogan J. M. and Pillinger C. T., 1997. Artificial weathering of the ordinary chondrite Allegan: Implications for the presence of Cl- as a structural component in akaganeite. *American Mineralogist*, 82(11-12), 1187-1197.

Blunt T.J., Kotvis P.V. and Tysoe W.T., 1989. Surface chemistry of chlorinated hydrocarbon lubricant additives. *Tribology Transactions*, 41(1), 129-139.

Bohm, G.G.A., 2003. Diffusion theory of the post-irradiated oxidation of polyethylene. *Polymer Physics*, 5(4), 639-652.

Bommel M, Gibson LT, Watts S, Kontozova V and Halsberghe L , 1997. *A Comparison of Diffusion Tube Determinations of Formic and Acetic Acid Concentrations in Air.* The 6th Indoor Air Quality Meeting, Padova, 10-12 November 2004, Available at < http://www.isac.cnr.it/iaq2004/pdfabstract/vanbommel_abstract.pdf > [Accessed 12 August 2011].

Boucherit N., Hugot-Le-Goff, A. and Joiret, S., 1991. Raman studies of corrosion films grown on Fe and Fe6Mo in pitting conditions. Corrosion Science, 32, 497-507.

Bozorth R.M., 1951. *Ferromagnetism*. New York , van Nostrand, 242.

Brimblecombe, P. and Rarner R. 1983 Museum display cases and the exchange of water vapour. *Studies in Conservation* 28, 179-188.

British Musuem. 1996, British Museum Materials Testing Service test numbers 3372-3379 and 3423-3425.

Brokerhof, A.W. and van Bommel M., 1996. Deterioration of Calcareous Materials by Acetic Acid Vapour: A Model Study. In *Preprints of 11th Triennial Meeting of ICOM Committee for Conservation* , Edinburgh, 1-6 September 1996, London, James and James, 769-775.

Brown D., 2007. *Archaeological Archives: A Guide to best practice in Creation, Compilation, Transfer and Curation*. London Institute of Field Archaeologists.

Buchwald V.F. and Clarke R., 1989. Corrosion of Fe-Ni alloys by Cl-containing akaganeite. *American Mineralogist*, 74, 656-667.

Burke, E. A. J., 2008. Tidying up Mineral Names: An IMA scheme for Suffixes, Hyphens and Diacritical Marks. *Mineralogical Record*, 39, 131-135.

Cambier, P., 1986. Infrared study of Goethites of varying crystallinity and particle sizes: I interpretation of OH and lattice vibration frequencies. *Clay Minerals*, 21, 191-200.

Camuffo D., 2010, The role of temperature and humidity. In: *Basic Environmental Mechanisms* Florence, Nardini Editore.

Calver A., Holbrook A., Thickett D. and Weintraub S., 2005. Simple methods to measure air exchange rates and detect leaks in display and storage

enclosures. In PrePrints of ICOM-CC 14th Triennial Meeting, The Hague, 12-16 September 2005, London James and James, 597-609.

Carlson L. and Schwertmann U. , 1981. Natural ferrihydrites in surface deposits from Finland and their association with silica. *Geochimica Cosmochimica Acta*, 45, 421-429.

Carver M.O.H., 1989. Anglo-Saxon Discoveries at Sutton Hoo, 1987-1988. *Old English Newsletter,* 22(2).

Cass, G. R., Drusik J. R., Grosjean D., Nazaroff W.W>, Whitmore P.M. and Wittman C.L., 1989 *Protection of works from atmospheric ozone*. Research in Conservation 5. [online] Los Angeles (Published 1989) Available at: <http://www.getty.edu/conservation/publications/pdf_publications/ ozone.pdf > [Accessed 23 July 2011].

Cermakova D. and Vlchova Y., 1966. Metallic corrosion in an atmosphere polluted with formaldehyde. *Proceedings of the 3rd International Congress on Metallic Corrosion*. Moscow, 497-508.

Chambaere D. and de Grave E., 1984. A study of the non-stoichiometric halogen and water content of β-FeOOH. *Physical Statistical Solids A*, 83, .93-102.

Childs C.W., Goodman B.A., Paterson E. and Woodhams F.W.D., 1980. The nature of iron in akaganeite. *Australian Journal of Chemistry*, 33, 15-26.

Chitraker R., Tezuka S., Sonoda A., Sakane K., Ooi K,. and Hirotsu T., 2009. Phosphate adsorption on synthetic goethite and akaganeite. *Journal of Colloid and Interface Science*, 298(2), 602-608.

Chitty W-J., Dillmann P., L'Hostis V. and Lombard C., 2005. Long-term corrosion resistance of metallic reinforcements in concrete – a study of corrosion mechanisms based on archaeological artefacts. *Corrosion Science*, 47, 1555-1581.

Clogg P. and Caple C., 1996. Conservation image enhancement at Durham University. In A. Higgins, P. Main and J. Lang, eds. *Imaging the Past – Electronic Imaging and Computer Graphics in Museums and Archaeology*, British Museum Occasional Paper 114, 13-22.

Coblenz W.W., 1905. *Investigations of Infra-red Specroscopy*. Washington DC, Carnegie Institution of Washington.

Commission Internationale de 'Eclairage,. 2004. CIE Technical Report Colorimetry 3rd edition. Vienna, CIE Central Bureau.

Cornell R.M. and Giovaoli R., 1990. Transformation of akaganeite into Goethite and hematite in alkaline media.*Clays and Clay Minerals*, 38, 469-476

Cornell R.M. and Schwertmann U., 1986. *The Iron Oxides*, Weinheim, VCH BverlagsgesellschaftmbH, 490.

Cornell R.M. and Schwertmann U., 2003, *The Iron Oxides Structure, Properties, Reactions, Occurences and Uses*, Weinheim, Wiley-VCH.

Corvo F., Betancourt N. and Mendoza A., 1995. The influence of airborne salinity on the atmospheric corrosion of steel. *Corrosion Science*, 37, 1889-1901.

Costain, C., 1984. *Cross sectional examination of nails: an evaluation following hot-wash or ethylenediamine treatment*. Analytical Research Services Report No. 2315. Ottawa, Canadian Conservation Institute.

Daniel, V. and Maekawa, S, 1992. The moisture buffering capability of museum case in Materials Research Society Symposium Proceedings, 27 April-1May 1992, San Francisco, Pittsburgh, Materials Research Society, 453-458.

Daniels, V. and Wilthew S., 1982. An investigation into the use of cobalt salt impregnated papers for the measurement of relative humidity. *Studies in Conservation*, 28, 80-84.

DeGrigny C., Durivault L., Chevalier B. and Darriet B., 1999. *Réalisation et caractérisation d'éprouvettes base fer simulant l'altération des objets archéologiques. PCR 'Fer chlorures'*, Institut de Chimie de la Matière Condensée de Bordeaux, Arc'Antique Laboratoire de Restauration et de Recherche sur les objets d'art de Nantes, Septembre 1999.

de Faria D.L.A., Venancio Silva S. and de Oliveira M.T., 1997. Raman microspectroscopy of some iron oxides and oxyhydroxides, *Journal of Raman Spectroscopy*, 28, 873–878.

Derrick M., Stulik D. and Landry J.M., 1999. *Infrared Spectroscopy in Conservation Science*, Los Angeles, Getty Conservation Institute.

deSantis, F., Allegrini I., Fazio, M.C. and Pasella D., 1996. Characterisation of indoor air quality in the Church of San Luigi dei Francesci, Rome, Italy. *International Journal of Environmental Analytical Chemistry*, 64, 71-81.

Deutsch FD., Godoi R.G., Spolnik Z.S., Wei WW, Kontozova-Deutsch, V. and Van Grieken R., 2008 Application of EPMA and XRF for the investigation of particulate pollutants in the field of cultural heritage. *Microchimica Acta*, 161 (3-4), 465-469.

DiPietro, G. and Ligterink F., 1999. Prediction of the relative humidity response of backboard-protected canvas paintings. *Studies in Conservation*, 44, 269-277.

Dinesen A.R., Pedersen C.T. and Bender Koch C., 2001. The thermal conversion of lepidocrite revisited. *Journal of Thermal Analysis and Calorimetry*, 62, 1303-1310.

Donovan P.D. and Stringer J., 1972. The corrosion of metals by organic acid vapours. In *Proceedings of the 4th International Congress on Metallic Corrosion*. Houston, National Association of Corrosion Engineers, 537-543.

Doren J.E. and Hodson F.R., 1975. *Mathematics and Computers in Archaeology*, Harvard, Harvard University Press.

Drude P., 1902. The Theory of Optics, London, Longmans Green, 299-301

Dungworth D. 2005 Discussion on chloride sensitivity of SEM-EDX with Joel 840 and Isis detection system [discussion], personal communication, 5 June 2010.

Dunnwald, J., and Otto, A., 1989. An investigation of phase transitions in rust layers using Raman spectroscopy. *Corrosion Science*, 29, 1167-1176.

Ebringer-Rist N., Peek C., Stelzner J. and Gauβ F., 2011. Computer tomography: a powerful tool for non-destructive mass documentation of archaeological metals. In Mardikian P., Chemello C., Watters C. and Hull P. Eds. *Postprints of Metals 2010,* 11-15 October 2010, Charleston South Carolina, Clemson University, 458-463.

English Heritage, 2010. Heritage Counts 2010 England, English Heritage [online] available at < http://hc.english-heritage.org.uk/HC-Economic-Impact > [Accessed 12 August 2011].

Ellis J., Giovani R. and Stumm W., 1976. Anion exchange properties of β-FeOOH. *Chimia*, 30, 194-197.

Eremin, K. and Wilthew P., 1996. The effectiveness of barrier materials in reducing emissions of organic gases from fibreboard: results of preliminary tests. *In Preprints of 11th Triennial Meeting of ICOM Committee for Conservation*, Edinburgh, 1-6 September 1996, London, James and James, 27-35.

European Commission, 1997. *European Collaborative Action Indoor Air Quality and Its Impact on Man. Evaluation of VOC Emissions from Building Products*, Report No. 18, Luxembourg, European Commission.

Evans U.R., 1981. *An Introduction to Metallic Corrosion*, London, Edward Arnold Ltd.

Farrer T.W., Biek L. and Wormwell F., 1953. The role of tannates and phosphates in the preservation of ancient buried iron objects. *Journal of Applied Chemistry*, 3, 80.

Fell, V. and Ward M., 1998. Iron sulphides corrosion products on artifacts from waterlogged deposits. In *Metal 98 Proceedings of the International Conference on Metals Conservation* Draguignan-Figanieres, France 27-29 May 1998, London, James and James, 111-115.

Fowler P.J., 1992. *The Past in Contemporary Society*, London, Routledge.

Freestone I., 2010. Discussion on chloride sensitivity of SEM-EDX with Joel 840 and Isis detection system [discussion] personal communication 18 August 2010.

Fry C, Xavier-Rowe A., Stanley B. and Halahan F., 2007. What's causing the damage! The use of a combined, solution-based risk assessment and condition audit in *Museum Microclimates*, Hvidovre Bogtryk, 107-114.

Gaines R.V., Skinner C., Foord E.E., Mason, B. and Rosenzweig A., 1997, *Dana's New Mineralogy*, New York, John Wiley and Sons, Inc..

Gallagher P.K. and Warne S.S.J., 1981. Thermo-magnetometry and thermal decomposition of siderite. *Thermochimica. Acta*, 43, 253-267.

Garcia K.E., Barrere C.A., Morales A.L. and Greneche J.M., 2008. Characterization of agakaneite synthesized in presence of Al^{3+}, Cr^{3+} and Cu^{2+} ions and urea. *Materials Chemistry and Physics*, 122, 120-126.

Gardiner C.P. and Melchers R.E., 2002. Corrosion of mild steel by coal and iron ore. *Corrosion Science*, 44, 2459-2478.

Garrels R.M. and ChristC.L., 1965. *Solutions, Minerals and Equilibria*, London, Harper and Row.

Gerwin W., 1999. Die Korrosion archaologischer eisenfunde im boden, *Arbeitsblatter fur Restaurattoren*, 32, 173-182.

Gettens R.J., 1961. Mineral alteration products of ancient metal objects. in *Recent advances in Conservation* IIC Conference Rome, Rome, 6-10 July 1987, London, Butterworths, 89-92.

Gibson LT, Cooksey BG, Littlejohn D and Tennent NH., 1997a, Determination of experimental diffusion coefficients of acetic acid and formic Acid vapours in air using a passive sampler. *Analytica Chimica Acta*, 341, 01-10.

Gibson L.T., Cooksey B.G., Littlejohn D. and Tennent N.H., 1997b. Determination of acetic acid and formic acid in the museum environment by passive sampling *Analytica Chimica Acta,* 341, 11-19.

Gibson L., 2005. Discussion on materials for diffusion tubes [discussion] personal communication. 10 July 2005.

Gibson, L.T. and Watt C.M., 2010 Acetic and formic acids emitted from wood samples and their effect on selected materials in museum environments. *Corrosion Science*, 52(1), 173-178.

Gilberg, M.R., Seeley N.J., 1981. The identity of compounds containing chloride ions in marine iron corrosion products: a critical review. *Studies in Conservation*, 26, 50-56.

Glasius, M., Carlsen, M.F., Hansen, T.S., Lohse, C., 1999. Measurements of nitrogen dioxide on Funen using diffusion tubes. *Atmospheric Environment*, 33, 1177.

Goni-Elizalde S. and Garcia-Clavel M.E., 1988. Thermal behavior in air of iron oxyhydroxides obtained from the method of homogeneous precipitation. *Thermo Chimica Acta*, 129, 325-334.

Gonzalez-Calbet J.M.and Alario Franco M.A., 1982. A thermogravimetric and electron microscopy study of the decomposition of akaganeite. *Thermo Chimica. Acta*, 58, 45-51.

Grace, 2012. Silica gel, [online] available at <http://www.grace.com/EngineeredMaterials/MaterialSciences/SilicaGel/Default.aspx > [accessed on 13 March 2012]

Green L.R. and Thickett D., 1992. *Re-evaluation of the Oddy test for assessment of materials for storage and display in the British Museum*, Conservation research report, no. 1992/4, London, The British Museum.

Green, L. R. and Thickett D., 1995. Testing materials for use in the storage and display of antiquities, a revised methodology. *Studies in Conservation.* 40, 145-152.

Greenwood, N.n. and Earnshaw, A., 1997. *Chemistry of the Elements*, Butterworth-Heinemann, Oxford.

Grossman, A. K., 2006. Keeping it together: conservation, context and cultural materials. In *The Object in Context: Crossing Conservation Boundaries* -

Contributions to the Munich Congress 28 August - 1 September 2006. ed. D. Saunders, J. H. Townsend and S. Woodcock. London, IIC, 1-6.

Grzywacz C. and Tennent N. H., 1994. Pollution monitoring in storage and display cabinets: carbonyl pollutant levels in relation to artifact deterioration, in Roy A. and Smith P. (eds) *Preventive conservation: practice, theory and research. Preprints of the contributions to the Ottawa Congress*, 12-16 September 1994, London, International Institute for Conservation of Historic and Artistic Works,164-170.

Grzywacz C. M. and Stulik, D.C., 1993. Carbonyl pollutants in the museum environment, *SSCR Journal***,** 4, 16-19.

Gysels K., Delalieux F., Deutsch F., van Grieken R. and Camuffo D., 2004. Indoor environment and conservation in the Royal Museum of Fine Arts, Antwerp, Belgium. *Journal of Cultural Heritage,* 5(2), 221-230.

Hanesch M., 2009. Raman spectroscopy of iron oxides and (oxy) hydroxides at low laser power and possible applications in environmental magnetic studies. *International Journal of Geophysics*, 177, 941-948.

Harder S., 2010. *Iron storage: where are we now?* Durham University MA Museum and Artefact Studies Thesis.

Harrick N.J. and du Pre F.K., 1966. Effective thickness of bulk materials and of thin films for internal reflection spectroscopy. *Applied Optics,* 5, 1739-1743.

Hatchfield, P. B. and Carpenter J.M., 1987. *Formaldehyde: How great is the danger to museum collections?* Cambridge, Mass, Center for Conservation and Technical Studies, Harvard University Art Museums.

Heller W., Kratky O. and Nowotny H., 1936. La constitution des sol d'oxyde de fer. *Comptes Rendus Hebdomadaires des Seances de l@Academie des Sciences,* 200, 1171-1173.

Hill J.D., 2001. A new cart/chariot burial from Wetwang, East Yorkshire, *Past*, 38, 2-3.

Hill J.D., 2002. Wetwang chariot burial. *Current Archaeology,*15 (178), 410-412.

Hofer L.J.E., Peebles W.C. and Dieter W.E., 1946. X-ray diffraction and magnetic studies on unreduced ferric oxide Fischer-Tropsch catalysts. *Journal of the American Chemical Society*, 68(10), 1953-1956.

Howell, D., Brimblecombe P., Lithgow, K., Lloyd H. and Knight B.. 2002. Monitoring dust in historic houses. *Conservation Science 2002*, Edinburgh, 22-24 May 2002, London, Archetype, 8-10.

Hu H., Chen Q., Yin, Z. and Zhang P., 2003. Thermal behaviours of mechanically activated pyrites by thermogravimetry. *Thermo Chimica. Acta*, 398, 233-240.

Huang H., Sumitana K., Oike T., Suzuki K., Watanabe F., Hasanati M and Kobayashi N., 2007. Effect of microwave irradiation on water vapour desorption capacity of zeolite, *Proceedings of International Symposium on EcoTopia Science*, s.l., s.n. 370-373.

Hunt C. P. and Moskowitz, B.P., 1995. Magnetic properties of rocks and minerals, in Ahrens, T. J., *Rock Physics and Phase Relations: A Handbook of Physical Constants*, Washington, DC, American Geophysical Union, 189–204.

International Standards Organisation, 2000. *ISO12569:2000 Thermal performance of building determination of air change in buildings – tracer gas dilution method of a tracer gas dilution.* Geneva: ISO.

Ishikawa T. and Inouye K., 1975. Role of chloride in β-FeOOH on its thermal change and reactivity to sulfur dioxide. *Bulletin of the Chemical Society of Japan,* 48, 1580-1584.

Ishikawa T. and Inouye K., 1972. The structural transformation of ferric oxyhydroxides and their activity to sulfur dioxide. *Bulletin of the Chemical Society of Japan*, 45, 2350-2354.

Ishikawa T. and Inouye K., 1973a. Variations of heat of immersion of ferric oxyhydroxides in water with structural changes by heating. *Bulletin of the Chemical Society of Japan* 46, 2665-2668.

Ishikawa T., Kondo Y., Yasukawa A, and Kandori K. 1998 Formation of magnetite in the presence of ferric oxyhydroxides. *Corrosion Science*, 40, 1239-1251.

Ishikawa, T., M. Kumagai, A. Yasukawa, K.Kandori, T. Nakayama, F. Yuse, 2002. Influences of metal ions on the formation of gamma-FeOOH and magnetite rusts. *Corrosion Science*, 44, 1073-1086.

Ishikawa,T., Katoh,R., Yasukawa A., Kandori K., Nakayama T. and Yuse F., 2001. Influences of metal ions on the formation of β-FeOOH particles. *Corrosion Science*, 43, 1727-1738.

Ishilawa T., Kondo Y., Akemi Y. and Kandori, K., 1998. Formation of magnetite in the presence of ferric oxyhydroxides. *Corrosion Science*, 40(7), 1239-1251.

IUPAC. Compendium of Chemical Terminology, 2nd ed. (the "Gold Book"). Compiled by A. D. McNaught and A. Wilkinson. Blackwell Scientific Publications, Oxford (1997). XML on-line corrected version: http://goldbook.iupac.org (2006-) created by M. Nic, J. Jirat, B. Kosata; updates compiled by A. Jenkins. ISBN 0-9678550-9-8. doi:10.1351/goldbook.

Ivanov A. V., Trakhtenberg S., Bertram A.K., Gershenzon Y.M., and Molina M. J., 2007. OH, HO_2, and ozone gaseous diffusion coefficients, *Journal of Physical Chemistry* A, 111(9), 1632-1637.

Jakes K.A. and Sibley L.R., 1984 An examination of the phenomenon of textile fabric pseudomorphism. In Gould R.F. ed. *Archaeological Chemistry*, Washington, American Chemical Society, 403-424.

JIS K 0129, 1994. General principles of thermal analysis.

Johnston J.H. and Logan N.E., 1979. Mossbauer spectroscopic studies of iron (III) in the octahedral and channel sites in akaganeite. *Journal of Chemical Society, Dalton Transactions*, 13-16.

Kaneko K. and Inouye K., 1974. Electrical properties of ferric oxyhydroxides. *Bulletin of the Chemical Society of Japan*, 47(5), 1139-1142.

Kaneko K, Serizawa M., Ishikawa T. and Inouye K., 1975. Dielectric behaviour of water molecules adsorbed on iron (III) oxide hydroxides. *Bulletin of the Chemical Society of Japan*, 49, 3689-3690.

Kaneko, K. and Inouye K., 1979. Adsorption of water on FeOOH as studied by electrical conductivity measurements. *Bulletin of the Chemical Society of Japan*, 52(2), 315-320.

Karmazsin, E., Satre, P. and Vergnon, P., 1983. Simultaneous thermomagnetic and dilatometric measurements in a study of metastable transformation. *Journal of Thermal Analysis*, 28, 279-284.

Keller P., 1948. Uber Hydroxide und basissche Salze des Zwertigen Eisens und deren dunkelgrunen Oxydationprodukte. PhD Bern.

Keller P., 1970. Eigenschaften von $(Cl,OH)_2Fe_8(OOH)_{16}$ und akaganeit. *Neues Jahrbuch der Mineralodie*, 113, 29-49.

Keller P., 1979. Eigenschaften von $(Cl,F,OH)_{<2}Fe_8(O,OH)_{16}$ und akaganeit. *Neues Jahrbuch fur Mineralogie Abhandlungen*, 113, 29-49.

Kellner R., Mermet, J.M., Otto, M. and Widmer H.M., 1998. *Analytical Chemistry* Weinheim New York.

Kibrya, R. and Shashoua Y., 1996. *Evaluation of the suitability of polypropylene Stewart plastic containers for storing metals*. British Museum Conservation Research Group Internal Report 1996/4, The British Museum, London

Knight B., 1982. Why do some iron objects break up in store? *National Maritime Museum Monograph 53*, Greenwich, National Maritime Museum, 50-51.

Knight B., 1990. A review of the corrosion of iron from terrestrial sites and the problem of post-excavation corrosion. *The Conservator*, 14, 37-43.

Koshy V.J., Rao K.V., Kalpana G. and Garg V.N., 1992. Application of electron probe micro-analysis to the estimation of chlorine in alumina based heterogeneous catalysts. *Talenta*, 39(1), 17-19.

Kuu W.Y., Chilamkurti R. and Chen C., 1989. Effect of relative humidity and temperature on moisture sorption and stability of sodium bicarbonate powder, *International Journal of Pharmaceutics*, 166(2), 167-175.

Kwan K.S., 1998, *The role of penetrant structure on the transport and mechanical properties of a thermoset polymer*. PhD thesis, Virginia Polytechnic Institute and State University.

Lansberg G.S. and Mandelstam L.I., 1928 Eine neue Erscheinung bei der Lichtzerstreuung in Krystallen, *Nature*, 16, 557–558.

Lang J. and Middleton A., 1997. *Radiography of Cultural Material*, London, Butterworth-Heinemann.

Larkin N., Blades N. and Makridou E. 2000 Investigation of volatile organic compounds associated with polyethylene and polypropylene containers used for conservation storage. *The Conservator*, 24, 42-51.

Larkin, N., Makridou E, and Comerford G., 1998. Plastic storage containers: a comparison. *The Conservator*, 22, 81-87.

Lee, M.R. and Bland, P.A., 2004. Mechanisms of weathering of meteorites recovered from hot and cold deserts and the formation of phyllosilicates. *Geochimica et Cosmochimica Acta*, 68, 893-916.

Lee, L.R. and Bradley S., 1995. An investigation of strategies for the long term storage of archaeological iron. In *Proceedings of Metal 95*, Semuer en Auxois, 25-28 September 1995, London, James and James Scientific Publishers, 305-309.

Legrand, L., Sagon, G., Lecomte, S., Chausse, A. and Messina, R., 2001. A Raman and infrared study of a new carbonate green rust obtained the electrochemical way. *Corrosion Science*, 43, 1739-1749.

Lehmann J. and Nosek, E.M., 1978. Research and conservation of iron objects discovered in a shipwreck lifted from Gdansk gulf. in Organ R.M., Nosekand E.M. and Lehmann J. Eds. *Conservation of Iron Objects Found in Salty Environments*, Warsaw, 1978, Warsaw, Historical Monuments Documentation Centre, 3-50.

Lehto, V.-P. and Lankinen, T., 2004. Moisture transfer into medicament chambers equipped with a double barrier- desiccant system. *International Journal of Pharmaceutics*, 275, 155-164.

Lewis, D.G. and Farmer, V.C., 1986. Infrared absorption of surface hydroxyl groups and lattice vibrations in lepidocrite (γ-FeOOH) and boehmite (γ-AlOOH). *Clay Minerals*, 21, 93-100.

Libowitzky, E. and Rossman, G.R., 1997. An IR absorption calibration for water in minerals. *American Mineralogist*, 82, 1111-1115.

Ligocki, M.P., Harvey, I.H.L., Cass, G.R., 1990. Measurements of particulate deposition rates inside Southern Californian museums. *Aerosol Science and Technology*, 13, 85-101.

Lu Y.Q., Yalamanchili M.R. and Miller J.D., 1998. FT-IR internal reflection spectroscopy using regular polygonal internal reflection elements. *Applied Spectroscopy*, 52(6), 851-854.

MacKay A.L., 1966. Some aspects of the topochemistry of the iron oxides and hydroxides. In De Boer Ed. *4th international symposium on Reactivity of Solids*, Amsterdam, Elsevier, 571-583

Mackay A.L., 1960. β-ferric oxyhydroxide. *Mineralogial Magazine*, 32(250), 545-557.

Mackay A.L.,1962. β-ferric oxyhydroxide: akaganeite. *Mineralogial Magazine,* 33(259), 220-280.

MacKenzie R.C., 1970. *Differential Thermal Analysis*, London, Academic Press.

Maeda Y., Matsuo Y., Sugihara S., Momoshima N. and Takashima Y., 1992. Mossbauer studies of first stage corrosion products on iron powder and corrosion products on highly corroded nails. *Corrosion Science*, 33, 1557-1567.

Maish, J. P., 2005. A note on the evaluation of a solid state air drier. *Studies in Conservation,* 50, 137-142.

Makkonen U. and Juntto S., 1997. Field comparison of measurement methods for sulphur dioxide and aerosol sulphate. *Atmospheric Environment,* 31(7), 983-990.

Matthiesen H. and Wonsyld K., 2009. In situ measurement of oxygen consumption to estimate corrosion rates, *Proceedings of EUROCORR 2009*, Nice, France, September 2009, Nice, The European Federation of Corrosion, Paper WS D-O-7856.

Melendres C.A., Pankuch M., Li Y.S. and Knight, R.L., 1992. Surface enhanced Raman spectroelectrochemcial studies of the corrosion films on iron and chromium in aqueous solution environments. *Electrochimica Acta,* 37 (15), 2747-2754.

Michalski, S., 1994. Leakage prediction for buildings, cases, bags and bottles. *Studies in Conservation,* 39(3), 169-186.

Michalski S., 2008. Social discount rate: modelling collection value to future generations, and understanding the difference between short-term and long-term preservation actions. In *Preprints of ICOM-CC, 15th Triennial Conference* New Delhi, 22-26 September 2008, New Delhi, Allied Publishers, 751-758.

Miliani C., Doherty B., Daveri A., Loesch A. Ulbricht H., Brunetti B.G. and Sgamellotti A., 2009. In situ non-invasive investigation on the painting techniques of early Meissen Stoneware. *Spectrochimica Acta Part A,* 73(4), 587-592.

Miner C.S. and Dalton N.N., 1953. *Glycerol*, New York, Reinhold, 269.

Misawa T., Suetaka W. and Shimodaira S., 1970. Formation of iron oxide and oxyhydroxides and aqueous solutions and their physical properties. *Zairyo,* 19, 537-542.

Misawa T., Suetaka W. and Shimodaira S., 1969. Infrared absorption spectra and oxidation of iron(II) hydroxide and green rust 1. *Bulletin of the Chemical Society of Japan*, 42, 3339-3340.

Misawa, T., Asami, K., Hashimoto, K and Shimodaira, S., 1974. The mechanism of atmospheric rusting and the protective amorphous rust on low allow steel. *Corrosion Science*, 14, 279-289.

Misawa, T., K. Hashimoto, and Shimodaira S., 1974. The mechanism of formation of iron oxide and oxyhydroxides in aqueous solutions at room temperature. *Corrosion Science*, 14, 131-149.

Mould R.F., 1993. *A Century of X-Rays and Radioactivity in Medicine*, London, Taylor and Francis Group.

Munsell Corporation, 2009. *Munsell Washable Soil Color Charts*, North Brunswick.

Murad E. and Bishop J.L., 2000. The infrared spectrum of synthetic akaganeite, *American Mineralogist*, 85(5-6), 716-721.

Music S., Maljkovic M. and Nagy C.I., 1997. Thermal decomposition of β-FeOOH. *Materials Letters*, 31, 444-448.

Nagai N.T., Matsunobe T. and Imai T., 2005. Infrared analysis of depth profiles in UV-photochemical degradation of polymers. *Polymer Degradation. and Stability*, 88, 224.

Naono H., Fujiwara R., Sugioka H, Sumiya K. and Yanazawa H., 1982. Micropore formation due to thermal decomposition of acicular microcrystals of β-FeOOH. *Journal of Colloid and Interface Science*, 87, 317-332.

Nauer G., Strecha P., Brinda-Konopik N. and Lipstay G, 1985. Spectroscopic and thermoanalytical characterization of standard substances for the identification of reaction products on iron electrodes. *Journal of Thermal Analysis*, 30(40), 813-830.

Neff, D., Dillmann P., Bellot-Gurlet L. and Beranger G., 2005. Corrosion of iron archaeological artefacts in soil. *Corrosion Science*, 47, 515-535.

Nelson, M. C. and Shears B., 1996. From the Field to the Files: Curation and the Future of Academic Archaeology. Common Ground 1(2): [online] Available at <http://www.nps.gov/history/archeology/Cg/vol1_num2/files.htm >[Accessed 28/04/2011].

Niklasson A., 2007. *Atmospheric corrosion of historic lead organ pipes*. PhD Chalmers University of Technology, Goteborgin, 53.

North N.A. and C. Pearson, 1975. Alkaline sulfite reduction treatment of marine iron. In *ICOM Committee for Conservation 4th Triennial Meeting*, Venice, 13-18 October 1975, Paris, International Council of Museums, 13/3-1-14.

North N.A., 1976. Formation of coral concretions on marine iron. *International Journal of Nautical Archaeology*, 5, 253-258.

North N. A., 1982. Corrosion products on marine iron. *Studies in Conservation*, 27, 75-83.

Nosek E.M., 1978. Research and conservation of the iron objects currently displayed at the salt mine museum. in *Conservation of Iron Objects Found in Salty Environments*, Ed: R.M. Organ, E.M. Nosekand J. Lehmann, Historical Monuments Documentation Centre, Warsaw, 9-20.

Nyquist R.A. and Kagel R.O., 1971. *Infrared Spectra of Inorganic Compounds*. London, Academic Press.

Oblonsky, L.J. and Devine, T.M., 1995. A surface enhanced Raman spectroscopic study of the passive films formed in borate buffer on iron, nickel, chromium and stainless steel. *Corrosion Science*, 37(1), 17-41.

O'Brian D., 2010, Measuring the value of culture: a report to the Department for Culture Media and Sport. DCMS [online], Available at: http://www.culture.gov.uk/publications/7660.aspx <Accessed 12 August 2011>.

Oddy W. A., 1973. An unsuspected danger in display. *Museums Journal*, 73, 27–28.

Odziemkowski M.S., Schuhmacher T.T., Gillham R.W. and Reardon E.J., 1998. Mechanism of oxide film formation on iron in simulating groundwater solutions: Raman spectroscopic studies. *Corrosion Science*, 40(2/3), 371-389.

Oesch S., 1996. The effect of SO_2, NO_2 and O_3 on the corrosion of unalloyed carbon steel and weathering steel – the results of laboratory exposures. *Corrosion Science*, 38(8), 1357-1368.

Ohtsuka T., Kubo K. and Sato N., 1986. Raman spectroscopy in thin corrosion films on iron at 100 to 150ºC in air. *Corrosion*, 42(8), 497-481.

Okamato S., 1968. Structure of δ-FeOOH. *Journal of the American Ceramic Society*, 51(10), 594-599.

Organ R.M., 1977. The current status of the treatment of corroded metal artifacts. In: *Corrosion and Metal Artifacts, A dialogue between conservators and*

conservation scientists, 17-18 March 1976, Gaithersburg, Maryland, Washington, National Bureau of Standards, 107-142.

Padfield, T., 1966. The control of relative humidity and air pollution in show-cases and picture frames. *Studies in Conservation*, 11, 8-30.

Palmes E.D., Gunnison A.F., DiMattio J. and Tomczyk, C., 1976. Personal sampler for nitrogen dioxide. *American Industrial Hygene Association Journal*, 37, 570-577.

Parfitt, R.L. and Smart, S.C., 1977. Infrared spectra from binuclear bridging complexes of sulphate adsorbed on goethite (α-FeOOH). *Journal of the Chemical Society Faraday Transactions*, 173, 796-802.

Paterson E., Swaffield R. and Clark D.R., 1982. Thermal decomposition of synthetic akaganeite. *Thermochim. Acta*, 54, 201-211.

Pearson C., 1972. The preservation of iron cannon after 200 years under the sea. *Studies in Conservation*, 17, 91-110.

Perkhina E.V. and Yu Strakhov S., 2008. Experimental and numerical modelling of attenuated total reflectance method in the process of hazard substances contact detection. *Optical Memory and Neural Networks*, 18(4), 337-342.

Pfaff, J.D., 1993. Method 300.0 Determination of inorganic anions by ion chromatography, Environmental Protection Agency, Cincinnati.

Pickrell, J.A., Mokler, B.V., Griffis, L.C., Hobbs, C.H. and Bathija, A., 1983, 'Formaldehyde Release Rates from Selected Consumer Products', *Environmental Science and Technology*, 17, 753-757.

Post J.J. and Buchwald V.F., 1991. Crystal structure refinement of akaganeite. *American Mineralogist*, 76, 272-277.

Pourbaix, M., 1977. Electrochemical corrosion and reduction. In B.F. Brown, H.C. Burnett, W.T. Chase, M. Goodway, J. Kruger and M. Pourbaix, eds, *Corrosion and Metal Artefacts*, National Bureau of Standards Special Publication, 479, 17-18 March 1976, Gaithersburg, Maryland, Washington, National Bureau of Standards,.1-16.

Pullin M.J. and Cabaniss S. E., 2003. The effects of pH, ionic strength, and iron-fulvic acid interactions on the kinetics of non-photochemical iron transformations. II. The kinetics of thermal reduction. *Geochimica et Cosmochimica Acta*.,67, 4079-4089.

Pullin, M.J. and Cabaniss S.E., 2003. The effects of pH, ionic strength, and iron-fulvic acid interactions on the kinetics of non-photochemical iron transformations. I. Iron (II) oxidation and iron (III) colloid formation. *Geochimica et Cosmochimica Acta*, 67(21), 4067-4077.

Raman A., Kuban B. and Razvan A., 1991, The application of infrared spectroscopy to the study of atmospheric rust systems—I. Standard spectra and illustrative applications to identify rust phases in natural atmospheric corrosion products. *Corrosion Science,* 32(12), 1295-1306.

Raman C.A. and Krishnan K.S., 1928. A new type of secondary radiation, *Nature*, 121(3048), 501.

Rance, V. and Cole H.G., 1958. *Corrosion of metals from organic acids: a survey,* HMSO, London, 17.

Raychaudhuri, M. R. and Brimblecombe P., 2000. Formaldehyde oxidation and lead corrosion. *Studies in Conservation,* 45, 226-232.

Reibold M., Paufler P. , Levin A. A., Kochmann W., Pätzke N. and Meyer D. C., 2006. Carbon nanotubes in an ancient Damascus sabre, *Nature*, 444, 286 doi:10.1038/444286a; Received 24 July 2006; Published online 15 November 2006

Refait P. and Genin J.-M.R., 1997. The mechanism of oxidation of ferrous hydroxychloride, β-$Fe_2(OH)_3Cl$ in aqueous solution: the formation of akaganeite vs Goethite. *Corrosion Science*, 39, 539-553.

Refait P., Drissi S.H., Pytkiewicz J. and Génin,J.-M. R., 1997. The anionic species competition in iron aqueous corrosion: role of various green rust compounds. *Corrosion Science*, 39, 1699–1710.

Reguer S., Dillman P. and Mirambet F., 2007. Buried archaeological artefacts: corrosion mechanisms related to the presence of chloride containing phases. *Corrosion Science*, 49, 2726-2744.

Reguer S., Dillman P., Mirambet F., Susini J. and Lagarde P., 2006. Investigation of Cl corrosion products of iron archaeological artefacts using micro-focused synchrotron X-ray absorption spectroscopy. *Applied Physics A*, E3, 189-193.

Reguer S., Dillmann P., Mirambet F. and Bellot-Gurlet L., 2005. Local and structural characterisation of chlorinated phases formed on ferrous archaeological artefacts by μXRD and μXANES. *Nuclear Instruments and Methods in Physics Research B*, 240, 500-504.

Remazeille C. and Refait P., 2008. Formation fast oxidation and thermodynamic data of Fe(II) hydroxychlorides. *Corrosion Science*, 50, 856-864.

Rimmer, M.B., 2010. Investigating the treatment of chloride-infested archaeological iron. PhD Cardiff.

Robinet L. and Thickett D., 2005. Application of Raman Spectroscopy to Corrosion Products. in Edwards H.G.M. and Chalmers J.M. eds. *Raman Spectroscopy in Archaeology and Art History*, London, Royal Society of Chemistry, 325 – 333.

Robinet L.. 2006. The role of organic pollutants in the alteration of soda silicate glasses. PhD Edinburgh/Paris, Edinburgh/Paris VI.

Robinet, L. and Thickett D., 2004. A new methodology for accelerated corrosion testing. *Studies in Conservation*, 48, 263-268.

Roduit, B. and Maciejewski M., 1996. Influence of experimental conditions on the kinetic parameters of gas-solid reactions--parametric sensitivity of thermal analysis. *Thermoanalytical Studies of Materials,* 282-283, 101-119.

Roduit, B., 2000. Computational aspects of kinetic analysis.: Part E: The ICTAC Kinetics Project--numerical techniques and kinetics of solid state processes. *Thermochimica Acta,* 355(1-2), 171-180.

Roduit, B., 2002. Prediction of the progress of solid-state reactions under different temperature modes. *Thermochimica Acta,* 388(1-2), 377-387.

Rosi F., Burnstock A., Van der Berg K.J., Miliani C., Brunetti B.G. and Sgamellotti A., 2008. A non invasive XRF study supported by multivariate statistical reflectance FTIR to assess the composition of modern painting materials. *Spectrochimica Acta Part A*, 71(5), 1655-1662.

Ross S.D., *Inorganic Infrared and Raman Spectra.* London, McGraw Hill.

Ryhl-Svendsen, M. and Claussen G., 2009. The effect of ventilation, filtration and passive sorption on indoor air quality in museum storage rooms. *Studies in Conservation,* 54, 35-48.

Saheb M., Neff D., Dillmann P., Matthiesen H. and Foy E., 2008. Long term corrosion behaviour of low carbon steels in anoxic environments. *Journal of Nuclear Materials*, 379, 118-123.

Scharff W. and Huesmann L.A., 1995. Accelerated decay of metal soil finds due to soil pollution. In *Proceedings of Metal 95*, Semueren Auxois, 25-28 September 1995, London, James and James Scientific Publishers , 17-20.

Schieweck, A., 2009. *Airborne pollutants in museum showcases.* Academy of Fine Arts. Dresden.

Schwertmann U. and Cornell R.M., 1991. *Iron Oxides in the Laboratory Preparation and Characterization*, Wiley-VCH.

Schwertmann, U., Cambier, P. and Murad, E., 1985. Properties of goethites of varying crystallinities. *Clays and Clay Minerals*, 33, 369-378.

Schwertmann U. and Wolska E., 1990. The influence of aluminium on iron oxides. *Clay and Clay Minerals*, 38, 209-212.

Schwieck A. and Salthammer T., 2010. Indoor air quality in passive type museum showcases. *Journal of Cultural Heritage*, 12, 205-213.

Scott D.A. and Eggert G.E., 2009. *Iron and Steel in Art*. London, Archaeotype.

Selwyn L., 2004. Overview of archaeological iron: the corrosion problem, key factors affecting treatment, and gaps in current knowledge. In *Proceedings of Metal 2004*, Canberra, 4-8 October 2004, Canberra, National Museum of Australia, 294-306.

Selwyn, L.S., Sirois, P.J. and Argyropoulus V., 1999. The corrosion of archaeological iron. *Studies in Conservation*, 44, 217-232.

Serna, C.J., Rendon, J.L. and Iglesias, J.E., 1982. Infrared surface modes in corrundum type microcrystalline oxides. *Spectrachimica Acta*, 38A, 797-802.

Sharma S.K., 1974. Raman study of ferric chloride hexahydrate and ferric chloride hexadeutrate in crystalline, molten and glassy states. *Journal of Non-Crystalline Solids*, 15(1), 83-95.

Shashoua Y. and Matthiesen H., 2010. Protection of iron and steel in large outdoors industrial objects, *Corrosion Engineering, Science and Technology*, 45(5), 357-361.

Shyichuk A.V., White J.R., Craig I.H. and Syrotynska D., 2005. Comparison of UV degradation depth profiles in polyethylene, polypropylene and an ethylene-propylene copolymer. *Polymer Degradation and Stability*, 88, 415-419.

Simpson, L.J. and Melendres, C.A., 1996. Surface enhanced Raman spectroelectrochemical studies of corrosion films on iron in aqueous carbonate solution. *Journal of the Electrochemical Society*, 143(7), 2146-2152.

Smekal A., 1923. Zur Quantentheorie der Dispersion, *Naturwissenschaften*, 11(43), 873-877.

Smith L., 2006. *Uses of Heritage*. Abingdon, Routledge.

Spicer, C. W., Kenny D.V. l., 1993. Transformations, lifetimes and sources of NO_2, HONO, and HNO3 in indoor environments. *Journal of the Air and Waste Management Association*, 43, 1479-1485.

Stahl, K., Nielsen K.,Jiang J., Lebech B., Hanson J.C., Norby P., and Van Lanschot J., 2003. On the akaganeite crystal structure, phase transformations and possible role in post-excavational corrosion of iron artefacts. *Corrosion Science*, 45, 2563-2575.

Stanley, B., Xavier-Rowe A., and Knight B., 2003. Displaying the Werner Collection: a pragmatic approach to display cases. *The Conservator*, 27, 34-46.

Suensen-Taylor K, Sully D. and Orton C., 1999. Data in conservation; the missing link in the process. *Studies in Conservation*, 44, 184-194

Svendby T. and Henriksen J.K., 2004. Homogeneous reaction of air pollutants: modelling and testing in *Innovative Modelling of Museum Pollution and Conservation Thresholds*, Final Report. N. Blades. London, UCL Centre for Sustainable Heritage, 97-114.

Taylor, R.M., 1980. Formation and properties of Fe(II)Fe(III) hydroxy-carbonate and its possible significance in soil formation. *Clay Minerals*, 15, 369-382.

Taylor, P. and Lopata, V. J. , 1984. Stability and solubility relationships between some solids in the system lead oxide-carbon dioxide-water. *Canadian Journal of Chemistry*, 62, 395-402.

Tetreault, J. 2003 *Airborne Pollutants in Museums, Galleries and Archives*. Ottawa, Canadian Conservation Institute.

Tétreault, J., Cano E., van BrommelM., Scott D., Dennis M., Barthes-Labrousse M.G, Minel L. and Robbiola L., 2003. Corrosion of Copper and Lead by Formaldehyde, Formic and Acetic Acid Vapours. *Studies in Conservation*, 48, 237-250.

Tétreault, J., 1999. *Showcases*, [CD] distributed by Canadian Conservation Institute

Tétreault, J., 2001. Coatings for display and storage in museums. *CCI Technical Bulletin* , 21, 5-7.

Tétreault, J., 2010. Carbonyl vapours and their impact on paper, 9th Indoor Air Quality Meeting Chalon sur Saone 21-23 April 2010, oral communication.

Tétreault, J., Sirois J., and Stamatopoulou, E., 1998. Study of lead corrosion in acetic acid environment. *Studies in Conservation*, 43, 17–32.

Thibeau, R.J., Brown, C.W. and Heidersbach, R.H., 1978. Raman spectra of possible corrosion products of iron . *Applied Spectroscopy*, 32, 532-535.

Thickett, D., 1997. Relative effects of formaldehyde, formic and acetic acids on lead, copper and silver, The British Museum Report 1997/12.

Thickett, D., 1998a. Sealing MDF to Prevent Corrosive Emissions, *The Conservator*, 22 49–56.

Thickett D., 1998b. Assessment of the risks to metal artifacts posed by volatile carbonyl pollutants.in *Metal 98 Proceedings of the international conference on Metals Conservation*, Draguignan, 27-29 May 1998, London, James and James, 260-264.

Thickett D., 1998c. Sealing methods for timber composites British Museum Department of Conservation internal report 1998/4

Thickett D., 2005a.The use of Infra-red and Raman Spectroscopies for Iron Corrosion Products, in *Postprints of Sixth Infra-Red Users Group*, Florence, 29 March – 1 April 2004,Padua, Il PratoElsevier, 86-93.

Thickett D. and Odlyha M., 2005b. Application of thermo-magnetometry to Corrosion Studies of Archaeological Iron, *Journal of Thermal Analysis and Calorimetry*, 80(3), 565-571.

Thickett, D., David F. and Luxford N., 2006. Air Exchange Rate; A dominant parameter for showcases. *The Conservator*, 29, 19-34.

Thickett D., Fletcher P., Calver A. and Lambarth S., 2007. The effect of air tightness on RH buffering and control, in *Museum Microclimates*, Ed: T. Padfield and K. Borchersen, LP 19-23 November 2007, Hvidovre , Nielsen Bogtryk, 245-252.

Thickett, D., 2008a. Investigation into role of inert dusts in corrosion and corrosion mitigation in an aggressive marine environment. *Ligas Metalicos*, Porto, Univeristy of Porto, 75-90.

Thickett, D., 2008b. Presentation in situ through microclimates, in *Conservation and Access, 22nd IIC Congress*, London, 15-19 September 2008, London, International Institute of Conservation, 98-96.

Thickett D., 2008c. Determining the Stability and Durability of Archaeological Materials, in *Art08*, Jerusalem June 2008 online

Thickett, D., Stanley B. and Booth K,. 2008d. Refitting old display cases. In *15th Triennial Meeting of ICOM-CC*, New Delhi. 22-29 September 2008, New Delhi, Allied Publishers, 775-782.

Thickett D. and Odlyha M., 2010. Assessment of dry storage microenvironments for archaeological iron, *Post prints of The Conservation of Archaeological Materials: Current trends and future directions*, Williamsburg 13-17 November 2005, London, Archaeopress, 187-199.

Thickett, D. and Short-Traxler K., 2011. Practical application of sorbents. In *Metal 2010,* Charleston, South Carolina, 11-15 October 2010. Charleston.Clemson Univeristy, 414-420.

Thierry, D., Persson, D., Leygraf, C., Boucherit, N. and Hugot-Le-Goff, A., 1991. Raman spectroscopy and XPS investigations of anodic corrosion films formed on Fe-Mo alloys in alkaline solutions. *Corrosion Science*, 32, 273-284.

Thomsen, G.,1977. Stabilization of RH in exhibition cases: hygrometric half-time. *Studies in Conservation,* 22, 85-102.

Turgoose S., 1982a. The nature of surviving iron objects in Conservation of iron, *National Maritime Museum Monographs and Report* 53, Greenwich, 4 July 1980, Greenwich, National Maritime Museum, 1-7.

Turgoose S., 1982b. Post-excavation changes in iron antiquities. *Studies in Conservation*, 27, 97-101.

Turgoose S., 1993. Structure, composition and deterioration of unearthed iron objects In *Reports on the 13th International Symposium on the Conservation and Restoration of Cultural Properties*, 4-9 October 1989, Tokyo Kokuritsu Bunkazai Kenkyujo Hozon Kagakubu, 20-41.

United Kingdom Institute for Conservation Archaeology Section, 1983. *Conservation Guidelines No. 2, Packaging and Storage of Freshly Excavated Artifacts from Archaeological Sites.* London.

Ushioda, S., 1972. Raman scattering from phonons in iron pyrite (FeS2). *Solid State Communications*, 10(3), 307-320.

Vernon, W. H. J., 1935. A Laboratory study of the atmospheric corrosion of metals: Part II, iron: the primary oxide film; Part III, the secondary product or rust (influence of sulphur dioxide, carbon dioxide, and suspended particles on the rusting of iron). *Transactions of the Faraday Society,* 31, 1668-1700.

Vogh, H., Chattopadhyay, Y. and Stolz, H.J., 1982. Complete first order spectra of the pyrite structure compounds FeS_2, MnS_2, SiP_2 . *Journal of physics and chemistry of solids* , 44(9), 869- 873.

Waller, C., Desipak bags, http://www.cwaller.de/english.htm <accessed 1 Sept 2011>.

Wang Q., 2007a. An investigation of deterioration of archaeological iron, *Studies in Conservation*, 52, 125-134.

Wang Q., 2007b. Effect of relative humidity on the corrosion of iron: an experimental view. *The British Museum Technical Research Bulletin*, 1, 65-73.

Wang, Z., Xu C. C., Cao X. and Xu B., 2007. The morphology, phase composition and effect of corrosion product on simulated archaeological iron. *Chinese Journal of Chemical Engineering*, 15(3), 433-438.

Warne S.S.J, Hurst H.J.J. and Stuart W.I., 1998. Application of thermo-magnetometry in mineralogy, metallurgy and geology. *Thermal Analysis Abstracts*, 17(1), 1-6.

Watkinson, D., 1983. Degree of mineralization: its significance for the stability and treatment of excavated ironwork. *Studies in Conservation*, 28, 85-90.

Watkinson D. and Neal V., 1987. *First Aid for Finds* London: RESCUE.

Watkinson D. and Al-Zahrani A., 2008. Towards quantified assessment of aqueous chloride extraction methods for archaeological iron: de-oxygenated treatment environments, *The Conservator*, 31, 75-86.

Watkinson D and Lewis. M., 2004. SS Great Britain iron hull: modeling corrosion to define storage relative humidity. in *Preprints of Metal04*, Canberra, Canberra, National Museum of Australia 88-100.

Watkinson D. and Lewis M.T., 2005. Dessicated storage of chloride contaminated archaeological iron objects. *Studies in Conservation*, 50, 241-252.

Watkinson D.and Lewis M.R.T., 2005 The Role of [beta]FeOOH in the corrosion of archaeological iron in *Materials Issues in Art and Archaeology VII: Materials Research Society Symposium*, November 30-December 3, 2004, Boston, Massechusis, Materials Research Society, 103-114.

Weckler B. and Lutz H.H., 1998. Lattice vibration spectra. *European Journal of Solid State Inorganic Chemistry*, 35, 531-544.

Weintraub, S., 2002, Demystifying silica gel, Object Specialty Group Postprints (vol. 9), 2002. Washington, D.C.: American Institute for Conservation.

Weiser H. and Milligan W.O., 1935. X-ray studies on the hydrous oxides V. Beta ferric oxide monohydrate. *Journal of the American Chemical Society,* 57, 238-241.

Weschler, C. J., Shields H., Naik, D.V., 1989. Indoor ozone exposures. *Journal of the Air and Waste Management Association*, 39, 1562-1568.

Wilson, M.J. ed., 1994. *Clay Mineralogy: Spectroscopic and Chemical Determinative Methods*, London, Chapman Hall.

Wolska E., Szajda W. and Piszora P., 1992. Determination of solid solution limits based on the thermal behaviour of aluminium substituted iron hydroxides and oxides. *Journal of Thermal Analysis*, 38, 2115-2122.

Worobiec, A., Stefaniak E.A., Kontzova V., Samek L., Karaszkiewicz P., Van Meel K. and Van Grieken R., 2006. Characterisation of individual atmospheric particles in the royal museum of the Wawel castle in Krakow, Poland. *e-Preservation Science*, 3, 63-68.

Wunderlich B., 1990. *Thermal Analysis*, London, Academic Press, 417-431.

Xavier-Rowe A., Fry C. and Stanley B., 2008. Power to prioritize: applying risk and condition information, *Conservation and Access: Contributions to the 2008 IIC Congress, London*, London James and James, 186-191.

Xavier-Rowe A., Fry C. and Stanley B., 2011. Collections at risk, In: *Preprints of 16th Triennial Meeting of ICOM-CC,* ICOM-CC

Yakimets I., Lai D. and Guigon M., 2004. Effects of photo-oxidation cracks on behaviour of thick polypropylene samples. *Polymer Degradation and Stability*, 86(1), 59-67.

Yang L., Pabalan, R.T., Browning L. and Dunn D.S., 2003. Corrosion behavior of carbon steel and stainless steel materials under salt deposits in simulated dry repository environments. *Materials Research Society Symposium Proceedings*, 757, II4.14.1-II4.14.7.

Yunlan H. Bixia L. Changsui W. Jinhua L. and Suzuki M., 1994. The structural characteristics of corrosion products of ancient ironware, *Science*, 263, 23-28.

Zucchi F., Morigi G.and Bertolasi V., 1977. Beta iron hydroxide formation in localized active corrosion of iron artifacts. In B.F. Brown, H.C. Burnett, W.T.

Chase, M. Goodway, J. Kruger and M. Pourbaix, Eds, *Corrosion and Metal Artefacts, A dialogue between conservators and conservation scientists.* 17-18 March 1976, Gaithersburg, Maryland, Washington, National Bureau of Standards, 103-106.

Appendix 1 FTIR Spectra of Standard Materials by Different Sampling Techniques.

The FTIR spectra described in 3.1 are presented in this appendix. Figure A1.1 shows the spectra of Goethite collected with potassium bromide disc, diamond cell, microscope and DRIFTS. Spectra are presented in % reflectance or transmission due to the microscope spectra.

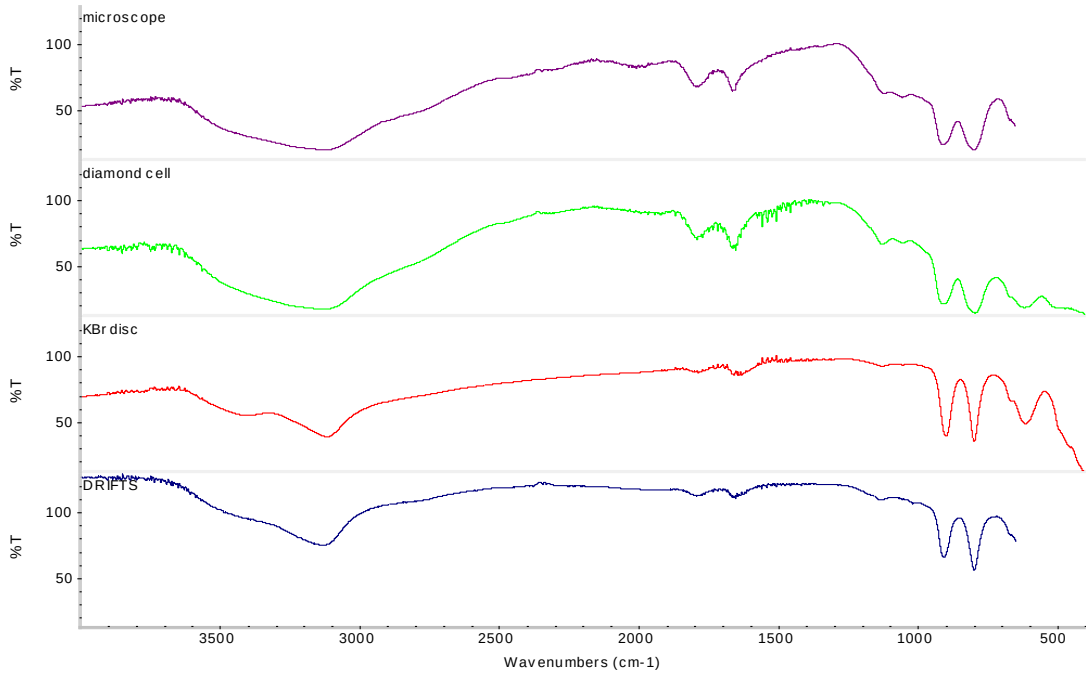

Figure A1.1 FTIR spectra of Goethite collected with different sampling techniques. Upper spectrum (purple) microscope; upper mid spectra (green) diamond cell; lower mid spectrum (red) potassium bromide disc; lower spectrum (blue) DRIFTS.

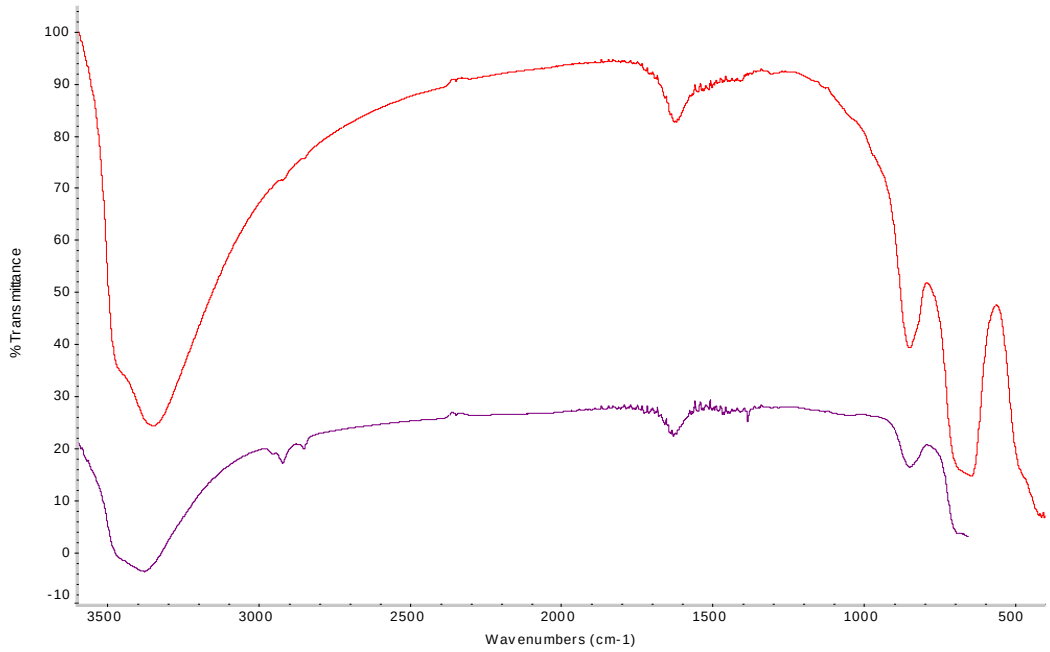

Figure A1.2 FTIR spectra of akaganeite. Upper spectrum (red) potassium bromide disc; lower spectrum (purple) microscope.

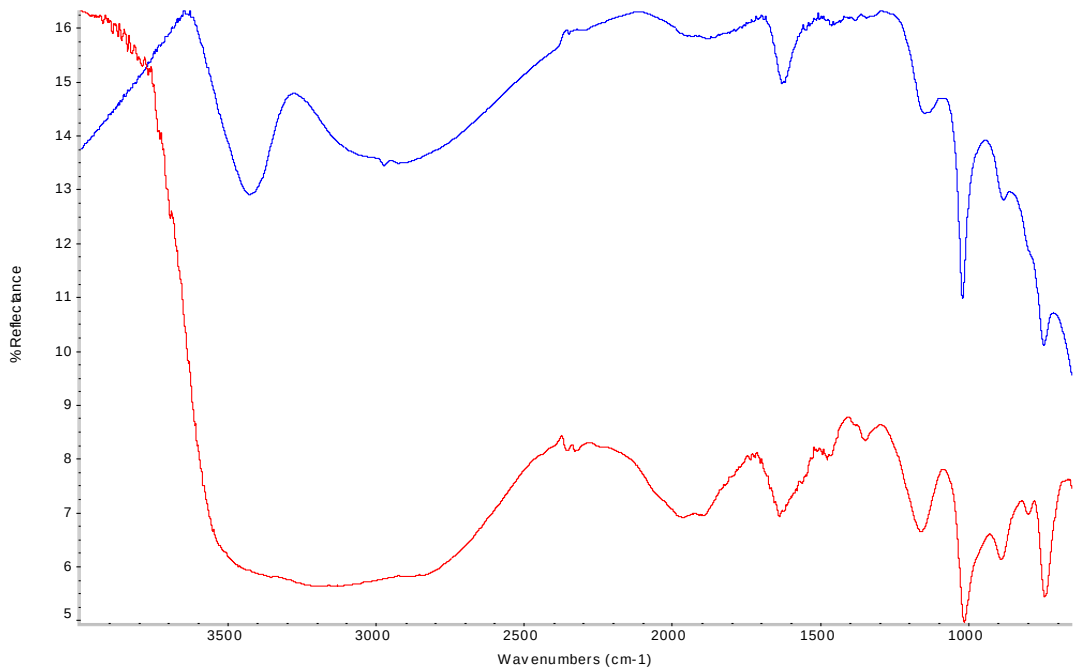

Figure A1.3 FTIR spectra of lepidocrite. Upper spectrum (blue) potassium bromide disc; lower spectrum (red) microscope.

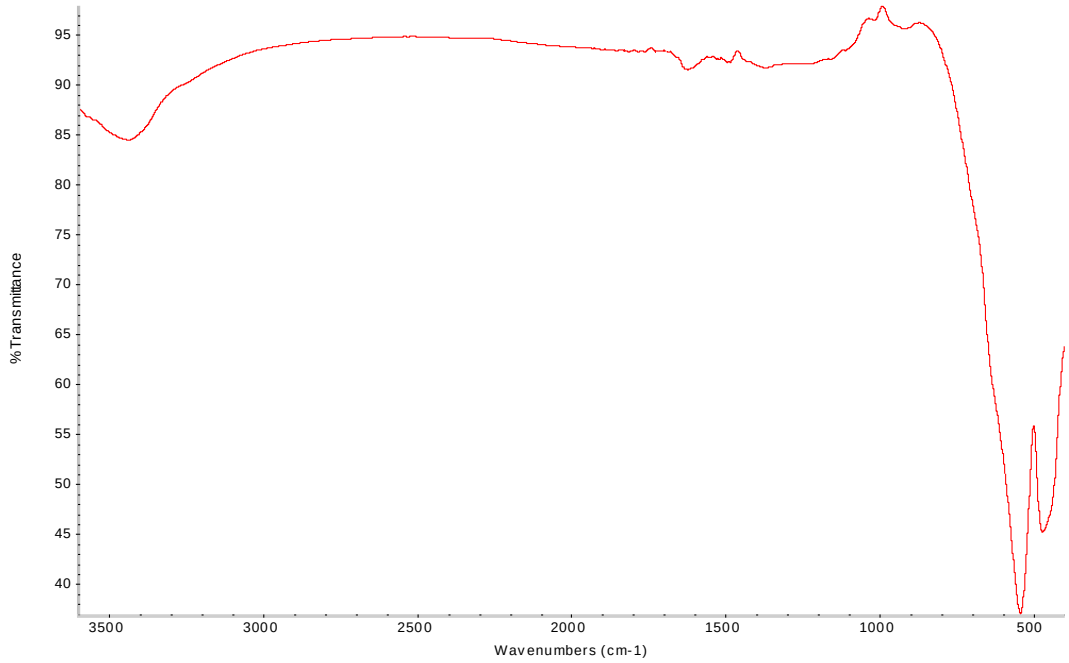

Figure A1.4 FTIR spectra of hematite by potassium bromide disc. There are no significant absorptions above 650cm-1 and hence microscope spectra is not displayed

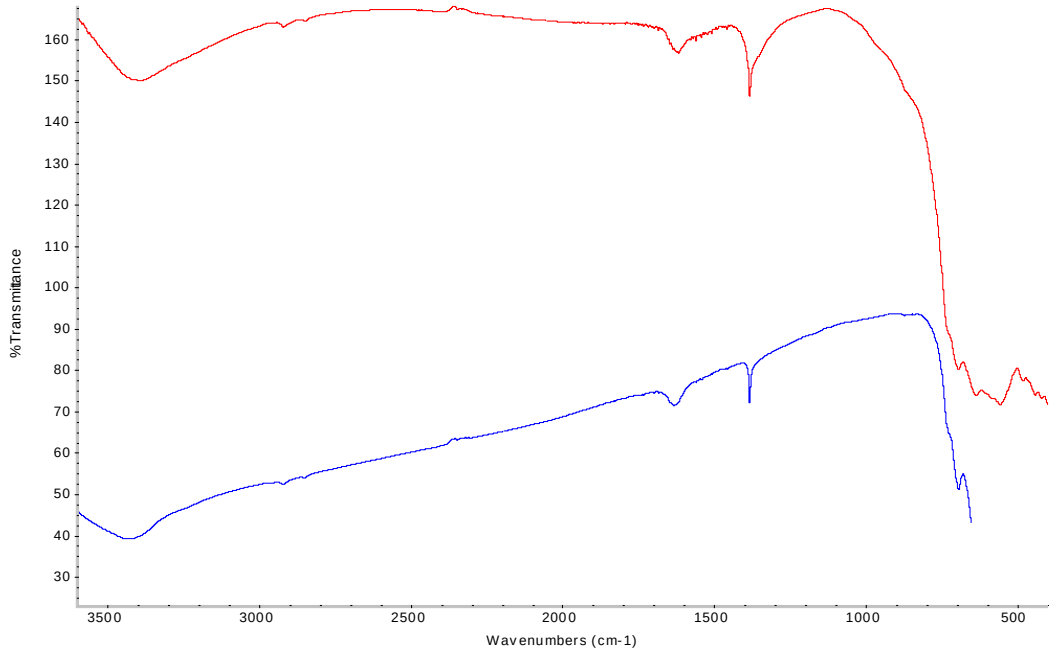

Figure A1.5 FTIR spectra of maghemite. Upper spectrum (red) potassium bromide disc; lower spectrum (blue) microscope.

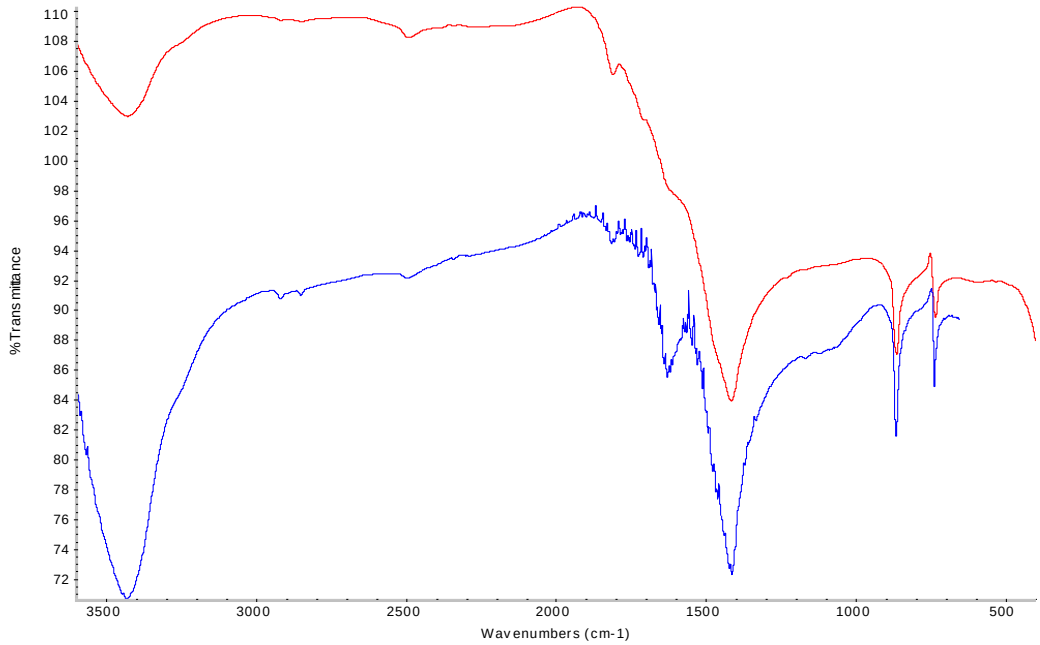

Figure A1.6 FTIR spectra of siderite,iron carbonate. Upper spectrum (red) potassium bromide disc; lower spectrum (blue) microscope.

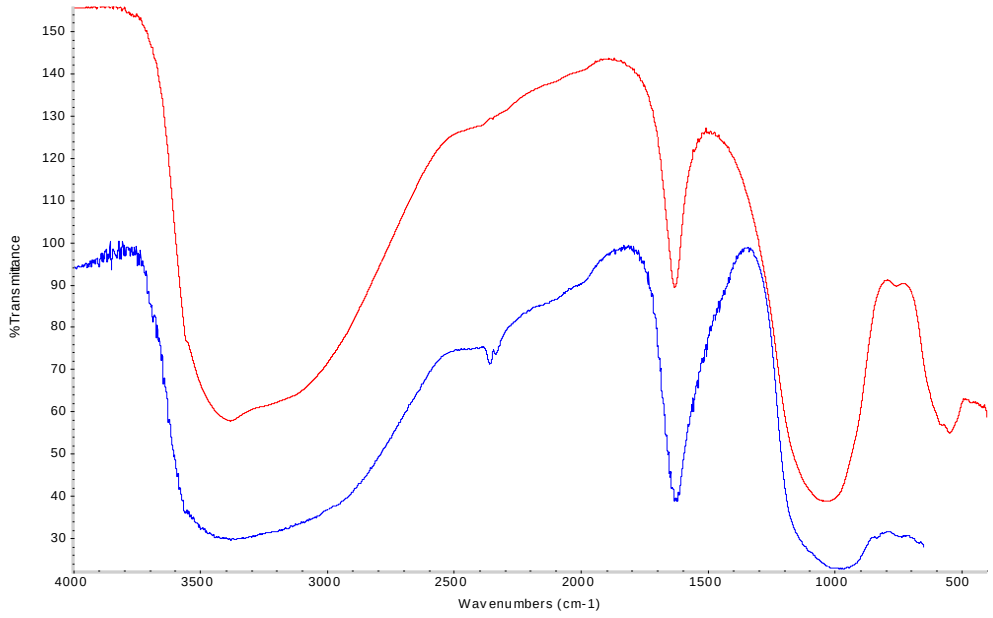

Figure A1.7 FTIR spectra of iron phosphate. Upper spectrum (red) potassium bromide disc; lower spectrum (blue) microscope.

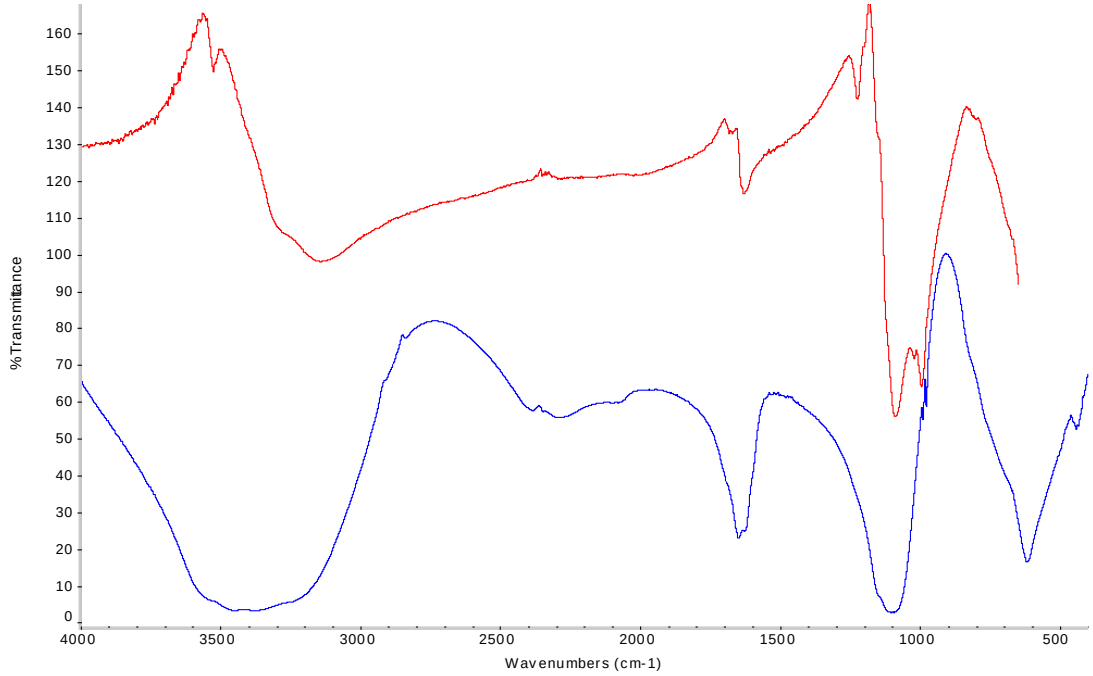

Figure A1.8 FTIR spectra of iron sulfate. Upper spectrum (red) microscope; lower spectrum (blue) potassium bromide disc.

The microscope spectra show water rotation bands above 3200cm^{-1} and between 1400 and 1900cm^{-1} due to the open beam path allowing exposure to water vapour. The microscope spectra A1.6 and A1.8 show derivative peaks although these are also present in the potassium bromide disc spectrum in A1.6.

Appendix2 Full Set of Pollution data from MASTER Project

Figures A2.1-A2.6 show the full set of concentration data measured in the project.

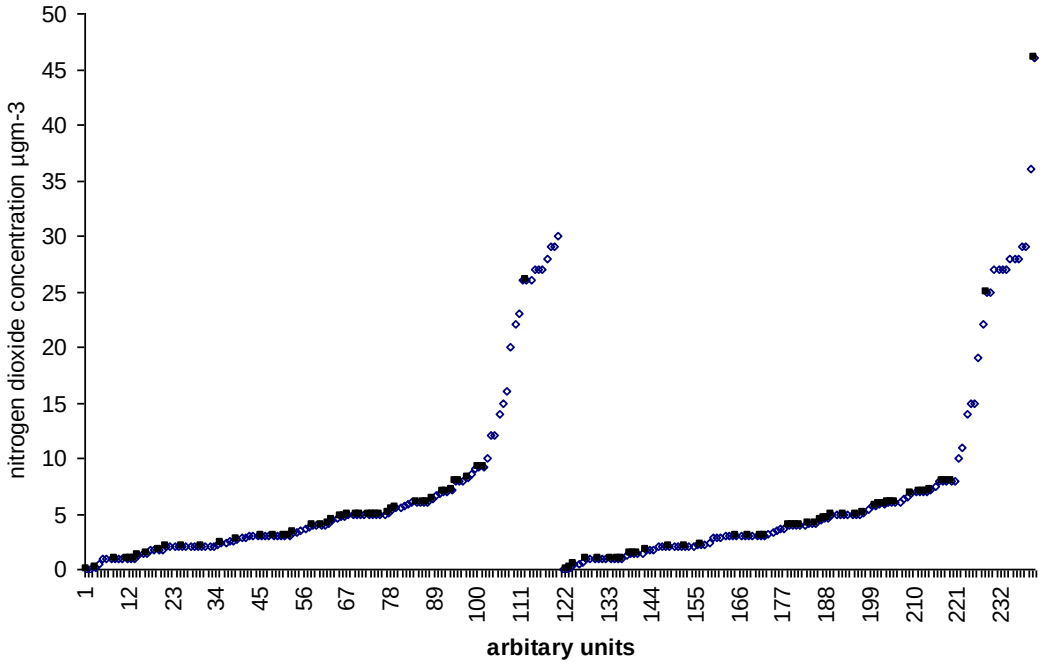

Figure A2.1 Nitrogen dioxide concentration in rooms measured in MASTER project

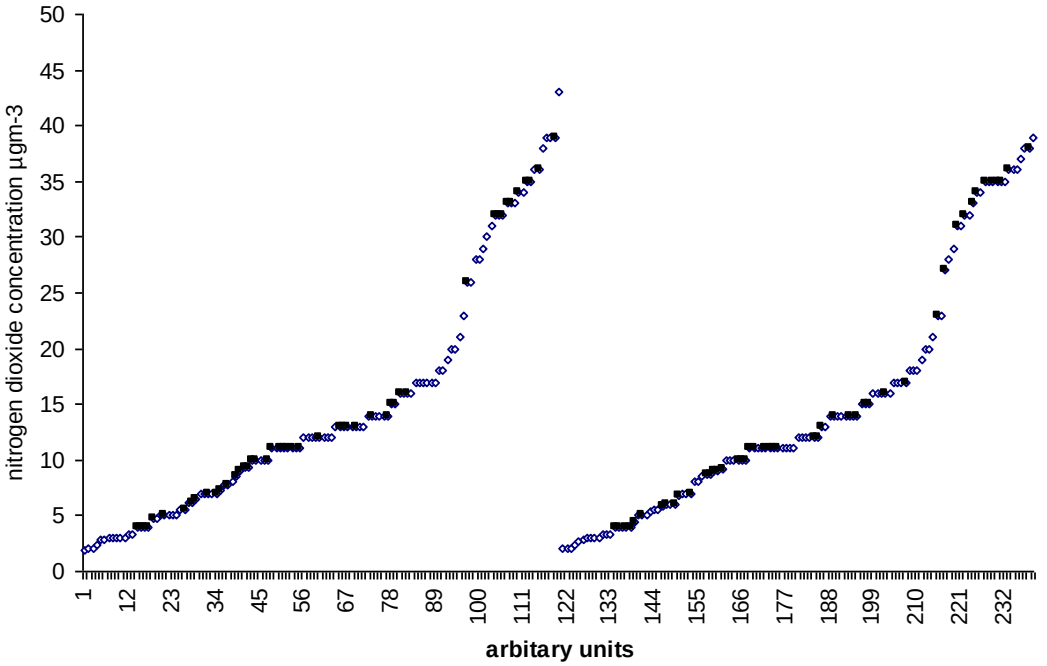

Figure A2.2 Nitrogen dioxide concentration inside showcases measured in MASTER project

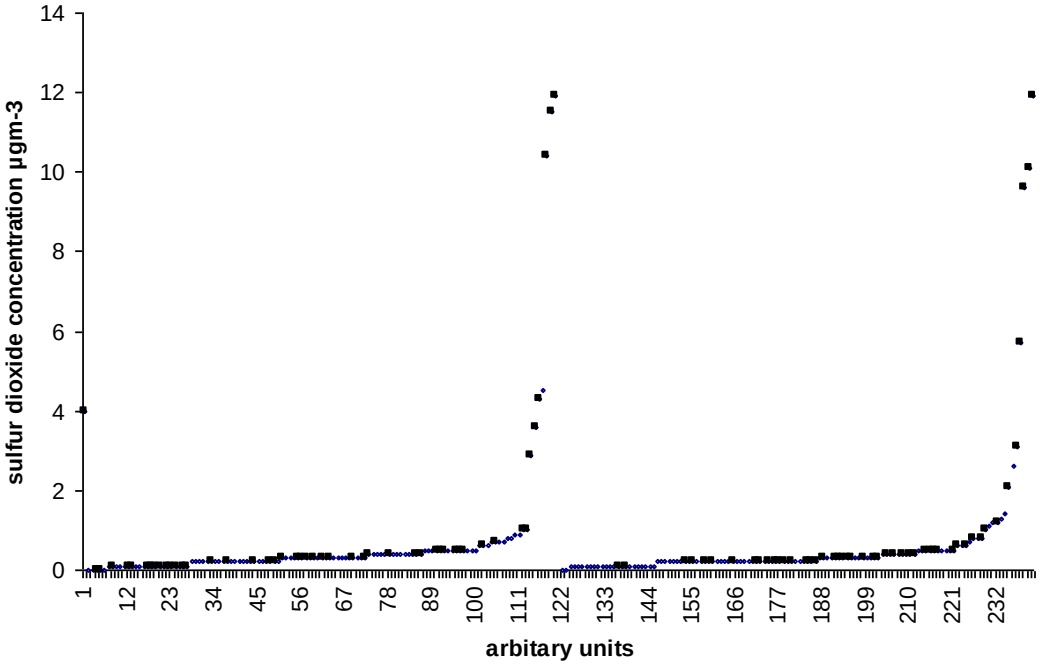

Figure A2.3 Sulfur dioxide concentration in rooms measured in MASTER project

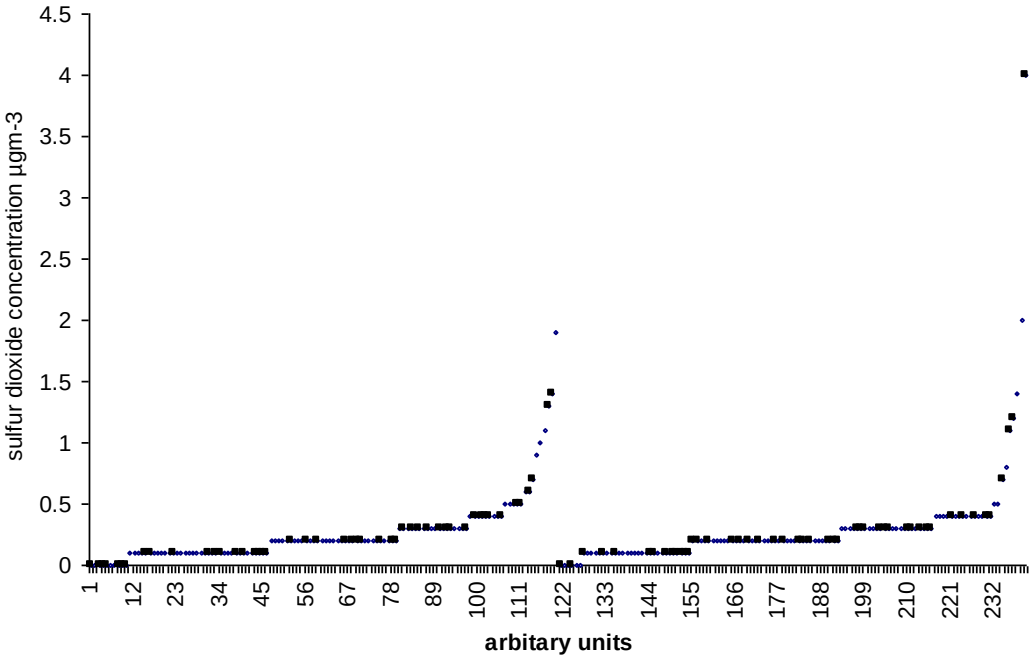

Figure A2.4 Sulfur dioxide concentration inside showcases measured in MASTER project

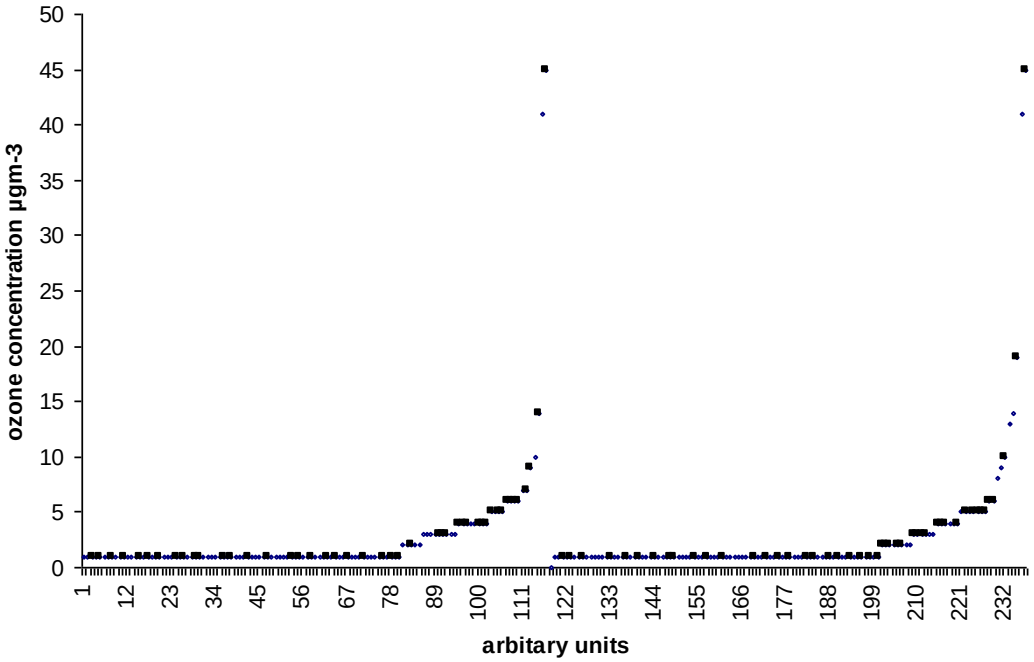

Figure A2.5 Ozone concentration in rooms measured in MASTER project

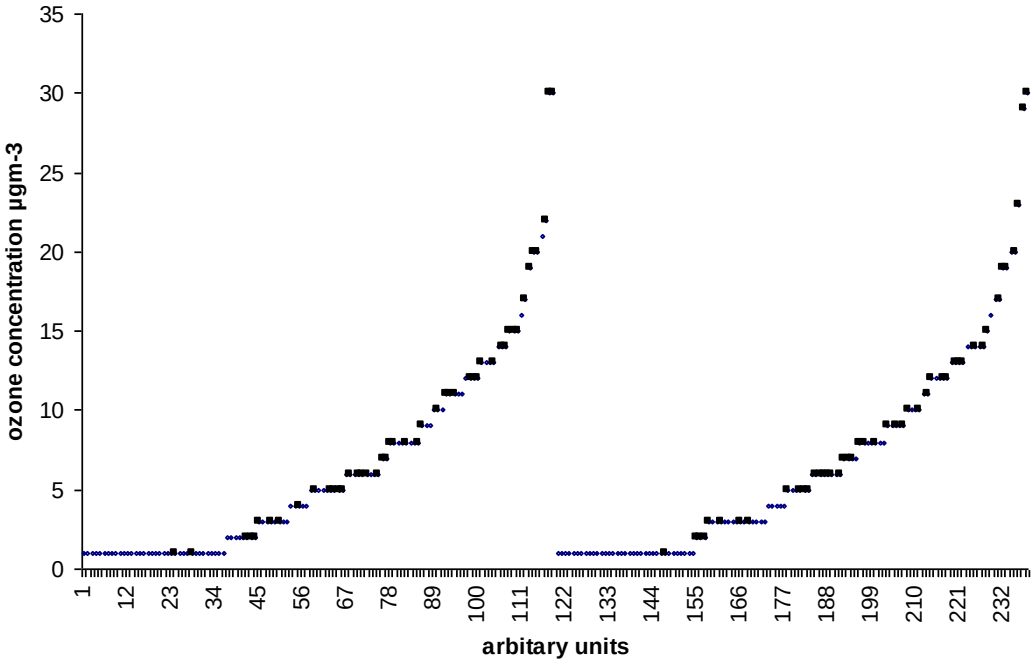

Figure A2.6 Ozone concentration inside showcases measured in MASTER project

The open lozenges are the full set of data and the black squares the data from the sites selected. This gave a good coverage of the span of data and the best and worst performing showcases. There are only two points on the very low concentration rooms for all gases, but all of the higher concentrations were well represented in the data set selected. The low concentrations were predominantly measured at Blickling Hall, Norfolk UK and The Jan Matejko House, Krakow, Poland, both rural sites with very little traffic.

Appendix3 Models for Relative Humidity Inside Enclosures

A3.1 Thomsen (1977)

Application of equation 7.4 is discussed in detail in Chapter 7.3.2.

$$T_{1/2} = 4MB/n \qquad (7.4)$$

Where $T_{1/2}$ is the hygrometric half life, the time taken for the RH inside the case to move half way to the value of the RH outside the case in days

B is the loading of buffer material in kg/m^3

M is the specific reserve of the buffer, the amount of water vapour adsorbed for a 1% increase in RH in g/kg, for most materials this is a function of RH and a single value cannot be used over wide RH ranges

n is the air exchange rate, day^{-1}

The equation assumes the temperature of the showcase is equal to that of the room it is in and that there is perfect mixing between the silica gel and the display volume. There are several heat sources commonly encountered in showcases. Internal lighting, environmental control equipment, AV equipment and the impingement of artificial and sunlight can all cause heating. Limited mixing was shown in Chapters 7.5.3 and 7.7.1. The internal RH in over forty showcases and thirty Stewart boxes has been modelled from room RH conditions. The model appeared robust with temperature differences up to 1.5ºC between the showcase and the room (no temperature differences above 0.3 ºC were observed for the Stewart boxes). Poor mixing did introduce a significant delay in the showcase RH and the model did not perform well in these instances.

The spreadsheet is available from

http://www.english-heritage.org.uk/professional/research/heritage-science/collections-conservation/collections-care-guidance/

(Calculating lifetime of silica gel in low RH showcases (60 minutes data intervals))

A3.2 Tetreault and Weintraub (2003)

Weintraub and Tetrault developed an equation to determine the amount of silica gel required to buffer to given RH fluctuation, which can be modified to estimate the time taken to reach a given RH (Tetrault 2003:58):

$$t_{RH} = MFB_H/C_{eq}Dn \quad \text{(A1)}$$

Where t_{RH} is time to reach a specifed RH (days)

F is targeted range of RH fluctuation (%)

B_H is specific moisture reservoir corrected for hysteresis (this effect is negligible for regular silica gel below 30% RH)

C_{eq} is equilibrium concentration of water vapour, calculated from T and RH, using Camuffo (2010:29) (g/m3).

D is decimal difference between external RH and enclosure RH.

The equation was iterated by calculating the time to reach 0.001% RH intervals and adding the RH increase for which the time that was the closest to 1 hour (the logger time interval) to the previous reading.

This assumes perfect mixing and failed when this was not the case.

A3.3 DePietro and Ligterink (1999)

DiPietro and Ligterink (1999) published a model to determine water vapor ingress through the backboard of picture frames:

$$t_{½} = \ln 2MB/PAC_{eq} \quad \text{(A2)}$$

Where $t_{½}$ is hygrometric half life (days)

P is permeance (measured at kg/m2sPa)

A is surface area (m^2)

C_{eq} is equilibrium concentration of water vapour, calculated from T and RH, using Camuffo (2010:29) (g/m3).

The model was iterated using a modification of the Thomsen.xls spreadsheet, Depietro.xls and the permeance value

A3.4 Lehto and Laninen (2004)

Many pharmaceutical products are RH sensitive, and models have been developed in that industry. The most recent was published by Lehto and Lankinen (2004). This is an iterative model for a desiccant container (silica gel bag), chamber, and external environment. It uses the following equations:

$$P_{con}(RH_{ch}-RH_{con}) = p_{ch}(RH_{env}-RH_{ch}) \quad (A3)$$

$$A_i = A_{i-1} + (B_{i-1} - D_{i-1}) \quad (A4)$$

$$B_i = P_{ch}\Delta_t\{RH_{env} -(100A_i/m_{max}) + RH_{init}\} \quad (A5)$$

$$C_i = 100(A_i+B_i)/m_{max} + RH_{init} \quad (A6)$$

$$D_i = P_{con}\Delta_t(C_i-F_{i-1}) \quad (A7)$$

$$E_i - E_{i-1} + D_i \quad (A8)$$

$$F_i = (100m_{init}+100E_i)/((m_{desc}W_mC_L)-C_L(100m_{init}+100E) \quad (A9)$$

Where P_{con} is permeability of desiccant container (ng/min%);

P_{ch} is permeability of chamber (ng/min%);

RH_{ch} is RH of chamber (%);

RH_{con} is RH of desiccant container (%);

RH_{env} is RH of external environment (75%);

A_i is total moisture content inside chamber (mg);

B_i is amount of water that permeates from environment into chamber during time interval Δt;

C_i is RH inside chamber, RH_{ch} (%);

D_i is amount of water that permeates into desiccant container from chamber during Δt (mg);

E_i is total amount of water that has permeated into desiccant container (mg);

F_i is RH inside the desiccant container, RH_{con} (%).

Lehto and Laninen provided the formula in a manner to feed easily in a spreadsheet.

A3.5 Brimblecombe and Ramer (1983)

Brimblecombe and Ramer published results from a model for the RH inside an enclosure written in Basic. Unfortunately the original program will not run on any computer with an operating system post Windows 95 and a suitable computer could not be found.

If you require an alternative accessible version of this document (for instance in audio, Braille or large print) please contact our Customer Services Department:
Telephone: 0870 333 1181
Fax: 01793 414926
Textphone: 0800 015 0516
E-mail: customers@english-heritage.org.uk